الجـــمـــهوريـــــة الجـــــزائريـــــة الـديمقـــراطيـة الـشعبيـــــة
People's Democratic republic of Algeria
وزارة التـعليـــــم الـعالـي و البحـث الـعلـــــمي
Ministry of Higher Education and Scientific Research
جـــــامعـــــة عبد الحميـــد بن باديـــس – مستغانـــــم
Abdelhamid Ibn Badis University – Mostaganem
كليـــــة العلـــــوم و الـتكنولـــوجـــــيا
Faculty of Sciences and Technology
قسم هندسة الطرائق
Department of Process Engineering

- **N° D'ORDRE: D…GP/2025**

THÈSE

Présenté pour obtenir le

DIPLÔME DE DOCTORAT 3ème cycle

Filière : **Génie des procédés**

Spécialité : **Génie des procédés de l'environnement**

Par:

BAGHDAD BENABED Fatma

Préparation d'un charbon actif à porosité contrôlée pour le traitement des eaux usées

Soutenue le **: 30 / 06 / 2025**

Devant le jury composé de :

Pr. CHOUAIH Abdelkader	Président	Université de Mostaganem
Pr. HADJEL Mohammed	Examinateur	Université des Sciences et de la Technologie d'Oran (USTO)
Pr. DRIOUCH Aouatef	Examinatrice	Université de Mostaganem
Dr. BENZEKRI BENALLOU Mokhtar	Examinateur	Université de Mostaganem
Dr. ATTOUTI Salima	Directeur de thèse	Université de Mostaganem
Dr. DOUARA Nadia	Co-directeur de thèse	Université de Mostaganem
Pr. BENDERDOUCHE Nouredine	Membre invité	Université de Mostaganem
Pr. BESTANI Benaouda	Membre invité	Université de Mostaganem

ANNEE UNIVERSITAIRE: 2024/2025

الجـــمـــهوريـــة الجـــزائريـــة الـديمقـــراطيـة الـشعبيـــة
People's Democratic republic of Algeria
وزارة الـتـعـليـــم الـعـالـي و الـبـحـث الـعـلـــمـي
Ministry of Higher Education and Scientific Research
جـــامـعـــة عبد الحميـــد بن باديـــس – مستغانـــم
Abdelhamid Ibn Badis University – Mostaganem
كليـــة العلـــوم و الـتكنولـوجـــيـا
Faculty of Sciences and Technology
قسم هندسة الطرائق
Department of Process Engineering

- **N° D'ORDRE: D…GP/2025**

THÈSE

Présenté pour obtenir le

DIPLÔME DE DOCTORAT 3ème cycle

Filière : **Génie des procédés**

Spécialité : **Génie des procédés de l'environnement**

Par:

BAGHDAD BENABED Fatma

Preparation of Activated Carbon with Controlled Porosity for Wastewater Treatment

Soutenue le: **30 / 06 / 2025**

Devant le jury composé de :

Pr. CHOUAIH Abdelkader	Président	Université de Mostaganem
Pr. HADJEL Mohammed	Examinateur	Université des Sciences et de la Technologie d'Oran (USTO)
Pr. DRIOUCH Aouatef	Examinatrice	Université de Mostaganem
Dr. BENZEKRI BENALLOU Mokhtar	Examinateur	Université de Mostaganem
Dr. ATTOUTI Salima	Directeur de thèse	Université de Mostaganem
Dr. DOUARA Nadia	Co-directeur de thèse	Université de Mostaganem
Pr. BENDERDOUCHE Nouredine	Membre invité	Université de Mostaganem
Pr. BESTANI Benaouda	Membre invité	Université de Mostaganem

ANNEE UNIVERSITAIRE: 2024/2025

Acknowledgments

I would like to start by mentioning that this doctoral research was carried out at the Structure, Development, and Application of Molecular Materials **(SEA2M)** Laboratory at Abdelhamid Ibn Badis University, Mostaganem.

A special thank you to **Dr. Salima ATTOUTI**, our team leader and my thesis supervisor, whose guidance, unwavering commitment, and motivation have been essential pillars of my academic journey. Her presence has been a constant source of inspiration and has significantly contributed to the quality and success of this research.

I would also like to express my gratitude to **Dr. Nadia DOUARA**, my co-supervisor, whose advice, invaluable expertise, and support played a crucial role in the completion of this ambitious project.

I wish to extend my gratitude to **Pr. Abdelkader CHOUAIH**, president of the jury and professor at the University of Mostaganem, for his essential role in supervising this defense and for his contribution to the evaluation of my thesis. I am deeply grateful to **Pr. Mohammed HADJEL** from the University of Science and Technology (USTO-MB), **Dr. Mokhtar BENZEKRI BENALLOU**, and **Pr. Aouatef DRIOUCH** from the University of Mostaganem, for their insightful and diligent examination of my work. Their unwavering commitment, constructive criticism, and expertise have significantly enriched my research.

I sincerely thank **Pr. Nouredine BENDERDOUCHE** and **Pr. Benaouda BESTANI** from the University of Mostaganem for the time and interest they devoted to this work, particularly through their constructive feedback. Their scientific knowledge and continuous support have enabled me to acquire valuable expertise in the field.

I also wish to express my heartfelt thanks to **Dr. Mourad TERMOUL** and **Dr. Mokhtar BENZEKRI BENALLOU** for their valuable support, insightful advice, and availability, as well as their constant encouragement, which have been a great help and are deeply appreciated.

I would like to express my heartfelt thanks to **Dr. Zohra MEKIBES**, Head of the Process Engineering Department, at Abdelhamid Ibn Badis University of Mostaganem, for her support, her availability, and her guidance in both scientific and administrative matters.

My sincere gratitude to **Pr. Nourdine BOUKABCHA** and **Pr. Abdelkader CHOUAIH** from Abdelhamid Ibn Badis University of Mostaganem, Laboratory of Technology and Solid Properties (LTPS), for agreeing to collaborate to carry out the theoretical study of our studied molecule.

I am profoundly grateful to **Prof. Dr Mustafa İmamoğlu** for welcoming me into the Analytical Chemistry Research Laboratory, as well as to **Prof. Dr Ali Çoruh**, and **Prof. Dr Yusuf ATALAY**, I sincerely thank them for their invaluable assistance with the characterization analyses conducted in their laboratory, as well as for their availability and good spirit throughout my stay.

A heartfelt thanks to **Halima DELALI,** teacher at Motaganem University, and all current and former Ph.D. students at Abdelhamid Ibn Badis University of Mostaganem, namely: Amina LAHOUALI DIT YAHYAOUI, Dr. Zohra Douaa BENYAHLOU, Sabrina SMATI, Dr. Mohammed Hadj Mortada BELHACHEMI, Asmae BENNABOU, Maamar CHERFI, Mohamed ALLAL, Yaslem Saleh Gamel Saleh, Salima DAOUI, Asmaa OUALI, Chaimaa MAITI, Khadidja KHALILI, and Soumia Abir AMIAR, who supported me, whether directly or indirectly, in the completion of this thesis.

Dedication

I dedicate this humble work to:

My dear parents, whose unconditional love, sacrifices, and unwavering support have shaped the person I am today,

*To my father, **Ali Cherif**, whose wisdom, hard work, and encouragement have always been a source of strength and inspiration,*

*To my mother, **Doha**, whose kindness, patience, endless devotion, and unlimited giving have guided me through every challenge,*

Their belief in me has been my greatest motivation,

I love you both with all my heart, and I pray that Allah blesses you with good health and a long life.

*To my beloved sister, **Imene**, and my dear brothers, **Yassine** and **Younes**, who bring joy and meaning to my life,*

To every close person to my heart, whose presence, love, kindness, and encouragement have been a source of comfort and motivation,

May Allah always keep you as my strength and pillar.

To my big family, who have always surrounded me with warmth and encouragement.

Fatma Baghdad Benabed

Abstract

Abstract

This study focused on preparing activated carbon from pine cone using potassium hydroxide (KOH) activation for pesticide removal from water. Two activation methods were compared: one-step and two-step activation. The results showed that the two-step activation produced activated carbon with higher porosity and better adsorption properties. The best-performing materials were the two-step activated carbon (K-AC_2), prepared in a muffle furnace, and AC_2', similarly prepared but in a tubular furnace under nitrogen. K-AC_2 had a yield of 72.25% and a BET surface area of 430.504 m^2 g^{-1}, an iodine number of 666.38 mg. g^{-1}, and a Methylene blue index of 72.77 mg g^{-1}, indicating a well-developed microporous structure. AC_2' had a higher micropore surface area of 1039.22 m^2 g^{-1}, an iodine number of 888.51 mg g^{-1}, and a yield of 72.57%, making it the most microporous material. The adsorption experiments demonstrated that these activated carbons effectively removed herbicides from aqueous solutions. For para-chlorophenoxyacetic acid (P-CPA), K-AC_2 achieved a maximum adsorption capacity of 266.5 mg g^{-1}, while AC_2' exhibited an even higher capacity of 284.8 mg g^{-1}. For Linuron (Lin), K-AC_2 reached 43.76 mg. g^{-1}, whereas AC_2' achieved 62.37 mg g^{-1}, where the adsorption isotherm was studied using several models (Langmuir, Freundlich, Temkin, Dubinin Radushkevich, and Redlich Paterson models). The kinetic study showed that the pseudo-second-order kinetics confirmed strong interactions between the adsorbent and pollutants. Thermodynamic studies showed that P-CPA adsorption was spontaneous and endothermic for both activated carbons, while Lin adsorption was exothermic for AC_2' but endothermic for K-AC_2. A desorption study revealed that K-AC_2 could be regenerated with a 69.72% desorption rate, demonstrating its potential for reuse in multiple cycles. These findings highlight that pine cone-based activated carbon, particularly the two-step activated carbon prepared in a tube furnace under nitrogen (AC_2') is a promising adsorbent material for herbicide removal and sustainable wastewater treatment.

Keywords: Pine cone, activated carbon, controlled porosity, adsorption, wastewater, para-chlorophenoxyacetic acid, Linuron.

Résumé

Cette étude porte sur la préparation de charbon actif à partir de cônes de pin en utilisant une activation par l'hydroxyde de potassium (KOH) pour l'élimination des pesticides dans l'eau. Deux méthodes d'activation ont été comparées : un procédé en une seule étape et une procédure en deux étapes. Les résultats ont montré que l'activation en deux étapes a produit un charbon actif avec une porosité plus élevée et de meilleures propriétés d'adsorption. Les matériaux les plus performants étaient : K-AC_2, préparé dans un four à moufle, et AC_2', préparé dans un four tubulaire sous atmosphère d'azote. K-AC_2 a présenté un rendement de 72,25 %, une surface BET de 430,504 m^2g^{-1}, un indice d'iode de 666,38 mg g^{-1}, et un indice de bleu de méthylène de 72,77 mg g^{-1}, indiquant une structure microporeuse bien développée. AC_2' a affiché une surface microporeuse plus élevée de 1039,22 m^2 g^{-1}, un indice d'iode de 888,51 mg g^{-1}, et un rendement de 72,57 %, ce qui en fait le matériau le plus microporeux. Les expériences d'adsorption ont démontré que ces charbons activés éliminent efficacement les herbicides des solutions aqueuses. Pour l'acide para-chlorophénoxyacétique (P-CPA), K-AC_2 a atteint une capacité maximale d'adsorption de 266,5 mg g^{-1}, tandis que AC_2' a atteint 284,8 mg g^{-1}. Pour le Linuron (Lin), K-AC_2 a atteint 43,76 mg g^{-1}, tandis que AC_2' a atteint 62,37 mg g^{-1}. L'étude des isothermes d'adsorption a été réalisée à l'aide de plusieurs modèles (Langmuir, Freundlich, Temkin, Dubinin-Radushkevich et Redlich-Peterson), et l'étude cinétique a montré que l'adsorption suivait un modèle cinétique du pseudo-second ordre, confirmant de fortes interactions entre l'adsorbant et les polluants. Les études thermodynamiques ont révélé que l'adsorption du P-CPA était spontanée et endothermique pour les deux charbons activés, tandis que l'adsorption du Lin était exothermique pour AC_2' mais endothermique pour K-AC_2. Une étude de désorption a montré que K-AC_2 pouvait être régénéré avec un taux de désorption de 69,72%, démontrant son potentiel de réutilisation sur plusieurs cycles. Ces résultats soulignent que le charbon actif dérivé des cônes de pin, en particulier AC_2', est un matériau prometteur pour l'élimination des herbicides et le traitement durable des eaux usées.

Mots clés : Cône de Pine, charbon actif, porosité contrôlée, adsorption, eaux usées, acide para-chlorophénoxyacétique, Linuron.

ملخص

تتمحور هذه الدراسة حول تحضير الكربون النشط من مخاريط الصنوبر باستخدام التنشيط بهيدروكسيد البوتاسيوم (KOH)لإزالة المبيدات من المياه. تم مقارنة طريقتين للتنشيط: عملية من خطوة واحدة وأخرى من خطوتين. أظهرت النتائج أن التنشيط المكون من خطوتين أدى إلى إنتاج كربون نشط بخصائص مسامية أعلى وقدرة امتزاز أفضل. كانت أفضل المواد أداءً هي $K\text{-}AC_2$، المحضرة في فرن المفل، وAC_2'، المحضرة في فرن أنبوبي تحت غاز النيتروجين .حقق $K\text{-}AC_2$ مردودًا بنسبة 72,25%، ومساحة سطح BET بلغت 430,504 م²/غ، ورقم اليود 666,38 ملغ/غ، ورقم أزرق الميثيلين 72,77ملغ/غ، مما يشير إلى بنية ميكروية متطورة. في المقابل، أظهر AC_2' مساحة سطح ميكروية أعلى بلغت 1039,22م²/غ، ورقم اليود 888,51 ملغ/غ، ومردودًا بنسبة 72,57%، مما يجعله المادة الأكثر مسامية .أثبتت تجارب الامتزاز أن هذه الكربونات النشطة فعالة في إزالة مبيدات الأعشاب من المحاليل المائية. بالنسبة إلى حمض بارا-كلوروفينوكسيسيتيك (P-CPA) ، وصلت قدرة الامتزاز القصوى لـ $K\text{-}AC_2$ إلى 266,5 ملغ/غ، في حين أن AC_2'أظهر قدرة امتزاز أعلى بلغت 284,8 ملغ/غ .أما بالنسبة إلى مبيد اللينورون (Lin) ، فقد بلغ الامتزاز الأقصى 43,76ملغ/غ لـ $K\text{-}AC_2$، بينما حقق AC_2' قدرة امتزاز بلغت 62,37 ملغ/غ .تمت دراسة متساويات حرارة الامتزاز باستخدام عدة نماذج (لانغموير، فروندليش، تيمكين، دوبينين-رادوشكيفيتش، وريدليش-باترسون)، وأظهرت الدراسة الحركية أن الامتزاز اتبع نموذج الدرجة الثانية الكاذب، مما يؤكد وجود تفاعلات قوية بين المادة الممتزة والملوثات .كشفت الدراسات الديناميكية الحرارية أن امتزاز P-CPA كان تلقائيًا وماصًا للحرارة لكلا الكربونين النشطين، بينما كان امتزاز اللينورون طاردًا للحرارة لـ AC_2' ولكنه ماص للحرارة لـ $K\text{-}AC_2$. كما أظهرت دراسة إزالة الامتزاز أن $K\text{-}AC_2$يمكن تجديده بمعدل إزالة امتزاز بلغ 69,72%، مما يثبت إمكانية إعادة استخدامه في دورات متعددة .تؤكد هذه النتائج أن الكربون النشط المستخلص من مخاريط الصنوبر، وخاصة AC_2' ، هو مادة واعدة لإزالة مبيدات الأعشاب ومعالجة المياه العادمة بشكل مستدام.

الكلمات المفتاحية: مخروط الصنوبر, الكربون المنشط ,المسامية المتحكم فيها, الامتزاز, مياه الصرف الصحي، حمض بارا-كلوروفينوكسيسيتيك, لينورون.

Table of Contents

List of abbreviations

AC	Activated Carbon
TGA	Thermogravimetric Analysis
BET	Brunauer-Emmett-Teller (Surface Area Analysis Method)
XRD	X-ray Diffraction
SEM	Scanning Electron Microscopy
EDS	Energy Dispersive Spectroscopy
SEM-EDS	Scanning Electron Microscopy with Energy Dispersive Spectroscopy
FT-IR	Fourier Transform Infrared Spectroscopy
pH_{pzc}	pH at Point of Zero Charge
MB	Methylene Blue
KOH	Potassium Hydroxide
NaOH	Sodium Hydroxide
HCl	Hydrochloric Acid
PAAs	Phenoxyacetic Acids
CPA	Chlorophenoxyacetic Acid
P-CPA	Para-chlorophenoxyacetic Acid
Lin	Linuron
2.4-D	2.4-Dichlorophenoxyacetic Acid
2.4.5-T	2.4.5-Trichlorophenoxyacetic Acid
MCPA	4-Chloro-2-Methylphenoxyacetic Acid
IUPAC	International Union of Pure and Applied Chemistry

List of figures

Section A: Literature review

CHAPTER I: WASTEWATER TREATMENT BY ADSORPTION TECHNIQUE

CHAPTER II: ACTIVATED CARBON

CHAPTER III: PESTICIDES

Section B: Experimental procedure and findings

CHAPTER IV: MATERIALS AND METHODS

CHAPTER V: RESULTS AND DISCUSSION

V. 1. Part 1

V. 2. Part 2

V. 3. Part 3

List of tables

Section A: Literature review

CHAPTER I: WASTEWATER TREATMENT BY ADSORPTION TECHNIQUE

CHAPTER II: ACTIVATED CARBON

CHAPTER III: PESTICIDES

Section B: Experimental procedure and findings

CHAPTER IV: MATERIALS AND METHODS

CHAPTER V: RESULTS AND DISCUSSION

V. 1. Part 1

V. 2. Part 2

Introduction

Introduction

Water is essential for all living beings, playing a crucial role in growth, nutrition, and sanitation. The well-known phrase "water is life" reflects its importance for human survival and ecosystems. Despite covering about 70% of the Earth's surface, freshwater remains a limited and unevenly distributed resource [1]. In 2015, WHO and UNICEF estimated that approximately 844 million people worldwide still lack access to safe drinking water [2] due to rapid population growth and climate change [3].

Sustainable water management has become a major challenge as water resources face both quantity and quality issues. One of the biggest concerns is the overuse of freshwater. Increasing demand from agriculture, industry, and households depletes groundwater and surface water reserves, leading to shortages in many regions [4]. At the same time, pollution from human activities further reduces water quality [5]. Industrial, agricultural, and domestic waste releases chemicals, heavy metals, and nutrients into water bodies, making them unsafe for consumption and harming aquatic ecosystems [6]. Pollution also includes synthetic compounds such as dyes, fertilizers, pesticides [7], and persistent organic pollutants from waste incineration [8].

Climate change complicates these issues by changing rainfall patterns, intensifying droughts and floods, and distorting the natural water cycle. These changes increase water stress and affect resource management. Furthermore, competition for water availability can lead to geopolitical tensions, resulting in confrontations between countries, regions, or communities [9]. These difficulties require long-term water management techniques that maintain both availability and quality [10]. According to the global sustainable development goals, preserving freshwater resources is vital for the planet and its inhabitants [11].

Pesticides are widely used in agriculture to protect crops from pests, weeds, and plant diseases. They are classified into different types, including herbicides (used to kill weeds), insecticides (targeting insects), rodenticides (for rodents), and fungicides (controlling fungi). Among these, herbicides make up about 45% of pesticide use, while insecticides account for around 30%. Every year, approximately 3.5 million tons of pesticides are applied worldwide to increase agricultural productivity and ensure food security [12, 13]. However, despite their benefits, pesticides pose serious risks to both the environment and human health [14, 15]. Studies show that only about 0.1% of applied pesticides reach their intended targets, while the remaining 99.9% contaminate soil, water, and air. These chemicals can persist in ecosystems for long periods and

accumulate in living organisms through bioaccumulation, bioconcentration, and biomagnifications [16]. As a result, they enter the food chain and can cause harmful effects on wildlife and human health. Long-term exposure to pesticides has been linked to weakened immune systems, increased susceptibility to infections, and higher risks of cancer in both humans and animals [17].

Phenoxyacetic acids (PAAs) or chlorophenoxyacetic acids (CPAs), which include: 2,4-Dichlorophenoxyacetic acid (2,4-D), 4-Chloro-2-methylphenoxyacetic acid (MCPA)[18, 19], 2-(4-Chlorophenoxy)-2-methylpropionicacid (CFA or clofibric acid)[15], 2,4,5-Trichlorophenoxyacetic acid (2,4,5-T)[20], and p-chlorophenoxyacetic acid (p-CPA or 4-CPA)[18, 21], are herbicides that work by disrupting the growth of broadleaf weeds and dicotyledonous plants. However, they are resistant to biodegradation [22, 23], meaning they persist in the environment for a long time. This increases the risk of contamination in water and soil, making them dangerous to human health and wildlife. Studies have shown that exposure to PAAs can increase the risk of infectious diseases and cancer in mammals [17].

Linuron (3-(3,4-dichlorophenyl)-1-methoxy-1-methylurea) is a widely used herbicide, often called "killer grass" due to its strong ability to eliminate weeds. It works by blocking photosynthesis, preventing unwanted plants from growing and competing with crops like carrots, potatoes, soybeans, and cereals [24]. While it is effective in improving agricultural productivity, Linuron also poses significant environmental and health risks. This herbicide remains in soil and water for long periods, leading to contamination of rivers, lakes, and groundwater. When washed away by rain, it can harm aquatic plants and animals. Because it does not break down easily, Linuron can accumulate in the food chain, affecting non-target organisms, including mammals [25].

Exposure to Linuron can be harmful to humans and animals [26]. It may interfere with hormone function, potentially leading to reproductive and developmental problems [27]. Some studies suggest that long-term exposure increases the risk of certain diseases, including cancer. Due to these risks, the European Union has banned or restricted its use, while other countries continue to monitor its effects closely [28].

Due to the environmental and health hazards posed by pesticides and herbicides, finding effective removal methods is essential [29]. Various techniques have been developed [30], including chemical degradation, which uses chemical reactions to break down pesticides, biodegradation, which uses bacteria and microorganisms to naturally degrade pollutants. Electrochemical methods use anodic oxidation and indirect electrooxidation to destroy harmful chemicals [31].

Adsorption is another removal method that has attracted the most interest due to its efficiency, low cost, and ability to produce high-quality treated water [15, 18, 20, 32-35]. Activated carbon, particularly derived from lignocellulosic waste materials, has proven to be the most effective adsorbent for removing a wide range of organic and inorganic contaminants, including herbicides, from industrial wastewater [36]. This method offers a simple and energy-efficient solution for pesticide removal, making it one of the most widely used techniques for sustainable water treatment [37].

One of the main challenges in the development of activated carbon is controlling its porosity to optimize its performance for specific applications. The adsorption capacity and efficiency of activated carbon depend on its pore size distribution, which includes micropores, mesopores, and macropores [38]. However, achieving the right balance between these pores is complex, as it is influenced by several factors, such as the choice of precursor, activation method, carbonization conditions, and post-treatment modifications. Improper control of porosity can lead to low adsorption efficiency, structural instability, or limited application in pollutant removal [39, 40]. Therefore, a major research focus is on optimizing the preparation process to achieve well-controlled porosity, ensuring high-performance activated carbon for environmental and industrial applications [41, 42].

In this research, we selected pine cone as a raw material (PCP) to prepare activated carbon with controlled porosity. To achieve this, we conducted a series of activation experiments using both a muffle furnace and a tube furnace under a nitrogen atmosphere. We applied chemical activation using potassium hydroxide (KOH) as the activating agent. A comparative study was performed between one-step and two-step activation procedures, along with a parametric study by varying activation conditions to optimize porosity.

After preparation, the activated carbons were characterized using the BET method to determine surface area and porosity, SEM-EDS, X-ray Diffraction, FT-IR, as well as overall quality parameters such as iodine number, Methylene blue index, yield, and burn-off etc. Based on these analyses, we selected the two best-performing activated carbons, one from the muffle furnace and the other from the tube furnace, according to their superior porosity, textural, and structural properties. These selected activated carbons were used for the removal of para-chlorophenoxyacetic acid (P-CPA) and Linuron (Lin) from aqueous solutions.

Based on these research steps, and after a general introduction, our thesis is divided into two main sections:

Section A: provides a literature review consisting of three chapters:

- Chapter I: discusses wastewater treatment using the adsorption technique, highlighting its importance and effectiveness in removing pollutants.
- Chapter II: focuses on activated carbon, explaining its properties, preparation methods, and applications in adsorption.
- Chapter III: examines pesticides and herbicides, their environmental impact, and the challenges they pose in water contamination.

Section B: presents the experimental work and findings. It includes Chapters IV and V.

- Chapter IV: provides materials and methods, describing the activated carbons preparation protocols, characterization techniques, and adsorption experiments.
- Chapter V: includes results and discussions, analyzing the adsorption performance of activated carbon and evaluating its efficiency in removing para-chlorophenoxyacetic acid (P-CPA) and Linuron (Lin) herbicides.

Finally, a general conclusion and future perspectives are presented.

Introduction References

[1] C.T. Chekem, Matériaux carbonés multifonctionnels à porosité contrôlée à partir des ressources végétales tropicales : application au traitement de l'eau par photocatalyse. Thesis (2017).

[2] World Health Organization., Progress on Drinking Water, Sanitation and Hygiene/ Update and SDGBaselines:"ISBN978-92-4-151289-3",(2017).
https://apps.who.int/iris/bitstream/handle/10665/258617/9789241512893eng.pdfsequence=9789

[3] Q.I. Shafi, H. Ihsan, Y. Hao, X. Wu, N. Ullah, M. Younas, B. He, M. Rezakazemi, Multi-ionic electrolytes and E.coli removal from wastewater using chitosan-based in-situ mediated thin film composite nanofiltration membrane, J Environ Manage, 294 (2021).

[4] L. Jaber, S.N. Backer, T. Laoui, F. Abumadi, M.M.S. Koujan, K.A. Khalil, A. Shanableh, M.A. Atieh, Recent Trends in Surface Impregnation Techniques on Activated Carbon for Efficient Pollutant Removal from Wastewater, Desalination and Water Treatment, (2024).

[5] S. Khettaf, R. Boumaraf, F. Benmahdi, K.-E. Bouhidel, M. Bouhelassa, Removal of the Neutral Dissolved Organic Matter (NDOM) from Surface Water by Coagulation/Flocculation and Nanofiltration, Analytical Letters, 54 (2021).

[6] K. Kalsoom, Z.A. Khan, S. Khan, N. Muhammad, F. Jabeen, M. Ziad, A. Khan, Comparative adsorption of selected pesticides from aqueous solutions by activated carbon and biochar, AQUA—Water Infrastructure, Ecosystems and Society, (2024).

[7] M.T. Chafia, Synthèse et caractérisation des matériaux naturels et mésoporeux. Application à l'élimination des micropolluants, Thesis, (2016).

[8] S. Bhandari, Environmental Pollution Caused by Organic Pollutants, Their Harmful Impacts, and Treatment through a Microbiological Approach, in: Nano-phytoremediation and Environmental Pollution, CRC Press, (2024).

[9] A. CHAHMI GHEIDENE, Combinaison des procédés biologiques et chimiques pour la réduction de la charge polluante des lixiviats issus du CET de Mascara, Thesis, (2024).

[10] K.N. Palansooriya, Y. Yang, Y.F. Tsang, B. Sarkar, D. Hou, X. Cao, E. Meers, J. Rinklebe, K.-H. Kim, Y.S. Ok, Occurrence of contaminants in drinking water sources and the potential of biochar for water quality improvement: A review, Critical Reviews in Environmental Science and Technology, 50 (2019).

[11] S. Khettaf, I. Khouni, G. Louhichi, A. Ghrabi, L. Bousselmi, K.-E. Bouhidel, M. Bouhelassa, Optimization of coagulation–flocculation process in the treatment of surface water for a maximum dissolved organic matter removal using RSM approach, Water Supply, 21 (2021).

[12] M.M. Steingrímsdóttir, A. Petersen, P. Fantke, A screening framework for pesticide substitution in agriculture, Journal of Cleaner Production, 192 (2018).

[13] F. Huang, Z. Li, C. Zhang, T. Habumugisha, F. Liu, X. Luo, Pesticides in the typical agricultural groundwater in Songnen plain, northeast China: occurrence, spatial distribution and health risks, Environ Geochem Health, 41 (2019).

[14] S.G. Mohammad, S.M. Ahmed, Preparation of environmentally friendly activated carbon for removal of pesticide from aqueous media, International Journal of Industrial Chemistry, 8 (2017).

[15] A. Derylo-Marczewska, M. Blachnio, A.W. Marczewski, A. Swiatkowski, B. Buczek, Adsorption of chlorophenoxy pesticides on activated carbon with gradually removed external particle layers, Chemical Engineering Journal, 308 (2017).

[16] N. Ates, N. Uzal, U. Yetis, F.B. Dilek, Removal of pesticides from secondary treated urban wastewater by reverse osmosis, Environ Sci Pollut Res Int, 30 (2022).

[17] F.L. Martin, E.Z. Martinez, H. Stopper, S.B. Garcia, S.A. Uyemura, V. Kannen, Increased exposure to pesticides and colon cancer: Early evidence in Brazil, Chemosphere, 209 (2018).

[18] K. Kuśmierek, L. Dąbek, A. Świątkowski, Removal of phenoxy herbicides from aqueous solutions using lignite as a low-cost adsorbent, Desalination and Water Treatment, 260 (2022).

[19] K. Das, D. Majhi, Y.P. Bhoi, B.G. Mishra, Combustion synthesis, characterization and photocatalytic application of CuS/Bi4Ti3O12 p-n heterojunction materials towards efficient degradation of 2-methyl-4-chlorophenoxyacetic acid herbicide under visible light, Chemical Engineering Journal, 362 (2019).

[20] A. Naboulsi, L. El Mersly, H. Yazid, M. El Himri, S. Rafqah, M. El Haddad, Adsorption behaviors and mechanisms by theoretical study of herbicide 2,4,5-Trichlorophenoxyacetic on activated carbon as a new biosorbent material, Journal of the Taiwan Institute of Chemical Engineers, 142 (2023).

[21] B. Alimnazarov, Kh., Ashurov, J. M, Eshimbetov, A. G, Turaev, Kh. Kh, Ibragimov, B. T. Electronic structure of diaquabis(p-chlorophenoxyacetato) copper(II) complex by DFT method. ISJ Theoretical & Applied Science, 10 (102), (2021).

[22] S. L. Levine, C. J. Borgert, Review and recommendations on criteria to evaluate the relevance of pesticide interaction data for ecological risk assessments, Chemosphere, 209 (2018).

[23] A. Derylo-Marczewska, M. Blachnio, A.W. Marczewski, M. Seczkowska, B. Tarasiuk, Phenoxyacid pesticide adsorption on activated carbon - Equilibrium and kinetics, Chemosphere, 214 (2019).

[24] J. Singh, B. Singh, Agar-gelatin-derived hydrogel-based controlled delivery devices for linuron herbicide to prevent environmental hazards, Environmental Chemistry and Ecotoxicology, (2024).

[25] D. Chaara, F. Bruna, K. Draoui, M. Ulibarri, C. Barriga, I. Pavlovic, Study of key parameters affecting adsorption of the herbicide Linuron on organohydrotalcites, Applied clay science, 58 (2012).

[26] S. Maharaj, N. El Ahmadie, S. Rheingold, J. El Chehouri, L. Yang, C.L. Souders II, C.J. Martyniuk, Sub-lethal toxicity assessment of the phenylurea herbicide linuron in developing zebrafish (Danio rerio) embryo/larvae, Neurotoxicology and Teratology, 81 (2020).

[27] H. Ding, W. Zheng, H. Han, X. Hu, B. Hu, F. Wang, L. Su, H. Li, Y. Li, Reproductive toxicity of linuron following gestational exposure in rats and underlying mechanisms, Toxicology letters, 266 (2017).

[28] U.S.E.P. Agency, Prevention, Pesticides And Toxic Substances, in, March 1995.

[29] L.H. Mendoza-Huizar, Chemical reactivity of isoproturon, diuron, linuron, and chlorotoluron herbicides in aqueous phase: a theoretical quantum study employing global and local reactivity descriptors, Journal of Chemistry, (2015).

[30] A. Marican, E.F. Durán-Lara, A review on pesticide removal through different processes, Environmental Science and Pollution Research, 25 (2018).

[31] L. H. Mendoza-huizar, C.H. Rios-reyes, G.A. álvarez-romero, M.T. Ramírez-silva, M.E. Palomar-pardavé, Electrophilic and nucleophilic chemical reactivity of neutral and anionic forms of 4-CPA, 24D-CPA, 34-CPA and 245T-CPA through conceptual DFT reactivity descriptors., (2017)

[32] A. Niaz, K.A. Spokas, B. Gamiz, D. Mulla, K.R. Arshad, S. Hussain, 2-Methyl-4-chlorophenoxyacetic acid (MCPA) sorption and desorption as a function of biochar properties and pyrolysis temperature, PLoS One, 18 (2023).

[33] T.Y. Kim, Adsorption Behavior of p-chlorophenoxyacetic Acid on activated carbon (2004).

[34] R. Boumaraf, S. Khettaf, F. Benmahdi, R. Masmoudi, A. Ferhati, Removal of 2,4-dichlorophenoxyacetic acid from aqueous solutions by nanofiltration and activated carbon, Biomass Conversion and Biorefinery, (2024)

[35] H.K. Hue, L.V. Anh, D.B. Trong, Study of the adsorption of 2,4-dichlorophenoxyacetic acid from the aqueous solution onto activated carbon, Vietnam Journal of Chemistry, 56 (2018) 208-213.

[36] S. Attouti, B. Bestani, N Benderdouche, Chemical surface modification of seaweed species for cationin dyes removal from simulated water, Indian Journal of Environmental Protection, (2020).

[37] G. Asgari, H. Abdipour, A.M. Shadjou, A review of novel methods for Diuron removal from aqueous environments, Heliyon, 9 (2023).

[38] L.S. Blankenship, R. Mokaya, Modulating the porosity of carbons for improved adsorption of hydrogen, carbon dioxide, and methane: a review, Materials Advances, 3 (2022).

[39] K. Phothong, C. Tangsathitkulchai, P. Lawtae, The analysis of pore development and formation of surface functional groups in bamboo-based activated carbon during CO2 activation, Molecules, 26 (2021).

[40] R. Ruiz-Rosas, F.J. García-Mateos, M.d.C. Gutiérrez, J. Rodríguez-Mirasol, T. Cordero, About the role of porosity and surface chemistry of phosphorus-containing activated carbons in the removal of micropollutants, Frontiers in materials, 6 (2019).

[41] M.R. Haghbin, M.N. Shahrak, Process conditions optimization for the fabrication of highly porous activated carbon from date palm bark wastes for removing pollutants from water, Powder Technology, 377 (2021).

[42] M. Louarrat, G. Enaime, A. Baçaoui, A. Yaacoubi, J. Blin, L. Martin, Optimization of conditions for the preparation of activated carbon from olive stones for application in gold recovery, Journal of the Southern African Institute of Mining and Metallurgy, 119 (2019).

Section A

Literature review

CHAPTER I:

WASTEWATER TREATMENT BY ADSORPTION TECHNIQUE

Introduction

Wastewater treatment is essential to remove contaminants before water is released into the environment or reused. This process generally occurs in wastewater treatment plants, which vary in size and complexity according to the community's or industry's needs. Various treatment methods are applied, depending on the quality of raw water, intended end use, and required standards [1].

Adsorption is a widely used separation and purification technique that finds applications in petrochemicals, chemicals, pharmaceuticals, and environmental protection [2]. It is also extensively used for air and water purification, where contaminants adhere to the adsorbent surface, improving environmental quality [3]. This process relies on intermolecular forces, such as van der Waals forces, to attract molecules to the surface of the adsorbent without modifying their structure, enabling molecule recovery and adsorbent regeneration [4].

Understanding the mechanisms and properties of adsorption is essential for advancing technologies in science and industry. By analyzing adsorption kinetics and isotherms, we can determine the adsorbent's reaction mechanisms and textural characteristics, enabling us to optimize treatment approaches.

I.1. Adsorption phenomena

Adsorption is a physical and chemical process that describes how molecules from a liquid or gas phase attach to the surface of a solid known as the adsorbent [5]. Kayser introduced this term in 1881 to explain the transfer of molecules from an effluent to a solid surface [6]. Adsorption is important in chemistry and physics because it occurs when molecules, atoms, or ions of a substance (called adsorbates) adhere to surfaces in a generally reversible manner [7].

Unlike absorption, where molecules penetrate inside a material, adsorption occurs only at the surface. It represents the transition of substances from a dissolved state to an adsorbed state, while desorption is the reverse process. This phenomenon applies to all dissolved substances, whether electrically charged or not, and access to the adsorption surfaces occurs through diffusion in pores, which can limit both the rate and the amount of adsorption [8].

To better understand adsorption, three types of experimental data are used [9]:

- Adsorption isotherms, which show how many molecules are adsorbed at equilibrium,
- Kinetic studies, which measure how fast adsorption occurs,

- Characteristics of the adsorbed molecules, which are related to their chemical structure and ability to desorb.

I.2. Mechanism of the adsorption process

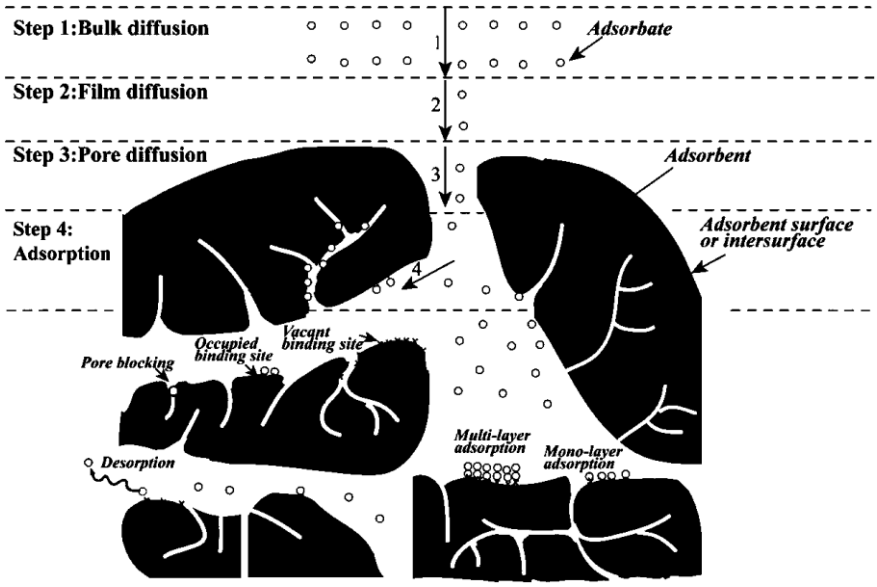

Figure I.1: Solute transfer steps during adsorption onto a microporous material

Adsorption involves the transfer of a solute from the liquid phase to a solid called the adsorbent. This process occurs in four main stages [10, 11]:

1. **Step 1** Transfer to the liquid film: The molecule is transported to the interface between the liquid and adsorbent (extra granular or bulk diffusion). The solute moves from the liquid phase to the liquid film surrounding the adsorbent through diffusion, driven by a concentration gradient.
2. **Step 2** Diffusion through the liquid film: Movement within the boundary layer near the substrate (external film diffusion). The solute diffuses through the liquid film to reach the surface of the adsorbent, moving through larger pores known as macropores and mesopores.
3. **Step 3** Diffusion into micropores: Diffusion within the pores (internal or pore diffusion). The solute travels toward the adsorbent's micropores, influenced by a concentration gradient, both in the free and bound states on the adsorbent surface.
4. **Step 4** Adsorption: The solute adheres to the adsorbent's internal surface via physicochemical interactions. It initially occupies the most active sites. The micropores fill up until a saturation point, after which multilayer adsorption can continue.

I.3. Factors affecting the adsorption process

Several main factors influence the equilibrium between an adsorbent and an adsorbate in adsorption processes:

a. Adsorbate Characteristics

- **Molecular size**: The molecule size should be smaller than the adsorbent pore size for efficient adsorption to ensure rapid diffusion. Activated carbon, a microporous adsorbent, is especially effective for smaller molecules.
- **Solubility**: According to Lun Delius's rule, less soluble compounds are generally adsorbed more effectively. This principle aligns with observed relationships between adsorption constants and molecular properties.
- **Polarity and polarizability**: The adsorption behavior is influenced by the molecule's surface area, volume, and functional groups, as well as its polarity. Polar molecules tend to have a higher affinity for polar adsorbents.
- **Molecular orientation**: The orientation of molecules on the adsorbent surface is determined by molecular interactions with the surface, although it can be complex to predict accurately.

b. Adsorbent characteristics

- **Surface area**: Adsorption is proportional to the adsorbent's accessible surface area; however, pore dimensions also play a role, as large molecules cannot enter smaller pores. Increasing surface area through grinding can enhance adsorption.
- **Pore size distribution**: A suitable pore size distribution is necessary to accommodate the adsorbate. Chemical activation can expand pore size, improving access for larger adsorbates.
- **Functional groups and pH_{pzc}**: The surface chemistry, including functional groups and pH at the point of zero charge (pH_{pzc}), is critical in determining adsorption capacity by affecting interactions with the adsorbate [11].

c. Physical parameters [12]

- **Contact time**: It plays a crucial role in the adsorption process, as it directly influences adsorption kinetics and, consequently, the economic efficiency of the process. Thus, optimizing contact time is essential for achieving high performance in adsorption.
- **Adsorbent dose**: Generally, increasing the adsorbent dose enhances the adsorption of a solute due to the higher number of active adsorption sites. However, beyond a certain point,

the adsorption efficiency per unit weight of adsorbent may decrease. This is often due to interference from interactions between the adsorbent's active sites at higher concentrations.

- **pH**: pH is a critical factor in the adsorption process, and has a significant influence on adsorption, as it can affect the structure and charge of both adsorbent and adsorbate. Adjusting the pH can significantly influence adsorption efficiency and capacity.
- **Temperature**: Physical adsorption generally occurs at lower temperatures, while chemisorption can increase with temperature up to a certain point before declining.

I.4. Adsorption types

Adsorption can be classified into two types based on the underlying mechanisms: physical adsorption, or physisorption, and chemical adsorption, or chemisorption. Adsorbent/adsorbate interactions are often electrostatic, making them weak and reversible, which is characteristic of physisorption. In contrast, chemisorption is generally an irreversible process that involves the formation of a covalent bond between the adsorbate and the adsorbent [13].

I.4.1. Physical adsorption (physisorption)

It involves a weak intermolecular interaction that occurs due to fluctuations in electronic charge and molecular polarization. The van der Waals forces responsible for physical adsorption mainly include[14]:

- **London dispersion forces**: These forces arise from temporary fluctuations in the electronic distribution of atoms and molecules, creating attractive interactions between regions of temporary positive and negative charge.
- **Dipole-dipole forces**: These forces occur when molecules have permanent dipole moments and interact due to their mutual orientation.
- **Hydrogen bonding (in certain cases)**: Although weaker than covalent bonds, hydrogen bonding can also contribute to physical adsorption when functional groups capable of forming hydrogen bonds are present on the adsorbent surface.

Physical adsorption is generally reversible, meaning that adsorbate molecules can be released from the adsorbent surface by changing environmental conditions, such as temperature or pressure variations [15]. There is no chemical modification of the adsorbed molecules, which can form multiple layers. The adsorption energy is low, typically below 20 kJ/mol [16]. Physical adsorption is commonly observed in applications such as gas physisorption on activated carbons, the formation

of thin films on solid surfaces, the separation of chemical compounds by chromatography, and various fields in chemistry and materials science [17].

I.4.2. Chemical adsorption (chemisorption)

Unlike physical adsorption, which relies on weaker intermolecular forces like van der Waals forces, chemisorption involves the formation of chemical bonds, such as covalent or ionic bonds, between the adsorbate and the adsorbent [18]. This process is typically slow, irreversible, and results in an alteration of the adsorbed molecules, forming a monolayer. The adsorption energy is relatively high, usually ranging from 20 to 200 kJ mol^{-1} [19].

Key characteristics of chemisorption include:

- **Chemical bonds**: Adsorbate molecules bond to active sites on the adsorbent surface through strong, specific chemical bonds. These bonds can be covalent, ionic, or other types.
- **Irreversibility**: Unlike physical adsorption, chemisorption is generally harder to reverse. Desorption of the adsorbate molecules often requires significant energy changes, such as a substantial shift in temperature or pH.
- **Selectivity**: Chemisorption can be highly selective depending on the nature of the chemical bonds formed between the adsorbate and the adsorbent. This selectivity allows certain compounds to be adsorbed while others are excluded based on their chemical affinity with the adsorbent.
- **Potential for chemical reactions**: In some cases, chemisorption can lead to additional chemical reactions between the adsorbate molecules and the adsorbent, which has applications in catalysis and surface modification.

Chemisorption is widely used in various applications, including industrial chemistry, gas separation, heterogeneous catalysis, water purification, and selective adsorption of chemical compounds. It plays a crucial role in numerous industrial processes and is fundamental to many areas of research in chemistry and materials science [20].

I.5. Adsorption isotherms

Adsorption isotherms provide a valuable representation of the relationship between the concentration of the adsorbate (C_e) in the liquid or gas phase and the amount adsorbed (q_e) at the solid-liquid or solid-gas interface at a given temperature. These are non-kinetic relationships expressed as $q_e = f(C_e)$, termed as isotherms. The adsorbed quantity can be calculated using the following equation:

$$qe = \frac{C_o - C_e}{1000 \times m} \times V \qquad (1)$$

Where:

- V is the volume of solution (mL),

- m is the mass of adsorbent (g),

- C_0 is the initial concentration of adsorbate,

- C_e is the equilibrium concentration of adsorbate.

Many researchers have proposed models to describe the relationship between the adsorbed quantity at equilibrium, these isotherms are essential for understanding and characterizing interactions between the adsorbent and adsorbate, as well as for evaluating the efficiency of adsorbent materials in various applications. By examining different types of isotherms, such as the Langmuir isotherm, the Freundlich isotherm, the Temkin isotherm, and other models, we can obtain insights into the adsorption capacity, specific surface area, and other key properties of adsorbent materials[21].

I.5.1. Adsorption isotherms classification

I.5.1.1. BET classification

In 1940, Brunauer, Emmett, and Teller introduced six types of isotherm classifications, with illustrations that highlight each form [22]. The shape of these curves enables the development of hypotheses about the underlying mechanisms, including whether adsorption occurs in monolayers or multiple layers, and whether interactions exist among adsorbed molecules.

- **Type I:** Also known as Langmuir isotherm, is characterized by monomolecular adsorption on homogeneous and uniform adsorption sites. The adsorbed quantity increases rapidly with pressure or concentration until reaching saturation.

- **Type II:** Commonly associated with the Freundlich model, represents multilayer adsorption on a heterogeneous surface. The adsorbed quantity gradually increases with pressure or concentration without reaching a definite saturation.
- **Type III:** Reflects mixed isotherms, where initial multilayer adsorption is followed by monolayer adsorption at higher concentrations or pressures.
- **Type IV:** This isotherm, often associated with porous materials, shows multilayer adsorption, beginning with an initial multilayer phase followed by monolayer adsorption, and then a gradual increase in the adsorbed layer.
- **Type V:** Indicates initial multilayer adsorption followed by monolayer adsorption, similar to Type IV, but with a slower increase in the adsorbed layer at higher concentrations or pressures.
- **Type VI:** Characterized by distinct steps, each indicating the successive formation of adsorbed layers on the surface of the adsorbent.

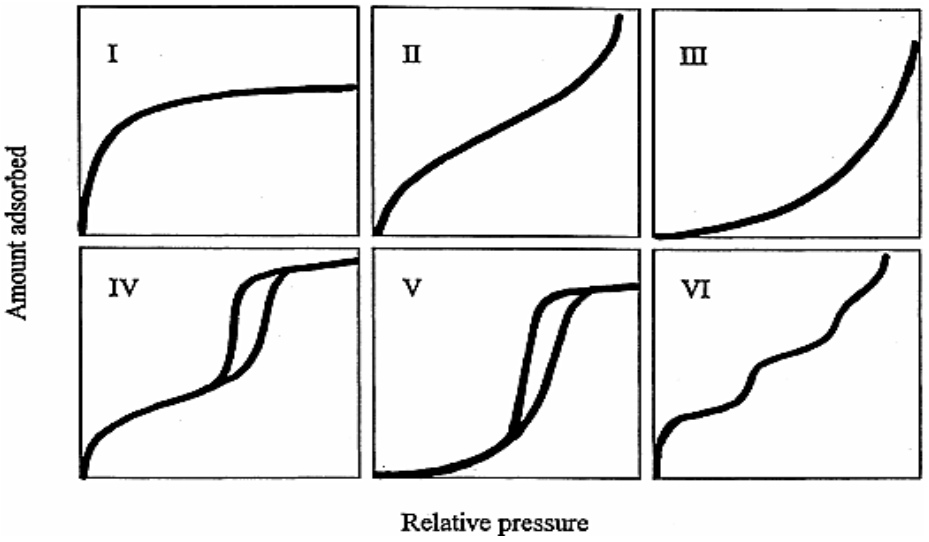

Figure I.2: BET isotherm classification

I.5.1.2. Classification of adsorption/desorption hysteresis loops

The H_1 and H_2 hysteresis loops appear in type IV isotherms showing a saturation level and typically indicate mesoporous adsorbents. The H_1 loop has almost vertical, parallel adsorption and desorption lines, often found in adsorbents with a very uniform mesopore size. The H_2 loop occurs with adsorbents that have interconnected mesopores.

Hysteresis loops H_3 and H_4 appear in Type II isotherms, which do not have a saturation point. In these cases, the desorption line may vary and often depends on the highest amount adsorbed at relative pressures close to 1. The H_3 loop, observed in adsorbents that form aggregates, is due to

capillary condensation in a flexible structure and does not represent a specific mesopore size. The H_4 loop is common with microporous adsorbents, where layers are loosely connected, allowing capillary condensation between them [23].

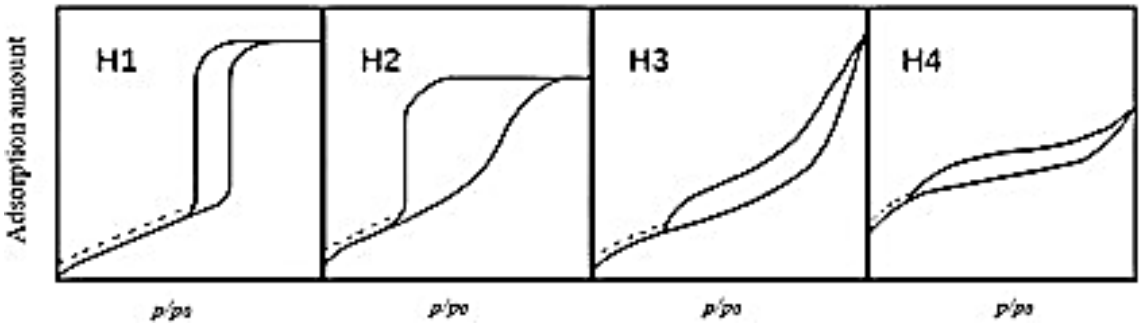

Figure I.3: Classification of adsorption/desorption hysteresis loops (IUPAC, 1985)

I.5.1.3. Giles classification

When an adsorbate comes into contact with a solute, a thermodynamic equilibrium is established between the adsorbed molecules and those remaining in the liquid phase. The adsorption equilibrium isotherm represents the number of molecules adsorbed per mass unit of adsorbent as a function of the concentration of the same molecule in the liquid phase when the system reaches equilibrium [24]. The shape of this curve provides insights into the mechanisms involved in adsorption.

There are various ways to classify adsorption equilibrium isotherms. Giles et al. (1974) identified four types in the context of liquid-phase molecule adsorption [25].

• **Type L** isotherm is characteristic of microporous adsorbents and reflects a strong affinity between the adsorbate and adsorbent.

• **Type S** isotherm corresponds to solids with heterogeneous porosity and suggests competitive adsorption, with interactions occurring between adsorbate-adsorbate and adsorbate-adsorbent.

• **Type H** isotherm is an extreme case of the Type L isotherm and indicates a very high affinity between the adsorbate and adsorbent.

• **Type C** or linear isotherm, represents a linear solute distribution between the solid and liquid phases (often used to remove organic micropollutants).

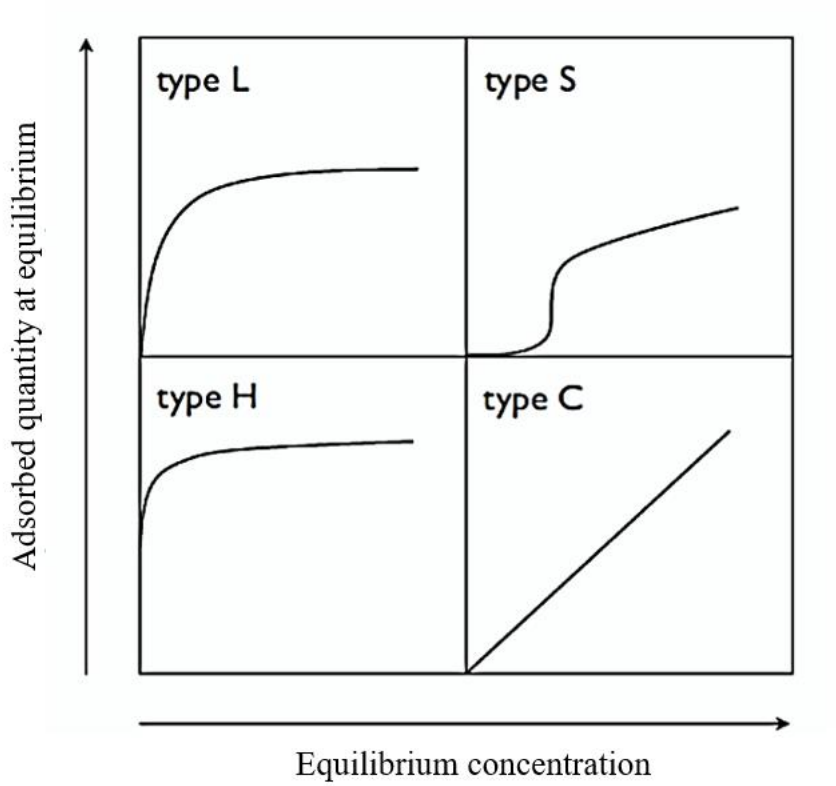

Figure I.4: Different types of liquid-phase adsorption equilibrium isotherms [26]

I.5.2. Modeling of adsorption isotherms

Isotherm adsorption modeling offers important data about the adsorption mechanism, adsorbent-adsorbate affinity, and adsorption type. It also describes the amount of adsorbate present on the adsorbent as a function of the amount of adsorbate left in the solution [27] when equilibrium is reached (between the two phases) at a certain temperature.

I.5.2.1. Langmuir isotherm model

Langmuir isotherm is an empirical model that considers the adsorbed layer thickness as one molecule (monolayer adsorption) and that the adsorption process happens in similar and equal localized locations [28]. The separation factor R_L (equation 2) is a dimensionless constant that expresses the crucial properties of the Langmuir isotherm [29]. The adsorption process is unfavorable when $R_L > 1$, it is linear when $R_L = 1$, favorable when $0 < R_L < 1$, and irreversible when $R_L = 0$ [30].

$$qe = \frac{q_m * K_L * Ce}{1 + (K_L * Ce)} \quad (2)$$

$$R_L = 1/1 + K_L * C_0 \quad (3)$$

q_e: adsorption capacity in the equilibrium (mg. g^{-1}), q_m: maximum adsorption capacity (mg. g^{-1})

K_L: Langmuir constant (mg. g^{-1}), C_e: equilibrium concentration (mg. L^{-1}), R_L: separation factor

I.5.2.2. Freundlich isotherm model

Unlike the Langmuir isotherm, the Freundlich isotherm describes multi-layer adsorption on a heterogeneous surface [31]. This isotherm is characterized by a continuous increase in adsorbed amount as pressure or concentration rises, without reaching a clear saturation point. The equation representing the Freundlich model is as follows [32]:

$$q_e = K_F\, Ce^{1/n} \qquad (4)$$

where K_F is the Freundlich constant or adsorption capacity ((mg. L^{-1})^n. (mg. g^{-1})) and n is a constant related to adsorption intensity/relative distribution of energy and the heterogeneity of adsorbate sites

I.5.2.3. Temkin isotherm model

Temkin assumes that the decrease in adsorption heat with increased surface coverage is not logarithmic, as in systems leading to the Freundlich equation, but rather linear, especially at medium and low coverage levels. This linearity may be due to:

- Repulsion between adsorbed species on a uniform surface,
- Surface heterogeneity [33].

The Temkin isotherm model is generally applied in the following form:

$$qe = B_T \ln (K_T * Ce) \qquad (5)$$

$$B_T = \frac{RT}{b} \qquad (6)$$

where B_T is the retention capacity at equilibrium, K_T is the Temkin constant, R is the ideal gas constant (8.314 J. mol^{-1}. K^{-1}), T is the absolute temperature (K), and b is a constant related to the heat of sorption in (J. mol^{-1}).

I.5.2.4. Dubinin-Radushkevich (D-R) model

It is an empirical adsorption simulation that is commonly used to represent adsorption mechanisms on heterogeneous surfaces with Gaussian energy distribution. It adopts a multilayer nature with van der Waals forces, pertinent to physical adsorption processes [30, 34]. the adsorption potential for

this model is variable and the free enthalpy of adsorption is linked to the recovery rate [35]. It is assumed that the adsorption energy is independent of temperature and depends on the nature of the adsorbate/adsorbent pair. It is used to estimate the type of adsorption: if the value of E is between 8-16 kJ mol^{-1}, the adsorption process is chemical, and if E < 8 kJ mol^{-1}, it is physical [29, 35].

$$q_e = q_{mD-R} \times \exp(-\beta\, \varepsilon^2) \quad (7)$$

$$\varepsilon = R \times T \times \ln\left(1 + \frac{1}{Ce}\right) \quad (8)$$

$$E = \frac{1}{\sqrt{2\times\beta}} \quad (9)$$

where q_{mD-R} is the maximum adsorption capacity (mg. g^{-1}), β: activity coefficient relative to adsorption energy (mol^2. J^{-2}), ε: the potential of Polanyi, and E: adsorption energy E (kj. mol^{-1}).

I.5.2.5. Redlich-Peterson isotherm model

It is the most widely cited and used three-parameter model in the literature [36-38] because it can be applied over a wide concentration range, in either homogenous or heterogeneous systems, therefore, it is versatile. The empirical equation developed by Redlich-Peterson incorporates three parameters to improve the fit of the Langmuir and Freundlich equation [35], being a compromise between the Freundlich and Langmuir models; this model approaches the Freundlich model for high concentrations, and the Langmuir equation for low concentrations and has the benefit of approaching the Henry region at infinite dilution. the mechanism of adsorption is a mix and does not follow ideal monolayer adsorption [30, 35].

$$qe = \frac{a_{r-p} * Ce}{1 + K_{r-p} * Ce^{\beta}} \quad (10)$$

where a_{r-p} is the constant of Redlich-Peterson isotherm (L. g^{-1}), K_{r-p} is a constant (L. mg^{-1}) and β is a heterogeneity parameter (mol^2. J^{-2}).

I.6. Adsorption kinetics

Adsorption kinetics examines the rate at which molecules or ions are attached to the surface of a solid or liquid material [39], focusing on the mechanisms and factors that influence the speed of this process, which is essential for understanding and optimizing adsorption applications [40]. Kinetic studies are a key element in this field, as they provide valuable information on the adsorption mechanism [41], determine the adsorption rate, and calculate the maximum adsorption capacity [42]. The major elements of adsorption kinetics are as follows:

- **Adsorption rate**: This is the speed at which molecules or ions are retained on the surface of the adsorbent material. This rate can vary depending on factors like the concentration of the substances to be adsorbed, the nature of the adsorbent material, the temperature, etc.
- **Adsorption equilibrium**: Adsorption kinetics often focuses on reaching adsorption equilibrium, the point at which the adsorption rate matches the desorption rate, with no significant change in the adsorption level. The time required to reach this equilibrium depends on the characteristics of the adsorption system.
- **Temperature effect**: Temperature has a significant impact on adsorption kinetics. Generally, an increase in temperature speeds up adsorption by raising the kinetic energy of the molecules and enhancing interactions with the material's surface.
- **Diffusion**: The diffusion of molecules to be adsorbed through the liquid or gas phase to the adsorbent surface is often a limiting factor in adsorption kinetics. Diffusion can be influenced by factors like the pore size of the adsorbent material and the viscosity of the medium, among others.
- **Kinetic models**: Various kinetic models describe adsorption kinetics across different systems, including Lagergren's pseudo-first and pseudo-second-order models that are applied to comprehend adsorption kinetics. In contrast, the intraparticle diffusion model proposed by **Weber–Morris** can be used to clarify diffusion mechanisms during adsorption [43, 44].

I.6.1. Adsorption kinetic models

The study of adsorption kinetic models is important for understanding and optimizing adsorption processes.

I.6.1.1. Pseudo-first order model

The pseudo-first-order model is one of the simplest and most widely used kinetic models to describe adsorption kinetics. It is based on the assumption that the adsorption rate is proportional to the difference between the initial adsorption capacity and the amount of adsorbate at a given time.

I.6.1.2. Pseudo-second order model

The pseudo-second-order model is another widely used kinetic model for describing adsorption kinetics. Unlike the pseudo-first-order model, this model assumes surface-dependent adsorption kinetics, with a rate that decreases over time [45].

I.6.1.3. Intraparticle diffusion model

The intra-particle diffusion model, also known as the Weber and Morris model, posits that diffusion is the dominant rate-limiting step in adsorption, Thus, it is the slowest phase governing the adsorption process [46].

Table I.1 summaries the equations of each model

Table I.1: Kinetic model equations

Kinetic Models	Nonlinear Equation	Linear Equation
Pseudo first order	$q_t = q_e(1 - e^{K_1 t})$	$\ln(q_e - q_t) = \ln q_e - K_1 t$
Pseudo second order	$q_t = \frac{{q_e}^2 K_2 t}{1 + q_t K_2 t}$	$\frac{t}{q_t} = \frac{1}{K_2 {q_e}^2} + \frac{1}{q_e} t$
Intraparticle diffusion	$q_t = K_{id} t^{1/2} + C$	$q_t = K_{id} t^{1/2} + C$

- Where qe is the quantity of herbicide adsorbed at equilibrium time (mg g^{-1}), qt is the amount of herbicide adsorbed at time t (mg g^{-1}), and k_1 is the pseudo-first-order rate constant (min^{-1}). qe and k_1 are calculated by plotting $\ln(q_e-q_t)$ as a function of time, applying the nonlinear regression,
- k_2 is the pseudo-second-order rate constant (g mg^{-1} min^{-1}), which is calculated using qe from the plot of t/qt as a function of t, applying the nonlinear equation,
- The y-intercept (C) and intra-particle diffusion rate constant (K_{id}) can be obtained by plotting q_t as a function of $t^{1/2}$, in the nonlinear form.

I.6.2. Analysis by error functions

In the field of adsorption, the use of error measurements can be highly relevant for assessing the goodness of fit of isotherm and adsorption kinetic models [47]. The root-mean-square error (RMSE), the chi-square statistic (χ^2), and the average percentage error (APE) are the most used error analyses in research papers. The RMSE quantifies the difference between observed and predicted values, while the χ^2 test assesses the fit between observed and theoretical distributions. A lower RMSE indicates a better model fit to the data, whereas a higher χ^2 can suggest a poor alignment between the model's predictions and observations. By using these metrics, one can choose the most suitable model and refine adsorption process predictions. The equations are shown in Table I.2.

Table I.2: Error functions equations [48, 49]

Error function	Equation
χ^2	$\sum \frac{(qe.exp - qe.cal)\text{^}2}{qe.cal}$
RMSE	$\sqrt{(\frac{1}{N-2})\sum_{1}^{N}(qe.exp - qe.cal)\text{^}2}$
APE	$\left(\sum_{1}^{N}(\frac{(\lvert qe.exp - qe.cal\rvert / qe.exp)}{N})\right) x\ 100$

qe.exp and qe.cal is experimental and calculates adsorption capacities respectively

N is the number of observations in the experimental data

I.7 Adsorption thermodynamic parameters

Adsorption is generally an exothermic process that releases heat, causing the solid to warm up and reducing adsorbed amounts [50]. Temperature variations are often significant in industrial adsorption processes and can be one of the main factors leading to performance degradation [51].

Thermodynamic studies are useful for determining the Gibbs free energy change (ΔG°), which is a function of the equilibrium adsorption constant of the isotherm fit (K_d) (the equilibrium constant), enthalpy change (ΔH°) that provides the type of thermal process associated with

adsorption [52], and entropy change (ΔS°) that indicates the degree of overall unrest at the liquid/solid interface during the adsorption process. These thermodynamic parameters can be determined following an experimental study of the influence of temperature on the adsorption process [53] and can be calculated from van't Hoff equations [54] :

$$\Delta G° = \Delta H° - T\Delta S° \quad (11)$$

$$\Delta G° = -RTLn(K_d) \quad (12)$$

where T is the absolute temperature (Kelvin), R is the universal gas constant (8.314 J mol^{-1} K^{-1}.), C_s (mg. L^{-1}) is the amount of herbicide adsorbed on adsorbent per liter of solution at equilibrium ($C_s = C_o - C_e$), C_o is the initial concentration (mg. L^{-1}), C_e is the equilibrium concentration (mg. L^{-1}), and $K_d = \frac{C_s}{C_e}$ called the distribution coefficient.

The distribution coefficient is a specific case of the Langmuir relationship, defined for adsorbed species at low concentrations. It is defined as the ratio of the amount adsorbed per gram of solid to the remaining solute per solution volume. The distribution coefficient characterizes the solute's affinity for the adsorbent and can be expressed by linking the formulas (10) and (11):

$$\ln(K_d) = \frac{-\Delta H°}{R}\left(\frac{1}{T}\right) + \frac{\Delta S°}{R} \quad (13)$$

Plotting ln K_d as a function of 1/T, which results in a straight line, allows the determination of the thermodynamic parameters ΔH° and ΔS° from the intercept and slope. For adsorption to be effective, the free energy must be negative. The negative ΔG° values demonstrate the spontaneous and thermodynamically favorable adsorption. Moreover, the decrease in the negative values of ΔG° with temperature indicates that adsorption is more advantageous at higher temperatures [55].

A positive enthalpy value indicates that the process is endothermic, and a high value suggests that the behavior is of a chemical nature (chemisorption). If it ranges between 20 and 80 kJ mol^{-1}, or less than 40 kj. mol^{-1}, the process is physical [56]. The positive value of ΔS^{o} indicates an increase in the randomness at the adsorbent/adsorbate interface during the adsorption process. In addition, a positive value gives an idea about the existing affinity of the prepared activated carbon towards pollutants.

References of Chapter I

[1] G. K. C. Ding, Wastewater treatment and reuse-The future source of water supply, Encyclopedia of sustainable technologies, (2017).
[2] M. S. Reza, C.S. Yun, S. Afroze, N. Radenahmad, M.S.A. Bakar, R. Saidur, J. Taweekun, A.K. Azad, Preparation of activated carbon from biomass and it's applications in water and gas purification, a review, Arab Journal of Basic and Applied Sciences, 27 (2020).
[3] A. Saravanan, P.S. Kumar, S. Jeevanantham, S. Karishma, B. Tajsabreen, P. Yaashikaa, B. Reshma, Effective water/wastewater treatment methodologies for toxic pollutants removal: Processes and applications towards sustainable development, Chemosphere, 280 (2021).
[4] N. E. Hira, S.S.M. Lock, N.F. Shoparwe, I.S.M. Lock, L.G. Lim, C.L. Yiin, Y.H. Chan, M. Hassam, Review of adsorption studies for contaminant removal from wastewater using molecular simulation, Sustainability, 15 (2023).
[5] M. Alaqarbeh, Adsorption phenomena: definition, mechanisms, and adsorption types: short review, RHAZES: Green and Applied Chemistry, 13 (2021).
[6] Amrutha, G. Jeppu, C. Girish, B. Prabhu, K. Mayer, Multi-component adsorption isotherms: review and modeling studies, Environmental Processes, 10 (2023).
[7] D.V. Shah, Role of Absorption and Adsorption in the Removal of Waste, in: Emerging trends in environmental biotechnology, CRC Press, (2022).
[8] A.S. Pundir, K. Singh, S. Rajoriya, Agricultural Waste, Utilization of Waste Biomass in Energy, Environment and Catalysis, (2022).
[9] S. Attouti, Activation de deux algues méditerranéennes par diverses méthodes pour l'élimination de colorants, Thesis 2013.
[10] E. SOGBOCHI, Elaboration par voies thermochimiques de charbons actifs dérivés de coproduits de Lophira lanceolata : essais d'adsorption de micropolluants de l'eau, Thesis, (2023).
[11] Z. Bahnes, Activation des noyaux de jujube pour l'obtention d'un charbon actif, Thesis, (2018).
[12] S. Iftekhar, D.L. Ramasamy, V. Srivastava, M.B. Asif, M. Sillanpää, Understanding the factors affecting the adsorption of Lanthanum using different adsorbents: a critical review, Chemosphere, 204 (2018).
[13] N. M. Aljamali, R. Khdur, I.O. Alfatlawi, Physical and chemical adsorption and its applications, International Journal of Thermodynamics and Chemical Kinetics, 7 (2021).
[14] J. Hermann, R.A. DiStasio Jr, A. Tkatchenko, First-principles models for van der Waals interactions in molecules and materials: Concepts, theory, and applications, Chemical Reviews, 117 (2017).
[15] O. H. Gunawardene, C.A. Gunathilake, K. Vikrant, S.M. Amaraweera, Carbon Dioxide capture through physical and chemical adsorption using porous carbon materials: A review, Atmosphere, 13 (2022).
[16] L. Ding, B. Zou, W. Gao, Q. Liu, Z. Wang, Y. Guo, X. Wang, Y. Liu, Adsorption of Rhodamine-B from aqueous solution using treated rice husk-based activated carbon, Colloids and Surfaces A: Physicochemical and Engineering Aspects, 446 (2014).
[17] A. A. Abd, S. Z. Naji, A.S. Hashim, M.R. Othman, Carbon dioxide removal through physical adsorption using carbonaceous and non-carbonaceous adsorbents: a review, Journal of Environmental Chemical Engineering, 8 (2020).
[18] A. S. Dobrota, I.A. Pašti, Chemisorption as the essential step in electrochemical energy conversion, Journal of Electrochemical Science and Engineering, 10 (2020).

[19] A. Gil, Classical and new insights into the methodology for characterizing adsorbents and metal catalysts by chemical adsorption, Catalysis Today, 423 (2023).
[20] B. K. Nesrine, Elaboration et caractérisation d'un matériau hybride pour le traitement des eaux usées, Thesis, (2024).

[21] X. Xing, N.S. Alharbi, X. Ren, C. Chen, A comprehensive review on emerging natural and tailored materials for chromium-contaminated water treatment and environmental remediation, Journal of Environmental Chemical Engineering, 10 (2022).
[22] V. J. Inglezakis, S.G. Poulopoulos, H. Kazemian, Insights into the S-shaped sorption isotherms and their dimensionless forms, Microporous and Mesoporous Materials, 272 (2018).
[23] M. S. Mel'gunov, Application of the simple Bayesian classifier for the N2 (77 K) adsorption/desorption hysteresis loop recognition, Adsorption, 29 (2023).
[24] R. Saadi, Z. Saadi, R. Fazaeli, N.E. Fard, Monolayer and multilayer adsorption isotherm models for sorption from aqueous media, Korean Journal of Chemical Engineering, 32 (2015).
[25] G. Alberti, V. Amendola, M. Pesavento, R. Biesuz, Beyond the synthesis of novel solid phases: review on modelling of sorption phenomena, Coordination Chemistry Reviews, 256 (2012).
[26] R. Guillossou, Élimination des micropolluants organiques dans les eaux résiduaires urbaines par adsorption sur charbon actif: compréhension des processus et implications opérationnelles, (2021).
[27] R. Boumaraf, S. Khettaf, F. Benmahdi, R. Masmoudi, A. Ferhati, Removal of 2,4-dichlorophenoxyacetic acid from aqueous solutions by nanofiltration and activated carbon, Biomass Conversion and Biorefinery, (2022).
[28] M. A. Al-Ghouti, D.A. Da'ana, Guidelines for the use and interpretation of adsorption isotherm models: A review, J Hazard Mater, 393 (2020).
[29] H. N. Otheman Amrahr, Mohammed S. Elyoubi, Application of nonlinear regression analysis to select the optimum absorption isotherm for Methylene Blue adsorption onto Natural Illitic Clay, (2015).
[30] N. Ayawei, A.N. Ebelegi, D. Wankasi, Modelling and Interpretation of Adsorption Isotherms, Journal of Chemistry, 2017 (2017).
[31] Y. Cai, B. Tang, L. Bin, S. Huang, P. Li, F. Fu, Constructing a multi-layer adsorbent for controllably selective adsorption of various ionic dyes from aqueous solution by simply adjusting pH, Chemical Engineering Journal, 382 (2020).
[32] B. O. Isiuku, P.C. Okonkwo, C.D. Emeagwara, Batch adsorption isotherm models applied in single and multicomponent adsorption systems–a review, Journal of Dispersion Science and Technology, 42 (2021) .
[33] N. Douara, Adsorption de composés phénoliques par un déchet traité chimiquement, Thesis, (2015).
[34] Y. Vieira, C. Schnorr, A.C. Piazzi, M.S. Netto, W.M. Piccini, D.S. Franco, E.S. Mallmann, J. Georgin, L.F. Silva, G.L. Dotto, An advanced combination of density functional theory simulations and statistical physics modeling in the unveiling and prediction of adsorption mechanisms of 2, 4-D pesticide to activated carbon, Journal of Molecular Liquids, 361 (2022).
[35] B. SALIM, Etude de la dégradation photocatalytique et de l'adsorption du Phénol sur TiO2 P25. Influence de la présence des métaux lourds et des ultrasons, Thesis, (2012).

[36] C. R. Girish, Various isotherm models for multicomponent adsorption: A review, International Journal of Civil Engineering and Technology (2017).
[37] K. V. Kumar, K. Porkodi, Relation between some two- and three-parameter isotherm models for the sorption of methylene blue onto lemon peel, J Hazard Mater, 138 (2006).
[38] F. C. Wu, B.-L. Liu, K.-T. Wu, R.-L. Tseng, A new linear form analysis of Redlich–Peterson isotherm equation for the adsorptions of dyes, Chemical Engineering Journal, 162 (2010).
[39] J. Wang, X. Guo, Adsorption kinetic models: Physical meanings, applications, and solving methods, Journal of Hazardous materials, 390 (2020).
[40] É. C. Lima, M. A. Adebayo, F.M. Machado, Kinetic and equilibrium models of adsorption, Carbon nanomaterials as adsorbents for environmental and biological applications, (2015).
[41] F .M. Machado, C.P. Bergmann, T.H. Fernandes, E.C. Lima, B. Royer, T. Calvete, S.B. Fagan, Adsorption of Reactive Red M-2BE dye from water solutions by multi-walled carbon nanotubes and activated carbon, J Hazard Mater, 192 (2011).
[42] N. Kaya, Z.Y. Uzun, Investigation of effectiveness of pine cone biochar activated with KOH for methyl orange adsorption and CO2 capture, Biomass Conversion and Biorefinery, 11 (2020).
[43] S. Cheng, L. Zhang, H. Xia, S. Zhang, J. Peng, S. Wang, Crofton weed derived activated carbon by microwave-induced KOH activation and application to wastewater treatment, Journal of Porous Materials, 23 (2016).
[44] Z. Mekibes, B. Bestani, N. Douara, N. Benderdouche, M. Benzekri-Benallou, Simultaneous activation of Ficus carica L. leaves for the removal of emerging pollutants from aqueous solutions, Desalination and Water Treatment, 222 (2021).
[45] H. Moussout, H. Ahlafi, M. Aazza, H. Maghat, Critical of linear and nonlinear equations of pseudo-first order and pseudo-second order kinetic models, Karbala International Journal of Modern Science, 4 (2018).
[46] F. Ugbe, N. Abdus-Salam, Kinetics and thermodynamic modelling of natural and synthetic goethite for dyes scavenging from aqueous systems, Arabian Journal of Chemical and Environmental Research, 7 (2020).
[47] O. Amrhar, H. Nassali, M.S. Elyoubi, Application of nonlinear regression analysis to select the optimum absorption isotherm for Methylene Blue adsorption onto Natural Illitic Clay, Bulletin de la Société Royale des Sciences de Liège, (2015).
[48] M. Hamzaoui, B. Bestani. N. Benderdouche, The use of linear and nonlinear methods for adsorption isotherm optimization of basic green 4-dye onto sawdust-based activated carbon, Journal of Materials and Environmental Sciences, (2018).

[49] N. Douara, M. Benzekri Benallou, M. Termoul, Z Mekibes, B. Bestani, N. Benderdouche, Removal of Textile Dyes on a Biosorbent Based on the Leaves of Atriplex Halimus, Iran. J. Chem. Chem. Eng., (2022).
[50] D. Lefebvre, F.H. Tezel, A review of energy storage technologies with a focus on adsorption thermal energy storage processes for heating applications, Renewable and Sustainable Energy Reviews, 67 (2017).
[51] P. Saha, S. Chowdhury, Insight into adsorption thermodynamics, Thermodynamics, 16 (2011) 349-364.
[52] A. Valero, A. Valero, P. Vieillard, The thermodynamic properties of the upper continental crust: Exergy, Gibbs free energy and enthalpy, Energy, 41 (2012).

[53] J. Li, Q. Lv, L. Bi, F. Fang, J. Hou, G. Di, J. Wei, X. Wu, X. Li, Metal-organic frameworks as superior adsorbents for pesticide removal from water: The cutting-edge in characterization, tailoring, and application potentials, Coordination Chemistry Reviews, 493 (2023).
[54] A. Naboulsi, L. El Mersly, H. Yazid, M. El Himri, S. Rafqah, M. El Haddad, Adsorption behaviors and mechanisms by theoretical study of herbicide 2,4,5-Trichlorophenoxyacetic on activated carbon as a new biosorbent material, Journal of the Taiwan Institute of Chemical Engineers, 142 (2023).
[55] S. Arif, S. Zafar, M.I. Khan, S. Manzoor, A. Shanableh, J.F. Garcia, M. Hayat, Removal of chromium (VI) by commercial anion exchange membrane BII from an aqueous solution: Adsorption kinetic, equilibrium and thermodynamic studies, Inorganic Chemistry Communications, 152 (2023).
[56] M. Li, Y. Wang, Y. Liu, H. Wang, H. Song, Preparation of active carbon through one-step NaOH activation of coconut shell biomass for phenolic wastewater treatment, Research on Chemical Intermediates, 48 (2022).
[57] A. Pandiarajan, R. Kamaraj, S. Vasudevan, S. Vasudevan, OPAC (orange peel activated carbon) derived from waste orange peel for the adsorption of chlorophenoxyacetic acid herbicides from water: Adsorption isotherm, kinetic modelling and thermodynamic studies, Bioresour Technol, (2018).

CHAPTER II:

ACTIVATED CARBON

Introduction

In theory, all solids possess adsorptive characteristics. The most commonly used adsorbents in industry include activated carbon, zeolites, silica gels, and alumina. Their exceptional adsorption capacity is due to their porous structure and large surface area [1].

Charcoal is one of the first substances discovered by humans, and it appeared when the first fire was ignited. It is a material obtained by the calcination of any organic matter. Due to its medicinal properties, it was used as early as 1500 BC in Egypt as a common remedy for food poisoning for several centuries. The ancient Hindus also used charcoal to filter water and make it drinkable. Activated carbon production began in the early 20^{th} century to meet the needs of sugar refineries, where it was used as a decolorizing agent. These initial activated carbons were obtained by carbonizing plant materials in the presence of metallic chloride and by treating charcoal with carbon dioxide or steam [2].

Nowadays, activated carbon is the most widely used industrial adsorbent. The U.S. Environmental Protection Agency (EPA) recognizes it as one of the best technologies for environmental control [3]. The low cost of activated carbon and its non-selective nature secure its position in the adsorbent market, with global annual production reaching 800,000 tons. Additionally, the variety of activated carbons in terms of chemical composition and texture accounts for their wide range of applications. It is estimated that the global consumption of commercial activated carbon (CAC) is around 400 kilotons per year, with 80% used in liquid-phase applications and the remainder primarily in the form of extruded carbon for gas-phase applications. Numerous sectors are involved, including those for treating water, air, and gases [4].

The global interest in preserving the environment from solid waste generated by various human activities and transformations has drawn researchers' attention to finding technical means to recycle these wastes[5]. Producing activated carbon from plant waste is economically attractive because it involves simple processes that enable direct applications of these materials [6].

Another significant advantage of using activated carbon is that it does not generate by-products unlike chemical oxidation methods. Activated carbons are also used in industry for the production and recycling of process water and for treating water before discharge. The growing public interest in drinking water quality has increased the demand for activated carbon in household filters, which can be installed directly on taps or at the point of entry of water pipes in homes. This sector is currently experiencing rapid growth [7].

II.1 Activated carbon

Activated carbon, also called activated charcoal, is a carbon-based material with a highly porous structure. It is processed at extremely high temperatures to develop an extensive specific surface area [8]. It is composed of carbon atoms arranged in layers with a structure similar to graphite [9]. These carbon sheets are grouped into a granular or monolithic structure (solid structure), containing pores that range from a few angstroms (interlayer spaces) to several dozen nanometers [10]. The interconnected pore system consists of channels formed within a rigid framework of disordered carbon atom layers that are unevenly stacked. This configuration produces a highly porous structure with various crevices, cracks, and voids between the carbon sheets [11]. It is characterized by an almost non-polar surface, allowing it to preferentially adsorb organic or non-polar compounds over polar ones, such as water. Unlike most other adsorbents, this property enables its use in gas separation/purification operations without needing prior dehumidification [12].

Activated carbon can be produced from a wide range of materials containing organic carbon of animal and plant origin. The raw materials (precursors) and the activation method used in its preparation influence the properties of activated carbon, which enhances its adsorption capacity for organic and inorganic substances [13].

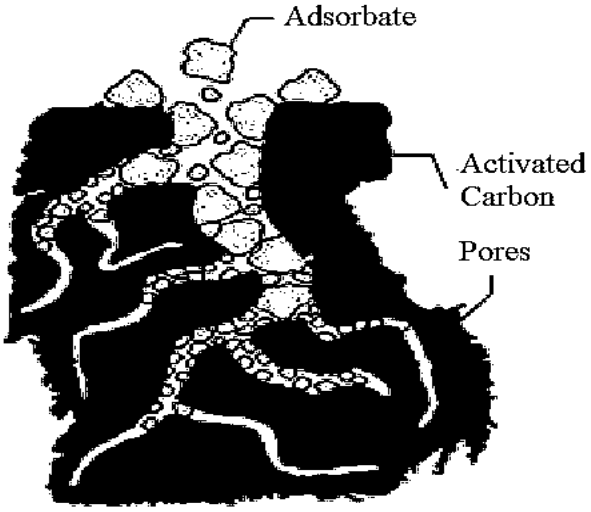

Figure II.1: Structure of activated carbon [14]

II.1.1 Activated carbon classification

Activated carbon is a material commonly used for purification and filtration. It comes in different forms, each with specific properties suited to various applications. Based on particle size,

it is generally classified into four types: powdered activated carbon (PAC), granular activated carbon (GAC), fibrous activated carbon (FAC), and extruded activated carbon (EAC) [15-18].

a. Powdered Activated Carbon (PAC): These are very fine particles, generally less than 0.1 mm, with a common particle size ranging from 0.015 to 0.025 mm. It is often used for drinking water treatment and in the purification processes of liquids and gases.
b. Granular Activated Carbon (GAC): Composed of larger particles than PAC, it has an average particle size between 0.6 and 4 mm. Its high bulk density, high hardness, and low abrasion index make GAC more suitable than PAC for various applications. It is used in continuous-flow filtration systems, such as water and air filters.
c. Extruded Activated Carbon (EAC): Formed by an extrusion process into rods or cylinders, it offers good mechanical strength and is used in applications requiring low-pressure drop, such as air or gas filtration systems.
d. Fibrous Activated Carbon (FAC): Presented in the form of fabrics, felts, or fibers, it is valued for its large specific surface area and rapid adsorption capacity. It is commonly used in filter masks, air filters, and applications requiring fast adsorption.

Powdered Activated Carbon (PAC)

Granular Activated Carbon (GAC):

Extruded Activated Carbon (EAC)

Fibrous Activated Carbon (FAC)

Figure II.2: Forms of activated carbon

II.2 Sources of activated carbon

II.2.1 Agroforestry coproducts

Trees and their elements, such as bark, needles, leaves, and branches, have been employed from the beginning of civilization. However, millions of tons of forestry residue such as bark, cones, needles, twigs, and so on, have been produced during wood harvesting in forested areas. These residues vary significantly in volume per hectare, size, and location. Furthermore, scientists and engineers have thoroughly researched a wide range of techniques to modify lignocellulosic materials chemically and physically to take advantage of their superior qualities and higher simplicity of use compared to their homologs [19].

Agricultural waste is estimated to comprise about 80% of each cultivated plant [20], leading to significant yield losses during harvest. The European Union generates around 700 million tons of agricultural waste annually, while global figures reach tens of billions of tons [21]. According to the 2020 report by the Food and Agriculture Organization (FAO), the world's forest cover now accounts for about 31% of total land area, compared to 66% four centuries ago, covering approximately 4.06 billion hectares. The same report states that annual deforestation averaged 7.8 million hectares per year during the 2010-2020 decade [22].

Most agricultural waste is typically burned, either as biomass fuel in power plants in developed countries or simply disposed of through open burning [23]. This process releases carbon dioxide, smog, particulate matter, and ash instead of being utilized to create added value. Plant biomass, which is made up of lignin, cellulose, and hemicellulose, could be repurposed for various uses, such as in the chemical industry, energy production, or composting [24].

Due to its surfactant properties, lignin is used as a binder, stabilizer, or emulsifier in chemistry. It is valuable for synthesizing phenol, catechol, benzene, and their derivatives. Cellulose is used to make paper and cotton materials and as additives or binders in the production of tablets, capsules, or granules in the pharmaceutical industry [25]. Hemicelluloses can synthesize sugars and organic acids such as butyric, acetic, and lactic acids [26].

In the energy sector, plant biomass can be used as a raw material for producing bioenergy. This includes biofuels, heat, electricity, and biogas [27]. Agroforestry by-products are also used to create activated carbon [28], nanoparticles [29], and nanomaterials [30]. To preserve agroforestry resources, utilizing by-products from oilseed species, for instance, helps prevent the excessive cutting down of trees, which could lead to their decline.

The production of activated carbon is a complex process that converts carbon-rich materials into a highly porous and reactive substance [31].

The precursor materials are divided into three categories: fossil materials (such as coal, lignite, and wood), plant-based materials (like fruit pits, coconut shells, and palm oil), and synthetic materials (including cellulose, viscose, rayon, and polyvinylidene chloride, a homopolymer of vinylidene chloride of formula $(C_2H_2Cl_2)_n$) [32].

In recent years, many fundamental studies have reported on the production of activated carbon from unconventional precursors, such as plant waste, agricultural by-products, and industrial by-products. Some of the most effective sources include apricot pits [33], pomegranate peels [34], tea leaves [35], sawdust [36], rice husks [37], Doum fiber [38], seed shells [39], corn kernels [40], orange peels (Citrus sinensis) [41], and sludges [42]. Using these precursors is economically appealing and aligns with sustainable development and waste valorization [43].

II.2.2 Chemical composition of lignocellulosic precursors

a. **Cellulose** is the most abundant natural polymer on Earth, as it is found in major proportions in nearly all plant species. It has always been widely used, especially in the manufacture of paper and cotton. Although the chemical structure of cellulose is well known, its tertiary structure, including its crystalline and fibrous structure, is not completely resolved. Cellulose is a homopolysaccharide (or carbohydrate polymer) composed of H-O glucopyranose units linked together by β (1-4) glycosidic bonds.
b. **Hemicellulose** is a type of polysaccharide found in all plants. It has a lower molecular weight than cellulose and has fewer regular structures due to the presence of different units in its chains. Hemicellulose molecules are very hydrophilic (water-attracting) and adhesive. These molecules dissolve easily in alkaline and basic substances. The backbone of hemicellulose is similar to that of cellulose but can have cross-linking with hexoses (like glucose, mannose, and galactose) and/or pentoses (like xylose and arabinose), as well as aromatic acids [44].
c. **Lignin** is the main component of wood, making up about 20 to 30% of the carbon in plant biomass. It is the second most abundant organic compound in the biosphere after cellulose, which means it is a renewable and abundant natural resource. Lignin is not easily broken down by biological processes, creating a physical barrier that helps protect plants from

pathogens and pest attacks. The term 'lignin' refers to a group of high molecular weight polyphenolic polymers that have complex and variable compositions and structures.

d. **Extractives** are not a part of the cell wall. They can be easily removed by natural solvents. They include various chemical substances such as certain fats, aromatic compounds, volatile oils, high molecular weight alcohols, and fatty acids. While extractives do not contribute to the mechanical properties of wood, they do add weight. They can also color the wood and give it a fragrance. Additionally, extractives are toxic and help make wood more resistant to decay and insect attacks [45].

II.2.3 Conversion of lignocellulosic waste into activated carbon

Research shows that the adsorptive properties of activated carbon depend on the raw materials used, particularly the biopolymers such as cellulose, hemicellulose, and lignin found in lignocellulosic precursors. These biopolymers are crucial for creating the porous structure of activated carbon. During carbonization and activation, they break down and are removed, forming pores. While the amount of these biopolymers can influence pore characteristics, their presence is essential for porosity, regardless of their specific ratios [46, 47]. Additionally, the type of lignocellulosic material chosen affects the surface area, pore volume, size, and distribution of the pores [48].

Compared to cellulose and hemicellulose, lignin has the highest carbon content, and a low oxygen content, while the water and hydrogen contents are similar and close [49]. It is generally accepted that lignin is responsible for microporosity, while hemicellulose and cellulose lead to mesoporous-activated carbons. Above 300 °C, lignin and cellulose decompose to produce three products: gas, tar, and a solid carbonaceous phase [50]. Furthermore, cellulose and hemicellulose are mostly released in the form of water vapor, carbon dioxide, and carbon monoxide, which leads to the formation of micropores [51].

In studies on the preparation of activated carbons from different precursors, it was shown that materials with high lignin content, such as grape seeds and cherry pits, resulted in macroporous activated carbons [52], while those with a higher cellulose content (apricot pits, almond shells) produced microporous activated carbons [53]. A high lignin content compared to cellulose favors the formation of mesopores [54]. According to several authors, lignin is the main contributor to the final weight of carbon [55]. In another study, pyrolyzing lignin with potassium bicarbonate ($KHCO_3$) led to the breakdown of hydroxyl groups in cellulose and hemicellulose, resulting in a

mainly macroporous structure, with hemicellulose and lignin having a higher ash content compared to cellulose [56, 57].

It can be concluded that high lignin content leads to the formation of macro- and mesoporous-activated carbons. In contrast, higher levels of other biomass components are more likely to produce smaller pores. However, the differing results in the literature could be due to the type and quantity of activating agents used [58].

II.3 Pine cone tree - Maritime pine

The trees from the Pinaceae family (i.e. pinus, Abies, Picea, Cedrus, Larix, etc.) are one of the most widely distributed worldwide. Pine cones (fruit from pine cone tree) are the most widespread conifer genus in the Pinaceae family, with over 10 genera and from 100 to 200 species [59], including the maritime pine (*Pinus pinaster* or *Pinus maritima*) [60].

Most Pinaceae species have been in temperate climates, ranging from subarctic to tropical lands. However, due to their high tolerance to dryness, and chilly weather, many Pinaceae species have been planted for protection against tides, producing fuels and substitution of wood-based materials.

The pine tree or maritime pine shares similar morphological characteristics with other species in the Pinus genus. It is native to the southwestern regions of Europe, with notable growth along the Atlantic coast of France, Spain, and Portugal, also in northwestern Africa and the Mediterranean region (Tunisia, Morocco, Algeria) [61]. It plays a key role in the production and consumption primarily along the Atlantic Ocean coasts and in North America, and even in the Mediterranean region [62]. It is considered invasive in South Africa, Australia, and Chile. In the 19th century, it was widely planted to drain wet soils and stabilize dunes.

The Maritime Pine can tolerate temperatures above 40°C for extended periods, but is not resistant to prolonged and severe cold. It grows faster in deep, well-drained soils but does not thrive in calcareous soils. This tree can grow up to 30 meters in height, reaches maturity at 40 to 50 years, and can live for up to 500 years [63].

Algeria has an area of 2.388 million km², with forests and scrubland covering 4.1 million hectares. This represents a forest coverage rate of 16.4% in northern Algeria.

The pine cone tree "Snouber" is the most dominant and common tree, which covers a surface area between 880,000 and 900,000 hectares and is mainly found in semi-arid areas [64, 65].

The fruits of the maritime pine are oval cones, brown in color, and about 2 cm long. The sapwood is pale yellow, while the heartwood is yellow with reddish-brown veining [47]. Pinus pinea, also known as the 'Stone Pine' or 'Umbrella Nut', gets its name from its ability to grow well in stony soil and its umbrella-like shape [66]. Another important species, maritime pine (*Pinus pinaster* Ait.), is widely used for producing wood-based panels and in the pulp and paper industry [67].

Figure II. 3: Photos of pine cone and maritime pine trees

II.3.1. Chemical constituents of pine cone

Several studies have shown that coniferous cones contain similar chemical components to wood, though in different proportions. Notably, they are rich in phenolic compounds. Typically, pine cones consist of approximately 41.7 % cellulose, 25.9 % lignin, and 20.5 % hemicelluloses [58]. It has also been found that a variety of compounds can be extracted from pine cones, including polysaccharides, lignin-related compounds, water- and solvent-soluble substances, and essential oils, with polysaccharides making up about 50 % (w/w) of the total content. It was proposed that the *pinus* and *picea* cone polysaccharides typically consisted of ribose, rhamnose, arabinose, xylose, mannose, glucose, and galactose in different molar ratios [19, 68, 69].

II.4. Preparation of activated carbon

The properties of activated carbons are greatly influenced by the choice of precursor, the activation process, the type of activating agent, as well as the temperature and duration of activation. Therefore, the process must be optimized to achieve the desired characteristics and meet the intended use of the final product [70]. In practice, there are two main methods for preparing activated carbon: single- and two-step activation [71]. The main goal of these processes is to develop a structure that is both durable and porous.

Single-step pyrolysis is commonly employed in the preparation of activated carbon using the chemical activation method. However, the traditional method for producing activated carbon through physical activation involves a two-step pyrolysis process, where carbonization and activation are conducted separately. There is also a two-step activation procedure using the chemical procedure, which involves initial carbonization to remove impurities and produce a base carbon. This is followed by activation carbonization that forms a porous structure with a chemical activating agent. Table II. 1 shows a comparison between the two processes used in the preparation of activated carbon. The product from two-step pyrolysis exhibits high surface area and porosity.

Table II.1: Comparison between one-step and two-step activation [2].

One step activation	Two-step activation
- One-step process - Low energy consumption, inexpensive - Shorter process time - Modest surface and porosity	- Two-step process - Energy consumption - Costly - Longer process times - High surface area and porosity

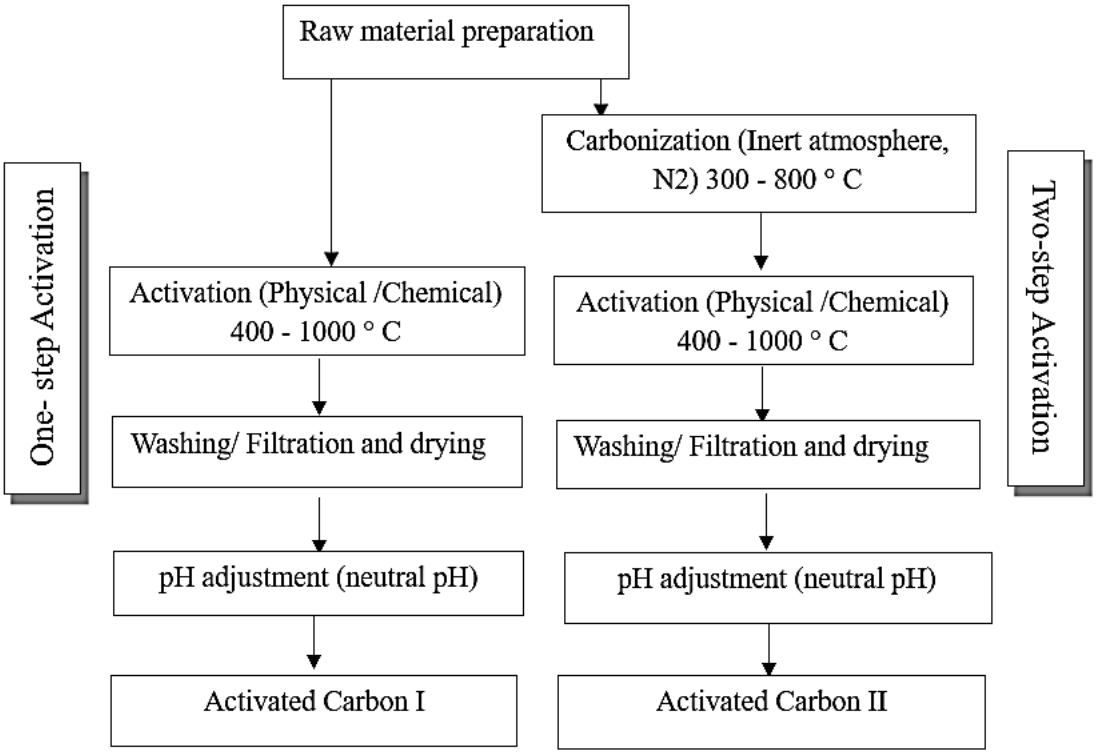

Figure II.4: Schematic diagram of the two procedures used to prepare activated carbon (one-step and two-step activation)

II.4.1. Thermogravimetric analysis (TGA) - Importance and principle

Pyrolysis is a thermal decomposition process in which organic material is heated to high temperatures without oxygen or other oxidizing agents, typically in specialized furnaces. During pyrolysis, macromolecules within the material undergo gradual decomposition through various thermochemical reactions. These reactions produce a range of gaseous compounds and leave behind a solid residue known as char, which has a dense carbon structure. The thermochemical changes occurring in biomass during pyrolysis have been extensively studied using thermogravimetric analysis (TGA).

Thermogravimetric analysis monitors the mass change of a sample over time and temperature, providing insights into the degradation behavior of biomass, including the determination of ash and volatile content [72]. The goal is to identify the optimal temperature for the activation process, which will yield high-quality activated carbon with favorable properties such as good yield, activation rate, and specific surface area [73].

Three primary mechanisms occur almost simultaneously within the biomass during pyrolysis, as it is described in Figure II.5.

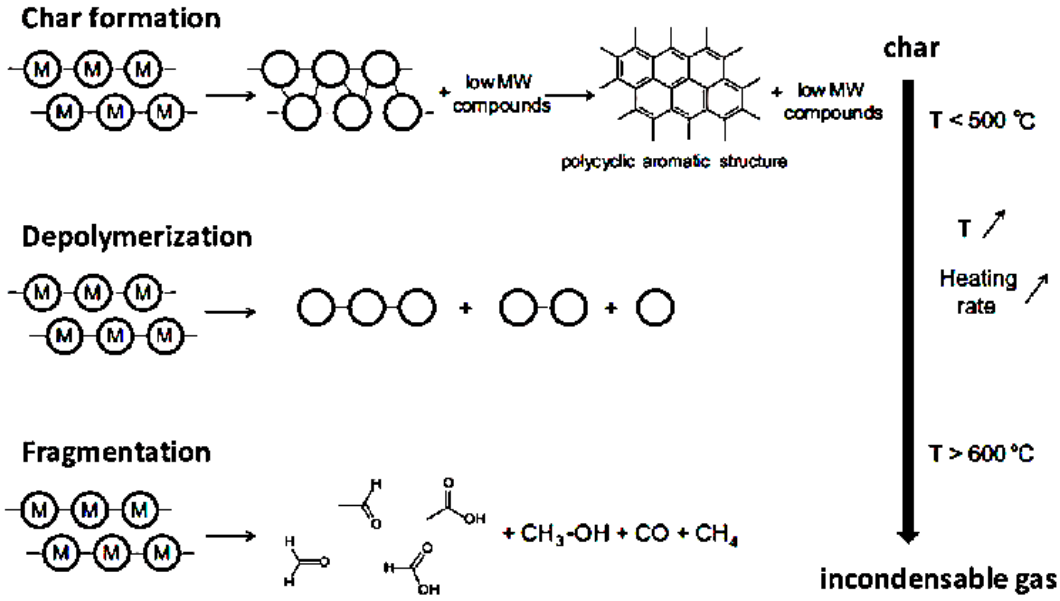

Figure II.5: Processes involved in the main mechanisms for converting biomass components (M: monomer, MW: molecular weight) [74]

II.4.2. Carbonization

Carbonization is a specific and targeted type of pyrolysis process with the specific goal of producing carbon-rich solids [75, 76], It involves heating organic material (like wood or biomass) at high temperatures in an inert atmosphere [77]. Through carbonization, most volatile components, such as water, gases, and non-carbon organic elements, are removed through pyrolytic decomposition of the initial material, transforming it into a form suitable for activation.

The remaining free carbon atoms are then organized into a crystalline structure known as elementary graphite crystallites. During carbonization, the product's carbon content reaches around 80%. The carbonized product has low adsorption capacity because its minimal internal surface area lacks a well-developed porous structure, which will be further developed during the activation process [78].

The key factors that influence the quality, properties, and yield of the pyrolyzed product are:

- Furnace heating rate (°C/min): This affects the pyrolysis process, a slower heating rate results in fewer volatile compounds and helps retain some of the original structure.

- Final carbonization temperature (°C): This controls the resulting carbon's mass loss and surface appearance.
- Residence time in the furnace (hours or minutes): This is a critical factor in the initial carbonization stage and should be optimized to achieve good yield.
- Nature of the starting material: The pyrolysis rate is highly impacted by the moisture content of the raw material [79].

II.4.3. Activation

Activation is a crucial step in the production of activated carbon. In single-step activation, it serves as the primary phase, while in two-step activation, it follows carbonization, where carbonized particles are treated with an activating agent at high temperatures. The main purpose of activation is to create a porous structure on the carbon's surface, significantly enhancing its specific surface area.

Two main activation methods are used:

II.4.3.1. Chemical activation

Chemical activation involves the thermal treatment of biomass or char previously impregnated with chemical substances [80, 81]. These substances can be either acidic or basic, depending on the specific properties desired in the activated carbon [82]. The main chemical agents used are acids (such as H_3PO_4, HCl, H_2SO_4) or bases like NaOH and KOH and also salts such as $ZnCl_2$ [83]. Their presence catalyzes gasification reactions, which are responsible for creating pores in the carbon matrix of the charcoal. Additionally, these agents affect the surface chemistry of the activated carbon by catalyzing oxidation and reduction reactions [78]. When directly impregnated into the biomass, their strong acidic and basic properties play a key role in the depolymerization and fragmentation of macromolecules [84].

KOH is one of the most commonly used chemical agents. Researchers agree that K^+ ions initially form bridges (bonds) between the molecules resulting from the fragmentation of macromolecules [85]. These ions gradually convert to their reduced form (mainly from ionic K^+ to metallic K), then leave the carbon matrix as the temperature rises, creating a porous imprint in the solid structure [86]. KOH also plays a role after the charcoal has already been formed, acting both as a catalyst and a reactant to gasify part of the carbon in the charcoal.

Equations 1- 4 show some of the reactions involved in gasification in the presence of KOH [87].

$$2KOH \longrightarrow H_2O + K_2O \quad (1)$$

$$C + H_2O \longrightarrow H_2 + CO \quad (2)$$

$$C + O_2 \longrightarrow CO_2 \quad (3)$$

$$C + CO_2 \longrightarrow 2CO \quad (4)$$

KOH tends to develop more micropores, whereas H_3PO_4 produces larger pore sizes [88].

II.4.3.2 Physical activation

This physical activation method involves first carbonizing the biomass (between 400 and 700°C) in an inert gas atmosphere (such as nitrogen, argon, or helium) [89]. The resulting charcoal is then gasified at temperatures between 750 and 1000°C using an oxidizing gas, like steam or CO_2 (or a mixture of both). The gasification process removes carbon atoms in a controlled and selective manner to create porosity [90]. The gasification reactions follow equations 2, 3, and 4 presented earlier [87].

Studies comparing both activation methods have shown that physical activation tends to produce more mesopores, while chemical activation generally creates more micropores and leads to higher specific surface areas. Additionally, chemical activation introduces more surface functional groups, allowing activated carbons (AC) to adsorb a broader range of pollutants compared to those produced through physical activation [87, 91].

II.5 Activated carbon properties

II.5.1 Porous structure of activated carbon

By definition, a pore is a cavity that is deeper than it is wide. The porous structures of adsorbents vary depending on the type of material used, the specific application, and the desired properties. For effective adsorption separation, the adsorbent must have a high internal volume (highly porous) [92].

According to the IUPAC (International Union of Pure and Applied Chemistry) classification, activated carbon porosity is divided into three main categories:

- macropores, which have diameters greater than 50 nm,
- mesopores, with diameters between 2 and 50 nm,

- micropores, with diameters below 2 nm. Micropores are further categorized as super micropores, with diameters between 0.7 and 2 nm, and ultra micropores, with diameters smaller than 0.7 nm. The total pore volume can be calculated based on the volume of fluid required to fill all open pores in one gram of the solid, which reflects the accessible surface area.

Table II.2: Properties of activated carbon porosity (IUPAC classification)

	Micropores	**Mesopores**	**Macropores**
Diameter (Å)	<20	20-500	>500
Pore volume (cm^3g^{-1})	0.15-0.5	0.02-0.1	0.2-0.5
Specific pore surface ($m^2\ g^{-1}$)	100-1000	10-100	0.5-2.0

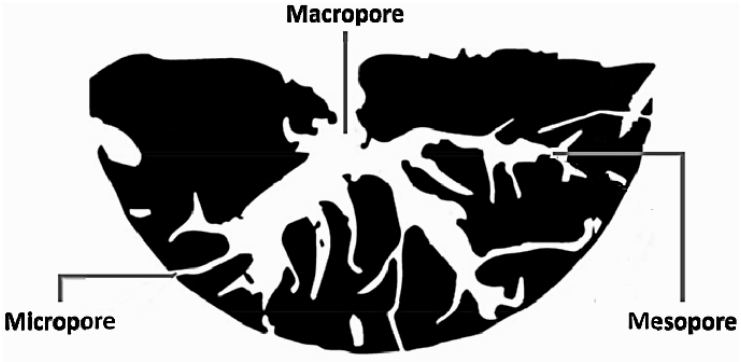

Figure II.6: Porosity of activated carbon [93]

II.5.2. Surface chemistry of activated carbon

II.5.2.1. Surface functional groups of activated carbon

The characteristics of activated carbon are shaped by its pore structure and surface chemistry. Activated carbon has oxygen-containing surface groups that play a crucial role in adsorption [94]. These surface groups are classified into two main types: acidic groups, which act as nucleophilic centers, and basic groups, which serve as electrophilic centers [95]. They are key in adsorbing polar or charged organic compounds in aqueous environments [96]. Acidic groups include carboxyl, hydroxyl, quinone, carbonyl, and lactone, while basic groups include pyrones and chromenes [97]. These groups contribute to the amphoteric nature of activated carbon, allowing it to develop either positive or negative charges depending on the pH of the environment, which in turn affects

contaminant adsorption [98]. The point of zero charge (PZC), where the surface has no detectable charge, is a critical factor in adsorption, especially when contaminants are near adsorption sites. These reactive sites enable interactions with a variety of pollutants in water [99].

Activated carbon is traditionally considered an adsorbent for non-polar compounds. Its arrangement of aromatic rings creates sites that encourage electrostatic interactions, such as van der Waals forces, which help adsorb non-polar pollutants and organic molecules with aromatic structures [100]. Thanks to its variety of chemical groups on the surface, the presence of heteroatoms, which impact its surface properties and its porous structure, activated carbon also adsorbs polar molecules [101]. As a result, activated carbon can efficiently adsorb a wide range of pollutants of different sizes and chemical characteristics [102].

II.6 Textural, structural, and chemical characterization of activated carbons

II.6.1 Brunauer, Emmett, and Teller (BET) theory

The first gas adsorption studies to determine the porosity of solids appeared in the early 19th century. In 1916, Irving Langmuir developed an ideal monolayer adsorption model, which assumes that adsorption occurs on a flat surface where all adsorption sites are identical [103].

Stephen Brunauer, Paul Hugh Emmett, and Edward Teller improved this model, leading to the development of the BET theory, published in 1938 in the Journal of the American Chemical Society. This theory takes into account the uneven surface of solids and hypothesizes that the first adsorbed layer consists of tightly packed gas molecules that completely cover the surface. Each molecule occupies an average surface area corresponding to its transversal cross-section, making it possible to accurately calculate the specific surface area of the porous material [104].

The BET isotherm is given by:

$$\frac{P}{V(P_o-P)} = \frac{1}{V_m.C} + \frac{C-1}{V_m.C}\left(\frac{P}{P_o}\right) \quad (5)$$

with

$$\frac{V}{V_m} = \frac{C.P}{(P_o-P).[1+(C-1)\frac{1}{P}]} \quad (6)$$

where V is the volume of adsorbed gas, P is the gas pressure, P_0 is the vapor pressure above several layers of adsorbed molecules and $V_{m\ is}$ the volume required to form a complete mono-molecular

layer on the surface of one gram of solid. C is a constant given by the expression:

$$C = \exp\left(\frac{H_J - H_L}{R.T}\right) \quad (7)$$

where H_J is differential heat (cal) and H_L is latent heat of evaporation (cal).

By plotting $\frac{P}{(V(P_o - P))}$ as a function of $\frac{P}{P_o}$, we should obtain a straight line with slope $\frac{C-1}{(C \times V_m)}$ and y-intercept $\frac{1}{(V_m \times C)}$.

We calculate the volume corresponding to a total overlap V_m, using the relationship:

$$V_m = \frac{1}{a+b} \quad (8)$$

With "a" and "b" are the slope and the y-intercept, respectively.

The specific surface S_{sp} can be directly calculated from V_m using the following relationship

$$S_{sp} = \frac{P_m.V_m}{R.T_m} \times 6.022 \times 10^{23} \times S_o \quad (9)$$

Where P_m and T_m are the pressure and temperature of the adsorbed gas, and S_o the surface area occupied by a molecule. S_o can be expressed by the following relationship:

$$S_o = 1.09 \times \left[\frac{M}{6.022 \times 10^{23} \times \rho}\right]^{2/3} \quad (10)$$

Where M is the molecular mass of the adsorbed gas, ρ is the density of the pure liquid at the temperature of the experiment (for nitrogen at -195.8°C, ρ = 0.808 g/cm^3).

II.6.2. Iodine number

Iodine number indicates the amount, in milligrams, of iodine adsorbed per gram of activated carbon when the residual equilibrium concentration is 0.02 N (ASTM D4607-94). Activated carbons with a high iodine number are suitable for adsorbing low-molecular-weight substances from aqueous solutions. This measure is essential for characterizing activated carbons, as it provides insight into the available surface area for capturing small substances that can reach micropores (an estimate of the micropores present in the activated carbon).

II.6.3. Methylene blue index

This measurement indicates the available mesoporous surface area in adsorbents. It represents the amount, in milligrams, of Methylene blue adsorbed per gram of activated carbon

when the equilibrium concentration of Methylene blue is 1 mg. L^{-1}. Values for this measure can reach up to 300 mg. g^{-1} [105].

II.6.3.1. SEM-EDS

SEM-EDS (Scanning Electron Microscopy with Energy-Dispersive Spectroscopy) is a combined technique that provides detailed information about the morphology and chemical composition of a sample. SEM uses an electron beam to scan the sample surface, producing high-resolution images that reveal its texture, and structure. As the electrons interact with the sample, characteristic X-rays are emitted from each chemical element. These X-rays are detected by the EDS spectrometer, which analyzes their energy to identify and measure the elements in the sample. This combined approach enables the mapping of both the microscopic structure and the surface's chemical composition, providing essential data for fields such as materials science, geology, chemistry, metallurgy, medicine, biology, and environmental protection [106].

II.6.3.2. X-ray diffraction

X-ray diffraction (XRD) is a powerful analytical technique used to study the crystalline structure of materials. It is based on the interaction between X-rays and the atoms of a material: when X-rays reach the material, they are diffracted at specific angles that depend on the atomic arrangement. Analysis of these diffraction angles and associated intensities provides detailed information on crystallite size, interlayer spacing**,** and the crystalline phases present in the sample. XRD is commonly applied in materials science, chemistry, mineralogy, and physics to study solid materials, identify compounds in mixtures, and verify crystalline purity [107].

II.6.3.3. FT-IR analysis

Infrared spectroscopy is a proven and simple technique. It provides information about the chemical composition of materials. This technique measures the decrease in intensity of radiation as it passes through a sample at different wavelengths. The absorption of radiation in this range induces molecular vibrations and rotations. These vibrations are mainly concentrated in functional groups without affecting the rest of the molecule. Therefore, functional groups can be identified by their unique absorption bands. Most applications use the near-infrared wavelength range ($2.5\ \mu m < \lambda < 50\ \mu m$), which corresponds to wavenumbers from 4000 cm^{-1} to 400 cm^{-1} (mid-infrared). Infrared spectroscopy is mainly used for qualitative analysis of a molecule, identifying the types of bonds present (functional groups) [108].

II.6.3.4. Boehm method

The Boehm titration method can be used to identify and quantify surface functional groups on activated carbon. The oxygen-containing functional groups on the carbon surface have different acidity levels, which can be assessed through acid-base titration with different basic solutions. In the Boehm method, the bases used are sodium bicarbonate ($NaHCO_3$), sodium carbonate (Na_2CO_3), and sodium hydroxide (NaOH). $NaHCO_3$ neutralizes only carboxylic groups, Na_2CO_3 neutralizes carboxylic and lactonic groups, and sodium hydroxide (NaOH) neutralizes acidic groups, including carboxylic, lactonic, and phenolic groups[109].

II.6.3.5. Point of zero charge (pH_{pzc})

This physicochemical property is very important when using activated carbon for liquid phase adsorption. It is defined as the pH of the aqueous solution where the solid has a neutral electrical charge. In other words, at the point of zero charge (pH_{pzc}), the positive charge of the surface sites is equal to the negative charge. If the pH of the solution is higher than pH_{pzc}, cation adsorption is favored, while if the pH is lower than pH_{pzc}, protonation occurs, favoring anion adsorption [110].

The experimental methodology will be described in Chapter IV: Materials and Methods.

II.7. Activated carbon regeneration

Activated carbon has many advantages over other adsorbent materials, however, it must be regenerated for industrial purposes and for increased added value. Regeneration is the process that removes or breaks down the pollutants trapped in saturated activated carbon (AC) so it can be used again. This allows AC to be reused for several months and is a major part of the activated carbon use costs. The regeneration method can vary based on the type of pollutant (organic or inorganic), its stability during regeneration, and the chosen method. Generally, these methods fall into three main categories: physical regeneration (including heat methods), microbiological regeneration, and chemical regeneration [111].

References of Chapter II

[1] K. Achelhi, Organo-apatites et nanocomposites zircone-hydroxyapatite pour le piégeage des métaux, in, Université Pierre et Marie Curie-Paris VI, 2012.

[2] B. Zohra, Activation des noyaux de jujube pour l'obtention d'un charbon actif, 2018.

[3] S. Khirani, Procédés hybrides associant la filtration membranaire et l'adsorption/échange ionique pour le traitement des eaux usées en vue de leur réutilisation, in, Toulouse, INSA, 2007.

[4] A. Chennouf, Préparation de charbon mésoporeux actif à base de polymères synthétiques et dérivés ligno-cellulosiques et application dans l'adsorption des polluants organiques, Thesis, 2017.

[5] I. Tchakala, L.M. Bawa, G. Djaneye-Boundjou, K. Doni, P. Nambo, Optimisation du procédé de préparation des Charbons Actifs par voie chimique (H_3PO_4) à partir des tourteaux de Karité et des tourteaux de Coton, International Journal of Biological and Chemical Sciences, 6 (2012).

[6] M. Trachi, N. Bourfis, S. Benamara, H. Gougam, Préparation et caractérisation d'un charbon actif à partir de la coquille d'amande (Prunus amygdalus) amère, BASE, (2014).

[7] N. Douara, Adsorption de composés phénoliques par un déchet traité chimiquement, Thesis, (2015).

[8] N. Chouikhi, Production de biométhane à partir de biogaz par technologie de séparation par adsorption PSA : optimisation numérique par approche multi-échelle, in, Université Paris-Saclay, (2020).

[9] J. W. Zondlo, Graphite: structure, properties, and applications, Graphite, Graphene, and Their Polymer Nanocomposites, (2012).

[10] Y. B. Melnichenko, Y.B. Melnichenko, Structural characterization of porous materials using SAS, Small-Angle Scattering from Confined and Interfacial Fluids: Applications to Energy Storage and Environmental Science, (2016).

[11] D. Boikanyo, M.L. Masheane, L.N. Nthunya, S.B. Mishra, S.D. Mhlanga, Carbon-supported photocatalysts for organic dye photodegradation, in: New Polymer Nanocomposites for Environmental Remediation, Elsevier, (2018).

[12] M. CLAUSSE, Étude d'un procédé d'adsorption TSA (temperature swing adsorption) à chauffage et refroidissement indirects, Thesis, (2003).

[13] T. W. Chew, P.S. H'Ng, B.C.T.G. Luqman Chuah Abdullah, K.L. Chin, C.L. Lee, B.M.S. Mohd Nor Hafizuddin, L. TaungMai, A Review of Bio-Based Activated Carbon Properties Produced from Different Activating Chemicals during Chemicals Activation Process on Biomass and Its Potential for Malaysia, Materials, 16 (2023).

[14] M. C. M. Amin, Elimination du mercure en phase aqueuse et en phase gazeuse par un nouvel adsorbant activé.

[15] M. F. Hassan, M.A. Sabri, H. Fazal, A. Hafeez, N. Shezad, M. Hussain, Recent trends in activated carbon fibers production from various precursors and applications—A comparative review, Journal of Analytical and Applied Pyrolysis, 145 (2020).

[16] A. Kumar, R. Aslam, C. Verma, O.M. Rodríguez-Narváez, Activated Carbon for Environmental Applications, (2023).

[17] W. Liu, S. Adanur, Desulfurization properties of activated carbon fibers, Journal of Engineered Fibers and Fabrics, (2014).

[18] R. Gembo, S. Odisitse, C. King'ondu, Transforming waste resources into efficient activated carbon for energy storage and environmental remediation: a comprehensive review, International Journal of Environmental Science and Technology, (2024).

[19] H. Sahin, O. Yalcin, Conifer cones: An alternative raw material for industry, British Journal of Pharmaceutical Research, (2017).

[20] O. Toundou, Evaluation des caractéristiques chimiques et agronomiques de cinq composts de déchets et étude de leurs effets sur les propriétés chimiques du sol, la physiologie et le rendement du maïs (Zea mays L. Var. Ikenne) et de la tomate (Lycop ersicum esculentum L. Var. Tropimech) sous deux régimes hydriques au Togo, Université de Limoges, Université de Lomé (Togo), (2016).

[21] C. Fritsch, A. Staebler, A. Happel, M.A. Cubero Márquez, I. Aguiló-Aguayo, M. Abadias, M. Gallur, I. M. Cigognini, A. Montanari, M.J. López, Processing, valorization and application of bio-waste derived compounds from potato, tomato, olive and cereals: A review, Sustainability, (2017).

[22] Organisation des nations unies pour l'alimentation et l'Agriculture, Situation forêts et agriculture: défis et possibilités concernant l'utilisation des terres des forêts du monde (2016).

[23] C. Ronneau, Énergie, pollution de l'air et développement durable, Presses univ. de Louvain, (2013).

[24] M. K. Awasthi, S. Sarsaiya, A. Patel, A. Juneja, R.P. Singh, B. Yan, S.K. Awasthi, A. Jain, T. Liu, Y. Duan, Refining biomass residues for sustainable energy and bio-products: An assessment of technology, its importance, and strategic applications in circular bio-economy, Renewable and Sustainable Energy Reviews, 127 (2020).

[25] I. Hasan, S. Walia, A review on properties and challenges associated with cellulose nanocrystals and nanocomposites, Materials Today: Proceedings, (2021).

[26] A. Kumar, V. Kumar, B. Singh, Cellulosic and hemicellulosic fractions of sugarcane bagasse: Potential, challenges and future perspective, International Journal of Biological Macromolecules, 169 (2021).

[27] J.C. Solarte-Toro, Y. Chacón-Pérez, C.A. Cardona-Alzate, Evaluation of biogas and syngas as energy vectors for heat and power generation using lignocellulosic biomass as raw material, Electronic Journal of Biotechnology, 33 (2018).

[28] C.V. Berenguer, R. Perestrelo, J.A. Pereira, J.S. Câmara, Management of Agri-Food Waste Based on Thermochemical Processes towards a Circular Bioeconomy Concept: The Case Study of the Portuguese Industry, Processes, 11 (2023).

[29] I.N.Z.N. Azmi, P.W. Chia, R.K. Liew, H.M. Yusoff, T.S. Chuah, F.S.J. Yong, C.G. Joseph, Z. Guo, E. Buchar, W. Winchester, Biowastes as sustainable source for nanoparticle synthesis and their pesticide properties: a review, ES Food & Agroforestry, 16 (2024).

[30] R.D. Prasad, N. Charmode, O.P. Shrivastav, S.R. Prasad, A. Moghe, P.D. Sarvalkar, N.R. Prasad, A review on concept of nanotechnology in veterinary medicine, ES Food & Agroforestry, 4 (2021).

[31] M. Hervy, Valorisation de chars issus de pyrogazéification de biomasse pour la purification de syngas: lien entre propriétés physico-chimiques, procédé de fonctionnalisation et efficacité du traitement, in, Ecole des Mines d'Albi-Carmaux, (2016).

[32] L. Meljac, Etude d'un procédé d'imprégnation de fibres de carbone activées, in, Ecole Nationale Supérieure des Mines de Saint-Etienne, (2004).

[33] U.S. Zhenisbekovna, M.I. Satayev, S.V. Viktorovich, Production of active carbons from apricot pit shells by thermal activation in the mixture of carbon dioxide and water vapors, Biosciences Biotechnology Research Asia, 13 (2016).

[34] A.H. Jawad, M.H. Sauodi, M.S. Mastuli, M.A. Aouda, K.A. Radzun, Pomegranate peels collected from fresh juice shop as a renewable precursor for high surface area activated carbon with potential application for methylene blue adsorption, Desalination and Water Treatment, 124 (2018).

[35] V. Thirumal, R. Yuvakkumar, G. Ravi, G. Dineshkumar, M. Ganesan, S.H. Alotaibi, D. Velauthapillai, Characterization of activated biomass carbon from tea leaf for supercapacitor applications, Chemosphere, 291 (2022).

[36] T.E. Oladimeji, B.O. Odunoye, F.B. Elehinafe, R.O. Oyinlola, A.O. Olayemi, Production of activated carbon from sawdust and its efficiency in the treatment of sewage water, Heliyon, 7 (2021).

[37] M.M. Alam, M.A. Hossain, M.D. Hossain, M. Johir, J. Hossen, M.S. Rahman, J.L. Zhou, A.K. Hasan, A.K. Karmakar, M.B. Ahmed, The potentiality of rice husk-derived activated carbon: From synthesis to application, Processes, 8 (2020).

[38] A. Grich, T. Bouzid, A. Naboulsi, A. Regti, A.A. Tahiri, M. El Himri, M. El Haddad, Preparation of low-cost activated carbon from Doum fiber (Chamaerops humilis) for the removal of methylene blue: Optimization process by DOE/FFD design, characterization, and mechanism, Journal of Molecular Structure, 1295 (2024).

[39] N. Thinakaran, P. Panneerselvam, P. Baskaralingam, D. Elango, S. Sivanesan, Equilibrium and kinetic studies on the removal of Acid Red 114 from aqueous solutions using activated carbons prepared from seed shells, Journal of hazardous materials, 158 (2008).

[40] R. Wu, Q. Ye, K. Wu, L. Wang, H. Dai, Highly efficient CO2 adsorption of corn kernel-derived porous carbon with abundant oxygen functional groups, Journal of CO_2 Utilization, 51 (2021).

[41] W. El Malti, A. Hijazi, Z. Abou Khalil, Z. Yaghi, M.K. Medlej, M. Reda, Comparative study of the elimination of copper, cadmium, and methylene blue from water by adsorption on the citrus Sinensis peel and its activated carbon, RSC advances, 12 (2022).

[42] P. Hadi, M. Xu, C. Ning, C.S.K. Lin, G. McKay, A critical review on preparation, characterization and utilization of sludge-derived activated carbons for wastewater treatment, Chemical Engineering Journal, 260 (2015).

[43] A. Kapoor, M. Raghunathan, B. Lal, P. Kumar, N. Srivastava, G. Devnani, D.B. Pal, Sustainable valorization of waste plastic into nanostructured materials for environmental, energy, catalytic and biomedical applications: A review, Chemosphere, (2024).

[44] S.-J. Jung, S.-H. Kim, I.-M. Chung, Comparison of lignin, cellulose, and hemicellulose contents for biofuels utilization among 4 types of lignocellulosic crops, Biomass and bioenergy, 83 (2015).

[45] R. Sun, Cereal straw as a resource for sustainable biomaterials and biofuels: chemistry, extractives, lignins, hemicelluloses and cellulose, Elsevier, (2010).

[46] M. Saeed, U. Shahzad, M. Fazle Rabbee, R. Manzar, J.Y. Al-Humaidi, A. Siddique, T.A. Sheikh, R.H. Althomali, T. Qamar, M.M. Rahman, Potential development of porous carbon composites generated from the biomass for energy storage applications, Chemistry–An Asian Journal, 19 (2024).

[47] A. Meullemiestre, Valorisation des déchets de la filière «bois» en deux étapes: isolation des molécules extractibles puis fabrication de charbon actif: cas du pin maritime, in, Université de La Rochelle, (2014).

[48] H.M. Boundzanga, B. Cagnon, M. Roulet, S. de Persis, C. Vautrin-Ul, S. Bonnamy, Contributions of hemicellulose, cellulose, and lignin to the mass and the porous characteristics of activated carbons produced from biomass residues by phosphoric acid activation, Biomass Conversion and Biorefinery, (2020).

[49] P. Zong, Y. Jiang, Y. Tian, J. Li, M. Yuan, Y. Ji, M. Chen, D. Li, Y. Qiao, Pyrolysis behavior and product distributions of biomass six group components: Starch, cellulose, hemicellulose, lignin, protein and oil, Energy Conversion and Management, 216 (2020).

[50] H. M. Boundzanga, Valorisation de la biomasse pour l'élaboration de carbones activés et le développement de dispositifs d'élimination et de détection de nitrates en milieu aqueux, in, Orléans, (2020).

[51] C. Xu, M. Strømme, Sustainable porous carbon materials derived from wood-based biopolymers for CO_2 capture, Nanomaterials, 9 (2019).

[52] M. Lewoyehu, Comprehensive review on synthesis and application of activated carbon from agricultural residues for the remediation of venomous pollutants in wastewater, Journal of Analytical and Applied Pyrolysis, 159 (2021).

[53] R. Goswami, A.K. Dey, Activated carbon from agricultural residues: a review, Desalin. Water Treat., 278 (2022).

[54] X. Zhao, P. Gao, B. Shen, X. Wang, T. Yue, Z. Han, Recent advances in lignin-derived mesoporous carbon based-on template methods, Renewable and Sustainable Energy Reviews, 188 (2023).

[55] L. A. Z. Torres, A.L. Woiciechowski, V.O. de Andrade Tanobe, S.G. Karp, L.C.G. Lorenci, C. Faulds, C.R. Soccol, Lignin as a potential source of high-added value compounds: A review, Journal of Cleaner Production, 263 (2020).

[56] J. Deng, T. Xiong, H. Wang, A. Zheng, Y. Wang, Effects of cellulose, hemicellulose, and lignin on the structure and morphology of porous carbons, ACS sustainable chemistry & engineering, 4 (2016).

[57] B. Cagnon, X. Py, A. Guillot, F. Stoeckli, G. Chambat, Contributions of hemicellulose, cellulose and lignin to the mass and the porous properties of chars and steam activated carbons from various lignocellulosic precursors, Bioresource Technology, 100 (2009).

[58] E. SOGBOCHI, Elaboration par voies thermochimiques de charbons actifs dérivés de coproduits de Lophira lanceolata : essais d'adsorption de micropolluants de l'eau, (2023).

[59] N. Ayotte, Dendroécologie du pin gris (Pinus banksiana Lamb) dans le Haut-Boréal du Québec, Institut National de la Recherche Scientifique (Canada), (2014).

[60] C. Ferracini, L. Dovigo, E.V. Fontana, S. Gallizia, P. Gonthier, G. Lione, C. Pogolotti, S. Prospero, I. Rollet, M. Vercelli, Manuels Mongefitofor. Surveillance et gestion de la processionnaire du pin et d'autres ravageurs du pin dans les zones alpines transfrontalières, (2024).

[61] L. Sterck, N. de María, R.A. Cañas, M. de Miguel, P. Perdiguero, A. Raffin, K.B. Budde, M. López-Hinojosa, F.R. Cantón, A.S. Rodrigues, Maritime pine genomics in focus, in: The Pine Genomes, Springer, (2022).

[62] M.A. Nuñez, M.C. Chiuffo, A. Torres, T. Paul, R.D. Dimarco, P. Raal, N. Policelli, J. Moyano, R.A. García, B.W. Van Wilgen, Ecology and management of invasive Pinaceae around the world: progress and challenges, Biological Invasions, 19 (2017).

[63] https://www.pepinieres-atlantique-mercier.com/nos-arbres/coniferes/pin-maritime/, in, 06/01/2025.

[64] https://www.fao.org/4/x6771f/X6771F02.htm, in, 06/01/2025.

[65] N. Kadri, B. Khettal, Y. Aid, S. Kherfellah, W. Sobhi, V. Barragan-Montero, Some physicochemical characteristics of pinus (Pinus halepensis Mill., Pinus pinea L., Pinus pinaster and Pinus canariensis) seeds from North Algeria, their lipid profiles and volatile contents, Food chemistry, 188 (2015).

[66] S. Mutke, R. Calama, S.C. González-Martínez, G. Montero, F. Javier Gordo, D. Bono, L. Gil, 4 mediterranean stone pine: Botany and horticulture, Horticultural reviews, 39 (2012).

[67] J. I. Alonso-Esteban, M. Carocho, D. Barros, M.V. Velho, S. Heleno, L. Barros, Chemical composition and industrial applications of Maritime pine (Pinus pinaster Ait.) bark and other non-wood parts, Reviews in Environmental Science and Bio/Technology, 21 (2022).

[68] M. Balaban Ucar, O. Gonultas, Chemical characterization of cone and wood of Pinus pinea, Lignocellulose, 2 (2014).

[69] B. M. Maya, A. Abedini, S.C. Gangloff, A. Kabouche, Z. Kabouche, L. Voutquenne-Nazabadioko, A new δ-tocotrienolic acid derivative and other constituents from the cones of Cedrus atlantica and their in vitro antimicrobial activity, Phytochemistry letters, 20 (2017).

[70] S. Z. Naji, C.T. Tye, A review of the synthesis of activated carbon for biodiesel production: Precursor, preparation, and modification, Energy Conversion and Management: X, 13 (2022).

[71] A. A. Ceyhan, Ö. Şahin, C. Saka, A. Yalçın, A novel thermal process for activated carbon production from the vetch biomass with air at low temperature by two-stage procedure, Journal of analytical and applied pyrolysis, 104 (2013).

[72] S. A. El-Sayed, T.M. Khass, M.E. Mostafa, Thermal degradation behaviour and chemical kinetic characteristics of biomass pyrolysis using TG/DTG/DTA techniques, Biomass Conversion and Biorefinery, 14 (2024).

[73] F. Koyuncu, F. Güzel, İ.I.G. İnal, High surface area and supermicroporous activated carbon from capsicum (Capsicum annuum L.) industrial processing pulp via single-step KOH-catalyzed pyrolysis: Production optimization, characterization and its some water pollutants removal and supercapacitor performance, Diamond and Related Materials, 124 (2022).

[74] F. X. Collard, J. Blin, A review on pyrolysis of biomass constituents: Mechanisms and composition of the products obtained from the conversion of cellulose, hemicelluloses and lignin, Renewable and sustainable energy reviews, 38 (2014).

[75] Y. X. Seow, Y.H. Tan, N. Mubarak, J. Kansedo, M. Khalid, M.L. Ibrahim, M. Ghasemi, A review on biochar production from different biomass wastes by recent carbonization technologies and its sustainable applications, Journal of Environmental Chemical Engineering, 10 (2022).

[76] F. Ronsse, R.W. Nachenius, W. Prins, Carbonization of biomass, in: Recent advances in thermo-chemical conversion of biomass, Elsevier, (2015).

[77] W. M. Lewandowski, M. Ryms, W. Kosakowski, Thermal biomass conversion: A review, Processes, 8 (2020).

[78] Y. Gao, Q. Yue, B. Gao, A. Li, Insight into activated carbon from different kinds of chemical activating agents: A review, Science of the Total Environment, 746 (2020).

[79] A. Al-Rumaihi, M. Shahbaz, G. Mckay, H. Mackey, T. Al-Ansari, A review of pyrolysis technologies and feedstock: A blending approach for plastic and biomass towards optimum biochar yield, Renewable and Sustainable Energy Reviews, 167 (2022).

[80] J. Alcañiz-Monge, M.d.C. Román-Martínez, M.Á. Lillo-Ródenas, Chemical activation of lignocellulosic precursors and residues: what else to consider?, Molecules, 27 (2022).

[81] B. Sajjadi, T. Zubatiuk, D. Leszczynska, J. Leszczynski, W.Y. Chen, Chemical activation of biochar for energy and environmental applications: a comprehensive review, Reviews in Chemical Engineering, 35 (2019).

[82] Z. Heidarinejad, M.H. Dehghani, M. Heidari, G. Javedan, I. Ali, M. Sillanpää, Methods for preparation and activation of activated carbon: a review, Environmental Chemistry Letters, 18 (2020).

[83] M. Saleem, Effect of chemical activating agents on surface area and methylene blue uptake capacity of activated carbons, Pakistan Journal of Scientific & Industrial Research Series A: Physical Sciences, 64 (2021).
[84] W. Schutyser, a.T. Renders, S. Van den Bosch, S.-F. Koelewijn, G. Beckham, B.F. Sels, Chemicals from lignin: an interplay of lignocellulose fractionation, depolymerisation, and upgrading, Chemical society reviews, 47 (2018).
[85] H. Ge, Y. Huang, Z. Liu, F. Liu, Y.-n. Chen, L. Guo, Alkaline pulping catalyzed ordered conversion of bark in supercritical water, Journal of Cleaner Production, 446 (2024).
[86] F. Destyorini, S. Priyono, H.S. Oktaviano, Y.-I. Hsu, R. Yudianti, H. Uyama, Porous Graphitic Carbon from Coconut Coir Biochar Developed by Ni–KOH Single-Pot Graphitization Process for Lithium-Ion Battery Anodes, Waste and Biomass Valorization, 15 (2024).
[87] C. T. Chekem, Matériaux carbonés multifonctionnels à porosité contrôlée à partir des ressources végétales tropicales : application au traitement de l'eau par photocatalyse, Thesis (2017).

[88] S. M. Villota, H. Lei, E. Villota, M. Qian, J. Lavarias, V. Taylan, I. Agulto, W. Mateo, M. Valentin, M. Denson, Microwave-assisted activation of waste cocoa pod husk by H3PO4 and KOH—comparative insight into textural properties and pore development, ACS Omega, 4 (2019).
[89] R. K. Liew, M.Y. Chong, O.U. Osazuwa, W.L. Nam, X.Y. Phang, M.H. Su, C.K. Cheng, C.T. Chong, S.S. Lam, Production of activated carbon as catalyst support by microwave pyrolysis of palm kernel shell: a comparative study of chemical versus physical activation, Research on Chemical Intermediates, 44 (2018).
[90] B. Sajjadi, W.-Y. Chen, N.O. Egiebor, A comprehensive review on physical activation of biochar for energy and environmental applications, Reviews in Chemical Engineering, 35 (2019).
[91] M. S. Contreras, C.A. Páez, L. Zubizarreta, A. Léonard, S. Blacher, C.G. Olivera-Fuentes, A. Arenillas, J.-P. Pirard, N. Job, A comparison of physical activation of carbon xerogels with carbon dioxide with chemical activation using hydroxides, Carbon, 48 (2010).
[92] B. K. Nesrine, Elaboration et caractérisation d'un matériau hybride pour le traitement des eaux usées, Thesis, (2024).

[93] J. Y. Lai, L.H. Ngu, S.S. Hashim, J.J. Chew, J. Sunarso, Review of oil palm-derived activated carbon for CO2 capture, Carbon Letters, 31 (2021).
[94] Y. Bian, Z. Bian, J. Zhang, A. Ding, S. Liu, L. Zheng, H. Wang, Adsorption of cadmium ions from aqueous solutions by activated carbon with oxygen-containing functional groups, Chinese Journal of Chemical Engineering, 23 (2015).

[95] A. Naboulsi, L. El Mersly, H. Yazid, M. El Himri, S. Rafqah, M. El Haddad, Adsorption behaviors and mechanisms by theoretical study of herbicide 2, 4, 5-Trichlorophenoxyacetic on activated carbon as a new biosorbent material, Journal of the Taiwan Institute of Chemical Engineers, 142 (2023).

[96] A. Bhatnagar, M. Sillanpää, Removal of natural organic matter (NOM) and its constituents from water by adsorption–a review, Chemosphere, 166 (2017).

[97] A. Barroso-Bogeat, M. Alexandre-Franco, C. Fernández-González, V. Gómez-Serrano, FT-IR analysis of pyrone and chromene structures in activated carbon, Energy & fuels, 28 (2014).

[98] V. Bernal, A. Erto, L. Giraldo, J.C. Moreno-Piraján, Effect of solution pH on the adsorption of paracetamol on chemically modified activated carbons, Molecules, 22 (2017).

[99] F. Mansour, M. Al-Hindi, R. Yahfoufi, G.M. Ayoub, M.N. Ahmad, The use of activated carbon for the removal of pharmaceuticals from aqueous solutions: a review, Reviews in Environmental Science and Bio/Technology, 17 (2018).

[100] V. I. Isaeva, M.D. Vedenyapina, A.Y. Kurmysheva, D. Weichgrebe, R.R. Nair, N.P.T. Nguyen, L.M. Kustov, Modern carbon–based materials for adsorptive removal of organic and inorganic pollutants from water and wastewater, Molecules, 26 (2021).

[101] P. Sinha, S. Banerjee, K.K. Kar, Characteristics of activated carbon, Handbook of nanocomposite supercapacitor materials I: characteristics, (2020).

[102] Y. Chen, Y. Zhu, Z. Wang, Y. Li, L. Wang, L. Ding, X. Gao, Y. Ma, Y. Guo, Application studies of activated carbon derived from rice husks produced by chemical-thermal process—A review, Advances in colloid and interface science, 163 (2011).

[103] M. Essalhi, Conception de nouveaux polymères de coordination poreux pour des applications énergétiques: études expérimentales et simulations moléculaires, in, Université du Québec à Trois-Rivières, (2024).

[104] A. Shaji, A.K. Zachariah, Surface area analysis of nanomaterials, in: Thermal and Rheological Measurement Techniques for Nanomaterials Characterization, Elsevier, (2017).

[105] Z. Mekibes, Fixation de polluants émergeants par des supports ligno-cellulosiques, Thesis, (2021).

[106] S. Erić, The application and limitations of the SEM-EDS method in food and textile technologies, Advanced Technologies, 6 (2017).

[107] A. Ali, Y.W. Chiang, R.M. Santos, X-ray diffraction techniques for mineral characterization: A review for engineers of the fundamentals, applications, and research directions, Minerals, 12 (2022).

[108] S. Attouti, Activation de deux algues méditerranéennes par diverses méthodes pour l'élimination de colorants, Thesis, (2013).
[109] R.R. Chad Spreadbury, and David Mazyck, Comparison Between FTIR and Boehm Titration for Activated Carbon Functional Group Quantification, (2017).
[110] M. Mohsin, H.W. Kamran, M.A. Nawaz, M.S. Hussain, A.S. Dahri, Assessing the impact of transition from nonrenewable to renewable energy consumption on economic growth environmental nexus from developing Asian economies, Journal of environmental management, 284 (2021).
[111] Y. Ma, X. Zhang, J. Wen, Study on the harm of waste activated carbon and novel regeneration technology of it, IOP Conference Series: Earth and Environmental Science, IOP Publishing, (2021).

CHAPTER III:

PESTICIDES

Introduction

The pollution problems we face today result from a variety of human activities, including domestic, industrial, and agricultural practices [1]. Pollutants come not only from natural sources such as oil and minerals but also from waste produced by sewage treatment plants and persistent organic pollutants generated by waste incineration. However, most harmful substances come from synthetic products the chemical industry creates, such as dyes, fertilizers, and pesticides [2].

Technological advances and their industrial applications have considerably transformed human activities, producing toxic organic and inorganic substances [3, 4].

A chemical pollutant is a toxic substance that has harmful effects on plants, animals, and human beings and is found in natural environments in concentrations sufficient to have an impact on ecosystems and human health [5]. Common examples of pollutants in effluents include nitrates, phosphates, detergents, chlorinated solvents, and various metals such as lead, nickel, mercury, chromium, and cadmium, as well as dyes and pigments [6].

In addition, there are lesser-known pollutants classified as priority hazardous substances, which include volatile organic compounds (VOCs), polycyclic aromatic hydrocarbons (PAHs) such as pentachlorophenol (PCP), and agricultural chemicals such as pesticides [7].

Recent studies have highlighted the presence of pesticide traces in food, as well as in groundwater and surface water. The toxicity of these organic pollutants is attributed to their stable molecular structure, which resists degradation, or to their breakdown into more harmful and carcinogenic by-products. Globally, hundreds of pesticide formulations and thousands of active ingredients are widely used to protect crops and enhance agricultural yields [8].

III.1. Pesticides

III. 1.1. Definition

A pesticide is a chemical compound used to repel, eliminate, or control organisms deemed harmful or parasitic to crops [9]. Pesticides help improve production yields by regulating plant growth, minimizing fruit loss due to premature drop, and preserving quality during storage and transport [10].

Pesticides fall into two broad categories: organic and inorganic, depending on their chemical composition. Organic pesticides contain carbon as their central element, meaning they are mainly derived from natural or synthetic organic materials. These pesticides are often more biodegradable and may include pyrethrins, organophosphates, or carbamates. Their versatility and targeted action mean that they are widely used in agricultural practices [11].

Inorganic pesticides, on the other hand, contain no carbon, except in specific forms such as carbonates or cyanides. They are generally derived from mineral sources and include compounds based on arsenic, mercury, fluorine, sulfur, and copper, as well as cyanide derivatives. Historically, inorganic pesticides were among the first to be used because of their availability and effectiveness. However, their environmental persistence and potential toxicity to non-target organisms have raised major environmental and health concerns [12].

III.1.2 Pesticides classification

Pesticides are classified according to their intended target and their application (Table III.1):

Table III.1: Classification of some pesticides according to their target [13]

Type of pesticide	Target	Example
Herbicides	To control weeds (unwanted plants)	Chloroacetanilide herbicides like Alachlor, Metolachlor and Organic phosphorus herbicides like glyphosate Chlorophenoxy acid herbicides like 2.4-D, 2.4.5-T, MCPA, and Silvex. Triazine herbicides like atrazine, cynazine, hexazinone, metribuzin, and simazine.
Fungicides	To destroy fungi	Captain, copper sulfate, folpet, mancozeb
Insecticides	To kill insects	Organochlorides like cyclodienes (which include aldrin, dieldrin, chlordane, heptachlor, and endrin), DDT, BHC, lindane, Chlorobenzilate, and methoxychlor. Organophosphates and carbamates like parathion, Chlorpyrifos, diazinon, carbaryl, carbofuran, oxamyl, and aldicarb. Repellants like DEET (N, N-Diethyl-m-toluamide) and Bio insecticides like Bacillus thuringiensis, Beauveria Bassiana.
Acaricides	To target Mites, ticks and spiders	DDT, Diazinon, carbaryl, permethrin, flumethrin, formamidines, and avermectins.
Rodenticides	To control moles (rats) and rodents	Warfarin, 1080 (sodium fluoroacetate), and red squill
Larvicides	Larvae	Microbial larvicides, Bacillus sphaericus and Bacillus thuringiensisisraelensis, temephos, methoprene, oils, and monomolecular films.
Nematicides	To control nematodes (Tiny worms)	TeloneII, Paladin (dimethyl disulphide or DMDS), Aldicarb (Temik), chloropicrin, Vapam (metam sodium).
Bactericide	Bacteria	Beta-lactam antibiotics and vancomycin, daptomycin, fluoroquinolones, metronidazole, nitrofurantoin, co-trimoxazole, and telithromycin. Amino glycosidic, antibiotics
Fumigants	Termites, bedbugs	Sulfur dioxide, carbon monoxide, hydrogen cyanide, and methyl bromide

The most commonly used pesticides are [14, 15]:

- **Herbicides:** These are the most widely used in quantity and treated areas. They are designed to eliminate unwanted weeds (adventitious plants) from crops. There are over 35 chemical families within this category, including carbamates (e.g., carbaryl, chlorpropham, triallate), chlorophenoxy acids (e.g., 2.4-D, 2.4.5-T, 4-CPA), amides (e.g., alachlor, propyzamide), substituted ureas (e.g., diuron, chlortoluron), and triazines (e.g., atrazine, simazine).
- **Fungicides:** These agents combat the spread of pathogenic fungi and address fungal diseases, such as potato blight, grapevine mildew, and cereal rusts, which historically caused significant agricultural losses. These diseases result from the invasion of plant tissues by fungal mycelium. The earliest fungicides were copper salts and sulfur-based products. Modern organic fungicides dominate the market, including triazoles (e.g., bromuconazole, triticonazole), benzene derivatives (e.g., chlorothalonil, quintozene), and dicarboximides (e.g., folpet, iprodione).
- **Insecticides:** These are specifically formulated to eliminate harmful insects. Common insecticides include carbamates (e.g., carbosulfan), pyrethroid derivatives, and organophosphates (e.g., bromophos).

Herbicides, fungicides, and insecticides can be designated according to the way they act on undesirable organisms [16]:

Table III.2: Classification based on how the pesticides act on undesirable organisms

Herbicide	
Contact	acts on plant parts with which it comes into contact.
Systemic	absorbed by the plant and moves within it.
Selective	targets only certain plants among those treated.
Non-selective	targets all treated plants
Residual	degrades slowly, providing long-term control of plants.
Non-residual	becomes inactive quickly after application and provides only short-term control
Fungicide	
Preventive	protects the plant by preventing the disease from developing.
Curative	Suppresses a disease that has already developed.
Insecticide	
Contact	acts when the insect comes into contact with the product.
Inhalation	acts when the insect breathes in the product.
Ingestion	acts when the insect consumes the product.

III.1.3. Pesticides evolution and environmental impacts

The use of pesticides dates back to antiquity when the insecticidal properties of arsenic were already known. However, their use increased considerably in the 19th century with advances in inorganic chemistry, particularly copper-based pesticides.

The discovery of chemicals such as DDT during the Second World War marked a turning point in the use of pesticides [17]. Between 1945 and 1985, pesticide consumption doubled

every ten years, due to their important role in increasing agricultural yields and combating diseases such as malaria [18].

Today, the widespread application of pesticides underscores their continued importance in agriculture. For instance, as shown in Figure III.1, Brazil emerged as the world's largest pesticide consumer in 2022, utilizing approximately 800.65 thousand metric tons. The United States followed in second place with 467.68 thousand metric tons, while global pesticide consumption reached a total of 3.69 million metric tons. This surge reflects the reliance on pesticides in intensive farming systems, especially in countries with large-scale monoculture.

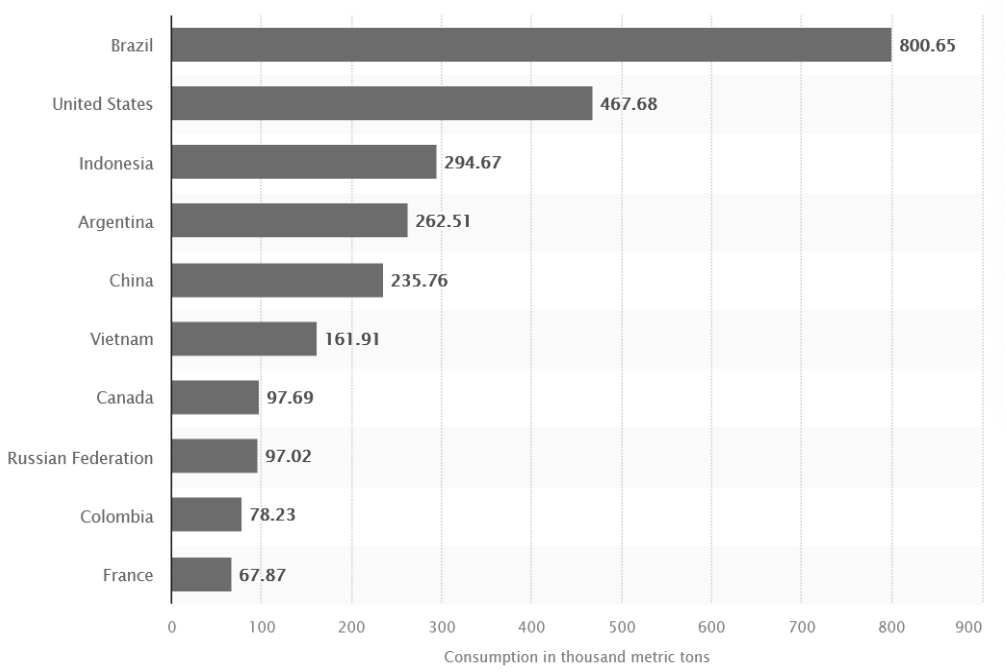

Figure III.1: Setting countries in pesticide usage in worldwide agriculture by 2022 (measured in thousand tons) [19]

In Algeria, the use of pesticides in agriculture is extensive and primarily driven by the need to combat various pests in intensive farming systems. According to the 2015 Algerian Index of Phytosanitary Products, approximately 4517 tons of pesticides were imported for agricultural use, comprising 39% fungicides, 7% insecticides, and 5% herbicides. These active ingredients, classified into 757 commercial formulations, are dominated by insecticides (38%), fungicides (35%), and herbicides (19%) [20].

However, the use of pesticides to increase productivity was accompanied by serious environmental and health consequences. Some pesticides, such as DDT, are poorly

biodegradable and accumulate in living organisms, leading to their gradual banning [21]. Pesticides contaminate water, air, and soil, impacting all parts of the biosphere [22]. This growing pollution is exacerbated by uncontrolled use and agricultural practices such as monoculture and excessive fertilization, which attract pests and increase pesticide dependence [23].

Since the end of the 20th century, environmental concerns have prompted the development of targeted treatments to reduce the impact of pesticides, and efforts to limit their use have become a global priority [24]. While pesticides remain essential to agriculture, their increasing use represents a major environmental challenge, requiring sustainable approaches to balance agricultural needs and ecosystem protection.

III.2. Pesticide toxicity

Pesticides are persistent organic pollutants (POPs) known for their stable physical and chemical properties, making them highly resistant to environmental degradation. They can also be transported over long distances, spreading through air, water, and soil. Once released, these chemicals often break down into various by-products, known as metabolites, which can remain in the environment for many years and continue to pose risks to ecosystems and health [25].

The main risk posed by these persistent substances or their by-products is their ability to enter the food chain. Because of their toxicity and resistance to degradation, pesticides can accumulate in the environment and into the food chain, a process known as bioaccumulation, which poses a serious threat to living organisms.

These characteristics make pesticides highly hazardous, necessitating detailed studies to understand their fate and behavior in the environment. Evaluating the effects of pesticide-related pollution on ecosystems is complex, as their impact depends on factors such as their mode of action (with some being significantly more toxic than others), their persistence over time (with some degrading much faster than others), and the nature of their degradation by-products (metabolites) [26]. These metabolites are often more toxic and degrade slowly than the parent compound.

III.2.1. Presence and behavior of pesticides as POPs in the environment

Research has confirmed the presence of organic pollutants in the environment, especially in aquatic ecosystems. The environmental impact of these compounds is closely tied to their behavior in soil. Once organic pollutants reach the soil, they follow three main pathways (Figure III.2):

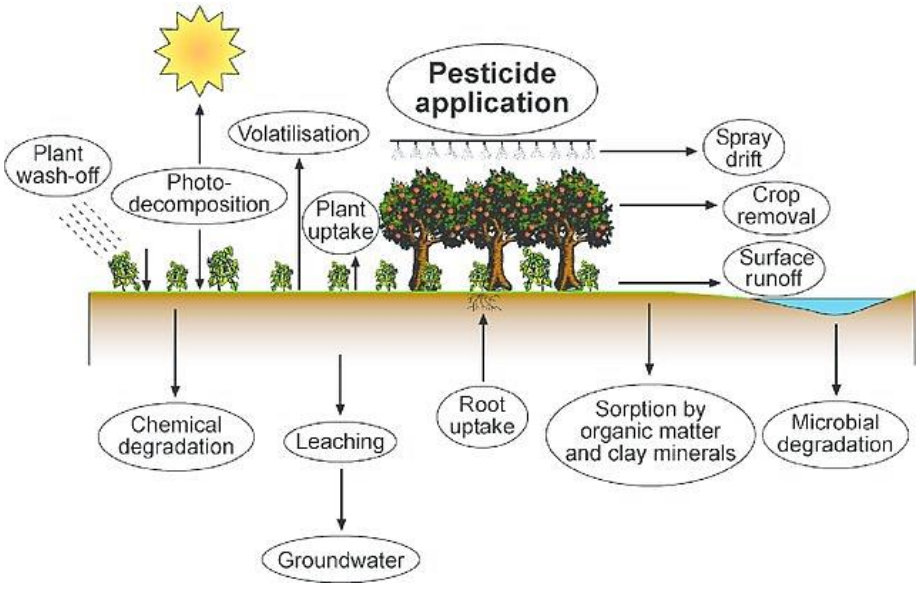

Figure III.2: Processes showing the fate of pesticides in the environment [27]

- **Degradation**

  Pesticides can break down into smaller molecules and eventually into carbon dioxide and water through photochemical, chemical, or biological reactions. During this process, pesticides produce by-products known as metabolites, which often have unique chemical properties and can be more toxic than the parent pesticides.

- **Adsorption by soil and plants**

Soil particles are crucial in trapping pesticides through adsorption, reducing their mobility, and preventing their spread. Plants can also absorb pesticides, lowering their availability and stopping further migration into the environment. Adsorption refers to the attachment of pesticides to soil particles and is influenced by factors such as soil characteristics and pesticide properties. The soil's pH significantly affects the adsorption process by altering the chemical structure of the pesticide.

- **Surface and subsurface movement**

Pesticides move in the environment through rain-induced processes like runoff, infiltration, and transfer to groundwater and water bodies. They can also volatilize and be carried by air currents, with droplets smaller than 100 µm capable of traveling long distances before settling through dry deposition or being washed out by rain. The transfer of pesticides to groundwater (Figure III.2) is a significant concern due to its environmental and health implications [13].

III.2.2. Human toxicological aspects of pesticides

Environmental exposure to pesticides is well documented in cases of acute exposure, often caused by accidents in the chemical industry. However, the risks associated with daily and long-term exposure to low doses of pesticides from food and water are still poorly understood.

This is concerning due to the toxicity of certain substances, which can specifically target the nervous system and cause various health effects. Chronic exposure to these substances has been linked to carcinogenic, immunosuppressive, mutagenic, neurotoxic, and teratogenic effects. Other studies suggest that some chemicals can also disrupt the human hormonal and immune systems [28, 29].

Long-term use of pesticides may also contribute to reduced sperm counts in men. These substances are most often ingested through food residues, but can also be absorbed through drinking water or inhaled air.

Acute pesticide poisoning occurs when symptoms appear shortly after a significant exposure, and these types of poisoning are the most familiar to health professionals [30].

Farmers and workers responsible for preparing mixtures and applying treatments are the most exposed to pesticide-related risks. In addition to their toxic effects, these substances can affect water quality by causing organoleptic nuisances, such as persistent odors or flavors, detectable at thresholds ranging from 0.1 to 1000 µg L^{-1} depending on the molecule. The World Health Organization (WHO) estimates that around one million people worldwide are seriously poisoned by pesticides every year, with approximately 220,000 deaths. Acute pesticide poisoning mainly affects the mucous membranes and skin, as well as the digestive and respiratory systems [31].

III.3. Herbicides

Herbicides account for around 45% of all pesticides used in agriculture [32]. They consist of active ingredients or formulated products capable of eliminating undesirable vegetation. These chemical substances vary according to their composition, their mode of absorption, their impact on weeds, and their elimination process [33].

Herbicides are essential products for controlling weeds that damage crops. Their use extends beyond agriculture to the maintenance of urban spaces, infrastructure such as railroads, and gardening.

Herbicides can be selective, targeting specific plant species, or non-selective, killing a wide range of vegetation. Their action can be either contact, destroying the parts where they are applied, or systemic, penetrating the plant and spreading through the leaves or roots, resulting in a widespread toxic effect [34].

III.3.1. Herbicide mechanisms of action

Herbicides exert their effects through a variety of mechanisms, including:

- Disruption of the photosynthesis process,
- Inhibition of lipid synthesis,
- Blockage of amino acid synthesis,
- Interference with auxin regulation,
- Cell division arrest at the metaphase stage (a process involving plant hormones linked to growth and essential to development),
- Inhibit the production of carotenoids, which protect chlorophyll pigments,
- Inhibit the enzyme PPO (protoporphyrinogen oxidase), which is crucial for chlorophyll synthesis,
- Causing pH imbalances in cellular compartments,
- Disrupting overall plant growth.

These mechanisms collectively target key physiological and biochemical processes in plants, leading to the elimination of unwanted vegetation [35].

III.3.2. Herbicide application methods and environmental impacts

Herbicides can be applied before (pre-emergence) or after (post-emergence) weed growth. However, their propagation in the environment poses major problems. Only a small proportion of the herbicide reaches the target plants, the rest being intercepted by soil,

vegetation, or washed away by rain.

Although some soils can retain herbicides and micro-organisms can break down some of them, many herbicides and their metabolites, which are often non-biodegradable, end up in surface and groundwater. These movements, through leaching or runoff, lead to the contamination of water resources, including those used for human consumption [36].

III.3.3. Herbicide toxicity in humans

Herbicides are extensively utilized in agriculture for weed control, but they pose significant risks to human health. The adverse effects of herbicides depend on various factors, such as chemical class, dosage, exposure duration, and entry route into the body (ingestion, inhalation, or skin contact). Many herbicides target specific plant processes that may also occur in humans and animals, leading to potential toxicity upon exposure [37]. Both low and high doses can be harmful, with increased severity correlating with higher exposure levels [38].

Long-term herbicide exposure is associated with numerous health issues, including cancers and neurodegenerative diseases like Parkinson's and Alzheimer’s [39, 40]. Glyphosate, a widely used herbicide, has been classified by some organizations as a possible human carcinogen. Additionally, herbicide exposure can result in respiratory problems and immune system suppression, heightening susceptibility to other diseases [41].

Dietary exposure to herbicides through food residues is a critical concern. Approximately 35% of cancer cases in the U.S. are linked to diet, with herbicide residues contributing to this risk. Crops genetically modified for herbicide resistance often exhibit higher residue levels, increasing human exposure risk [42].

Beyond cancer risk, studies indicate that high doses of specific herbicides may lead to weight loss due to metabolic disruptions. Herbicides like paraquat are known for severe acute toxicity, causing gastrointestinal distress and lung damage, potentially resulting in death if ingested in large amounts [43]. Long-term exposure to atrazine has been linked to hormonal imbalances affecting reproductive health and development in children [44].

While herbicides are vital for modern agriculture, their potential health impacts necessitate careful management. Enhanced regulations, improved application practices, and the development of safer alternatives are essential to reduce human exposure to these hazardous chemicals [45].

III.3.4. Regulations governing herbicides in water

Given the health and environmental risks posed by herbicides, the WHO, the European Union, and other national or international organizations have established guidelines since the late 1960s to control discharge concentrations, aiming to limit their impact and protect human health and the environment.

For example, on November 3rd, 1998, the European Parliament adopted a directive concerning the quality of water intended for human consumption (Directive N°. 98/83/EC, 1998). Directive N°. 98/83/EC allows a concentration of 0.1 µg L^{-1} for a single pesticide (herbicide, fungicide, or insecticide) and 0.5 µg L^{-1} for all pesticides combined in drinking water.

Later, on October 23, 2000, the European Union adopted Directive No. 2000/60/EC to enhance its water policy for the environment. This directive sets maximum acceptable pesticide and herbicide concentrations in groundwater and surface waters for member states [46].

Algeria, a key participant in the early stages of the United Nations Conferences on Environment and Sustainable Development, has been committed to promoting sustainable development that respects the global environment.

Since the creation of the National Institute for Plant Protection (INPV) in 1975, the mission of controlling plant protection products was carried out by a central structure and decentralized research and experimental stations. In 1987, the phytosanitary law N°. 87-17, passed on August 1st, 1987, expanded the scope of this mission to include all aspects related to the commercialization and storage of these products, including the involvement of phytosanitary inspectors at border posts. The approval process was overseen by the National Commission for Agricultural Phytosanitary Products.

The Algerian government's commitment to rational resource management is evident through the strengthening of the legislative and institutional framework, as well as the many environmental education programs launched.

In 2000, the Ministry of Agriculture established a central directorate for plant protection and technical controls. Executive Decree N°. 2000-234, dated August 14th, 2000, transferred the responsibility for this task from INPV to the Directorate of Plant Protection and Technical Controls (DPVCT). Since then, products subject to approval have been monitored by a biological evaluation committee, made up of experts from technical institutes under the Ministry of Agriculture and Rural Development (MADR), whose main task is to test these substances under real field conditions [47].

III. 4. Pesticide treatment methods

The treatment methods currently used for polluted water can be broadly divided into four categories:

- Physical treatments
- Chemical treatments
- Biological treatment
- Combined treatment methods

Nowadays, several conventional and modified methods are available for pesticide removal, like: hydrolysis, incineration, advanced oxidation processes (O_3/UV, Fenton oxidation, etc.), UV-TiO_2-based photocatalytic degradation, combined photo-Fenton and biological oxidation, membrane-filtration methods like nanofiltration, ultrafiltration, reverse osmosis and electrodialysis, ozonation, coagulation, fluid extraction, solid phase extraction, and adsorption, absorption or sorption (inorganic, organic absorbents and activated carbon), composting, bioaugmentation, phytoremediation, and aerobic degradation [48].

III. 4. 1. Physical treatments

Membrane Filtration Methods [49]: Effectively removing pesticide molecules based on size exclusion and chemical compatibility. Common techniques include:

- Nanofiltration (NF): Capable of removing organic micro-pollutants like atrazine, achieving retention rates of over 95%.
- Reverse Osmosis (RO): Can separate small pesticide molecules but requires high operational pressure, making it energy-intensive [50].
- Pre-treatment Integration: Membrane systems often incorporate pre-treatments like coagulation and adsorption to minimize fouling and enhance effectiveness.

The adsorption technique is one of the most cost-effective methods, relying on materials like activated carbon. Due to its large surface area and porosity, activated carbon is highly efficient in adsorbing a wide range of pesticides [51-53].

- Biochar: A low-cost alternative derived from biomass. For example, biochar from wood or agricultural residues demonstrates high sorption capacities for herbicides like atrazine.
- Synthetic Adsorbents: Engineered polymers, clays, and chitosan composites enhance adsorption capacities and reduce costs.

- Natural Adsorbents (Bio-adsorbents): Materials such as zeolites, clays, and ores offer eco-friendly options for water treatment.

III. 4. 2. Chemical treatments

Advanced Oxidation Processes (AOPs) [54, 55]: AOPs rely on highly reactive radicals like hydroxyl (OH•) or sulfate ($SO_4^{\bullet -}$) to degrade persistent pesticide molecules into simpler, less toxic forms. Key methods include:

- Ozonation: Ozone breaks down pesticides either directly or via free radical generation. For instance, ozonation effectively removes pesticides like atrazine and diuron, but its efficiency depends on the molecule and system design. Limitations include high energy costs and the potential formation of toxic byproducts[56].
- Fenton Processes: Hydrogen peroxide (H_2O_2) and ferrous iron (Fe^{2+}) are used to produce hydroxyl radicals. This method is particularly effective for degrading organic pollutants and can achieve high removal rates [57].
- Photochemical Degradation: Uses UV light and photocatalysts such as titanium dioxide (TiO_2) to oxidize pesticides. This method has been successful in mineralizing carbofuran and atrazine. New methods incorporate green nanocomposites for greater efficiency [58].

III. 4. 3. Biological treatments

This approach uses microorganisms or enzymes to degrade pesticides into less harmful components. Key strategies include:

- Bioaugmentation: Addition of specific microbial strains that can metabolize pesticides, enhancing natural degradation.
- Biomixtures and Biofilters: Contain humic materials, soil, and microorganisms tailored to degrade pesticides, particularly fungicides and herbicides.
- Ligninolytic Fungi: These fungi produce enzymes that break down pesticide molecules containing lignin-like structures, for instance, Trametes versicolor effectively degrades triazoles.

- Aerobic and Anaerobic Processes: Under aerobic conditions, microorganisms oxidize pesticides into biodegradable intermediates. Anaerobic processes, such as using bioreactors, break down organochlorines and other toxic compounds [48, 59].

However, not all pesticides are easily biodegradable, so pretreatment steps like photochemical oxidation may be required to improve biodegradability.

III. 4. 4. Hybrid methods - Integrated treatment approaches

Hybrid treatments are a form of combined treatment, where two or more methods are integrated to take advantage of their combined benefits and overcome the limitations of individual processes. For pesticide removal, hybrid treatments combine physical, chemical, or biological methods to increase the performance of the treatment, reduce operational costs, or address specific challenges caused by persistent pollutants [60, 61].

- Photo-Fenton and Biological Oxidation: Combine the advanced oxidation of Fenton's reaction with biological treatment, achieving high removal rates of bio-recalcitrant pesticides.
- Adsorption-Coagulation Systems: Improve overall efficiency compared to standalone methods. For instance, coagulation with nano-clays followed by activated carbon adsorption achieves 60% higher removal than coagulation alone.
- Membrane + Adsorption: Pairing ultrafiltration or nanofiltration membranes with powdered activated carbon enhances removal rates for persistent organics and reduces pollution [48, 62].

References of Chapter III

[1] A. Abbasi, A. Sajid, N. Haq, S. Rahman, Z.-t. Misbah, G. Sanober, M. Ashraf, A.G. Kazi, Agricultural pollution: an emerging issue, Improvement of Crops in the Era of Climatic Changes: Volume 1, (2014).

[2] R.R. Karri, G. Ravindran, M.H. Dehghani, Wastewater—sources, toxicity, and their consequences to human health, in: Soft computing techniques in solid waste and wastewater management, Elsevier, (2021).

[3] S.V. Rathod, P. Saras, S.M. Gondaliya, Environmental Pollution: Threats and Challenges for Management, in: Eco-Restoration of Polluted Environment, CRC Press, (2025).

[4] N. Akhtar, M.I. Syakir Ishak, S.A. Bhawani, K. Umar, Various natural and anthropogenic factors responsible for water quality degradation: A review, Water, 13 (2021).

[5] L. Rani, K. Thapa, N. Kanojia, N. Sharma, S. Singh, A.S. Grewal, A.L. Srivastav, J. Kaushal, An extensive review on the consequences of chemical pesticides on human health and environment, Journal of cleaner production, 283 (2021).

[6] A. Ahamad, S. Madhav, A.K. Singh, A. Kumar, P. Singh, Types of water pollutants: conventional and emerging, Sensors in water pollutants monitoring: Role of material, (2020).

[7] H. Zeliger, Human toxicology of chemical mixtures, William Andrew, (2011).

[8] K. Rajmohan, R. Chandrasekaran, S. Varjani, A review on occurrence of pesticides in environment and current technologies for their remediation and management, Indian journal of microbiology, 60 (2020).

[9] K. Paranjape, V. Gowariker, V. Krishnamurthy, S. Gowariker, The pesticide encyclopedia, Cabi, (2014).

[10] I. M. Brasil, M.W. Siddiqui, Postharvest quality of fruits and vegetables: An overview, Preharvest modulation of postharvest fruit and vegetable quality, (2018).

[11] M.F.B. Mfarrej, F.M. Rara, Competitive, sustainable natural pesticides, Acta Ecologica Sinica, 39 (2019.

[12] A. Hassan, Inorganic-based pesticides: A review article, Egypt Sci J Pestic, 5 (2019).

[13] H. ZAZOU, Dégradation de pesticides dans l'eau par les procédés d'oxydation avancée (POA), Thesis, (2015).

[14] R. Kaur, G.K. Mavi, S. Raghav, I. Khan, Pesticides classification and its impact on environment, Int. J. Curr. Microbiol. Appl. Sci, 8 (2019).

[15] S.U. Khan, Pesticides in the soil environment, Elsevier, book, (2016).

[16] cottineau, Https://www.cottineau.net/qu-est-ce-qu-un-pesticide/), cited in (2024)

[17] J.C. Whorton, Before Silent Spring: Pesticides and public health in pre-DDT America, Princeton University Press, (2015).

[18] G. Manasa, B. Karishma, C.S. Rout, Emerging agricultural and environmental pollutants: their impact on public health, in: Electrochemical Interfaces for the Detection of Agricultural Pollutants, IOP Publishing Bristol, UK, (2024).

[19] statista, https://www.statista.com/statistics/1263069/global-pesticide-use-by-country/, cited in, (2024).

[20] F. Bettiche, W. Chaib, A. Halfadji, H. Mancer, K. Bengouga, O. Grunberger, The human health problems of authorized agricultural pesticides: The Algerian case, Microbial Biosystems, 5 (2021).

[21] M. Bilal, H.M. Iqbal, D. Barceló, Persistence of pesticides-based contaminants in the environment and their effective degradation using laccase-assisted biocatalytic systems, Science of The Total Environment, 695 (2019).

[22] P. Rajak, S. Roy, A. Ganguly, M. Mandi, A. Dutta, K. Das, S. Nanda, S. Ghanty, G. Biswas, Agricultural pesticides–friends or foes to biosphere?, Journal of Hazardous Materials Advances, 10 (2023).

[23] S.J. Kraham, Environmental impacts of industrial livestock production, International Farm Animal, Wildlife and Food Safety Law, (2017).

[24] M. Tudi, H. Daniel Ruan, L. Wang, J. Lyu, R. Sadler, D. Connell, C. Chu, D.T. Phung, Agriculture development, pesticide application and its impact on the environment, International journal of environmental research and public health, 18 (2021).

[25] WHO, Health risks of persistent organic pollutants from long-range transboundary air pollution.

[26] L. Tison, L. Beaumelle, K. Monceau, D. Thiery, Transfer and bioaccumulation of pesticides in terrestrial arthropods and food webs: State of knowledge and perspectives for research, Chemosphere, 357 (2024).

[27] A.K. Sarmah, K. Müller, R. Ahmad, Fate and behaviour of pesticides in the agroecosystem, a review with a New Zealand perspective, Soil Research, 42 (2004).

[28] E.D. Caldas, Toxicological aspects of pesticides, Sustainable agrochemistry: A compendium of technologies, (2019).

[29] V.P. Kalyabina, E.N. Esimbekova, K.V. Kopylova, V.A. Kratasyuk, Pesticides: formulants, distribution pathways and effects on human health–a review, Toxicology reports, 8 (2021).

[30] W. Boedeker, M. Watts, P. Clausing, E. Marquez, The global distribution of acute unintentional pesticide poisoning: estimations based on a systematic review, BMC public health, 20 (2020).

[31] Z. Behnas, Activation des noyaux de jujube pour l'obtention d'un charbon actif, Thesis, (2018).

[32] F.B. Benabed, S. Attouti, N. Douara, M. Termoul, M. İmamoğlu, A. Çoruh, N. Boukabcha, N. Benderdouche, B. Bestanı, Theoretical study of the herbicide parachlorophenoxyacetic acid molecule and its removal by activated carbon prepared from pine cone, Desalination and Water Treatment, 320 (2024).

[33] C.M. Raffa, F. Chiampo, Bioremediation of agricultural soils polluted with pesticides: A review, Bioengineering, 8 (2021).

[34] S.I. Sherwani, I.A. Arif, H.A. Khan, Modes of action of different classes of herbicides, Herbicides, physiology of action, and safety, 10 (2015).

[35] I. Jablonkai, Molecular mechanism of action of herbicides, Herbicides—Mechanisms and Mode of Action, (2011).

[36] Didi. Mabrouka, Prédiction de la toxicité d'une série d'amides herbicides, Thesis, 2010.

[37] W. Aktar, D. Sengupta, A. Chowdhury, Impact of pesticides use in agriculture: their benefits and hazards, Interdisciplinary toxicology, 2 (2009).

[38] R. Mohd Ghazi, N.R. Nik Yusoff, N.S. Abdul Halim, I.R.A. Wahab, N. Ab Latif, S.H. Hasmoni, M.A. Ahmad Zaini, Z.A. Zakaria, Health effects of herbicides and its current removal strategies, Bioengineered, 14 (2023).

[39] K. Muthukumaran, A.J. Laframboise, S. Pandey, Herbicides and the risk of Neurodegenerative Disease, Herbicides-Mechanisms and Mode of Action, (2011).

[40] F.S. Galli, M. Mollari, V. Tassinari, C. Alimonti, A. Ubaldi, C. Cuva, D. Marcoccia, Overview of human health effects related to glyphosate exposure, Frontiers in Toxicology, 6 (2024).

[41] E. Nwanaforo, C.N. Obasi, C. Frazzoli, O. Bede-Ojimadu, O.E. Orisakwe, Exposure to Environmental Pollutants and Risk of Diarrhea: A Systematic Review, Environmental Health Insights, 18 (2024).

[42] interchopen, https://www.intechopen.com/chapters/44984#, cited in, 2024.

[43] T. Ustuner, A. Sakran, K. Almhemed, Effect of herbicides on living organisms in the ecosystem and available alternative control methods, Int. J. Sci. Res. Publ, 10 (2020).

[44] G. Van Maele-Fabry, L. Gamet-Payrastre, D. Lison, Residential exposure to pesticides as risk factor for childhood and young adult brain tumors: A systematic review and meta-analysis, Environment international, 106 (2017).
[45] G. Matthews, Pesticides: health, safety and the environment, John Wiley & Sons, (2015).
[46] A. M. ALI, Étude d'un procédé d'oxydation avancée couplé plasma non thermique/carbone activé fonctionnalisé pour le traitement d'herbicides dans l'eau, (2024).
[47] M. Ferfar, Toxicité et Bioaccumulation de Pesticides sur quelques Variétés de Blé dur (T. durum desf) Thesis, (2017)
[48] A. C. Gheidene, A. Zehhaf, S. Messekine, F. Z. Soufal, T. Laoui, Advanced leachate treatment at Mascara landfill (Algeria): A hybrid pilot approach with activated sludge and ferric chloride, Desalination and Water Treatment, 319 (2024) .
[49] S. Yadav, A.K. Chauhan, S. Kumar, N. Kataria, Advanced membrane technology for the removal of pesticides from water and wastewater, in: Pesticides remediation technologies from water and wastewater, Elsevier, (2022).
[50] K.V. Plakas, A.J. Karabelas, Removal of pesticides from water by NF and RO membranes, A review, Desalination, 287 (2012).
[51] K. Ignatowicz, Selection of sorbent for removing pesticides during water treatment, Journal of Hazardous Materials, 169 (2009).
[52] A. Mojiri, J.L. Zhou, B. Robinson, A. Ohashi, N. Ozaki, T. Kindaichi, H. Farraji, M. Vakili, Pesticides in aquatic environments and their removal by adsorption methods, Chemosphere, 253 (2020).
[53] K. Iwuozor, E. Emenike, F. Gbadamosi, J. Ighalo, G. Umenweke, F. Iwuchukwu, C. Nwakire, C. Igwegbe, Adsorption of organophosphate pesticides from aqueous solution: a review of recent advances, International Journal of Environmental Science and Technology, 20 (2023).
[54] A. Giwa, A. Yusuf, H.A. Balogun, N.S. Sambudi, M.R. Bilad, I. Adeyemi, S. Chakraborty, S. Curcio, Recent advances in advanced oxidation processes for removal of contaminants from water: A comprehensive review, Process Safety and Environmental Protection, 146 (2021).
[55] C. Martínez-Sánchez, I. Robles, L. Godínez, Review of recent developments in electrochemical advanced oxidation processes: application to remove dyes, pharmaceuticals, and pesticides, International Journal of Environmental Science and Technology, 19 (2022).
[56] C.V. Rekhate, J. Srivastava, Recent advances in ozone-based advanced oxidation processes for treatment of wastewater-A review, Chemical Engineering Journal Advances, 3 (2020).

[57] S. Sangami, B. Manu, Fenton's treatment of actual agriculture runoff water containing herbicides, Water Science and Technology, 75 (2017).

[58] M. Zeshan, I.A. Bhatti, M. Mohsin, M. Iqbal, N. Amjed, J. Nisar, N. AlMasoud, T.S. Alomar, Remediation of pesticides using TiO2 based photocatalytic strategies: A review, Chemosphere, 300 (2022) 134525.

[59] I.A. Saleh, N. Zouari, M.A. Al-Ghouti, Removal of pesticides from water and wastewater: Chemical, physical and biological treatment approaches, Environmental Technology & Innovation, 19 (2020) 101026.

[60] S. Akinapally, B. Dheeravath, K.K. Panga, H. Vurimindi, S. Sanaga, Treatment of pesticide intermediate industrial wastewater using hybrid methodologies, Applied Water Science, 11 (2021) 1-7.

[61] S.S. Rasooly, M. Anwer, G. Tsnim, A Review on Treatment Methods for Pesticide Contaminated Water, Journal of Environmental Science e Toxicology and Food Technology, 16 (2022) 24.

[62] A.A. de Almeida Alves, G.L. de Oliveira Ruiz, T.C.M. Nonato, C. Pelissari, A. Dervanoski, M.L. Sens, Combined microfiltration and adsorption process applied to public water supply treatment: water quality influence on pesticides removal, Environmental Technology, (2020).

Section B

Experimental procedure and findings

CHAPTER IV:

MATERIALS AND METHODS

Introduction

This chapter provides information on the chemical reagents used in the application of the analytical methods, the materials prepared, the methodologies adopted for the methods used in the study, and the various experimental protocols applied.

As part of our in-depth discussions, we explored the elaboration protocols and the various analytical methods implemented to characterize the prepared material, namely activated carbon. A detailed explanation of the techniques used to evaluate and understand the physicochemical properties, structures, and characteristics of the adsorbent material resulting from the protocols applied is given.

The growing demand for adsorbent materials for environmental protection processes has driven further research into the manufacture of activated carbons from alternative materials, in particular forestry waste.

In this study, we chose to produce activated carbons from a renewable and less expensive precursor, pine cone, also known as maritime pine, to obtain a product applicable to water treatment and, particularly, to the removal of herbicidal pollutants. We focused on two herbicides, para-chlorophenoxyacetic acid "*P-CPA*" and Linuron "*Lin*".

This chapter is divided into three parts:

The first part focuses on the protocols followed for preparing activated carbons, including the parametric study and optimization of activation parameters. It also covers the application of both chemical and physical methods to determine the most suitable protocol for obtaining activated carbon with controlled porosity.

The second part addresses the analytical methods used to characterize the prepared activated carbons. It outlines the techniques for assessing the overall quality of the adsorbent materials, their physicochemical properties, and textural and structural studies to examine the features of the developed activated carbons.

The third part is dedicated to application studies, including adsorption tests performed on the optimized activated carbons (prepared using chemical and physical activation) with these specific herbicides to evaluate their adsorption capacity and confirm the control of their porosity.

Ⅳ. 1. Part 1: Preparation of activated carbon from pine cone

Ⅳ. 1.1. Choice of the precursor "pine cone"

Pine cones are produced annually as a by-product of agriculture worldwide. Like all agricultural waste, this precursor primarily comprises lignin, cellulose, and tannins. Some of these components, such as phenolic groups of lignin, polysaccharides, and tannins, can stain treated water [1]. Various activation techniques have been investigated to improve its adsorption capacity of pine cone [2-6].

Several studies on Algerian pine have shown that stone pine cones are a valuable source of essential oils with therapeutic effects [7, 8]. However, activated carbon is made from the pine cones rejected by the tree, which are considered worthless waste. This aims to provide an alternative use for this waste and meet the needs of other industrial sectors [9].

Producing adsorbents from lignocellulosic materials helps preserve the environment and adds value to pine cone wood, which is often considered waste. Using pine cones to produce activated carbon addresses the issue of solid waste accumulation, including green waste from forestry and agriculture, while also finding applications for by-products from stone pine cultivation. This approach offers an environmentally friendly solution to managing large amounts of forestry waste left after fruit extraction. Therefore, the conditions of availability, abundance, and renewability, as well as the effectiveness of this waste, motivated us to valorize it as an adsorbent for removing herbicides [10].

In our research, Algerian pine cones (**pine cone precursor "PCP"**) were collected from the Touakas mountains in the Sig-Mascara area in western Algeria and served as raw material for preparing activated carbon.

Figure IV.1. 1: Photos of pine cones

Ⅳ. 1. 2. Preparation of activated carbons

Ⅳ. 1. 2. 1 Chemical activation using KOH as an activating agent in a muffle oven

IV. 1. 2. 1. a Comparison between one-step and two-step chemical activation protocols

The activated carbon preparation processes were carried out under similar experimental conditions. The as-collected material (PCP) underwent a series of preparation steps. Initially, pine cones were cleaned of dust using tap water. Then, they were air-dried until completely free of moisture. After drying, the pine cones were fragmented into smaller pieces and ground and sieved using a Retsch siever to a size of 0.14 mm and were rinsed several times with distilled water until the color of the rinsing water completely disappeared. Finally, they were dried in a drying oven set at 70 °C (**Consult Appendix 1**).

In the one-step activation process, 40 g of ground pine cone precursor "PCP" was directly impregnated at a 1:1 KOH activator/PCP impregnation weight ratio. The impregnated pine cones were filtered and placed in crucibles after being dried overnight in the oven at 70 °C, then subjected to a temperature of 800 °C in a muffle oven (**Consult Appendix 1**) for 30 min at a heating rate of 5 °C min^{-1} while in the two-step process, the **PCP** sample was first carbonized at 600 °C for 1 h at a 10 °C min^{-1} heating rate. The chemical activation procedure (impregnation and heating) was the same as the one-step activation procedure. Subsequently, the pyrolyzed material was rinsed with distilled water until it reached a neutral pH.

After drying, the resulting activated carbons, designated as **K-AC$_1$** and **K-AC$_2$**, were mechanically ground using a laboratory grinder FRITSCH pulverisette type 02.102 N° 4439 and finally sieved using a Retsch siever (Consult Appendix 1) to a particle size of 45 µm.

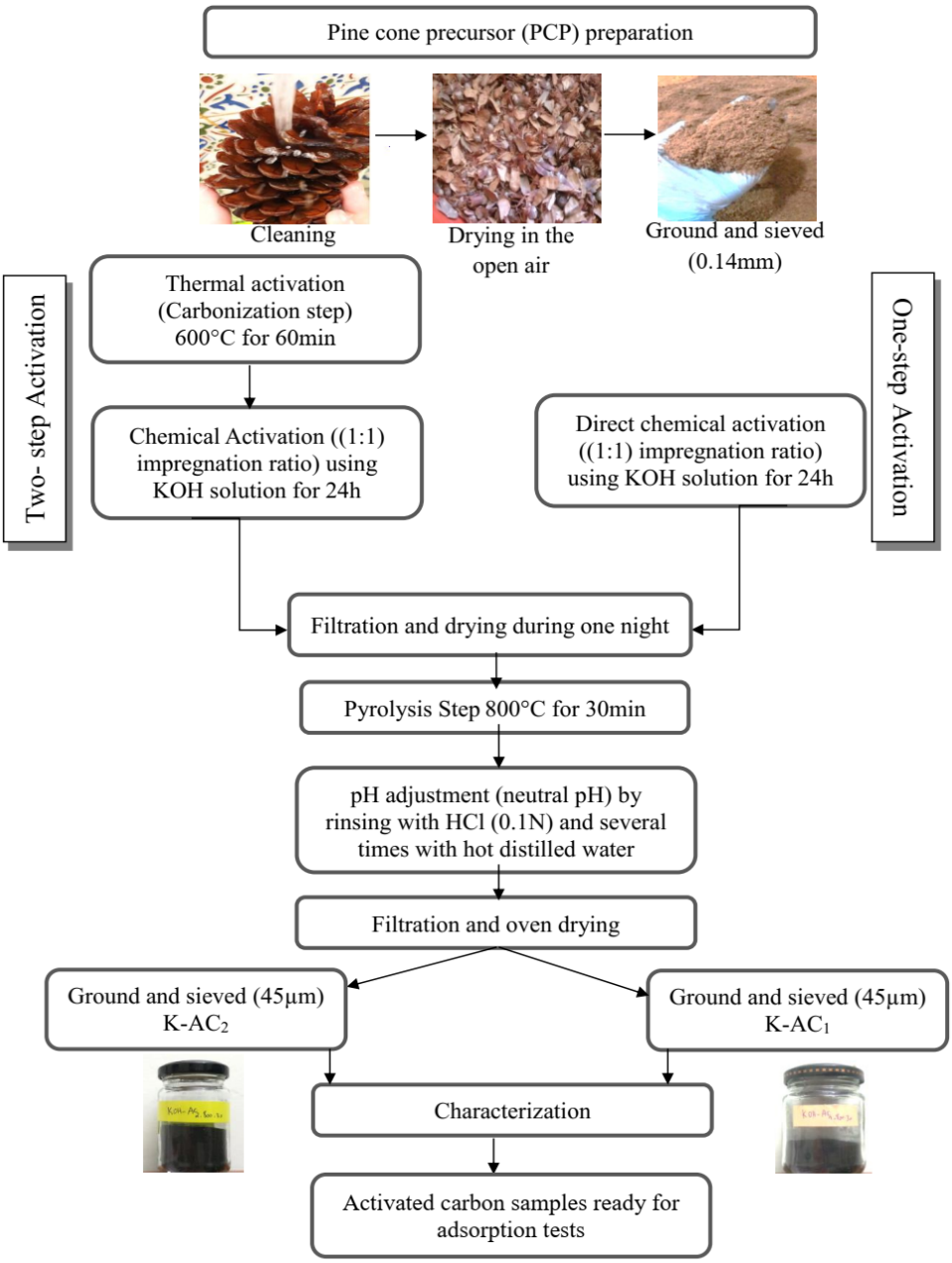

Figure IV.1. 2: Description of one-step and two-step activation protocols

IV. 1. 2. 1. b. Parametric study applied to control activated carbon's porosity

To prepare an activated carbon with controlled porosity, it is important to select the appropriate protocol that gives either a microporous or mesoporous activated carbon. For that reason, a parametric study was conducted by optimizing the activating parameters, which are

carbonization temperature (T(°C)), activation time (hour), and impregnation ratio. In a muffle oven, the activation parameters were optimized in one-step and two-step activation methods:

In one-step activation, the carbonization time was set to 30 minutes and only the activation temperature was changed. In this process, a mass of ground **PCP** was impregnated in a 1:1 ratio and then carbonized at 600°C for 30 minutes to produce **K-AC$_1$'**.

For two-step activation, an initial carbonization step was applied 600°C for 1 hour by activation under controlled conditions, where the activation temperature was varied between 600°C and 700°C for 30 minutes using an impregnation ratio of 1:1, leading to the formation of **AC$_{600.30}$** and **AC$_{700.30}$**.

To investigate the effect of the impregnation ratio on porosity, a two-stage protocol at 800°C for 30 minutes was applied, with the impregnation ratio increased to 1:2, producing **K-AC$_2$'**.

In addition, the activation temperature (for an impregnation ratio of 1:1) was varied to 600°C, 700°C and 800°C, with activation times of 45 and 60 minutes for each temperature. This process led to the preparation of **AC$_{600.45}$**, **AC$_{700.45}$**, **AC$_{800.45}$**, **AC$_{600.60}$**, **AC$_{700.60}$** and **AC$_{800.60}$**.

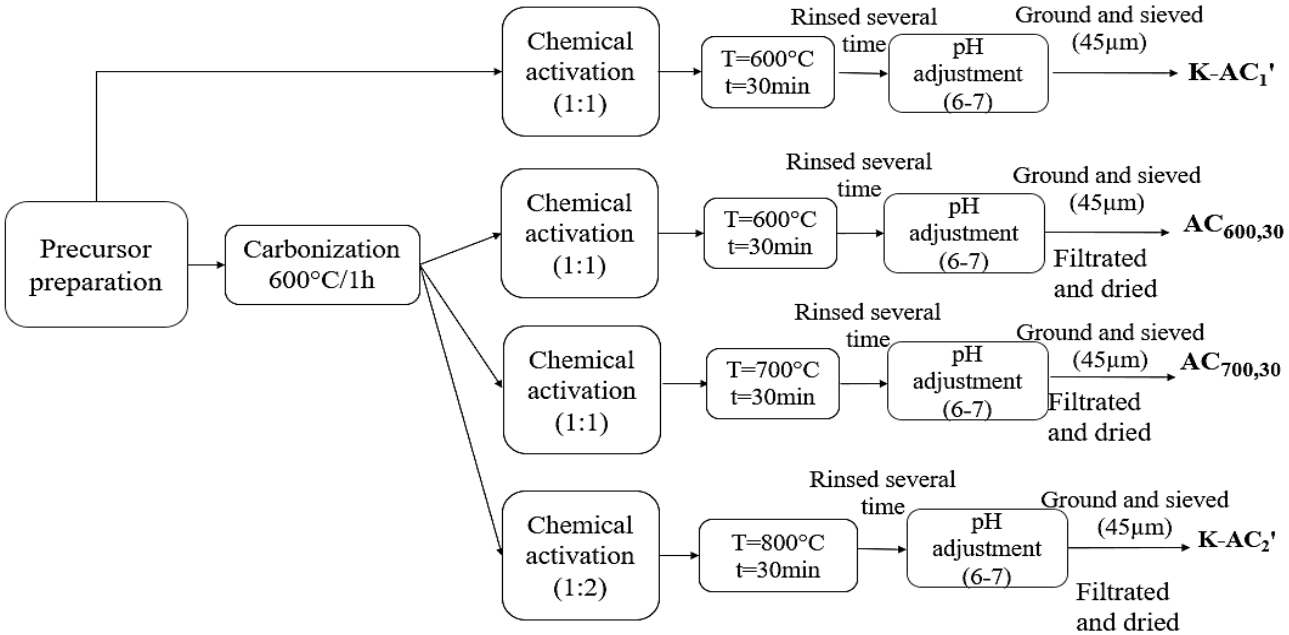

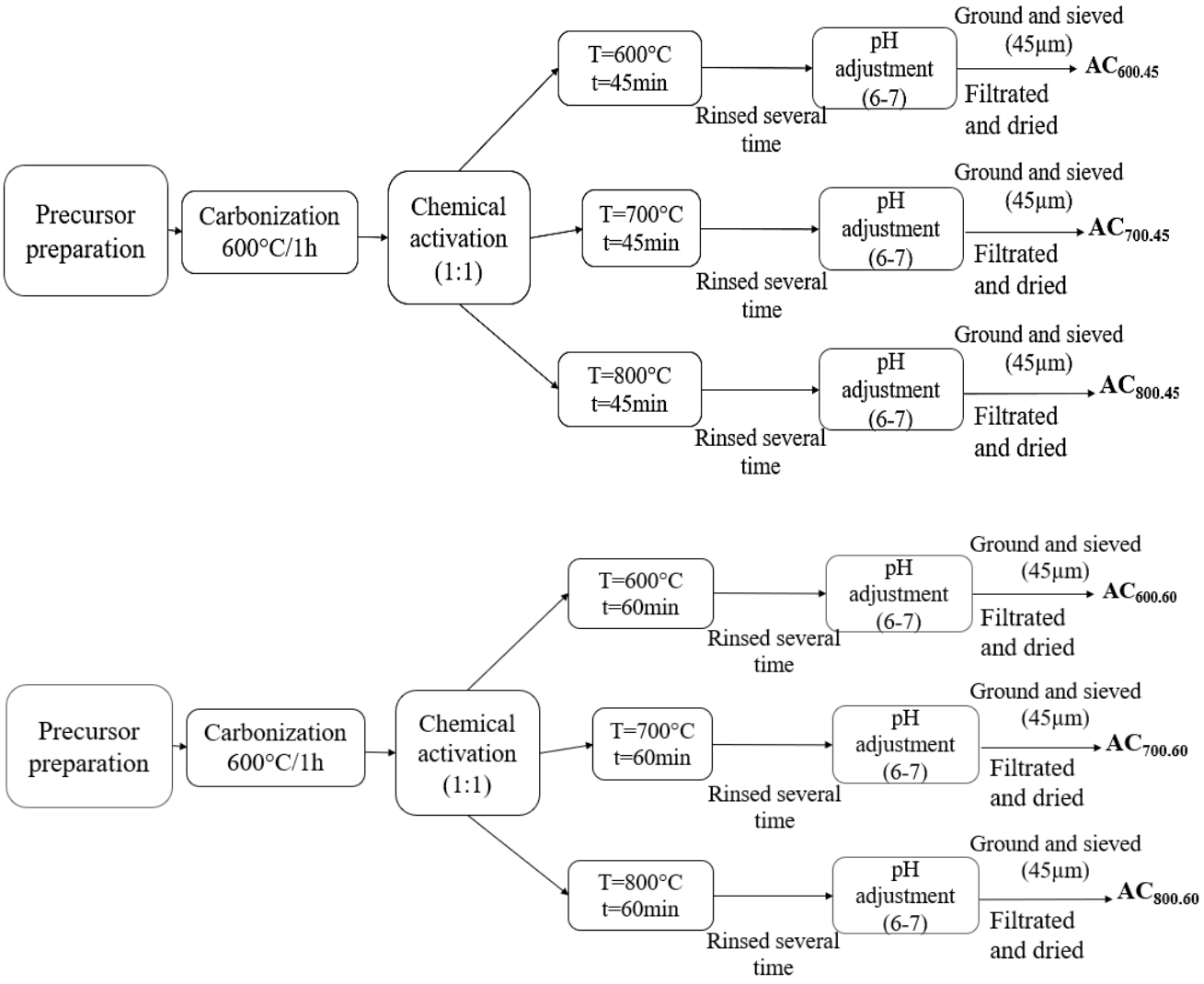

Figure IV.1. 3: Description of the parametric study protocols in a muffle oven

Ⅳ. 1. 2. 2. Combined activation using KOH as an activating agent in a tube furnace under nitrogen atmosphere

This research part performed a combined activation method. The activated carbons synthesis was executed under controlled experimental conditions, utilizing a PROTHERM tubular furnace. (**Consult Appendix 1**)

A mass of **PCP** was directly pyrolyzed for 30 min at 800°C in a PROTHERM tubular furnace under an inert nitrogen atmosphere to prepare **AC** as a charcoal.

In the one-step chemical activation process, a quantity of ground PCP was directly impregnated at a 1:1 rate to prepare **AC**$_1$ and a 1:2 ratio to prepare **AC**$_1$**'**. The impregnated PCP were filtered and placed in crucibles after being dried overnight in the oven at 70 °C, then

subjected to a temperature of 800 °C for 30 min at a heating rate of 5 °C min^{-1} in a PROTHERM tubular furnace (**Consult Appendix 1**), this protocol was applied to prepare the **AC_1** and **AC_1'.**

In the two-step activation using the same tube furnace, we have also prepared **AC_2** and **AC_2'**. A mass of **PCP** was first carbonized at 600 °C for 1 h at a 10 °C min^{-1} heating rate. The activation procedure was at two different impregnation ratios (1:1 and 1:2). The activation temperature and time were fixed at 800°C for 30min under an inert nitrogen atmosphere. The pyrolyzed materials were then washed with distilled water until they reached a neutral pH. After drying, **AC, AC_1, AC_1', AC_2,** and **AC_2'** were mechanically ground using a laboratory grinder FRITSCH pulverisette type 02.102 N° 4439 and finally sieved to a particle size of 63 µm.

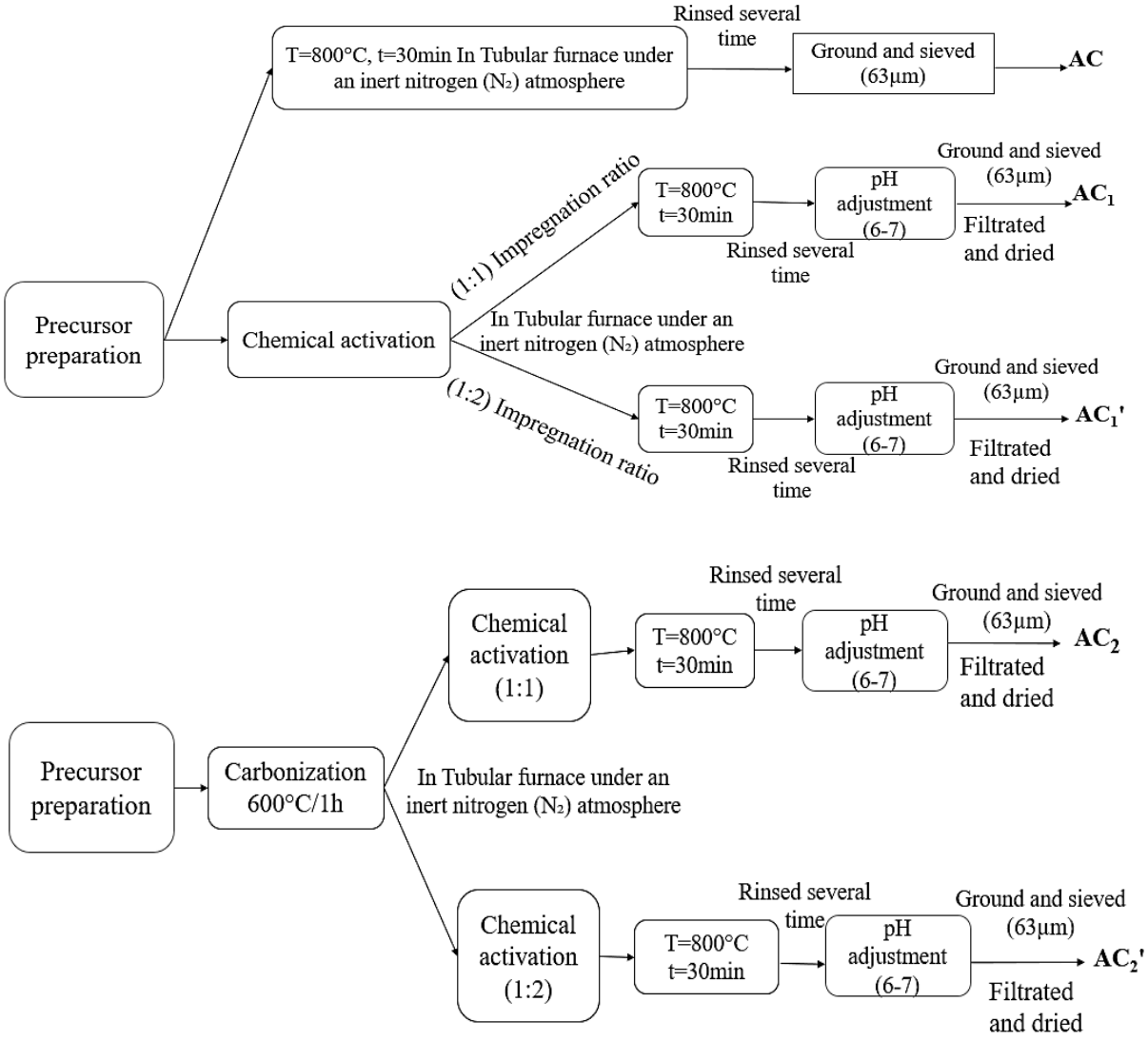

Figure IV.1. 4: Schematic description of the combined activation in a tube furnace under a nitrogen atmosphere

IV. 2. Part 2: Characterization methods and instruments used in the study

This section presents an overview of the main instruments and equipment used to prepare, characterize, and test activated carbon in this study. Each device is described below to facilitate understanding of the applied methodologies.

Ⅳ. 2. 1 Thermogravimetric analyzer (TGA)

A thermogravimetric analyzer was used to investigate the precursor material's thermal stability and decomposition behavior, as well as to evaluate the activation process. Thermogravimetric analysis was carried out using a TGA analyzer, Discovery TA-SDT650.

A quantity of the PCP sample was heated in an aluminum pan up to 800 °C at a ramp rate of 10 °C·min^{-1} in an inert atmosphere. The lost mass of the sample was plotted as a function of temperature (**Fig V. 1. 1.** in results and discussion chapter)

Figure IV.2. 1: Thermogravimetric analyzer Discovery TA-SDT650 used for thermal analysis

Ⅳ. 2. 2. BET Surface area analyzer

The standard method for measuring the specific surface area of an adsorbent is based on the physical adsorption of a gas on the surface of a solid. Nitrogen is commonly used for this purpose due to its low saturation vapor pressure at liquid nitrogen temperature.

Experimental data from the adsorption isotherm, combined with the Brunauer-Emmett-Teller (BET) equation, are used to determine the volume of gas required to form a monolayer on the surface of the sample. The amount of gas adsorbed at monolayer coverage is then used to calculate the specific surface area, expressed in m² g^{-1}. The BET analyzer Micromeritics

3Flex instrument was used to measure specific surface area, pore volume, and pore size distribution of the activated carbon, along with other parameters such as BJH adsorption/desorption surface area, Langmuir surface area, Dubinin volume, and micropore surface area. The measurements were performed within a relative pressure range (P/P_0) from 0.01 to 1. Before analysis, the samples were degassed overnight at 200 °C under a vacuum of 674.6 mm Hg. Nitrogen adsorption-desorption isotherms were then recorded, and the BET specific surface area was calculated using the BET equation. A sample weight of 0.2 g was used for each analysis.

For measurements using the Quantachrome NovaTouch BET surface area analyzer, a smaller sample weight of 0.02 g was used, with analyses conducted at 77 K within the relative pressure range of 0.01 to 1.

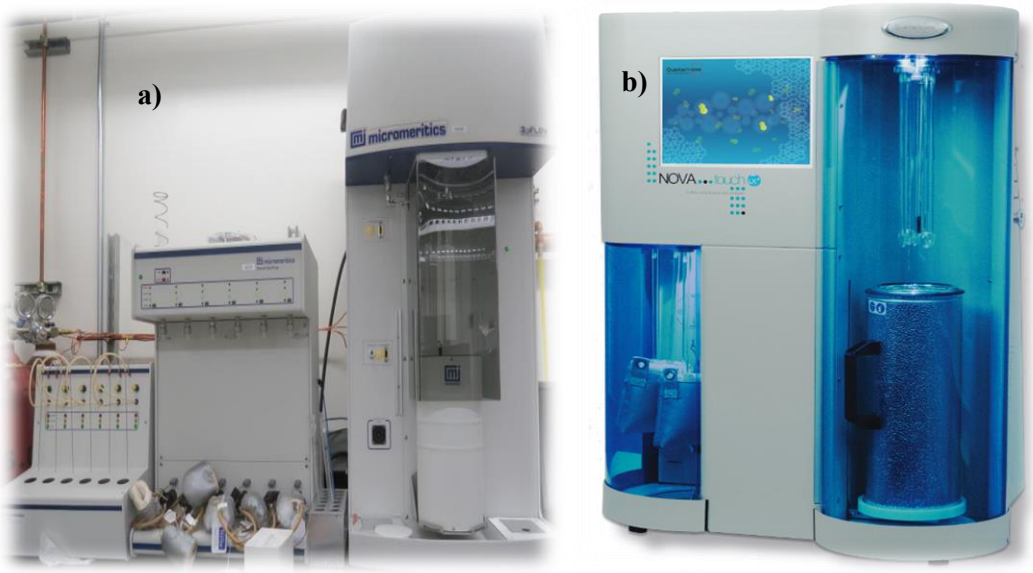

Figure IV. 2. 2: a) Micromeritics 3Flex BET Surface area analyzer [11]. **b)** Quantachrome Novatouch BET surface area analyzer [12] (representative instrument picture)

IV. 2. 3. Scanning electron microscope with energy dispersive spectroscopy (SEM-EDS)

The scanning electron microscope (SEM) (**Figure IV. 2. 3**) coupled with energy dispersive spectroscopy (EDS) was employed to analyze the textural morphology, surface structure, and elemental composition of the activated carbon.

The SEM provided detailed images of surface features, such as pore structure, and the EDS functionality enabled qualitative and quantitative elemental analysis, offering insights into the distribution of chemical elements across the material's surface. This combination was instrumental in correlating the morphological characteristics with the chemical properties of the activated carbon.

These characterizations were investigated using a scanning electron microscope EDAX TEAM) equipped with an X-ray spectrometer for energy dispersive spectroscopy (EDS)

Another instrument was also used named GRESHAM Sirius JEOL (JSM-6060LV) equipped with an X-ray spectrometer for energy dispersive spectroscopy (EDS).

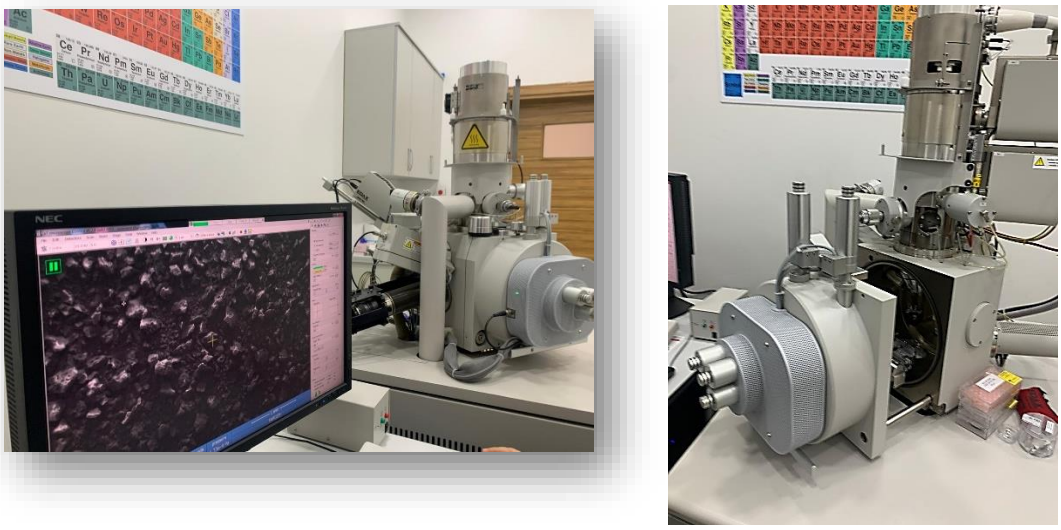

Figure IV. 2. 3: SEM-EDS used for morphological and elemental characterization

Ⅳ. 2. 4. X-ray diffraction (XRD)

The purpose of the X-ray diffraction (XRD) examination was to determine if the activated carbon was crystalline or amorphous. The method revealed details about the carbon atoms' structural arrangement as well as the existence of any residual crystalline phases from the activation process or precursor material. The instrument that was used for our characterization was named Rigaku X-Ray Diffractometer.

Figure IV. 2. 4: X-ray diffractometer (XRD) used for structural analysis

Ⅳ. 2. 5. FT-IR spectrometer

Infrared spectrometry is a nondestructive analytical method that studies the absorption of electromagnetic radiation by a sample in the wavelength range (λ) of 1 to 1000 μm, corresponding to wavenumbers (ν=1/λ) between 1 and 10^{-3} μm^{-1}. Spectra were recorded in absorbance mode at room temperature over a wavenumber range of 4000–400 cm^{-1}[13].

The surface functional groups of the adsorbents were identified using Fourier Transform Infrared Spectroscopy (FT-IR). Two instruments were used: the IR Prestige-21 SHIMADZU spectrophotometer provided a resolution of 4 cm^{-1}, (**Figure IV.12 a**) and the Perkin Elmer Spectrum Two spectrophotometer provided a resolution of 2 cm^{-1}, (**Figure IV.12 b**).

To prepare the KBr-supported sample pellets, a homogeneous mixture containing about 1% of the adsorbent sample and KBr powder was prepared and finely ground.

The mixture was placed into a mold and compressed under high pressure using a hydraulic press. The resulting pellet was removed from the mold, dried, and placed in the IR sample holder for analysis [14].

Figure IV 2. 5: FT-IR spectrometers used for functional group identification, **a)** Prestige-21 SHIMADZU spectrophotometer, **b)** Perkin Elmer Spectrum Two spectrophotometer.

Ⅳ. 2. 6. Boehm method

The Boehm method was applied as an additional experimental protocol to FT-IR for the chosen activated carbon to the adsorption test. It is a quantitative technique to describe surface functionalities. It revolves around identifying oxygenated acidic and basic functional groups on surfaces. These groups include acidic functions such as carboxylic, lactone, hydroxyl, and carbonyl groups, which are quantified using bases of varying strengths. Also, basic functions are determined using hydrochloric acid.

0.15 g of the chosen activated carbon was placed into 100 mL Earlen meyer flasks. In each one, 50 mL of 0.1 N concentration alkaline solutions were introduced followed by continuous agitation for 48 h, at a temperature of (25 ± 2) °C.

Figure IV.2. 6: Boehm titration procedure

The bases used in Boehm's method are sodium bicarbonate, $NaHCO_3$, which neutralizes only carboxylic acid functions, sodium carbonate, Na_2CO_3 doses both carboxylic acid and lactone functions, and sodium hydroxide NaOH, which neutralizes all acidic functions [15]. After filtration, the amount of base consumed by the activated carbon was determined by titrating a known volume of filtrate (10 mL) with hydrochloric acid (0.1 N) by adding a color indicator to each base. The neutralized quantity was determined following the equation [16].

$$\text{Quantity(meqg)} = (N_{base} - \left(\frac{N_{HCl}\ V_{HCl}\ (mL)}{V_{dosed\ base}}\right)) \times \frac{V_{base}}{m_{sample(g)}}) \qquad (1)$$

Ⅳ. 2. 7. Determination of pH of zero-point charge (pH_{ZPC})

The nature of activated carbon can be acidic, neutral, or basic, depending on the pH_{pzc}. The pH_{pzc} depends on the precursor's origin and the preparation method (chemical or physical). The pH_{pzc} serves as a valuable indicator of the chemical and electronic properties of functional groups. It is defined as the pH at which there is no positive or negative charge on the surface of the activated carbon, in other words, no discharge of H^+ or OH^- ions [17].

50 mL samples of NaCl solution (0.01 M) were introduced in stoppered flasks while the pH was adjusted from 2 to 12 by adding sodium hydroxide NaOH (0.1 N) or concentrated hydrochloric acid HCl (0.1 N). 0.15 g samples of the activated carbon were then added to the NaCl solutions. After 48 h of stirring, the final pH was measured. The pH value that corresponds to the point of intersection of the plot of (pH_i-pH_f) against the initial pH is the pH_{pzc} of the carbon. If the pH is lower than the pH_{pzc}, the adsorbent's surface charge becomes positive, promoting the adsorption of anionic species, conversely, at a pH higher than the pH_{pzc}, cationic species are preferentially adsorbed due to the favorable surface charge [18].

Ⅳ. 2. 9. Parameters evaluating the overall quality of the prepared activated carbons

IV. 2. 9. 1. Burn-off (%) is the mass percentage (%) that signifies the weight reduction observed during the activation process and that is calculated according to the following equation [19] :

$$\text{Burn} - \text{off}(\%) = \frac{m_{initial} - m_{final}}{m_{initial}} \times 100 \qquad (2)$$

IV. 2. 9. 2. Yield (%) or The activation effectiveness was assessed using the following equation[14]:

$$\text{Yield}(\%) = \frac{m_{final}}{m_{initial}} \times 100 \qquad (3)$$

IV. 2. 9. 3. Volatile meter (VC) **(%)** or the evaporation matter was calculated as follows [20]:

$$\text{Volatile matter (\%)} = 100(\%) - \text{yield (\%)} \qquad (4)$$

Ⅳ. 2. 9. 4. Ash ratio (%)

The ash content analysis is used to assess inorganic impurities in starting materials, It is conducted following the ASTMD2866-70 standard [21].

The procedure is as follows:

- Heat an empty crucible for one hour at 650°C, then cool it in a desiccator and weigh it to record its mass.
- Weigh a portion of the carbonized material and place the crucible with the sample in a furnace at 650°C for three hours. Weigh it again and return it to the furnace for another hour.
- Repeat this process until the mass becomes constant.

The ash content, expressed as a mass percentage (%), is calculated using the following equation:

$$Ac = \frac{F - G}{B - G} \times 100 \qquad (5)$$

Where

- B is the mass of the crucible plus the dried carbonized sample,
- F is the mass of the crucible plus the ash,

- G is the mass of the empty crucible.

This protocol ensures an accurate determination of inorganic impurities in the material.

Ⅳ. 2. 9. 5. Humidity rate (%)

The oven-drying test method was used to measure moisture content according to ASTM D2867-70 standard [21].

A 1 g sample of carbonized material is placed in a dry crucible with a cover (specified weight). The crucible containing the sample is precisely weighed before being placed in a preheated oven set to 150°C. The sample is dried for three hours under stable conditions before being taken from the oven (lid closed) and chilled to room temperature in a desiccator. The closed crucible is weighed again with precision. The percentage weight difference is calculated as the sample's humidity rate, using the following equation:

$$\mathrm{Mc} = \frac{\mathrm{B-F}}{\mathrm{B-G}} \times 100 \qquad (6)$$

where

- B is the mass of crucible with cover plus carbonized mass before drying,
- F is the mass of crucible with cover plus carbonized mass after drying,
- G is the mass of crucible and empty cover.

Ⅳ. 2. 9. 5. Carbon yield (%)

Carbon yield or fixed carbon is the carbon remaining after the elimination of volatile matter and ash. It is a value obtained by summing the percentage of moisture or the humidity rate, ash, and volatile matter subtracted from 100, according to ASTMD 3172-73 standard [22].

$$\text{Carbon yield (\%)} = 100 - (\mathrm{MC} + \mathrm{AC} + \mathrm{VC}) \qquad (7)$$

Mc is the Humidity rate (%), AC is the ash ratio (%), and VC is the volatile meter (%)

Ⅳ. 2. 9. 6. Apparent density (g cm^{-3})

The apparent density was determined by applying (ASTM D 2854-96) standard to estimate the amount of weight necessary to fill out a container. 1cm^3 of activated carbon was placed in a small graduated cylinder and placed in the drying oven for 24h to be weighed the day after [23], and the apparent density was calculated according to the following equation:

$$A_d = \frac{A-F}{1} \quad (8)$$

- F: Mass of the empty crucible
- A: Mass of the crucible with material after oven drying

Ⅳ. 2. 9. 7. Iodine number

Iodine number is defined as the quantity of iodine (in milligrams) absorbed per gram of adsorbent at a residual concentration of 0.02N and was evaluated by iodometric titration. This number represents the surface area available for adsorption.

Iodine is a tiny molecule; consequently, the iodine number represents activated carbon's capacity to adsorb smaller molecules. Iodometry is a reaction with a standard iodine solution that is related to the titration of iodine produced during chemical reactions.

$$I_2 + 2\,e^{-1} \rightarrow 2\,I^{-1} \quad (9)$$

Strong reducing agents such as stannous chloride, sulfurous acid, hydrogen sulfide, and sodium thiosulfate react with iodine even in an acidic solution.

$$2S_2O_3^{-2} + I_2 \rightarrow S_4O_6^{-2} + 2I^- \quad (10)$$

Reagents

- Iodine solution (0.1 N)
- Sodium thiosulfate pentahydrate solution (0.1 N)
- Starch solution (1%) in boiling water
- Hydrochloric acid (5% v/v)
- Potassium dichromate solution (0.1 N)
- Potassium iodide solution (0.1 N).

Procedure

To determine the iodine number of our activated carbon, we followed the steps below:

1. Accurately weigh 0.2 grams of the activated carbon and place it in a 250 mL Erlenmeyer flask.
2. Add 10 mL of hydrochloric acid and stir until the activated carbon is completely wetted.
3. Place the Erlenmeyer flask on a hot plate and heat until it starts boiling, then count for 30 seconds.

4. Allow the mixture to cool, then add 100 mL of 0.1 N iodine solution. Close the flask immediately and shake vigorously for 30 seconds.
5. Filter the solution using the Whatman N°2 paper. Take 50 mL of the filtrate and transfer it to another 250 mL Erlenmeyer flask.
6. Titrate the filtrate with sodium thiosulfate solution. At the end of the titration, add 2 mL of starch solution.
7. Record the final volume of sodium thiosulfate added and calculate the iodine number using the appropriate formula.

$$\text{Iodine index} = \frac{((V_2 - V_1) \times N \times 126.93)}{m} \quad (11)$$

Where

- m is the mass of activated carbon (g).
- V_2 is the volume of thiosulfate for blank titration (mL).
- V_1 is the volume of thiosulfate for titration after adsorption (mL).
- N is the normality of thiosulfate solution used (eq-g L^{-1}).

The iodine values of the prepared activated carbons are shown in the results and discussion chapter.

Ⅳ. 2. 9. 5. Methylene blue index

The Methylene blue index measures the amount of Methylene blue, in milligrams, adsorbed by one gram of activated carbon. This index was determined by Chemviron-Carbon's TM-11 method, which involves measuring the adsorption of filtrate containing the residual concentration of Methylene blue after 30 minutes' contact with activated carbon.

The Methylene blue index represents the quantity of Methylene blue, in mg g^{-1}, adsorbed by the activated carbon tested. To determine the Methylene Blue Index (MBI) of each activated carbon, the following solutions are required:

- 0.25% acetic acid solution
- 50 % acetic acid solution
- 1200 mg L^{-1} Methylene blue solution

Preparation of solutions

- ✓ To prepare a 0.25% acetic acid solution, add 2.5 mL glacial acetic acid to 900 mL of distilled water in a 1 L flask. Dilute the mixture to the calibration point.
- ✓ To prepare a 50% acetic acid solution, measure 253.11 ml of glacial acetic acid into a flask and dilute to the mark.
- ✓ To get 1200 mg L^{-1} of Methylene blue solution, weigh 1.2 grams of Methylene blue, dissolve it in 100 milliliters of 50% acetic acid, and dilute it to one liter.
- ✓ to obtain 120 mg L^{-1} of Methylene blue intermediate solution: Dilute the 1200 mg L^{-1} methylene blue solution with 0.25% acetic acid to a concentration of 120 mg L^{-1} per 100 mL.

Table IV. 1: Experimental data of the Methylene blue calibration curve

C (mg. L^{-1})	0	2.4	3.6	4.8	9.6	10.8
Absorbance	0	0.26	0.398	0.532	1.074	1.165

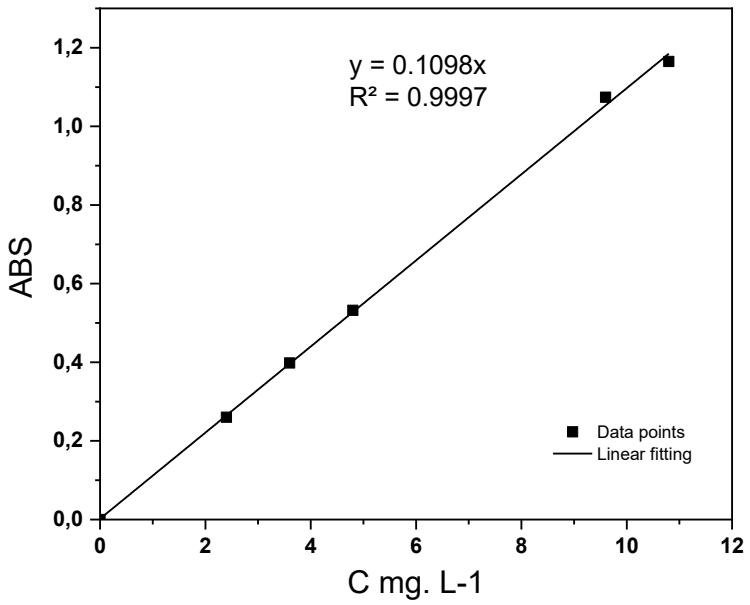

Figure IV 2. 7. Calibration curve of Methylene blue at 620 nm

Procedure

1. Prepare different concentrations of Methylene blue solution (120 mg L^{-1}) by pipetting specific volumes into 100 mL flasks and diluting with 0.25% acetic acid to the 1 L mark.
2. Weigh 0.1 g activated charcoal and mix with 25 mL Methylene blue solution (1200 mg L^{-1}). Shake the mixture for 30 minutes. The Methylene blue index is calculated using the equation below:

$$\text{MB index } (\text{mg g}^{-1}) = \frac{(1200-\text{Ceq})\,\text{V}}{1000\ \text{m}} \qquad (12)$$

➢ **UV-Visible Spectrophotometer**

The UV-visible spectrophotometer was used to evaluate the adsorption ability of activated carbon by measuring the concentration of contaminants in the solution before and after treatment. UV-Visible analysis was based on the Beer-Lambert law:

$$A = \log\frac{Io}{I} = \log\frac{1}{T} = \varepsilon \times \ell \times C \qquad (13)$$

where:

- T : is the transmission factor or transmittance,
- A : is the absorbance or optical density,
- C : is the mass concentration of the compound being measured (mol. L^{-1}),
- I, I_0 : are Intensities of the transmitted (emergent) and incident light beams, respectively,
- ε : is the specific absorption coefficient (L. mol^{-1}. cm^{-1}),
- ℓ is the path length (thickness of the cell), (cm).

This method measured the light absorption of the material to estimate the band gap, providing important insights into the material's electronic properties [24]. The analysis was carried out using a Shimadzu UV-1240 spectrophotometer (**Figure IV.11.)** equipped with quartz cells with a 1.0 cm optical path length, which was used to detect the UV absorption of each sample.

Figure IV.2. 8: UV-visible Shimadzu UV-1240 spectrophotometer used for adsorption studies

IV. 3. Part 3: Adsorption application studies

Ⅳ. 3. 1. Characteristics of the herbicide molecules studied

To validate activated carbon's adsorption ability, we chose two herbicides as target pollutants: para-chlorophenoxyacetic acid (P-CPA) and Linuron (Lin). These substances were chosen since they are commonly used in agriculture, persist in water sources, and pose significant environmental hazards.

Ⅳ. 3. 1. 1. Phenoxyacetic acids

The phenoxyacetic acids (PAAs) or chlorophenoxyacetic acids (CPAs) namely, 2,4-dichloro phenoxy acetic acid (2.4-D), 4-Chloro-2-methylphenoxyacetic acid (MCPA) [25, 26], 2-(4-chlorophenoxy)-2-methylpropionic acid (clofibric acid, CFA)[27], 2.4.5-trichloro phenoxy acetic acid (2.4.5-T) [28], P-chlorophenoxyacetic acid or 4-chlorophenoxyacetic acid (P-CPA or 4-CPA) [25, 29] are herbicides that are commonly used in agriculture, they work by disrupting the growth of broadleaf weeds and dicotyledons, making them effective in controlling undesirable plants in crops [30]. However, their use requires careful handling and application to minimize environmental and human health risks. CPAs have been observed to be resistant to biodegradation [31, 32] and hazardous to people and animals since they make mammals more susceptible to infectious illnesses and cancers [33].

IV. 3. 1. 1. 1. para-chlorophenoxyacetic acid or 4-Chlorophenoxyacetic Acid (P-CPA)

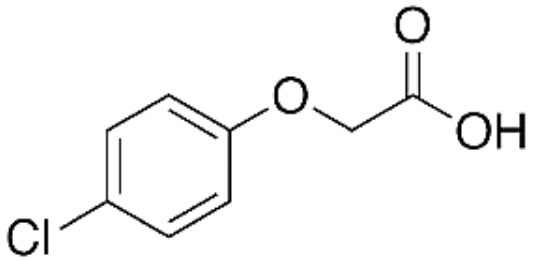

Figure IV. 3. 1: Chemical structural formula of p-chlorophenoxyacetic acid (P-CPA)

This cost-effective, highly efficient, water-soluble herbicide belongs to the group of chlorinated herbicides. It is commonly used as a plant growth regulator, particularly for thinning peaches and controlling root growth in mung beans. Due to its high water solubility, it can easily enter surface or groundwater, causing contamination. P-CPA, identified as a priority pollutant by the US EPA because of its high water solubility, has been the focus of numerous studies to address this issue [34, 35]. As a result, there is considerable interest in developing innovative methods for removing this herbicide from water and soil, such as electrochemical techniques like anodic oxidation and indirect electrooxidation methods [30]. The adsorption technique has also attracted the interest of scientists. It has generally become the most widely used technique for wastewater treatment and herbicide removal [36-39].

Table IV. 2: Experimental data of the para-chlorophenoxyacetic acid (P-CPA) herbicide Calibration curve

C(mg. L^{-1})	0	10	40	50	80	100	150	160	200
ABS	0	0.05	0.275	0.339	0.542	0.694	0.989	1.071	1.306

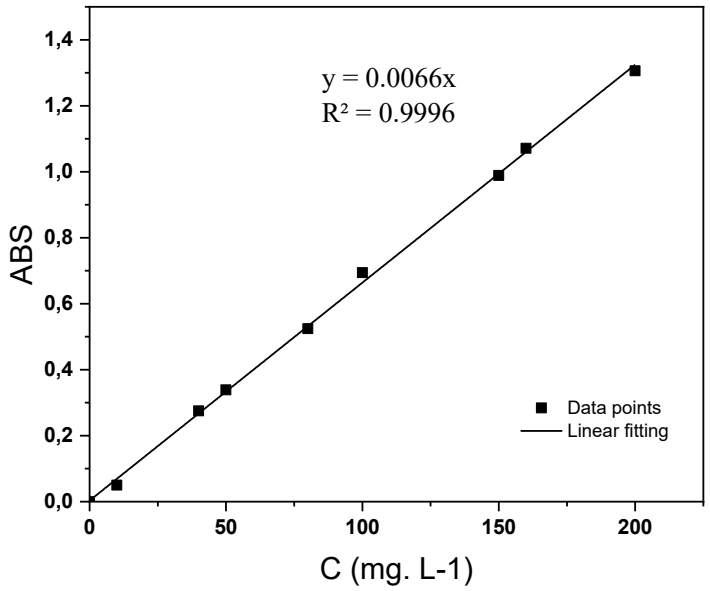

Figure IV. 3. 2. Calibration curve of para-chlorophenoxyacetic acid (P-CPA) at 278nm

Table IV. 3: Properties of the para-chlorophenoxyacetic acid (P-CPA) herbicide [40, 41]

Chemical formula	$C_8H_7ClO_3$
IUPAC name	(4-Chlorophenoxy) acetic acid
Appearance	White powder
Synonyms	P-CPA, Penta chlorophenoxyacetic acid, 4-CPA, (4 Chlorophenoxy) acetic acid, 2-(4 Chlorophenoxy) acetic acid
Molecular weight (g/mol)	186.59
Maximum wavelength λ_{max} (nm)	278
Water solubility(g/l)	0.957
pKa	3.56
***CAS number**	122-88-3 / C-0413 Lot 89F002125
Chemical safety	Irritant

*Source: Sigma cell culture (Information from the product bottle

Ⅳ. 3. 1. 2. Linuron

Linuron (3-(3,4-dichlorophenyl)-1-methoxy-1-methylurea) "Lin" is an herbicide from the substituted urea family, commonly used to control broadleaf weeds and certain grasses in agricultural crops. While effective in managing weeds, its use must be carefully managed to minimize environmental and human health risks. This includes adopting responsible application practices and exploring sustainable alternatives when possible[42].

Due to environmental and health concerns, linuron has been restricted or banned in several countries. For example, its approval was withdrawn in the European Union in 2017. However, it is still permitted in some other countries under strict regulations[43].

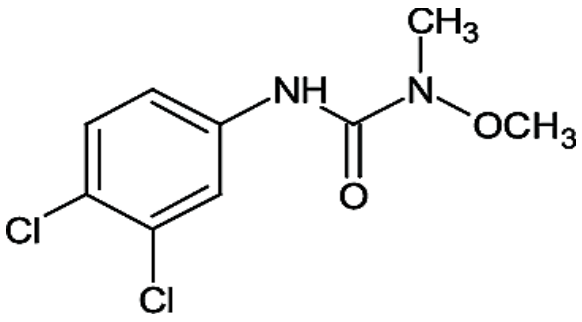

Figure IV. 3. 3. Chemical Structural Formula of Linuron (Lin)

Linuron is applied to control the spread of grass and weeds, facilitating the growth of economically valuable crops [44], however, it is an herbicide that is often referred to as 'killer grass.' It functions as a chemical herbicide by inhibiting photosynthesis by binding to a specific site in chlorophyll, effectively killing various weeds and plants.

Residues of linuron can pose risks to consumers and mammals. Alarmingly, only 0.1 percent of pesticides effectively target pests, while 99.9 percent contaminate the environment, particularly soil and water, thereby impacting the ecosystem and food chain[45].

Table IV. 4: Experimental data of the Linuron (Lin) herbicide Calibration curve

C (mg. L^{-1})	0	1	2	3	5	6	7	8	9	11	12	14	15
ABS	0	0.049	0.107	0.18	0.365	0.492	0.565	0.641	0.724	0.89	0.964	1.118	1.184

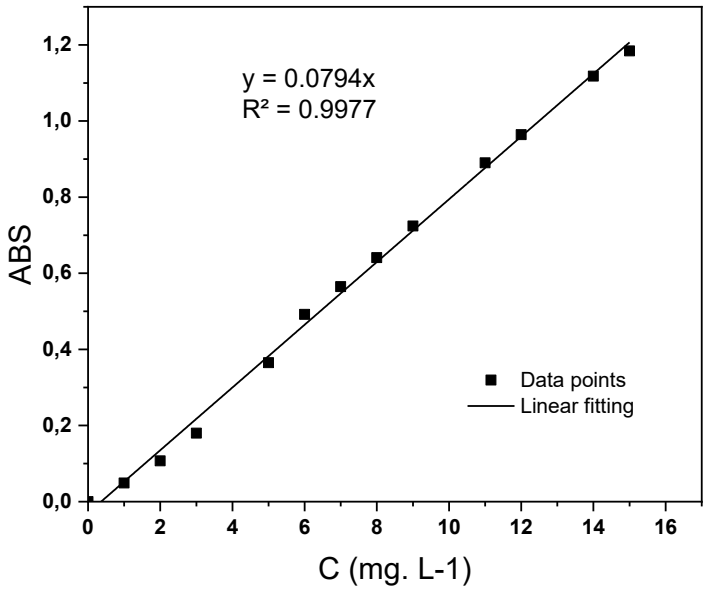

Figure IV. 3. 4: Calibration curve of Linuron herbicide (Lin) at 247nm

Table IV. 5: Properties of Linuron (Lin) herbicide [46, 47]

Chemical formulas	**$C_9H_{10}Cl_2N_2O_2$**
IUPAC name	3-(3,4-dichlorophenyl)-1-methoxy-1-methylurea
Appearance	colorless crystals
Synonyms	Linurex, Methoxydiuron, Afalon inuron, Liron, LOROX, LINEX, Lorex, LINNET, Laroks, Afolan, Norunil, Sarclex
Molecular weight (g/mol)	249.09
Maximum wavelength λ_{max} (nm)	247
Water solubility(g/l)	0.081
pKa	12.13
*CAS number	330-55-2
Chemical safety	Irritant- health hazard- environmental hazard

Ⅳ. 3. 2. Application of the Adsorption Process

Ⅳ. 3. 2. 1. Chemicals

BIOCHEM Chemopharma supplied potassium hydroxide (KOH), hydrochloric acid (HCl), sodium hydroxide (NaOH), and iodine (I_2) were purchased from SIGMA-ALDRICH and Biochemopharma, respectively, potassium iodide (KI) and Methyle Blue (MB) were supplied by MERCK company.

Para-chlorophenoxyacetic acid (P-CPA) was obtained from SIGMA CELL CULTURE C-0413 Lot 89F002125. Stock solutions of P-CPA herbicide (> 98 % purity) of known concentrations were prepared following the conventional approach by dissolving 500 mg of the substance in a 500 mL flask. Distilled water was added to the 500 mL mark to reach a concentration of 1 g L^{-1}.

Linuron was obtained from SIGMA-ALDRICH. The mother solution was prepared following the classic method by dissolving 250 mg of Linuron (*Lin*) in a 500 mL flask. The stock solutions were diluted and used to prepare working solutions of lower concentrations.

This study examined factors influencing herbicide adsorption, such as contact time, adsorbent dosage, and solution pH. Two of the best-activated carbons were chosen: one made in a muffle furnace (K-AC_2) and the other in a tube furnace under a nitrogen environment (AC_2').

IV. 3. 2. 2. Determination of Adsorption Equilibrium Time

To determine the adsorption equilibrium time, 25 mL volumes of known concentration solutions for each herbicide were successively brought into contact with 0.1 g of each adsorbent used. The mixtures were stirred for durations ranging from 10 to 150 minutes, then centrifuged at 5000 rpm for 15 minutes. A spectrophotometer (Shimadzu UV-mini-1240) was used to quantify the residual herbicide concentrations at the wavelength of the herbicide's maximum absorbance (λ_{max}).

IV. 3. 2. 3. Effect of Activated Carbon Dose

The dose of activated carbon is an important variable that affects adsorption effectiveness and may also be used to calculate the cost of activated carbon per unit of treated water. To determine the optimum adsorbent dose, 25 mL of the herbicide solution with a

specified concentration was mixed and agitated with 0.05 g, 0.1 g, 0.2 g, and 0.3 g of the studied activated carbons for a previously determined time. The samples were then centrifuged, and the herbicide content in the supernatant was determined.

IV. 3. 2. 4. Impact of pH

pH is a crucial factor in regulating the adsorption process since it influences the amount of material adsorbed[48]. It can affect the adsorbent's surface charge, the ionization of the adsorbate, and the dissociation of functional groups at the adsorbent's active sites [49]. In this experiment, 25 mL of herbicide solution at a specified concentration was added to a series of flasks. The pH was changed from 2 to 12 by adding sodium hydroxide or hydrochloric acid (0.1 N concentration). Each flask was then filled with the ideal amount of pine cone-derived activated carbon (K-AC_2 and AC_2'). This pH range was chosen to study how pollutant adsorption varies with the chemical forms present at different pH levels. Mixtures were stirred for a predetermined optimized time, filtered, and then analyzed using spectrophotometry to measure residual herbicide concentrations.

IV. 3. 2. 5. Adsorption isotherms

An adsorption isotherm is a curve that depicts the relationship between the amount of material adsorbed per unit mass of adsorbent and the concentration of the liquid phase at equilibrium and a constant temperature. This section of the study discusses the adsorption mechanism, such as whether it is single-layer (monolayer) or multi-layer adsorption, and whether lateral interactions occur between molecules [50]. The adsorption isotherm, which represents the thermodynamic equilibrium between an adsorbent and an adsorbate, is often determined by batch experiments [51]. These studies determine the stable residual equilibrium concentration of the adsorbate in the liquid phase after adsorption. The amount of adsorbate adsorbed is calculated using an equation mentioned in Chapter I- Section A.

For this study, the appropriate amount (g) of activated carbon was added to a series of beakers containing 25 mL of herbicide solution with known initial concentrations. The mixtures were stirred for a predetermined contact time. The obtained adsorption isotherms were modeled with the simple and well-known Langmuir, Freundlich and Temkin models. In addition, the Dubinin-Radushkevich (D-R) and Redlich-Peterson (R-P) models were used to validate the classical model results [16]. The determination coefficient R^2 was used to evaluate a theoretical

model's ability to accurately reflect experimental data. A value of R^2 near 1 indicates a good model fit.

IV. 3. 2. 6. Adsorption kinetics studies

Kinetics describes the rate at which a solute is adsorbed over time and is one of the most important studies conducted for evaluating the effectiveness of adsorption. The adsorption kinetics of p-chlorophenoxyacetic acid (P-CPA) and Linuron (Lin) were investigated with the prepared activated carbons (K-AC_2 and AC_2') as adsorbents. To evaluate the adsorption kinetics, tests were performed with 25 mL of the solution under study. The solution was combined with an optimized appropriate amount of adsorbent at a specific pH and herbicide concentrations. The contact time of herbicide with adsorbent was varied from 5 to 80 minutes (5, 10, 15, 20, 30, 40, 50, 60, 70, 80 min).

IV. 3. 2. 7. Thermodynamic studies

The temperature dependency of the adsorption process is a complex phenomenon. Thermodynamic characteristics such as heat of adsorption and activation energy are key predictors of adsorption behavior, and both are temperature dependent [52]. Numerous researchers have examined how temperature affects organic molecules adsorption [53, 54]. The relationship between temperature and adsorption is mostly determined by the adsorbent/adsorbate pair [14].

Using the Gibbs thermodynamic relation:

$$\Delta G° = \Delta H° - T\,\Delta S° \qquad (14)$$

and the vant' Hoff equation:

$$ln(K_d) = \frac{-\Delta H°}{R}\left(\frac{1}{T}\right) + \frac{\Delta S}{R} \qquad (15),$$

we can calculate the thermodynamic parameters (ΔG°, ΔH°, and ΔS°) of herbicides adsorption at different temperatures [55] (as described in Chapter I).

To investigate the influence of temperature on the adsorption of organic compounds by adsorbents, bottles holding 25 mL of solution with a known concentration were mixed with a predetermined quantity of adsorbent. These were placed in a water bath with a thermostat to regulate the temperature (20, 25, 30, and 40 °C). The mixture was agitated for a predetermined contact time before being centrifuged and spectrophotometrically evaluated.

The measurement of the adsorption heat ΔH is the main criterion parameter to differentiate chemisorption from physisorption. The sorption process is typically accompanied by a heat exchange, which is exothermic when $\Delta H < 0$ and endothermic when $\Delta H > 0$.

IV. 4. Part 4: Theoretical study of P-CPA ($C_8H_7O_3Cl$) molecule

Theoretical research is critical for understanding pollutant behavior at the molecular level, especially in adsorption processes. Computational chemistry approaches can help us understand the electrical characteristics, chemical reactivity, and adsorption mechanisms of organic pollutants. In addition to the experimental adsorption study, a theoretical investigation was conducted on para-chlorophenoxyacetic acid (P-CPA) to study critical electronic properties such as HOMO-LUMO energy gap, dipole moment, and global and local reactivity descriptors. The study also identified nucleophilic and electrophilic sites using Parr functions to predict potential interaction sites for adsorption.

These simulations anticipate the stability of the molecule, reactivity, and favored adsorption sites, providing insight into adsorption interactions such as electrostatic attraction, hydrogen bonding, and π-π stacking. Theoretical modeling improves understanding of adsorption mechanisms by identifying the most reactive molecular areas, which aids in the improvement of the treatment of water contaminated by P-CPA herbicide.

IV. 4. 1. HOMO-LUMO

HOMO (The most or the highest occupied molecular orbital) and LUMO (the least occupied molecular orbital) are the most important energy levels of a molecule. The difference in energy between these orbitals, known as the HOMO-LUMO gap, determines the degree of stability and reactivity of the molecule [56]. A low energy gap between frontier orbitals increases the polarizability of a molecule, which tends to be linked to high chemical reactivity [57]. The large intermolecular charge transfer (ICT) between the electron donor (HOMO) and electron acceptor (LUMO) along the conjugated π-pathways resulted in a notable separation of the HOMO and LUMO energy states. Furthermore, the HOMO-LUMO energy gap proved the presence of intramolecular charge transfer (ICT).

Using Global Chemical Reactivity Descriptor (GCRD) properties, the relationship between chemical reactivity and structural strength could be effectively demonstrated. Chemical reactivity descriptors, namely chemical potential (P) [58], electronegativity (χ) [59], hardness

(η) [60], softness (S) [61], electrophilicity index (ω) and nucleophilicity index (N) [62], were derived from HOMO and LUMO energies and calculated using the following equations [63]:

Electronegativity $\chi = -\frac{1}{2}(E_{LUMO} + E_{HOMO})$ (16)

Chemical potential $P = \frac{1}{2}(E_{LUMO} + E_{HOMO})$ (17)

Global hardness $\eta = \frac{1}{2}(E_{LUMO} - E_{HOMO})$ (18)

Global softness $S = \frac{1}{\eta}$ (19)

Electrophilicity index $\omega = \frac{P^2}{2\eta}$ (20)

Nucleophilicity index $N = E_{HOMO} - E_{HOMO\ (TCE)}$ (21)

IV. 4. 2. Local chemical reactivity descriptors

Research into the local selectivity of compounds involves the use of the Parr function P(r), derived from Mulliken atomic spin density (ASD) analysis at the radical anion and radical cation level of the corresponding reagents [64]. These local functions are used to determine the most electrophilic and nucleophilic locations in a molecule and are given by the equations that follow:

$P_k^-(r) = \rho_s^{rc}(r)$ for electrophilic attack (22)

$P_k^+(r) = \rho_s^{ra}(r)$ for nucleophilic attack (23)

Where $\rho_s^{rc}(r)$ represents the atomic spin density (ASD) of the radical cation, and $\rho_s^{ra}(r)$ is the atomic spin density of the radical anion. Each condensed atomic spin density on the individual atoms of the radical cation and radical anion generates our nucleophilic Pk and electrophilic Pk+ functions in the neutral system framework. Using these nucleophilic and electrophilic Parr functions, we can redefine the local electrophilicity indices ωk and local nucleophilicity indices Nk as follows:

$\omega_k = \omega . P_k^+$ (24)

$N_k = N . P_k^-$ (25)

Where ω and N are the global electrophilicity and nucleophilicity indices

References of Chapter IV

[1] O. Baatache, K. Derbal, A. Benalia, I. Aberkane, Q.E. Guizah, A. Khalfaoui, A. Pizzi, Valorization of pine cones (pinus nigras) for industrial wastewater treatment and crystal violet removal: a sustainable approach based on bio-coagulants and a bio-adsorbent, Water, 16 (2024) 260.

[2] M. E. Argun, S. Dursun, M. Karatas, M. Gürü, Activation of pine cone using Fenton oxidation for Cd (II) and Pb (II) removal, Bioresource technology, (2008).

[3] S. Valizadeh, H. Younesi, N. Bahramifar, Preparation and characterization of activated carbon from the cones of iranian pine trees (Pinus eldarica) by chemical activation with H_3PO_4 and its application for removal of sodium Dodecylbenzene Sulfonate removal from aqueous solution, Water Conservation Science and Engineering, (2018).

[4] P. Nowicki, I. Kuszyńska, J. Przepiórski, R. Pietrzak, The effect of chemical activation method on properties of activated carbons obtained from pine cones, Central European Journal of Chemistry, 11 (2013) .

[5] A. Muslim, Optimization of Pb (II) adsorption onto Australian pine cones-based activated carbon by pulsed microwave heating activation, Iran. J. Chem. Chem. Eng. Research Article Vol, 36 (2017).

[6] A. Özhan, Ö. Şahin, M.M. Küçük, C. Saka, Preparation and characterization of activated carbon from pine cone by microwave-induced ZnCl 2 activation and its effects on the adsorption of methylene blue, Cellulose, 21 (2014).

[7] N. Fekih, H. Allali, S. Merghache, F. Chaïb, D. Merghache, M. El Amine, N. Djabou, A. Muselli, B. Tabti, J. Costa, Chemical composition and antibacterial activity of Pinus halepensis Miller growing in West Northern of Algeria, Asian pacific journal of tropical disease, 4 (2014) 97-103.

[8] N. Kadri, B. Khettal, Y. Aid, S. Kherfellah, W. Sobhi, V. Barragan-Montero, Some physicochemical characteristics of pinus (Pinus halepensis Mill., Pinus pinea L., Pinus pinaster and Pinus canariensis) seeds from North Algeria, their lipid profiles and volatile contents, Food chemistry, 188 (2015).

[9] G. Liu, M. Zheng, X. Jiang, R. Jin, Y. Zhao, J. Zhan, Insights into the emission reductions of multiple unintentional persistent organic pollutants from industrial activities, Chemosphere, 144 (2016) .

[10] Y. Jari, N. Roche, M.C. Necibi, F.Z. Falil, S. Tayibi, K. Lyamlouli, A. Chehbouni, B. Gourich, Porous activated carbons derived from waste Moroccan pine cones for high-performance adsorption of bisphenol A from water, Heliyon, 10 (2024).

[11] J. Dombrowski, Micromeritics 3Flex Surface Characterization Analyzer, (September 2014).

[12] Q. Corporation, Quantachrome Novatouch version (2014).

[13] D. Nadia, ADSORPTION DE COMPOSÉS PHÉNOLIQUES PAR UN DÉCHET TRAITÉ CHIMIQUEMENT, (2015).

[14] Bahnes. Zohra, Activation des noyaux de jujube pour l'obtention d'un charbon actif, in, (2018).

[15] B. H., Some aspects of the surface chemistry of carbon blacks and other carbons. Carbon ;vol. 32(5):759–69, (1994).

[16] F.B. Benabed, S. Attouti, N. Douara, M. Termoul, M. İmamoğlu, A. Çoruh, N. Boukabcha, N. Benderdouche, B. Bestanı, Theoretical study of the herbicide parachlorophenoxyacetic acid molecule and its removal by activated carbon prepared from pine cone, Desalination and Water Treatment, 320 (2024).

[17] A. Medjdoub, F. Nemchi, H. Belayachi, B. Bestani, S. Bourahla, M. Belhakem, N. Benderdouche, Adsorptive potential of synthesized sea urchin-based hydroxyapatite for Supranol yellow and nickel ion recovery from aqueous media: kinetics and thermodynamic studies, Desalination and Water Treatment, (2022.

[18] M. B. Benallou, N. Douara, M. Chemrak, Z. Mekibes, N. Benderdouche, B. Bestani, Elimination of Malachite Green on granular activated carbon prepared from olive stones in discontinuous and continuous modes, Algerian Journal of Environmental Science and Technology, 7 (2021).

[19] V. S. Achari, A. S. Rajalakshmi, S. Jayasree, R. M Lopez, Surface Area and Porosity Development on Granular Activated Carbon by Zirconium: Adsorption Isotherm Studies, Journal of Applied Research and Technology, (2018).

[20] L. Azzouz, D. Belaloui, N. Bouchemal, Valorisation des cônes du pin pignon *Pinus pinea* L., par la synthèse du charbon actif, étude de caractérisation, 2170-1652 (2022).

[21] ASTMD 2866, Ash Content and Moisture of Activated carbon. Extracts were repinted; with permission from the Annual book of ASTM Standart copyright.

[22] A. 3172–73, Fixed carbon, Last previous edition D 3172 – 73. Annual Book of ASTM Standards, 05.05. (1984).

[23] A. Salima, B. Benaouda, B. Noureddine, L. Duclaux, Application of Ulva lactuca and Systoceira stricta algae-based activated carbons to hazardous cationic dyes removal from industrial effluents, Water Res, 47 (2013).

[24] Benkhemkhem. Kawther. Nesrine, Elaboration et caractérisation d'un matériau hybride pour le traitement des eaux usées, Thesis, (2024).

[25] K. Kuśmierek, L. Dąbek, A. Świątkowski, Removal of phenoxy herbicides from aqueous solutions using lignite as a low-cost adsorbent, Desalination and Water Treatment, 260 (2022) 111-118.

[26] K. Das, D. Majhi, Y.P. Bhoi, B.G. Mishra, Combustion synthesis, characterization and photocatalytic application of CuS/Bi4Ti3O12 p-n heterojunction materials towards efficient degradation of 2-methyl-4-chlorophenoxyacetic acid herbicide under visible light, Chemical Engineering Journal, (2019).

[27] A. Derylo-Marczewska, M. Blachnio, A.W. Marczewski, A. Swiatkowski, B. Buczek, Adsorption of chlorophenoxy pesticides on activated carbon with gradually removed external particle layers, Chemical Engineering Journal, 308 (2017).

[28] A. Naboulsi, L. El Mersly, H. Yazid, M. El Himri, S. Rafqah, M. El Haddad, Adsorption behaviors and mechanisms by theoretical study of herbicide 2,4,5-Trichlorophenoxyacetic on activated carbon as a new biosorbent material, Journal of the Taiwan Institute of Chemical Engineers, 142 (2023).

[29] B. K. Alimnazarov, J. M. Ashurov, A. G. Eshimbetov, K. K. Turaev, B. T. Ibragimov Electronic structure of diaquabis (p-chlorophenoxyacetato) copper (II) complex by DFT method, (2022).

[30] L. H. Mendoza-huizar, C.H. Rios-reyes, G.A. Álvarez-romero M.T. Ramírez-silva, M.E. Palomar-pardavé, Electrophilic and nucleophilic chemical reactivity of neutral and anionic forms of 4-CPA, 24D-CPA, 34-CPA, and 245T-CPA through conceptual DFT reactivity descriptors (2017)

[31] S.L. Levine, C.J. Borgert, Review and recommendations on criteria to evaluate the relevance of pesticide interaction data for ecological risk assessments, Chemosphere, 209 (2018).

[32] A. Derylo-Marczewska, M. Blachnio, A.W. Marczewski, M. Seczkowska, B. Tarasiuk, Phenoxyacid pesticide adsorption on activated carbon - Equilibrium and kinetics, Chemosphere, 214 (2019).

[33] F.L. Martin, E.Z. Martinez, H. Stopper, S.B. Garcia, S.A. Uyemura, V. Kannen, Increased exposure to pesticides and colon cancer: Early evidence in Brazil, Chemosphere, 209 (2018) 623-631.

[34] A. Abdelhaleem, W. Chu, Photodegradation of 4-chlorophenoxyacetic acid under visible LED activated N-doped TiO2 and the mechanism of stepwise rate increment of the reused catalyst, Journal of hazardous materials, (2017).

[35] F.L. Bohari, M.A.K.M. Hamzah, S.A.I.S.M. Ghazali, N.N. Dzulkifli, I. Fatimah, N. Adam, Synthesis and characterization of 4-chlorophenoxyacetic acid herbicide intercalated into calcium-aluminium layered double hydroxide through co-precipitation method, Malaysian Journal of Analytical Sciences, 25 (2021).

[36] A. Niaz, K.A. Spokas, B. Gámiz, D. Mulla, K.R. Arshad, S. Hussain, 2-Methyl-4-chlorophenoxyacetic acid (MCPA) sorption and desorption as a function of biochar properties and pyrolysis temperature, Plos one, (2023).

[37] T.Y. Kim, S.Y. Cho, Adsorption behavior of p-chlorophenoxyacetic acid on activated carbon, Journal of Industrial and Engineering Chemistry, 10 (2004).

[38] R. Boumaraf, S. Khettaf, F. Benmahdi, R. Masmoudi, A. Ferhati, Removal of 2, 4-dichlorophenoxyacetic acid from aqueous solutions by nanofiltration and activated carbon, Biomass Conversion and Biorefinery, 14 (2024).

[39] H.K. Hue, L.V. Anh, D.B. Trong, Study of the adsorption of 2, 4-dichlorophenoxyacetic acid from the aqueous solution onto activated carbon, Vietnam Journal of Chemistry, 56 (2018) 208-213.

[40] P.o.c. database, https://pubchem.ncbi.nlm.nih.gov/compound/26229 in, 2004.

[41] C.C.D.D. SOURCE, Structure of 4-CHLOROPHENOXYACETIC ACID (C8H7ClO3) https://www.molinstincts.com/structure/4-CHLOROPHENOXYACETIC-ACID-cstr-CT1001308635.html, (2022).

[42] U. States, E.P. Agency, Linuron, (1995).

[43] A. Székács, Herbicide mode of action, in: Herbicides, Elsevier, (2021).

[44] J. Singh, B. Singh, Agar-gelatin-derived hydrogel-based controlled delivery devices for linuron herbicide to prevent environmental hazards, Environmental Chemistry and Ecotoxicology, (2024).

[45] D. Chaara, F. Bruna, K. Draoui, M. Ulibarri, C. Barriga, I. Pavlovic, Study of key parameters affecting adsorption of the herbicide Linuron on organohydrotalcites, Applied clay science, 58 (2012).

[46]chemicalbook,https://www.chemicalbook.com/ChemicalProductProperty_EN_CB2749714.htm, cited in, 25.11.2024.

[47] pubchem, https://pubchem.ncbi.nlm.nih.gov/compound/Linuron#section=MeSH-Entry-Terms, cited in, 15.10.2024.

[48] M.P. Tavlieva, S.D. Genieva, V.G. Georgieva, L.T. Vlaev, Kinetic study of brilliant green adsorption from aqueous solution onto white rice husk ash, Journal of Colloid and Interface Science, 409 (2013).

[49] S. Attouti, M. Termoul, Z. Bahnes, F. Baghdad-Benabed, N. Boukabcha, B. Bestani, N. Benderdouche, A. Chouaih, J. Srénscek-Nazzal, B. Michalkiewicz, Reduction of 2, 4-dichlorophenoxy acetic acid herbicide toxicity from aqueous media by adsorption: Experimental and theoretical study using DFT method, Journal of Dispersion Science and Technology, (2024) 1-12.

[50] R. Saadi, Z. Saadi, R. Fazaeli, N.E. Fard, Monolayer and multilayer adsorption isotherm models for sorption from aqueous media, Korean Journal of Chemical Engineering, 32 (2015) 787-799.

[51] M.A.E. de Franco, C.B. de Carvalho, M.M. Bonetto, R. de Pelegrini Soares, L.A. Féris, Diclofenac removal from water by adsorption using activated carbon in batch mode and fixed-bed column: isotherms, thermodynamic study and breakthrough curves modeling, Journal of Cleaner Production, (2018).

[52] C. Erkey, M. Türk, Thermodynamics and kinetics of adsorption of metal complexes on surfaces from supercritical solutions, in: Supercritical Fluid Science and Technology, Elsevier, (2021).

[53] B. Qiu, Q. Shao, J. Shi, C. Yang, H. Chu, Application of biochar for the adsorption of organic pollutants from wastewater: Modification strategies, mechanisms and challenges, Separation and Purification Technology, (2022).

[54] E. Rápó, S. Tonk, Factors affecting synthetic dye adsorption; desorption studies: a review of results from the last five years (2017–2021), Molecules, 26 (2021).

[55] M.A. Khan, A. Ahmad, Kinetics and thermodynamic studies of phenol adsorption on nanocomposite, Desalination and Water Treatment, 57 (2016).

[56] A.R. Guerroudj, N. Boukabcha, A. Benmohammed, N. Dege, N.E.H. Belkafouf, N. Khelloul, A. Djafri, A. Chouaih, Synthesis, crystal structure, vibrational spectral investigation, intermolecular interactions, chemical reactivity, NLO properties and molecular docking analysis on (E)-N-(4-nitrobenzylidene)-3-chlorobenzenamine: A combined experimental and theoretical study, Journal of Molecular Structure, 1240 (2021).

[57] N. Boukabcha, A. Benmohammed, M.H.M. Belhachemi, M. Goudjil, S. Yahiaoui, Y. Megrouss, A. Djafri, N. Khelloul, Z.D. Benyehlou, A. Djafri, Spectral investigation, TD-DFT study, Hirshfeld surface analysis, NCI-RDG, HOMO-LUMO, chemical reactivity and NLO

properties of 1-(4-fluorobenzyl)-5-bromolindolin-2, 3-dione, Journal of Molecular Structure, 1285 (2023).

[58] N. E. H. Belkafouf, F.T. Baara, A. Altomare, R. Rizzi, A. Chouaih, A. Djafri, F. Hamzaoui, Synthesis, PXRD structural determination, Hirshfeld surface analysis and DFT/TD-DFT investigation of 3N-ethyl-2N'-(2-ethylphenylimino) thiazolidin-4-one, Journal of Molecular Structure, (2019).

[59] R.G. Pearson, Absolute electronegativity and hardness: applications to organic chemistry, The Journal of Organic Chemistry, (1989).

[60] R. Pearson, Chemical hardness, vol. 10, no. 3527606173, Weinheim: Wiley-VCH. sicity of amines. Journal of the American Chemical Society, (1997).

[61] P. Senet, Chemical hardnesses of atoms and molecules from frontier orbitals, Chemical physics letters, (1997).

[62] J. Padmanabhan, R. Parthasarathi, V. Subramanian, P. Chattaraj, Electrophilicity-based charge transfer descriptor, The Journal of Physical Chemistry A, (2007).

[63] H.P. Gümüş, Ö. Tamer, D. Avcı, Y. Atalay, Quantum chemical calculations on the geometrical, conformational, spectroscopic and nonlinear optical parameters of 5-(2-Chloroethyl)-2, 4-dichloro-6-methylpyrimidine, Spectrochimica Acta Part A: Molecular and Biomolecular Spectroscopy, (2014) .

[64] L.R. Domingo, P. Pérez, J.A. Sáez, Understanding the local reactivity in polar organic reactions through electrophilic and nucleophilic Parr functions, RSC advances, (2013)

CHAPTER V:

RESULTS AND DISCUSSIONS

Introduction

Chemical activation is commonly used to produce activated carbons from various bioresources such as forestry waste using potassium hydroxide as the activating agent. This method has several advantages [1, 2]. but the disadvantages of using KOH have often been overlooked [3].

The activated carbons obtained were analyzed using the physicochemical methods described above to obtain an overall assessment of their quality. In addition, textural and structural analyses were carried out to confirm the activation process and porosity control in the prepared activated carbons.

As mentioned in the materials and methods chapter, the prepared activated carbons were tested for the removal of two herbicides, para-chlorophenoxyacetic acid (P-CPA) and Linuron (Lin).

V. 1. Part 1: Preparation of Activated Carbon from Pine Cones

V. 1. 1. Pine cones precursor (PCP) characterization

V. 1. 1. 1. Thermogravimetric analysis of PCP

This characterization was applied before the selection of the activation temperature to determine the mass loss of the raw material (PCP) with temperature using a Discovery TA-SDT650 thermogravimetric analyzer.

The mass loss of the powdered precursor pine cone (PCP) was recorded over the temperature range from 19.397 to 800°C, as depicted in **Figure V. 1. 1**. The breakdown of the initial material occurred in four distinct phases. Initially, starting at 20°C and concluding around 100°C, a minor release of volatile compounds was observed on the TG curve. This was primarily ascribed to the elimination of water vapor due to the drying process, resulting in the removal of moisture and lightweight substances from the sample's surface during this stage [4].

Figure V. 1. 1 shows that the main breaking down range of the PCP started at 250°C and ended at 800°C. The raw material is a lignocellulosic biomass that consists of hemicellulose, cellulose, and lignin. As per the existing literature, the temperature intervals for the decomposition of hemicellulose, cellulose, and lignin are documented as 210–325, 310–400, and 160–900°C, respectively [5].

As shown, hemicellulose underwent decomposition between 110°C and 290°C. Subsequently, a significant mass loss occurred between 300°C and 400°C, which was linked to the degradation of cellulose. It's noteworthy that cellulose degradation takes place at a higher temperature range compared to hemicelluloses [6].

Finally, the lignin was decomposed in the range between 410°C to 800°C. Furthermore, we observed stabilization in the weight loss rate, revealing that the maximum decomposition temperature was 800°C.

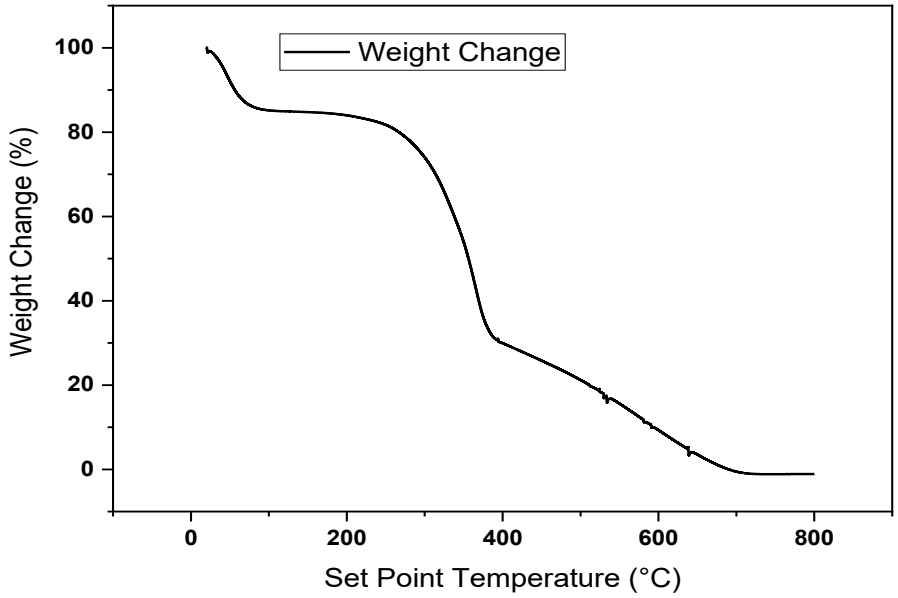

Figure V. 1. 1: TGA results for pine cone precursor

Ⅴ. 1. 1. 2. Global quality of the Pine cone raw material

Table V. 1. 1: Parameters evaluating the overall quality of the raw material

Properties	Pine Cone Precursor (PCP)
Volatile matter (%)	66.54
Humidity rate (%)	5.7
Ash ratio (%)	2.9
Carbon yield (%)	24.86
Apparent density (g. cm^{-3})	0.337
Iodine number (mg. g^{-1})	101.544
MB index (mg. g^{-1})	47.26

According to **Table V. 1. 1,** the PCP exhibited a substantial volatile matter content of 66.54% and a relatively low moisture content of 5.7%, which makes it suitable for thermochemical processes [6]. The immediate analysis of the PCP revealed low ash content (2.9 %) and a high carbon yield (24.86%). Consequently, pine cones are suitable for producing high-quality activated carbon due to their low ash content and high carbon yield [7].

Ⅴ. 1. 1. 3. SEM-EDS results for PCP

The SEM image of the pine cone precursor presented in **Figure V. 1. 2** shows a layered and uneven structure with apparent fissures and compact parts, which is typical of lignocellulosic materials made of cellulose, hemicellulose, and lignin [8, 9]. Small particles on the surface may be natural residues or fragments. At this point, the material has limited porosity, but the existence of cracks and voids suggests that pore creation could occur after activation.

This structural framework suggests that the precursor is suitable for chemical or physical activation procedures that can increase its surface area and porosity, allowing it to function as an effective adsorbent [10].

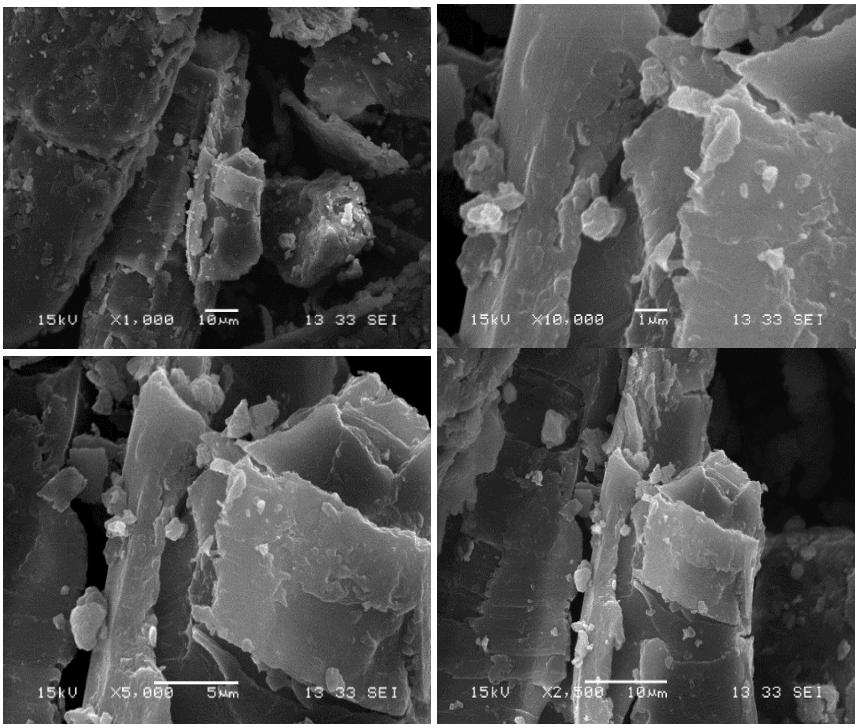

Figure V. 1. 2: SEM images of the PCP

EDS analysis of the pine cone precursor (**Figure V. 1. 3**) revealed the elemental composition with dominant peaks for carbon (C) and oxygen (O), expected in lignocellulosic materials, mainly composed of cellulose, hemicellulose, and lignin [11, 12]. The high carbon content indicates the organic nature of the precursor, making it a suitable material for conversion into activated carbon [13].

Smaller peaks for elements such as magnesium (Mg), silicon (Si), and aluminum (Al) suggest the presence of trace minerals [14], probably derived from the natural structure of the pine cone or exposure to the environment during growth. These minerals are generally in low concentrations and may not significantly affect the activation process.

The EDS results confirmed that the pinecone precursor is rich in carbon and oxygen, with minor amounts of mineral elements. This composition allows for further processing to develop porous activated carbon for adsorption applications.

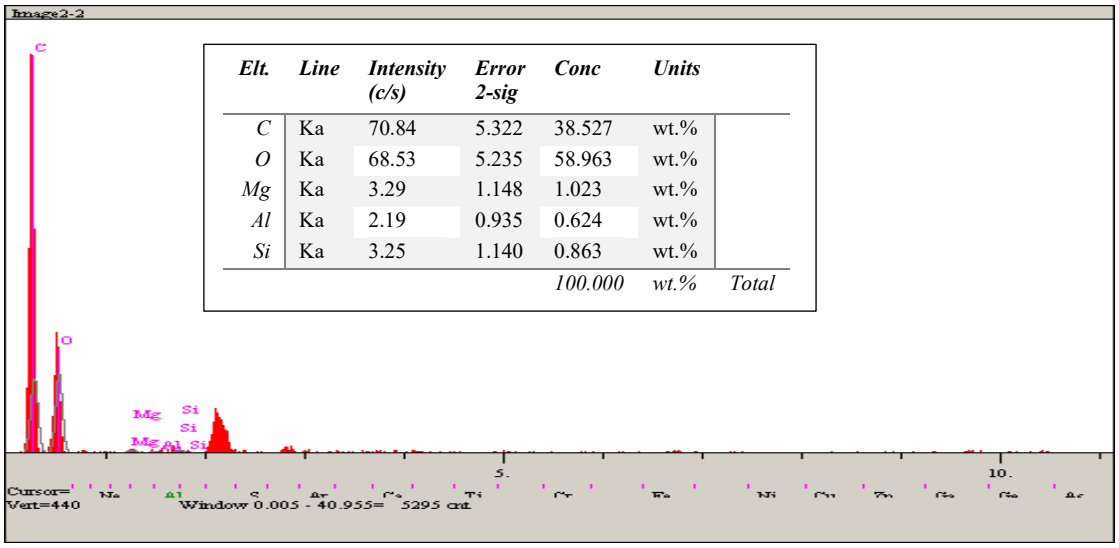

Elt.	Line	Intensity (c/s)	Error 2-sig	Conc	Units	
C	Ka	70.84	5.322	38.527	wt.%	
O	Ka	68.53	5.235	58.963	wt.%	
Mg	Ka	3.29	1.148	1.023	wt.%	
Al	Ka	2.19	0.935	0.624	wt.%	
Si	Ka	3.25	1.140	0.863	wt.%	
				100.000	wt.%	Total

Figure V. 1. 3: EDS spectrum of PCP

V. 1. 1. 4. FT-IR spectrum of PCP

Figure V. 1. 4 depicts the FT-IR spectrum of the pine cone precursor (PCP), The FT-IR spectrum indicates the presence of hydroxyl groups, aliphatic hydrocarbons, carbonyl groups, and aromatic structures, following its composition of lignin, cellulose, and hemicellulose. This provides valuable information on the chemical structure and functional groups present before the activation process. The large peak at 3393.68 cm^{-1} indicates O-H stretching, which is probably due to hydroxyl groups from water, alcohols, or phenols in the pine precursor. The peak at 2920.39 cm^{-1} is associated with C-H stretching from aliphatic hydrocarbons, most likely representing $–CH_2$ and $-CH_3$ groups found in organic molecules such as cellulose and lignin. The band observed at 1732 cm^{-1} corresponds to the C=O stretching of esters, carbonyl groups, or carboxylic acids, which may originate from hemicellulose or other organic precursor compounds. C=C elongation could indicate the presence of aromatic rings or conjugated alkenes in lignin at the 1621 cm^{-1} wavelength. The peak at 1378 cm^{-1} can be attributed to C-H bending (methyl or methylene groups), which is common in the structure of lignocellulosic materials. The signal at 1273.51 cm^{-1} can be ascribed to C-O stretching of aryl ethers or C-O-H deformation, observed in lignin or polysaccharides. Strong absorption band for C-O stretching in alcohols, ethers, or carbohydrates is observed at 1057.02 cm^{-1} wavelength, common in cellulose or hemicellulose structures. Finally, the peak at 568.44 cm^{-1} can be associated with out-of-plane bending of aromatic C-H bonds, possibly related to aromatic components in lignin [15-17].

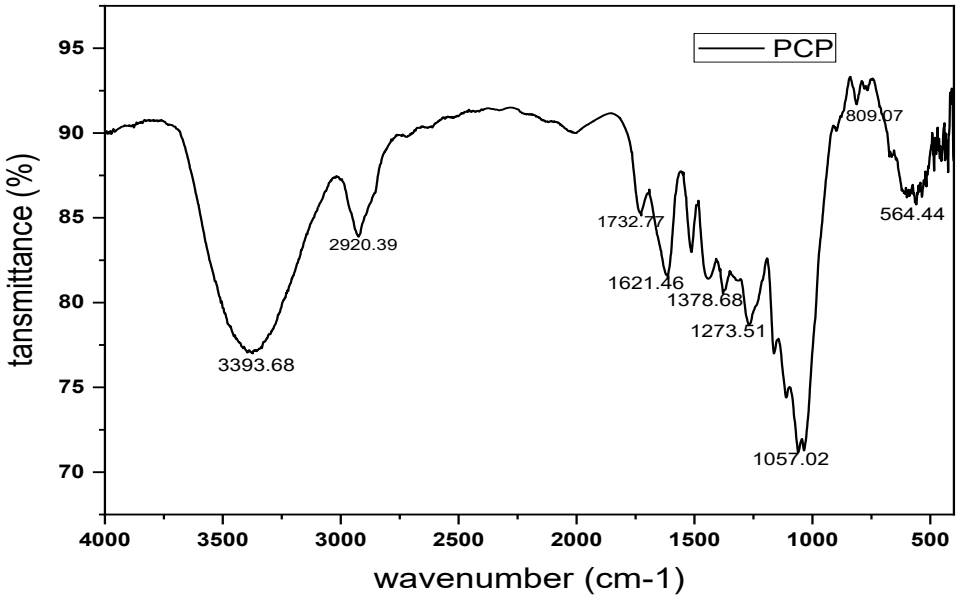

Figure V. 1. 4: FTIR spectrum of PCP

V. 1. 1. 5. X-ray diffraction analysis of the PCP

The XRD pattern of PCP in **Fig V. 1. 5** revealed a broad diffraction peak centered about 20-30° (2θ), basically indicating an amorphous structure with a few low-degree crystalline areas [18, 19]. The broad peak indicates the presence of cellulose, hemicellulose, and lignin, the primary organic components of organic precursors [20].

The lack of strong peaks suggests that the material has no well-defined crystalline domains, validating its classification as amorphous biomass [21]. Slight intensity changes in the 15-30° range may be due to residual semi-crystalline cellulose or inorganic components [22]. This amorphous nature is advantageous for activation operations because it promotes the formation of a porous structure during pyrolysis and activation, resulting in large-surface activated carbon [23].

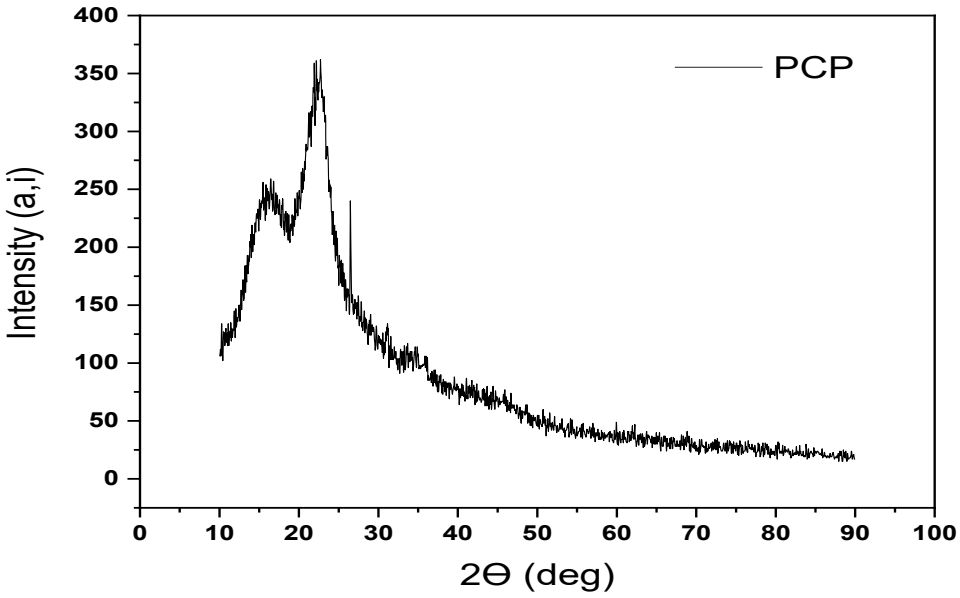

Figure V. 1. 5: XRD pattern of PCP

V. 1. 2. Characterization results of the activated carbons prepared in a muffle oven

V. 1. 2. 1. Comparison between one-step and two-step chemical activation protocols

V. 1. 2. 1. 1 Overall quality of the prepared activated carbon

The overall quality parameters of the prepared activated carbon with one-step and two-step are presented in **Table V. 1. 2.**

Table V. 1. 2: Parameters evaluating the overall quality of the activated carbons prepared using one-step and two-step activation processes (K-AC_1 and K-AC_2)

Property	Adsorbent	
	K-AC_1	**K-AC_2**
Burn-off (%)	63.55	27.74
Yield (%)	36.44	72.25
Volatile matter (%)	63.56	27.75
Humidity rate (%)	2.4	2
Ash ratio (%)	4	3
Carbon yield (%)	30.04	67.25
Apparent density (g cm^{-3})	0.227	0.451
Iodine number (mg g^{-1})	767.92	666.38
MB index (mg g^{-1})	122.859	72.768

Table V. 1. 2 and **Figure V. 1. 6** show that there was a significant weight loss (burn-off) during the activation process for K-AC_1 (63.55%). However, for K-AC_2, it was only 27.74%. This difference was visually observed in the laboratory, where the resulting K-AC_1 prepared through one-step activation produced less quantity of K-AC_1 than K-AC_2 that was prepared by applying the two-step activation protocol. We also noticed that the yields were 36.44% and 72.25% for K-AC_1 and K-AC_2, respectively. This result argues in favor of the synthesis of activated carbon from pine cone biomass using the two-step protocol, as only 27.75% of the material would be volatile after carbonization [24].

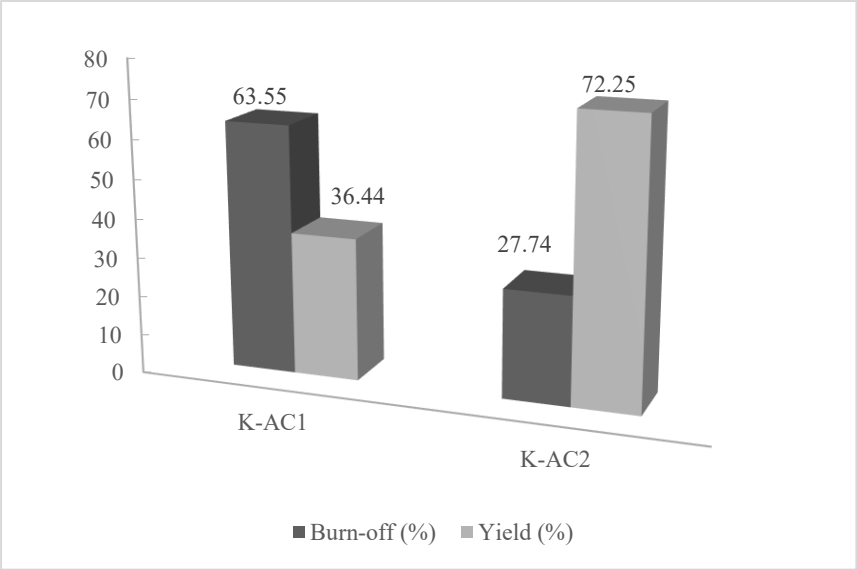

Figure V. 1. 6: Burn-off and yield of K-AC_1 and K-AC_2

As noticed from **Table V. 1. 2**, the resulting activated carbon samples K-AC_1 and K-AC_2 exhibited a very low moisture content compared to the raw material. It is also evident that K-AC_2 had a significantly lower volatile matter content (27.75%), indicating that the two-step activation process enhances the quality of the pine cone precursor activated with the KOH activating agent.

A low ash content was observed in the two-step prepared activated carbon K-AC_2 (3%), unlike the directly impregnated activated carbon, which exhibited a 4% ash content.

A low quantity of ash indicates the good quality of the adsorbent material [24]**.** A high ash ratio leads to contamination and clumping within the reactor. Simultaneously, it impacts the quality of pyrolysis, and results in higher operational expenses [25]. As a result, an adsorbent with high volatile and ash content is not appropriate [7].

Furthermore, the primary carbonization step applied to produce K-AC_2 enhanced the carbon content quality of the activated carbon. As noted in **Table V. 1. 2**, it contained the highest percentage of carbon yield (67.25%).

The iodine number is a parameter used to determine the presence of micropores in an adsorbent material. **Figure V. 1. 7** shows that the samples exhibited a good iodine adsorption capacity, indicating the presence of micropores. Consequently, activation with potassium hydroxide significantly enhanced the iodine number. Indeed, this number increased from 101.544 mg. g^{-1} for the raw material to 767.92 mg. g^{-1} for K-AC_1 activated carbon and 666.38

mg. g^{-1} for K-AC_2 activated carbon, in contrast to the activation of pine cones with phosphoric acid (H_3PO_4), which decreased this number according to the literature [24].

We also observe in **Figure V. 1. 7** that the Methylene blue values (which analyzes mesoporosity) were lower than the iodine index (which analyzes microporosity), confirming that activation with potassium hydroxide results in predominantly microporous activated carbon [26, 27]. KOH demonstrates greater efficacy in micropore formation, primarily attributed to the presence of layer interactions [28].

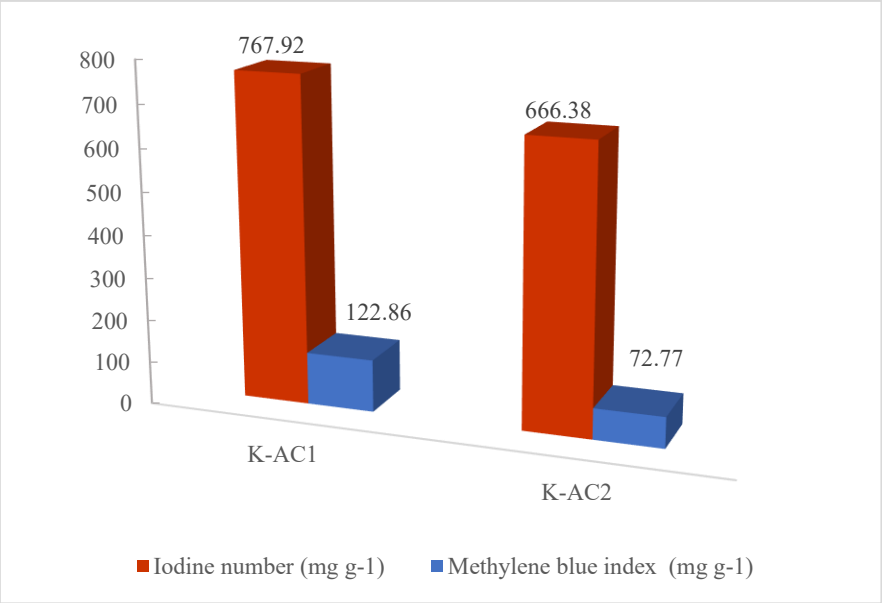

Figure V. 1. 7: Histograms of iodine number and Methylene blue index of K-AC_1 and K-AC_2

V. 1. 2. 1. 2 Textural and structural properties of the K-AC_2

A. Characterization of porous texture

Table V. 1. 3: BET adsorption-desorption results of K-AC_2

BET surface area (m^2 g^{-1})	430.504
BJH surface Area (m^2 g^{-1})	144.809
Langmuir surface area (m^2 g^{-1})	313.707
Micropore surface area (m^2 g^{-1})	270.52
Pore volume (cc g^{-1})	1.778
Pore radius Dv(r) (nm)	1.879

The results in **Table V. 1. 3** show that the activation process helped the prepared carbon acquire an acceptable specific surface area (430.5 m^2 g^{-1}). Consistent with the measured iodine number, the N_2 adsorption/desorption isotherms depicted in **Figure V. 1. 8** demonstrate an increase in adsorption at comparatively low pressures ($P/P_0 < 0.03$), suggesting the existence of micropores. On the other hand, a shift from monolayer to multilayer adsorption was seen for intermediate and higher P/P_0 levels. The isothermal curve exhibited a clear hysteresis loop and indicated the presence of a capillary condensation of N_2 above $P/P_0 > 0.98$ [29].

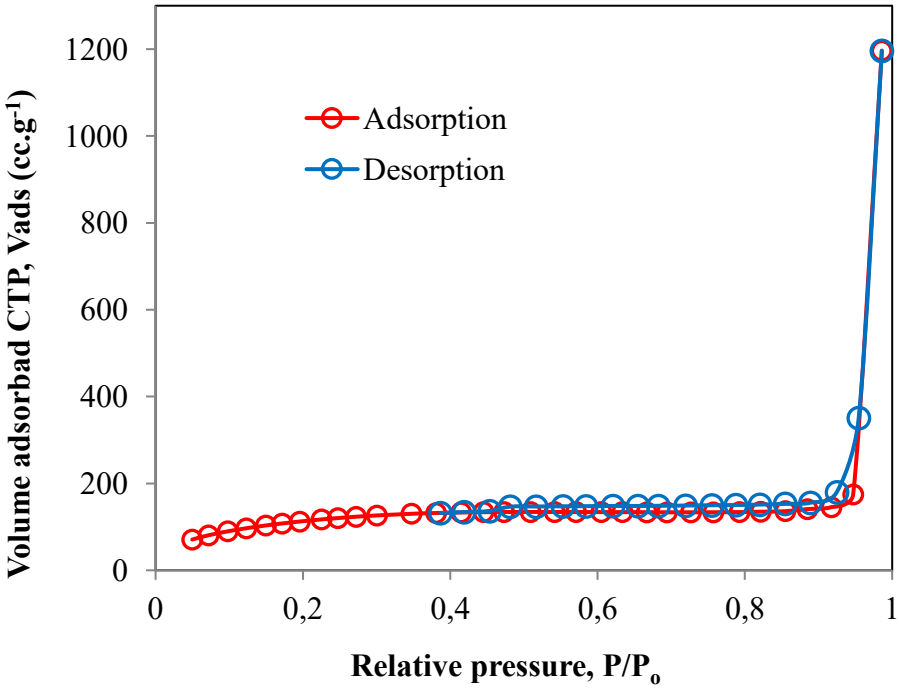

Figure V. 1. 8: N_2 adsorption/desorption isotherms of K-AC_2 activated carbon

Table V. 1. 4: Comparison of specific surface area and pore volume of KOH-activated carbons produced from different biomasses

Biomass	**S_{BET} ($m^2\ g^{-1}$)**	**V_{Tot} ($cm^3\ g^{-1}$)**	**Reference**
Pine cone	430.5	1.778	This study
Eucalyptus	92-200	/	[30]
Orange peel	592.471	0.242	[31]
Sewage sludge	130.7	0.13	[32]
Rice-husk	322.8	0.1734	[33]
Vine leaf	538	0.236	[34]
Sugar cane bagasse	851	0.442	[35]

B. Morphological structure and elemental composition of K-AC_2 by SEM-EDS

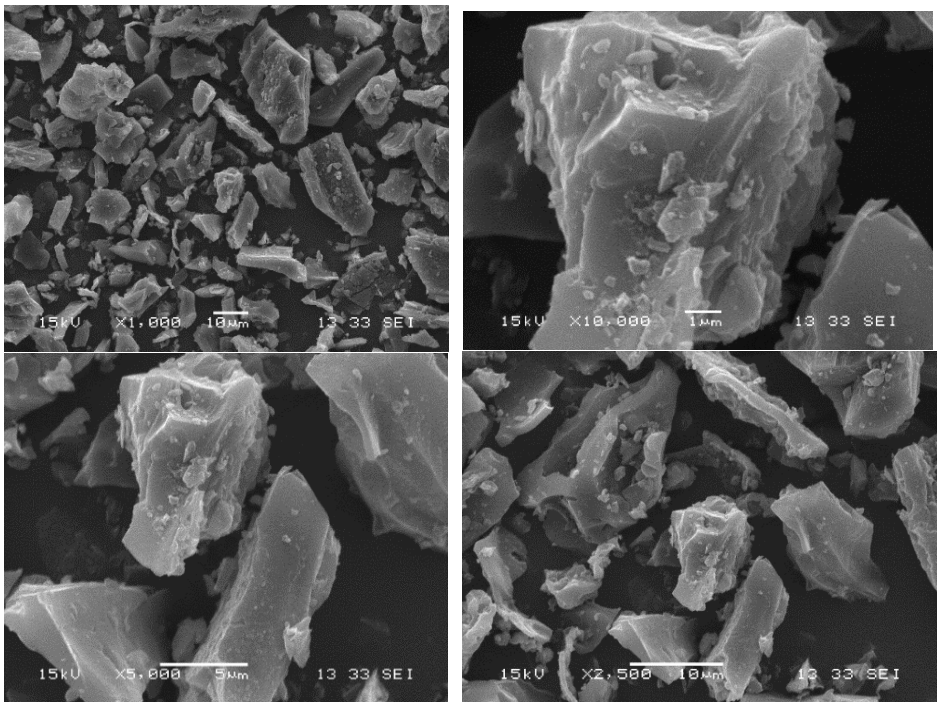

Figure V. 1. 9: SEM micrographs of K-AC_2

Figure V. 1. 9 shows the SEM images of K-AC_2 activated carbon. The results revealed a heterogeneous, dispersed morphology and porous surface, as well as the presence of cavities indicating a well-developed pore structure, essential for adsorption applications, compared to the SEM images of PCP presented in **Figure V. 1. 2**, where almost a clear surface is shown.

Further EDS analysis would confirm the elemental composition and identify potential impurities likely to influence performance.

The rise in carbon content in the activated carbon, from 38.527% from PCP EDS results that was presented in **Figure V. 1. 3** to 66.757% from **Figure V. 1. 10**, signifies the completion of the chemical activation process of the PCP, with the carbonization step being the initial stage. Minor amounts of inorganic elements, including silicon (1.57%), aluminum (0.34%), magnesium (0.21%), and calcium (0.17%), probably originate from the precursor material and may contribute to surface chemical modifications, such as pH adjustments and specific binding sites [36]. These results confirm the previous finding of low ash content overall, suggesting a good-quality activated carbon with minimal inorganic residues, guaranteeing effective adsorption performance for the targeted pollutants.

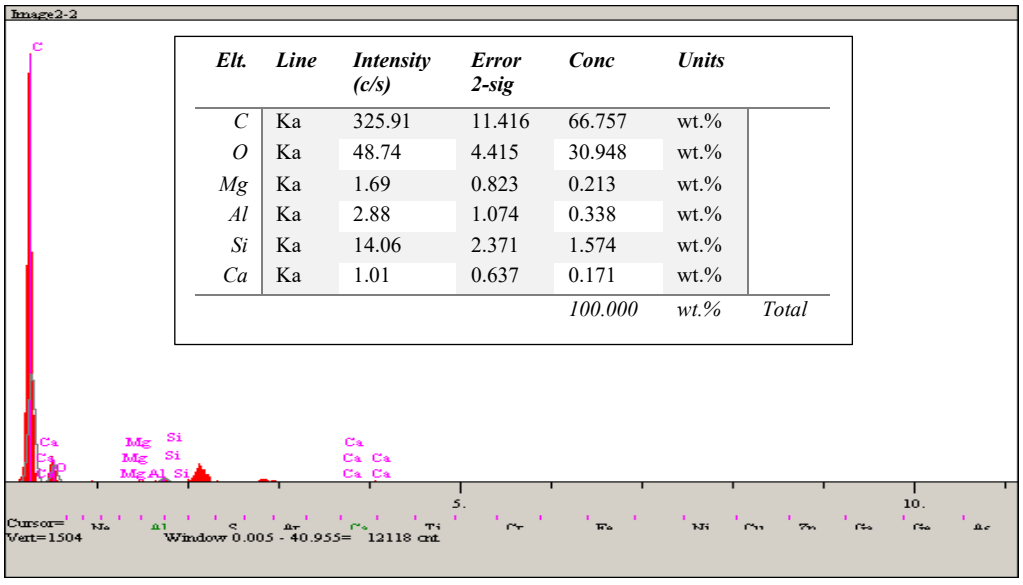

Elt.	*Line*	*Intensity (c/s)*	*Error 2-sig*	*Conc*	*Units*	
C	Ka	325.91	11.416	66.757	wt.%	
O	Ka	48.74	4.415	30.948	wt.%	
Mg	Ka	1.69	0.823	0.213	wt.%	
Al	Ka	2.88	1.074	0.338	wt.%	
Si	Ka	14.06	2.371	1.574	wt.%	
Ca	Ka	1.01	0.637	0.171	wt.%	
				100.000	*wt.%*	*Total*

Figure V. 1. 10: EDS spectrum of K-AC_2

C. FTIR analysis of K-AC$_2$

Figure V. 1. 11: FT-IR spectrum of K-AC$_2$

The FT-IR spectrum of activated carbon (**Figure V. 1. 11)** revealed the key functional groups that contribute to its adsorption properties [37]. The broadband observed around 3200-3500 cm^{-1} indicates O-H stretching of hydroxyl groups [38], The signals between 2949 and 2522 cm^{-1} can be attributed to the elongation vibrations of the C-H/OH and C-H groups of CHO, and the spectral bands around 2357 cm^{-1} for K-AC$_2$ may be due to ketene or ketone [39]. The peaks located between 1713 and 1627 cm^{-1} can be attributed to the symmetrical C=C and C=O stretching of the pyrone, aldehyde, or carboxylic groups, also the peak at 1644.91 cm^{-1} confirms the presence of the C=O carboxyl group and a weak carbonyl group peak at 1321.49 cm^{-1} can be linked to the COO$^-$ ion. A band observed between 1044.14 and 1612 cm^{-1} can be ascribed to the elongation of the C-O group of the functions of carboxylic acids, esters, ethers, or alcohols [40]. Peaks below 1000 cm^{-1} may indicate Si-O or metal-oxide bonds [41], consistent with EDS results showing traces of Si, Mg, and Ca. These functional groups play a crucial role in adsorption, enhancing interactions with polar pollutants in wastewater treatment applications [42].

The Boehm titrations result (**Table V. 1. 5)** revealed that the K-AC$_2$ activated charcoal used in this study has a higher quantity of basic functional groups (4.666 meq g^{-1}) compared to acidic groups (1.666 meq g^{-1}). This is confirmed by its basic nature, as indicated by its pH value (pH at the point of zero charge = 7.6).

Table V. 1. 5: Boehm method results of K-AC_2 activated carbon revealing the various groups

Carboxylic = N [$NaHCO_3$] (meqg g^{-1})	0.666
Lactone = N [Na_2CO_3]- N [$NaHCO_3$] (meqg g^{-1})	0.167
Phenol =N[NaOH]- N [Na_2CO_3] (meqg g^{-1})	3.833
Basic =N [NaOH] (meqg g^{-1})	4.666
Acidic = N [HCl] (meqg g^{-1})	1.666

D. pH_{pzc} results of K-AC_2

Table V. 1. 6: Initial and final pH values for the determination of pH_{pzc} of K-AC_2

pH_i	2	4	6	8	10	12
pH_f	2.38	6.3	7.04	7.85	9.07	11.85

The pH_{pzc} (point of zero charge) corresponds to the point of intersection of the curve with the line defined by the equation $pH_{final} = pH_{initial}$ (**Figure V. 1. 12**). pH_{pzc} of K-AC_2 is 7.6. Consequently, K-AC_2 exhibits a basic surface that releases OH^- ions. The overall surface charge is positive for solutions with a pH lower than this value, and it becomes negative when the pH values exceed the pH_{PZC}.

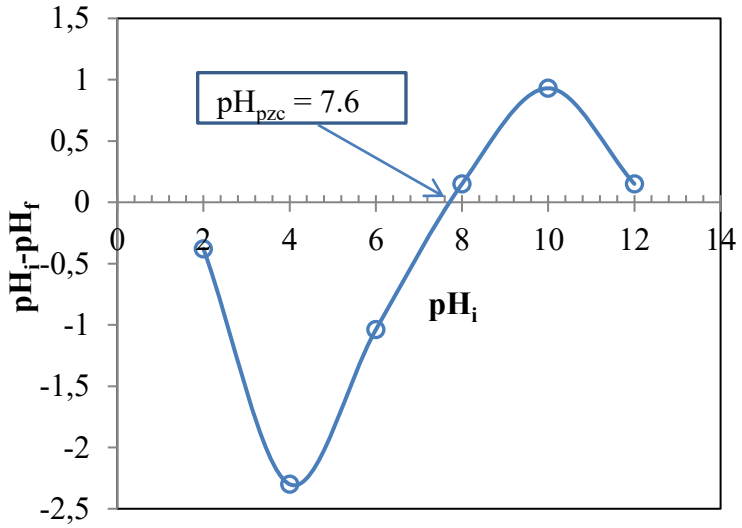

Figure V. 1. 12: Determination of pH_{pzc} of K-AC_2

Ⅴ. 1. 2. 2. Results of the Parametric study

Ⅴ. 1. 2. 2. 1 Overall quality of the prepared activated carbons

The parametric study was conducted by optimizing the activating parameters, which are the carbonization temperature (T(°C)), the activation period (hour), and the impregnation ratio.

As mentioned in the Materials and Methods chapter, the yield of the activated carbon wasn't acceptable or enough in the one-step activation, in this parametric study, we set the carbonization time to 30 min and varied only the temperature. We decreased the temperature to 600°C to prepare **K-AC$_1$'**.

For the two-step activation process, we prepared **AC$_{600.30}$, AC$_{700.30}$, K-AC$_2$' (AC$_{800.30}$), AC$_{600.45}$, AC$_{700.45}$, AC$_{800.45}$, AC$_{600.60}$, AC$_{700.60}$,** and **AC$_{800.60}$** activated carbons. (The protocols of each parametric study are detailed in the Materials and Methods chapter)

The parameters that evaluate the overall quality of the activated carbon prepared in this section are presented in Tables**:** V 1. 7, V.1. 8, V. 1. 9, and V. 1. 10.

A. Activated carbons prepared by the one-step activation process

Table V. 1. 7: K-AC_1' and K-AC_1 comparison results

	AC prepared in **one-step** activation	
AC	**K-AC_1'**	**K-AC_1**
Activation parameter	T= 600°C t = 30 min	T = 800°C t = 30 min
	1:1 impregnation ratio	
Yield (%)	49.52	36.44
Burn off (%)	50.47	63.55
Iodine number (mg g^{-1})	545.8	767.92
MB index (mg g^{-1})	20.4	122.86
Micropore surface area (m^2g^{-1})	320.32	758.8
Limiting micropore volume (cm^3 g^{-1})	0.135	0.27

The results in **Table V. 1. 7** show that the activation temperature of 800°C significantly reduced the yield from 49.52% to 36.44%, with a corresponding increase in burn-off from 50.47% to 63.55%. This indicates that higher temperatures led to excessive loss of material, resulting in a very low yield, which was also observed experimentally in the laboratory, where the amount of activated carbon prepared was insufficient for other adsorption applications.

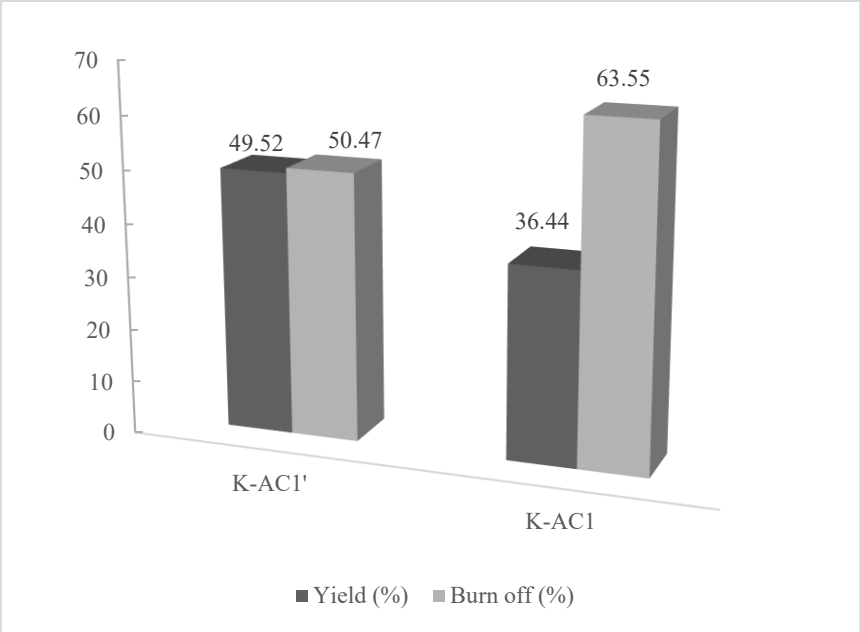

Figure V. 1. 13: Burn-off and yield of K-AC$_1$ and K-AC$_1$'

To remedy this problem, the activation temperature was lowered to 600°C for the remainder of the study. However, this adjustment did not improve the yield or quantity of activated carbon obtained.

On the other hand, higher temperatures improved porosity and adsorption properties. The iodine value increased from 545.8 to 767.92 mg g^{-1}, and the Methylene blue (MB) value strongly increased from 20.4 to 122.86 mg g^{-1} suggesting better development of micropores and mesopores in K-AC$_1$' (**Figure V. 1. 14**).

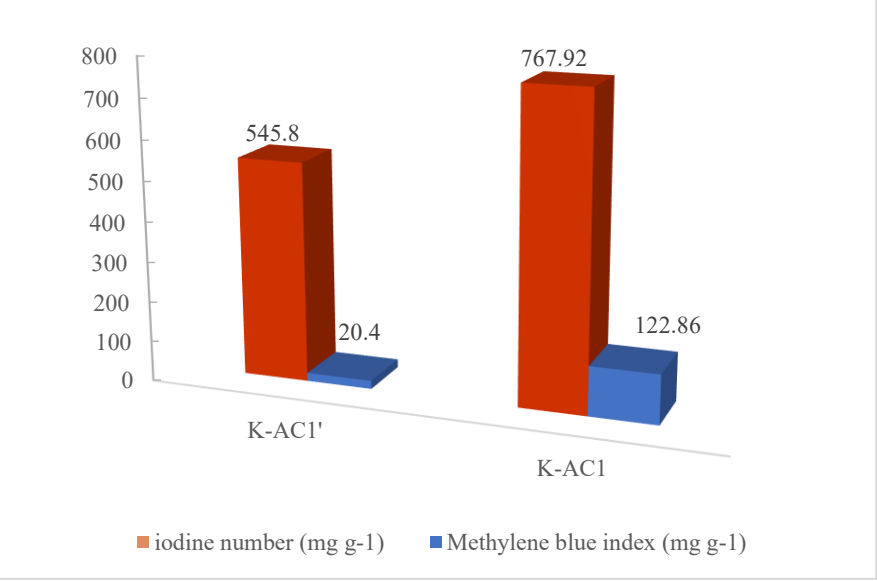

Figure V. 1. 14: Histograms of iodine number and Methylene blue index of K-AC$_1$ and K-AC$_1$'

Micropore surface area more than doubled, from 320.32 m^2 g^{-1} at 600°C to 758.8 m^2 g^{-1} at 800°C, and micropore volume also increased, from 0.135 cm^3 g^{-1} to 0.27 cm^3 g^{-1}, confirming that higher temperatures improved activated carbon porosity.

Although the 800°C temperature provided better textural and adsorption properties, the very low yield does not allow it to be used for large-scale applications, highlighting the need for further optimization.

For this reason, the two-stage activation process was selected for further optimization and parametric study.

B. Activated carbons produced by the two-step activation procedure

Table V. 1. 8: $AC_{600.30}$, $AC_{700.30}$, K-AC_2, K-AC_2' comparison results

	ACs prepared by **two-step** activation			
AC	**$AC_{600.30}$**	**$AC_{700.30}$**	**K-AC_2 ($AC_{800.30}$)**	**K-AC_2'**
Activation parameter	T = 600°C t = 30 min	T = 700°C t = 30min	T =800°C t = 30 min	T = 800°C t = 30 min
	1:1 Impregnation ratio			1:2 Impregnation ratio
Yield (%)	74.75	72.25	66.95	65.06
Burn off (%)	25.24	27.74	33.047	34.94
Iodine number (mg g^{-1})	507.72	539.45	666.38	609.27
MB index (mg g^{-1})	25.90	35.90	72.77	69.58
Micropore surface area (m^2 g^{-1})	210.71	276.26	270.52	792.80
Limiting micropore volume (cm^3 g^{-1})	0.085	0.11	0.10	0.30

The initial carbonization step is crucial as it allows the precursor material to be partially decomposed at a lower temperature before the activation step. This pre-treatment reduces the mass of the material and eliminates volatile components, creating a more stable structure better suited to the following activation process [43, 44]. In addition, this pretreatment increases yield by reducing excessive material losses during the activation stage, ultimately resulting in more efficient carbonization and activation [45]. The two-stage process allows better control of activated carbon properties, ensuring higher yields and more desirable textural characteristics for adsorption applications [46].

The results (**Table V. 1. 8**) of the two-stage activation process show that yield decreased with increasing activation temperature. The highest yield (74.75%) was obtained at 600°C for

30 minutes, while the lowest yield (65.06%) was observed at 800°C for 30 minutes with an impregnation ratio of 1:2.

This finding indicates that higher temperatures lead to greater material loss due to increased combustion. Burn-off increased with temperature, reaching 34.94 % at 800°C (1:2 ratio), confirming that more volatile components were removed at higher temperatures (**Table V. 1. 8** and **Figure V. 1. 15**).

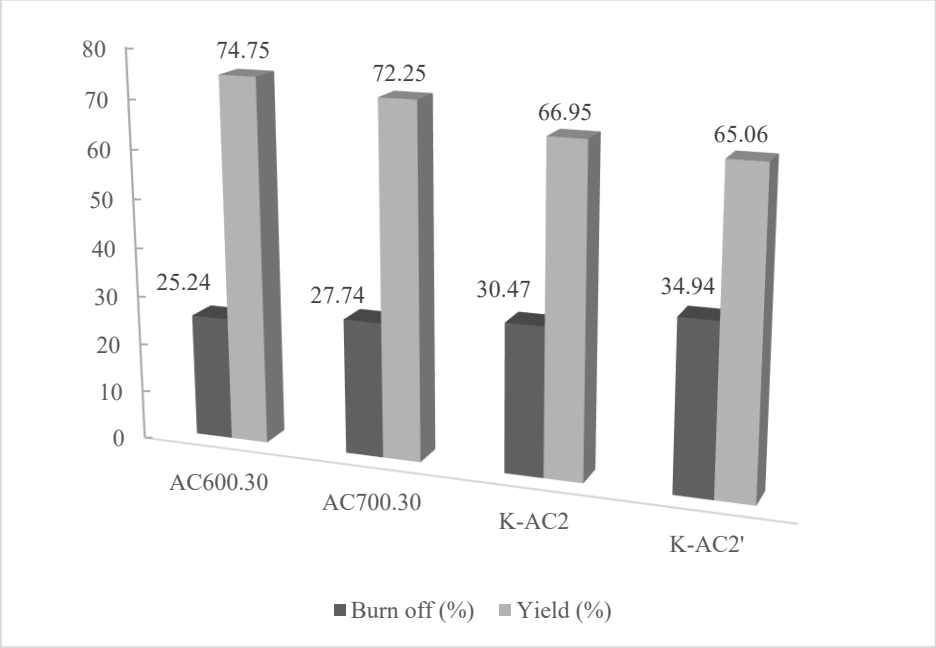

Figure V. 1. 15: Burn-off and yield of $AC_{600.30}$, $AC_{700.30}$, K-AC_2, and K-AC_2'

The iodine number and MB index, which reflect the adsorption capacity and surface properties of activated carbon, also improved with higher activation temperatures. The highest iodine number (666.38 mg g^{-1}) and MB number (72.77 mg g^{-1}) were obtained at 800°C (1:1 ratio) for K-AC_2, indicating an improvement in porosity and adsorption capacity (**Table V. 1. 8** and **Figure V. 1. 16**).

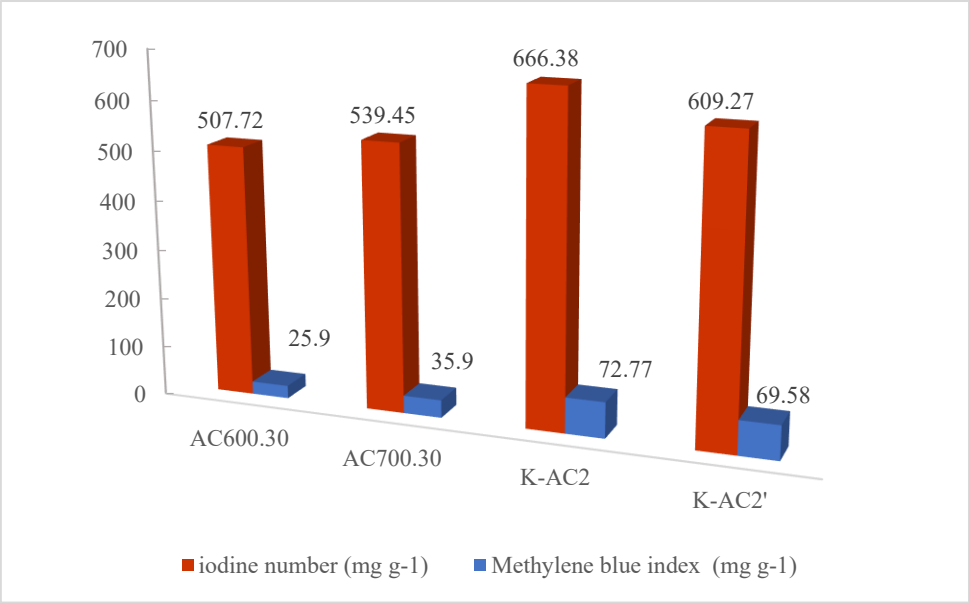

Figure V. 1. 16: Comparative histogram of iodine number and Methylene blue index of $AC_{600.30}$, $AC_{700.30}$, K-AC_2, and K-AC_2'

The micropore surface area increased with temperature, but a significant improvement was observed when the impregnation ratio was increased to 1:2 at 800°C, where it reached 792.80 $m^2\ g^{-1}$. This suggests that a higher impregnation ratio increases micropore surface area. meaning that a higher impregnation ratio improves pore development (**Table V. 1. 8)**.

Similarly, the micropore volume limit increased from 0.085 $cm^3\ g^{-1}$ at 600°C to 0.30 $cm^3\ g^{-1}$ at 800°C (1:2 ratio), confirming a substantial increase in microporosity. The increase in micropore surface area with a 1:2 impregnation ratio is mainly due to the higher concentration of KOH, which enhances the activation process [47, 48]. Excess KOH penetrates deeper into the carbon structure, resulting in a greater decomposition effect that removes disordered carbon and creates more micropores [49, 50]. However, according to our results, increasing the intensity of activation led to increased burn-off, which significantly reduced the overall yield of activated carbon. Although the 1:2 ratio favors the development of micropores, the loss of material makes it unsuitable for large-scale applications. In comparison (**Table V. 1. 8.**), the 1:1 impregnation ratio achieved a better balance between yield and adsorption qualities. It preserved sufficient activated carbon while ensuring good porosity, making it a more feasible option for future research and real-world applications. Overall, the two-step activation process offers a higher yield than the one-step method, while allowing better control of porosity and adsorption properties.

The results in **Table V. 1. 8** suggest that optimization of activation temperature and impregnation ratio is essential to obtain high-quality activated carbon with desirable textural and adsorption characteristics.

Table V. 1. 9: $AC_{600.45}$, $AC_{700.45}$, $AC_{800.45}$ comparison results

	AC prepared in **two-step** activation		
AC	**$AC_{600.45}$**	**$AC_{700.45}$**	**$AC_{800.45}$**
Activation parameter	T = 600°C t = 45 min	T = 700°C T = 45min	T = 800°C T = 45min
	1:1 Impregnation ratio		
Yield (%)	77.65	75.01	71.63
Burn off (%)	22.35	24.98	28.36
Iodine number (mg g^{-1})	545.8	590.22	602.91
MB index (mg g^{-1})	32.24	51.36	58.19
Micropore surface area (m^2 g^{-1})	234.32	327.08	301.90
Limiting micropore volume (cm^3 g^{-1})	0.084	0.117	0.115

The results of two-stage activation at 45 min show an improvement in yield compared with the two-stage activation process at 30 min. The yield was highest at 600°C (77.65%) and decreased with increasing activation temperature up to 700°C (75.01%) and 800°C (71.63%). This result is to be expected, as higher temperatures led to greater combustion, resulting in greater material loss (**Table V. 1. 9** and **Figure V. 1. 17**).

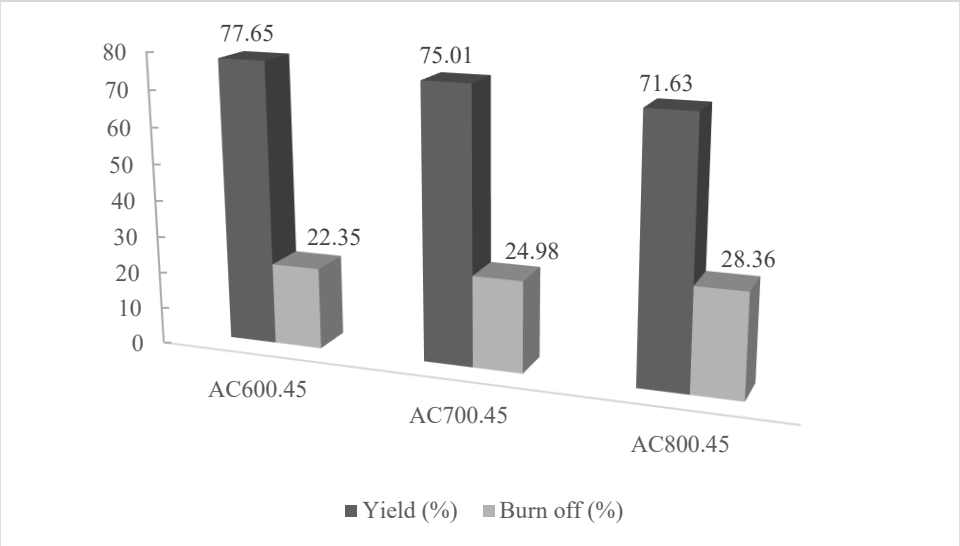

Figure V. 1. 17: Burn-off and yield of $AC_{600.45}$, $AC_{700.45}$, and $AC_{800.45}$

However, the iodine number, MB index, and micropore surface area all increased with temperature, indicating better pore development and adsorption properties (**Table V. 1. 9** and **Figure V. 1. 18**).

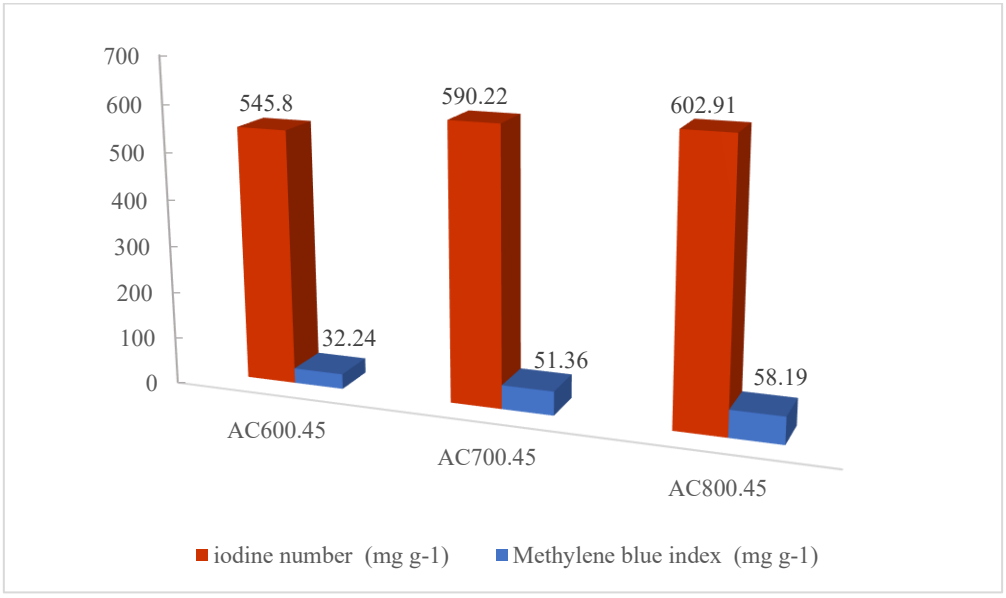

Figure V. 1. 18: Comparative histogram of iodine number and Methylene blue index of $AC_{600.45}$, $AC_{700.45}$, and $AC_{800.45}$

The two-stage 30 min-activation (**Table V. 1. 8**), compared to the 45 min-activation process, maintained higher yields while improving adsorption properties (**Table V. 1. 9**). The iodine number and MB index increased as the activation temperature rose, demonstrating that a longer activation time enables further pore formation.

However, the micropore surface area at 800°C (301.90 $m^2 g^{-1}$) was slightly lower than at 700°C (327.08 $m^2 g^{-1}$), suggesting that excessive activation may reduce microporosity.

Compared with one-step activation (**Table V. 1. 7**), the two-step process produced a much higher yield and better overall activated carbon quality. The one-step activation at 800°C for 30 min gave only 36.44 % yield (**Table V. 1. 8**), while the two-step process at 800°C for 45 min gave 71.63 % yield, almost doubling the yield (**Table V. 1. 9)**. This confirms that initial carbonization before activation stabilizes the structure, reducing excessive combustion and improving carbon retention.

Table V. 1. 10: $AC_{600.60}$, $AC_{700.60}$, $AC_{800.60}$ comparison results

	AC prepared in **two-step** activation		
AC	**$AC_{600.60}$**	**$AC_{700.60}$**	**$AC_{800.60}$**
Activation parameter	T = 600°C t = 60 min	T = 700°C t = 60 min	T = 800°C t = 60 min
	1:1 Impregnation ratio		
Yield (%)	58.39	52.016	46.57
Burn off (%)	41.61	47.98	53.42
Iodine number (mg g^{-1})	571.19	593.4	507.72
MB index (mg g^{-1})	34.06	45.44	54.09
Micropore surface area ($m^2 g^{-1}$)	203.85	392.43	273.38
Limiting micropore volume ($cm^3 g^{-1}$)	0.089	0.148	0.107

Increasing the activation time to 60 min, with higher temperature, resulted in a significant yield loss due to excessive degradation of the carbon structure, which resulted in more combustion (**Table V. 1. 10** and **Figure V. 1. 19)**

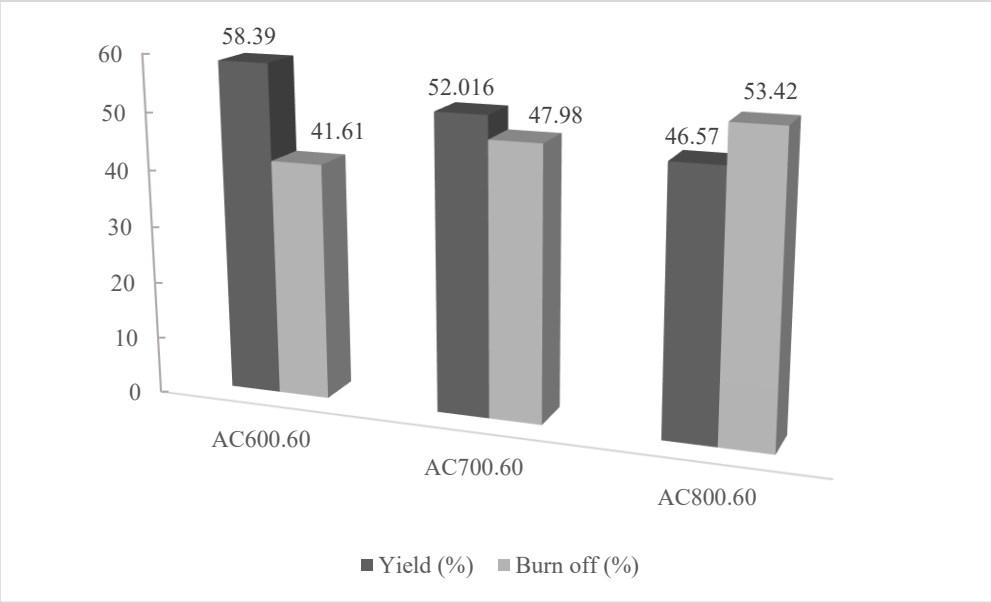

Figure V. 1. 19: Burn-off and yield of $AC_{600.60}$, $AC_{700.60}$, and $AC_{800.60}$

According to **Table V. 1. 10** and **Figure V. 1. 20**, the iodine number rose at 700°C (593.4 mg g^{-1}) but decreased at 800°C (507.72 mg g^{-1}), demonstrating that high activation inhibits micropore development [51]. Furthermore, the index of MB increased around 800°C, indicating the formation of a more mesoporous structure [52].

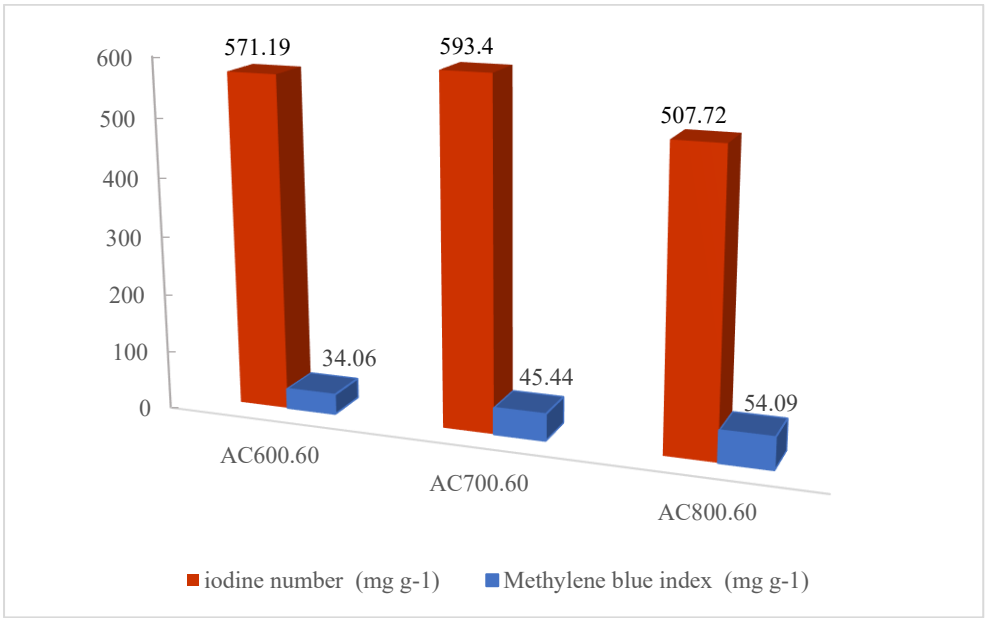

Figure V. 1. 20: Histograms of iodine number and Methylene blue index of $AC_{600.60}$, $AC_{700.60}$, and $AC_{800.60}$

This confirms that high temperatures damage the walls between micropores, resulting in structural degradation and the conversion of micropores to mesopores [53], which promotes MB adsorption but decreases iodine adsorption capability (**Figure V. 1. 20.**).

Micropore surface area followed a similar pattern, first increased at 700°C (392.43 m^2 g^{-1}), but then decreased at 800°C (273.38 m^2 g^{-1}), indicating that overactivation at higher temperatures can destroy micropores by transforming them into larger pores, as shown by several studies [51, 54].

The parametric investigation showed that activation temperature and time have a considerable impact on yield, porosity, and adsorption characteristics. Prolonged activation reduces carbon, weakening the structure and increasing material loss. Potassium hydroxide creates a microporous structure [55]. However, an extended activation period permits the activating agent to continue interacting with the carbon structure, resulting in pore enlargement [56], as confirmed by an increase in the MB index at 800°C.

As a result, while higher temperatures and longer activation durations may initially increase porosity, excessive activation reduces micropore volume and causes the material to develop a mesoporous texture. This emphasizes the importance of carefully controlling activation conditions to balance porosity enhancement and material conservation. Overall, the parametric study underlines the necessity to optimize activation parameters (temperature, time, and impregnation ratio) to balance yield, porosity, and adsorption capacity.

Ⅴ. 1. 3. Characterization results of the activated carbon prepared in a tube furnace under nitrogen atmosphere

This section includes the results and discussion of activated carbon produced via physicochemical activation with potassium hydroxide in a tube furnace under an inert nitrogen atmosphere. Five activated carbons were prepared using various activation methods. In the one-step activation technique, raw pine cones were immediately activated at 800°C for 30 minutes using two impregnation ratios (1:1 and 1:2). In the two-stage activation procedure, the material was first carbonized at 600°C for 1 hour, then activated at 800°C for 30 minutes, using the same impregnation ratios (1:1 and 1:2). The Materials and Methods chapter provides detailed experimental procedures.

Table V. 1. 11: Results of combined activation in a tube furnace under N_2 atmosphere (AC, AC_1, AC_1', AC_2, and AC_2' activated carbons)

	Direct Pyrolysis	**One-step activation**		**Two-step activation**	
AC	**Charcoal (AC)**	**AC_1**	**AC_1'**	**AC_2**	**AC_2'**
Activation parameters	T = 800°C t = 30min	T = 800°C t = 30min 1:1 ratio	T=800°C t = 30min 1:2 ratio	T=800°C t = 30 min 1:1 ratio	T=800°C t = 30min 1:2 ratio
Yield (%)	28.21	48.6	56.18	79.06	72.57
Burn off (%)	71.78	51.39	43.82	20.93	27.42
MB index (mg g^{-1})	80.51	95.67	96.89	174.23	50.60
Iodine number (mg g^{-1})	469.64	507.72	837.73	539.45	888.51
Micropore surface area (m^2 g^{-1})	27.94	745.30	850.19	227.28	1039.22
Limiting micropore volume (cm^3 g^{-1})	0.014	0.267	0.265	0.087	0.357

In this part, we compare the effects of different activation methods (physical activation, one-step physical chemical activation, and two-step physical chemical activation) on yield, burn-off, adsorption power, and material porosity.

The results (**Table V. 1.11)** reveal significant variations in these parameters, depending on the activation approach used. Physical treatment (Charcoal) (AC) produced the lowest yield (28.21%) and the largest burn-off (71.78%), demonstrating the aggressive nature of heat degradation in the absence of a chemical activating agent. One-step activation enhanced yield to 48.6% (AC_1) and 56.18% (AC_1'), while burn-off was reduced to 51.39% and 43.82%, respectively. A higher KOH ratio (1:2 in AC_1') results in better material retention and lower burn-off.

In contrast, two-step activation achieved the highest yields, with AC_2 reaching 79.06 % and AC_2' at 72.57 %, while their burn-off values were significantly lower (20.93% and 27.42%, respectively). The lower burn-off in this method suggests that the pre-treatment step in two-step activation stabilized the material, reducing excessive mass loss and leading to better carbon retention **(Table V. 1. 11** and **Figure V. 1. 21).**

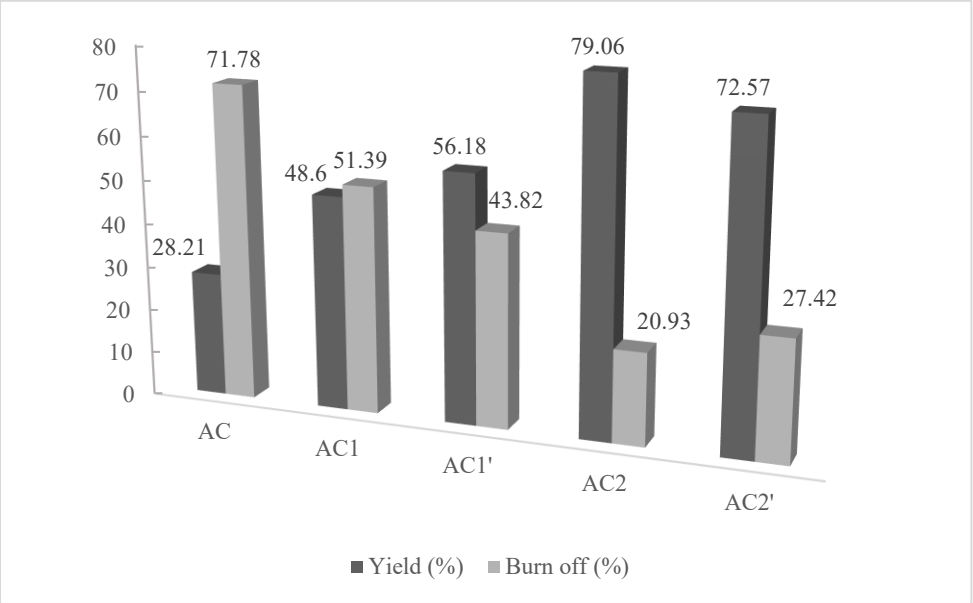

Figure V. 1. 21: Burn-off and yield of AC, AC_1, AC_1', AC_2, and AC_2'

As previously mentioned, the Methylene blue (MB) index measures the adsorption capacity of large molecules, indicating the presence of mesoporosity. In contrast, the iodine number measures the adsorption capacity of small molecules, giving an idea of microporosity.

Physical treatment yielded an MB index of 80.51 mg g^{-1}, indicating low mesoporosity. One-step activation resulted in a modest improvement, with values of 95.67 mg g^{-1} (AC_1) and 96.89 mg g^{-1} (AC_1'). However, the two-step activation showed larger values, AC_2 had the largest MB index (174.23 mg g^{-1}), indicating substantial mesoporosity, while AC_2' had the lowest MB value (50.60 mg g^{-1}), indicating the dominance of microporosity.

The iodine number showed a different pattern. AC yielded a value of 469.64 mg g^{-1}, slightly enhanced by one-step activation (507.72 mg g^{-1} for AC_1), and significantly increased with a higher KOH ratio (837.73 mg g^{-1} for AC_1'). The two-step activation resulted in the highest iodine number for AC_2' (888.51 mg g^{-1}), indicating greater microporosity. The value for AC_2 was 539.45 mg g^{-1}, indicating a mesoporous structure.

The results indicate that AC_2' is extremely microporous, while AC_2 has a more mesoporous structure (**Table V. 1. 11**. and **Figure V. 1. 22)**

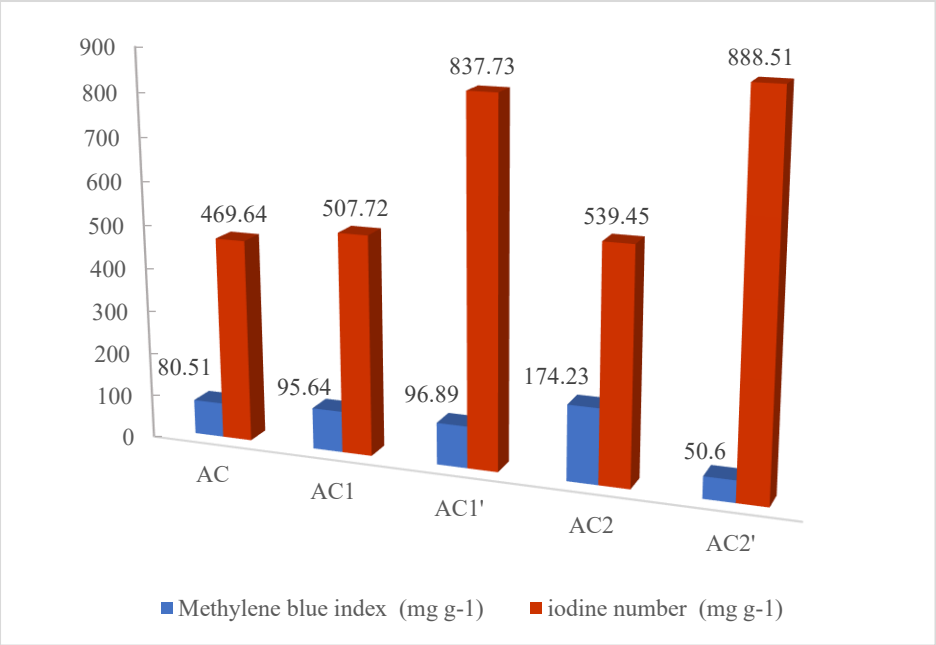

Figure V. 1. 22: Histograms of iodine number and Methylene blue index of AC, AC_1, AC_1', AC_2, and AC_2'

Microporosity was studied using micropore surface area and micropore volume. As shown in **Table V. 1. 11**, physical activation (AC) produced the smallest micropore surface area (27.94 m^2 g^{-1}) and volume (0.014 cm^3 g^{-1}), indicating ineffectual pore formation.

One-step activation significantly improved microporosity, with AC_1 achieving 745.30 m^2 g^{-1} and AC_1' increasing further to 850.19 m^2 g^{-1}. Their micropore volumes also improved (0.267 cm^3 g^{-1} and 0.265 cm^3 g^{-1}, respectively), demonstrating that a higher KOH ratio (1:2) enhances micropore development. The greatest creation in micropores was seen after two steps of activation. AC_2' activated carbon has the largest micropore surface area (1039.22 m^2 g^{-1}) and volume (0.357 cm^3 g^{-1}), indicating a superior microporous structure. AC_2 had a reduced micropore surface area (227.28 m^2 g^{-1}) and volume (0.087 cm^3 g^{-1}), suggestive of its mesoporous nature.

The choice of activation method plays a crucial role in studying the adsorption properties and pore structure of activated carbon. From our results, we can say that applying direct physical activation to the pine cone precursor (AC) produces low porosity and poor adsorption properties, making it the least effective process for the preparation of activated carbon by pine cone precursor.

One-step activation improves adsorption performance significantly, particularly in AC_1', which exhibited a high iodine number and enhanced micropore development.

However, the two-step activation yielded the best results, with AC_2' achieving the highest microporosity and AC_2 showing the best mesoporosity.

Overall, using a tube furnace under nitrogen atmosphere produced AC_1' and AC_2' as the most suitable for applications requiring high microporosity and adsorption of small molecules, with AC_2' being the best one, while the produced AC_2 is more appropriate for large-molecule adsorption due to its higher mesoporosity.

- **Point of zero charge (pH_{pzc}) of the AC_2' activated carbon**

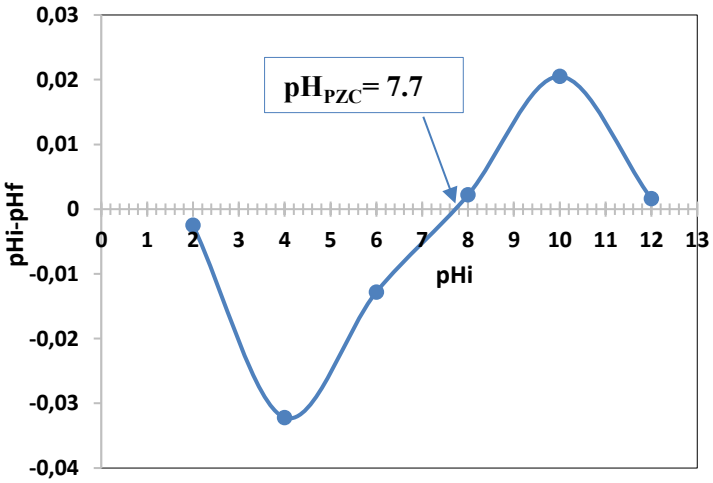

Figure V. 1. 23: pH_{pzc} of **AC_2'**

Figure V. 1. 23 shows the point of zero charge (pHpzc) of AC_2 illustrated by the intersection of the lines provided by the equation $pH_{initial}$-pH_{final}=$pH_{initial}$. The pH_{zpc} of AC_2 was 7.7. It is therefore a basic surface that releases OH^- ions. The charge on the AC_2 surface is positive for solutions with a pH below pH_{pzc} and negative when the pH exceeds this value [57].

- **Potassium Hydroxide chemical activation mechanism**

Potassium hydroxide plays a crucial role in porosity development through chemical attack, carbon oxidation, and gasification. The reaction between KOH and carbon at high temperatures generates potassium species: potassium metal (K), potassium oxide (K_2O), and potassium carbonate (K_2CO_3) that intercalate into the carbon structure, creating well-developed micropores. The chemical activation process can be described according to the following reactions:

$$4KOH + C \rightarrow 4K + CO_2 + 2H_2O \qquad (1)$$

According to reaction (1), potassium hydroxide (KOH) reacts with carbon (C) at high temperatures to produce potassium metal (K), carbon dioxide (CO_2), and water (H_2O). Potassium hydroxide acts as an activator, facilitating the decomposition of pine precursor carbon (PCP) into potassium metal and carbon dioxide. This reaction results in the engraving and activation of the carbon structure by removing some of the carbon in the form of CO_2, thereby increasing the number of pores (micropores and mesopores) in the carbonaceous material [58].

$$2KOH + CO_2 \rightarrow K_2CO_3 + H_2O \qquad (2)$$

Equation (2) shows the interaction between potassium hydroxide (KOH) and carbon dioxide (CO_2) liberated in the first reaction. At 400°C, potassium hydroxide reacts with carbon dioxide to form potassium carbonate (K_2CO_3) and water (H_2O). This is an oxidative reaction in which CO_2 is captured and converted to potassium carbonate. In the context of activated carbon preparation, potassium carbonate (K_2CO_3) is the compound that can contribute to micropore development and enhance the activation process [59].

$$6KOH + 2C \rightarrow 2K + 3H_2 + 2K_2CO_3 \qquad (3)$$

When the temperature reaches 700°C, potassium hydroxide (KOH) reacts with carbon (C) to produce potassium metal (K), hydrogen gas (H_2), and potassium carbonate (K_2CO_3).

Reaction (3) represents a more complicated activation process in which potassium hydroxide not only activates carbon, forming potassium metal and potassium carbonate but also liberates hydrogen gas. The formation of potassium carbonate suggests further oxidation of the carbon material, and the presence of hydrogen gas indicates gasification, which helps to open up the carbon structure and develop porosity [60].

$$K_2CO_3 \rightarrow K_2O + CO_2 \qquad (4)$$

Equation (4) presents a thermal decomposition reaction. Thermal decomposition of potassium carbonate generally takes place at high temperatures (800°C). Potassium carbonate (K_2CO_3) then decomposes into potassium oxide (K_2O) and carbon dioxide (CO_2). The formation of potassium oxide (K_2O) is important in this stage since it can react with carbon to continue the activation process, facilitating the formation of pores in the carbonaceous material.

$$CO_2 + C \rightarrow 2CO \qquad (5)$$

$$K_2O + C \rightarrow 2K + CO \qquad (6)$$

The emission of CO_2 gas in equation (4) also contributes to the removal of carbon from the structure, K_2O is reduced by C to produce metal K, thereby increasing the porosity and surface area of the activated carbon [50, 61]. The reactions lead to gasification, oxidation, and the production of potassium compounds (K_2CO_3 and K_2O), resulting in a more porous and reactive activated carbon structure [62]. These processes improve the adsorption capacity of the resulting activated carbon, making it useful in a variety of applications, including water treatment [63] and air purification [64].

- **Effect of furnace type on activated carbon properties**

This comparative study analyzed the effects of different activation parameters, including time, temperature, and impregnation rate, using the muffle furnace and the tubular furnace under nitrogen environment. Both types of ovens were evaluated for their ability to produce activated carbons with high quality. The muffle furnace ensured uniform temperature distribution but did not provide the level of control offered by the tube furnace under nitrogen atmosphere. Both methods demonstrated that increasing the activation temperature increased porosity. The tube furnace was more effective in developing micropores and preventing oxidation degradation. Its nitrogen atmosphere enabled a more controlled activation process, ensuring that the carbon structure was optimized for pore development without excessive oxidation or surface degradation.

V. 2. Part 2: Adsorption application results

Based on the results obtained, we selected the two prepared activated carbons K-AC_2 and AC_2' as the most suitable activated carbons for the removal of para-chlorophenoxyacetic acid (P-CPA) and Linuron (Lin) from aqueous solutions. These two materials demonstrated high surface area, well-developed microporosity, and superior adsorption capacity, making them ideal for pollutant removal.

By way of reminder, the K-AC_2 activated carbon, was prepared via two-step KOH activation (1:1 ratio) at 800°C for 30 minutes in a muffle furnace, provided a balanced porous structure with an MB index of 72.768 mg g^{-1}, a significant iodine number of 666.38 mg g^{-1}, a BET surface area of 430.504 m^2 g^{-1}, and a pore volume of 1.778 cm^3 g^{-1}, and a good yield (72.25 %).

These characteristics suggest that K-AC_2 activated carbon has a well-developed microporous structure suitable for the adsorption of small organic molecules.

However, The AC_2' activated carbon, obtained via a combined activation approach under inert nitrogen atmosphere in a tubular furnace using a higher KOH ratio (1:2), achieved the highest micropore surface area (1039.22 $m^2\ g^{-1}$) with an iodine number of 888.51 mg g^{-1}, micropore volume (0.357 $cm^3\ g^{-1}$), and 50.60 mg g^{-1} MB index, and a good yield (72.57%), indicating enhanced microporosity that can effectively fixe persistent pollutants from wastewater such as P-CPA and Lin herbicides.

Ⅴ. 2. 1. P-CPA removal from aqueous solution by K-AC_2 activated carbon

Ⅴ. 2. 1. 1. Contact time effect

The study investigated the effectiveness of adsorption over time to determine the contact time required for the adsorption of p-chlorophenoxyacetic acid onto the prepared K-AC_2. Two initial concentrations (200 and 300 mg L^{-1}) and the solution pH were fixed, while the contact time was varied from 10 to 60 minutes at 25 ± 1°C (using a thermostat).

The removal efficiency of P-CPA significantly improved over time due to the abundance of empty sites [65]. The removal process progressively stabilized at equilibrium (60 minutes) between K-AC_2 and P-CPA-herbicide. The optimal contact time was 45 minutes, as no significant increase in the elimination rate was observed beyond that. At the optimal time (45 minutes), the corresponding adsorption elimination rates of P-CPA were 90.15% for $C_{initial}$ = 200 mg L^{-1} and 84.70% for $C_{initial}$ = 300 mg L^{-1} (**Figure V. 2. 1**)

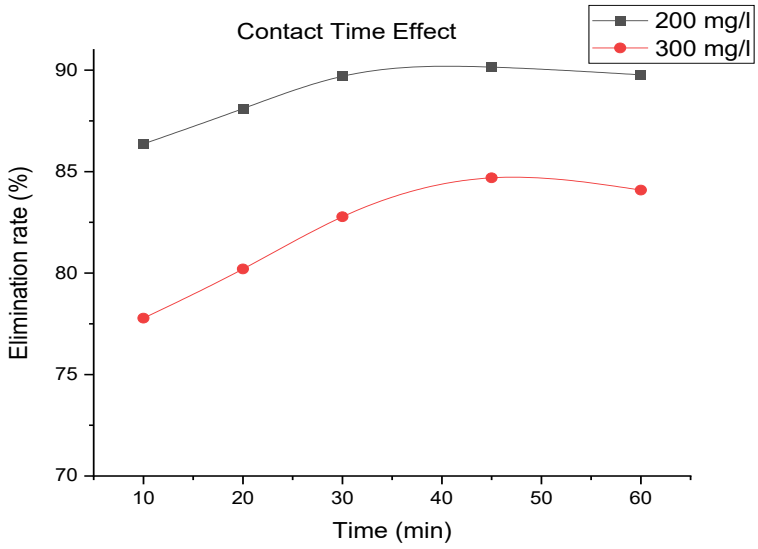

Figure V. 2. 1: Effect of contact time on P-CPA adsorption onto K-AC_2

V. 2. 1. 2. Effect of K-AC_2 dose on P-CPA adsorption

To determine the optimal dose of K-AC_2 for maximum P-CPA removal, we tested a range from 2 to 10 g L^{-1} activated carbon dose at ambient temperature and initial solution pH, with P-CPA concentrations of 200 and 300 mg L^{-1}. The results, shown in **Figure V 2. 2** demonstrated a significant increase in the removal rate of P-CPA as the activated carbon dose was raised from 2 to 6 g L^{-1}. For the 200 mg L^{-1} P-CPA concentration, the removal efficiency improved from 64.91% to 91.43%, and for the 300 mg L^{-1} concentration, it increased from 68.99 % to 92.88 %. This enhancement in removal efficiency can be attributed to the increased surface area and the presence of more active sites and contact surfaces on the K-AC_2 [65, 66]. However, at dose levels of 6 and 8 g L^{-1}, the adsorption process tended to stabilize, reaching a saturation point at 91.43% for 200 mg L^{-1} and 92.88 % for 300 mg L^{-1}. Beyond this stabilization point, further increases in the adsorbent dosage did not lead to higher adsorption efficiency. Higher doses (above 10 g L^{-1}) resulted in decreased adsorption capacity [67, 68], with values of 89.24 % for 200 mg L^{-1} and 92.73 % for 300 mg L^{-1}. Based on these results, the optimum activated carbon dose for P-CPA removal was 6 g L^{-1}.

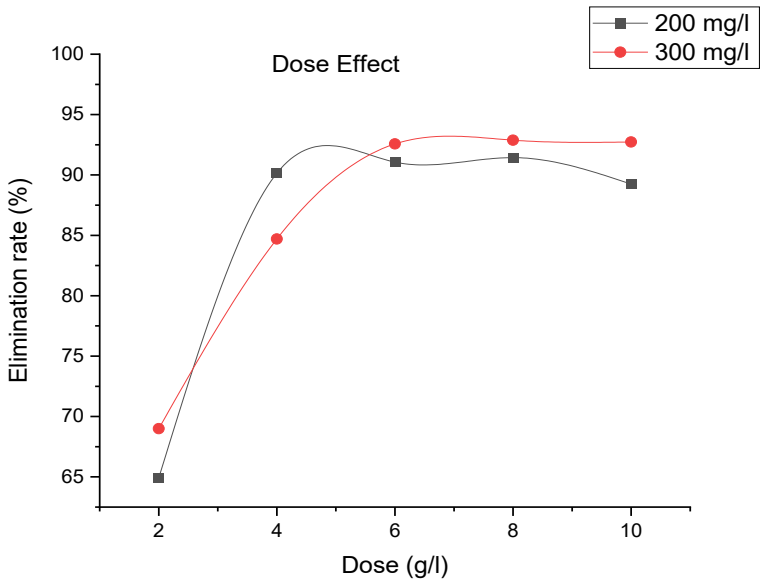

Figure V. 2. 2: Effect of K-AC_2 dose on P-CPA adsorption

V. 2. 1. 3. Study of the pH effect

The adsorption process is significantly influenced by the solution pH, which plays a critical role in various interactions, such as the surface charge of the adsorbent, electrostatic interactions, hydrogen bond formation, electron exchange, and π-π dispersion interactions in the solution [31, 69]. To investigate the impact of pH on P-CPA removal through adsorption on K-AC_2, several experiments were conducted at fixed concentrations (200 and 300 mg L^{-1}), a temperature of 25°C, an optimized adsorbent dosage of 6 g L^{-1}, and a contact time of 45 minutes. The adsorption performance of P-CPA with the solution pH is depicted in **Figure V. 2. 3**.

Observations revealed that the fixed amount of P-CPA adsorbed occurred at pH values of 2.1 and 3.75 (with 3.75 being the initial solution pH). As the solution pH increased, the elimination rate of P-CPA decreased, reaching 91.5 % to 65.68 % for the concentration of 200 mg L^{-1} and 92.6% to 66.46% for the concentration of 300 mg L^{-1}. According to the literature, in an aqueous environment with a basic solution pH, the carboxyl groups of P-CPA lose a proton (H^+) and acquire a negative charge. It is worth noting that the specific pH at which this deprotonation occurs depends on the molecule's pKa value. For P-CPA, the reported pKa values are 3.56 (experimental) and 3.27 (calculated), indicating that the anionic form of P-CPA is predominant when the pH is greater than 3.56 [70]. Moreover, when the solution's pH surpasses the pKa value of the adsorbate, the adsorbate predominantly exists in its deprotonated form ($RCOO^-$). This situation can enhance adsorption through electrostatic attraction with positively charged sites on the adsorbent surface, as supported by the pH_{pzc} results. At low pH values or

when pH < pH_{pzc} (pH_{pzc}= 7.76), the adsorbent surface acquires a positive charge, while P-CPA molecules become negatively charged within this pH range. Consequently, electrostatic attraction between the adsorbent surface and the pollutant occurs, resulting in a higher adsorption capacity [71]. Conversely, the opposite effect is observed when the pH is lower than the pKa value [72]. Furthermore, the activation of pine cone biochar using KOH introduced hydroxyl groups onto the adsorbent's surface. The adsorption process of P-CPA onto K-AC_2 possibly involved the substitution of the anionic group of P-CPA with the OH- group of the activated carbon [71].

Since the highest elimination rate was achieved at two different pH values, 2.1 and 3.75, we selected the pH value of 3.75 for subsequent steps in the study to avoid further adjustments. This choice aligns with findings from another scientific paper investigating the adsorption of chlorophenoxyacetic acid by OPAC (Orange Peals Activated Carbon), where authors also identified an optimum pH value of ″3″ [31].

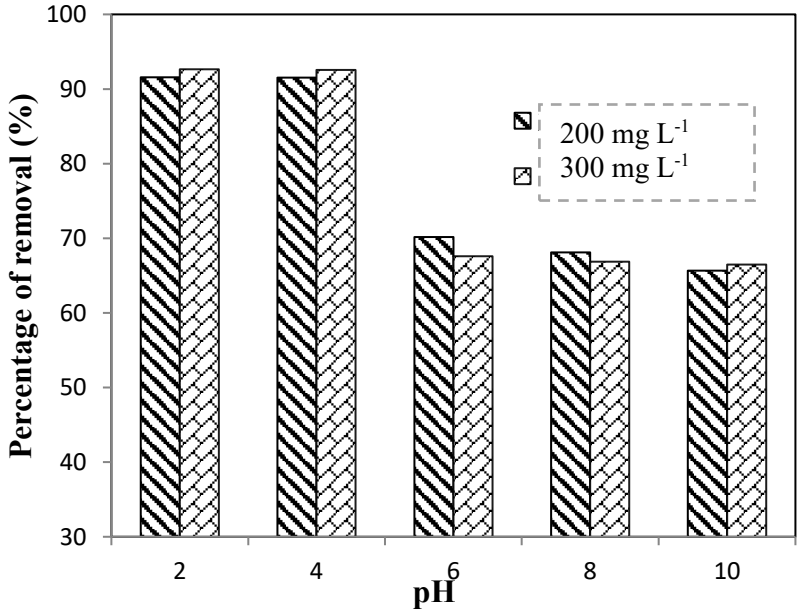

Figure V. 2. 3: Effect of pH on percent removal of P-CPA

Ⅴ. 2. 1. 4. Applied isotherm models for P-CPA adsorption by K-AC_2

Table V. 2. 1: Isotherm adsorption parameters

Model	Isotherm parameters results				χ^2	RMSE	APE
Langmuir	R^2	K_L (mg·g^{-1})	q_m (mg·g^{-1})				
	0.97	0.0185	266.5		28.90	1.44	11.51
Freundlich	R^2	n	K_F ((mg. L^{-1})^n. (mg· g^{-1}))				
	0.99	2.64	28.44		51.85	19.63	24.76
Temkin	R^2	B_T	b (J·mol^{-1})	K_T			
	0.98	52.38	43.33	0.26	15.20	10.96	7.92
(D-R)	R^2	β(mol^2·J^{-2})	q_{mD-R}(mg·g^{-1})	E			
	0.97	3.3×10^{-8}	224.7	3.892	46.49	16.27	15.39
(R-P)	R^2	β(mol^2·J^{-2})	a_{r-p} (L·g^{-1})	K_{RP} (L·mg^{-1})			
	0.98	0.87	7.17	0.059	20.65	11.03	12.48

The adsorption data of P-CPA onto K-AC_2 (**Table V. 1. 1**) were well fitted by the Langmuir isotherm (**Figure V. 2. 4**) model, with $R^2 > 0.97$ and low error functions. We obtained a significant maximum monolayer adsorption capacity of 266.5 mg g^{-1} based on this model. The calculation of different initial concentrations revealed that R_L of P-CPA adsorption on the studied activated carbon was $0<R< 1$ for the Langmuir model, which confirms that the adsorption process is favorable.

The Freundlich model (**Figure V. 2. 4)** fitted P-CPA adsorption data very well with a coefficient of determination of 0.99 and low error functions. The higher R^2 shows multi-layer adsorption, including interactions between herbicide molecules and heterogeneous adsorbent surfaces. A value of $n > 1$ shows that the prepared activated carbon has good adsorption properties. P-CPA is adsorbed in various ways due to powerful bonds between the adsorbent and adsorbate [73].

The Temkin model described the adsorption of P-CPA by K-AC_2 with a 0.98 determination coefficient and lower error functions (**Figure V. 2. 4**).

For the Dubinin-Radushkevich (D-R) model, the determination coefficient R^2= 0.97 (**Figure V. 2. 4**) and the low value of the error function mean that this model accurately described P-CPA adsorption using K-AC_2. The maximum adsorption capacity obtained by the Dubinin-Radushkevich (D-R) model (224.7 mg g^{-1}) was close to that obtained by the Langmuir model (266.5 mg g^{-1}). The value of adsorption energy obtained is lower than 8 kJ mol^{-1} (E = 3.892 kJ mol^{-1}) and denotes that the adsorption of P-CPA on K-AC_2 is physical.

The Redlich-Peterson isotherm constant β in between 0 and 1 (**Table V. 1. 1)** indicates that the isotherm approached the Freundlich isotherm (**Figure V. 2. 4**). It overlapped the Redlich-Peterson isotherm with a high coefficient of determination, up to 0.97, and a low error function, which confirms that the Freundlich isotherm is the most fitted isotherm model to the adsorption process of P-CPA on K-AC_2.

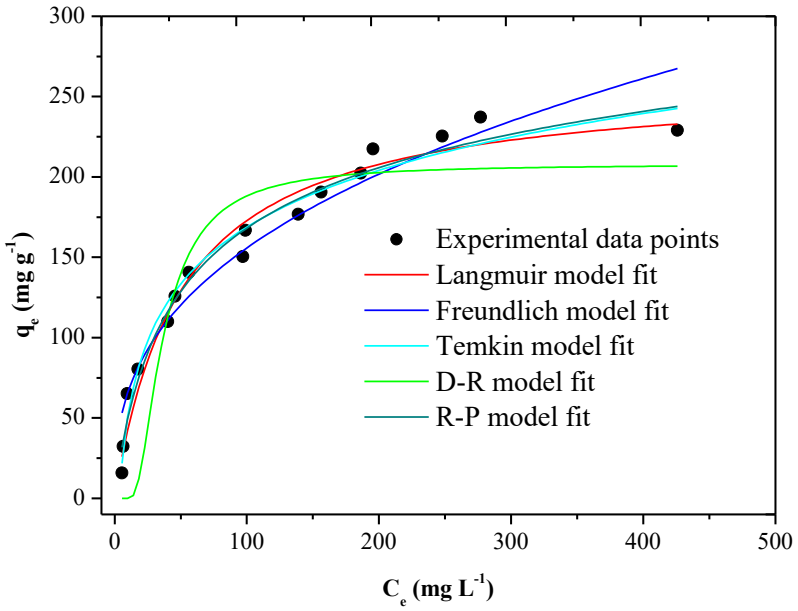

Figure V. 2. 4: Adsorption isotherm models of P-CPA on K-AC_2

Table V. 2. 2: Comparison of P-CPA maximum adsorption capacities on various adsorbents

Adsorbent	**q_m (mg g^{-1})**	**Reference**
Commercial NSX_2 powdered activated carbon	211.77	[74]
Functionalized Physalis peruviana biomass	333.3	[75]
Biomass-based ferrospinel composite	400	[76]
Activated carbon from tea waste	58.8	[77]
Activated carbon from Soybean waste	253.2	[78]
Pine cone based activated carbon treated with KOH	266.5	This study

V. 2. 1. 5. Kinetic study of P-CPA adsorption by K-AC_2

Table V. 2. 3: Fitting parameters for the pseudo-first-, the pseudo-second order adsorption kinetic and intraparticle diffusion models P-CPA adsorption by K-AC_2

C_o (mg L^{-1})	**200**	**300**
q_e(exp) (mg g^{-1})	**31.69**	**47.15**
Pseudo-first order model	R^2 = 0.98	R^2 = 0.91
q_e(calc) (mg g^{-1})	**2.247**	**2.218**
K_1 (min^{-1})	0.0506	0.0693
Pseudo-second order model	R^2 = 0.998	R^2= 0.999
q_e(calc) (mg g^{-1})	**32.33**	**47.73**
K_2 (g mg^{-1} min^{-1})	0.0187	0.0257
Intraparticle diffusion model	R^2=0.981	R^2=0.96
C_e (mg g^{-1})	**25.008**	**41.9**
K_{id} (mg g^{-1} $min^{-1/2}$)	0.9599	0.7746

The high values of the coefficient of determination (R^2>0.9) show fairly good linearity of the log (q_e-q_t) =f(t) curve (**Figure V. 2. 5**). The predicted adsorbed quantity values, q_{calc} (2.247 and 2.18 mg g^{-1} for 200 and 300 mg L^{-1} concentrations, respectively), were, however, lower than the experimentally measured values, q_{exp} (31.69 and 47.15 mg g^{-1} for 200 and 300 mg L^{-1} concentrations, respectively). This demonstrates that the pseudo–first–order model does not completely match the experimental data.

The figure indicates that plotting t/q_t vs t (**Figure V. 2. 6**) yields a good straight line with higher coefficients of determination (R^2 = 0.999), and the values of q_{calc} computed (32.33 and 47.73 mg g^{-1} for 200 and 300 mg L^{-1} respectively) using the pseudo-second-order equation are pretty similar to the experimental data for these two concentrations.

Table V. 1. 3 shows that the experimental results obtained perfectly follow the linear variation given by the pseudo-second-order kinetics equation for P-CPA adsorption on K-AC_2. Therefore, the pseudo-second-order model matched the experimental data better than the pseudo-first-order model. Similar results were found in other experimental works on the adsorption of herbicides [72, 79].

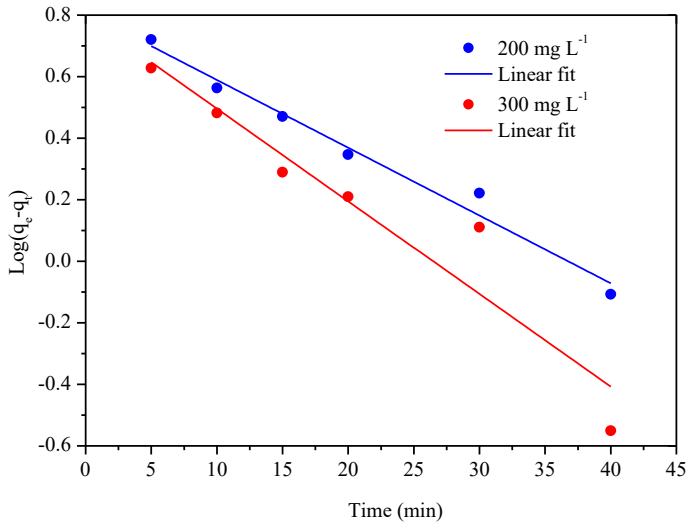

Figure V. 2. 5: Linear fit of the pseudo-first-order kinetic model of P-CPA adsorption onto K-AC_2.

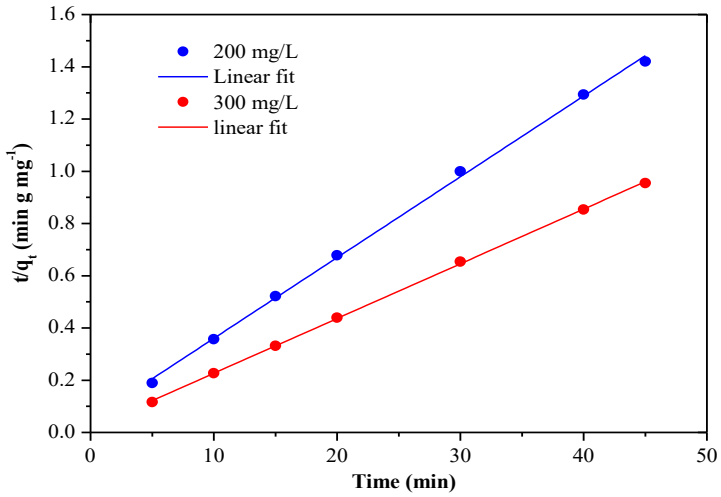

Figure V. 2. 6: Linear fit of the pseudo-second-order kinetic model of P-CPA adsorption onto K-AC_2.

Since the determination coefficient was greater than 0.98 (**Figure V. 2. 7**), we can say that intraparticle diffusion well fits the Lin adsorption process by K-AC_2. Also, we noticed that the diffusion rate constant (k_{id}) values decreased with increasing concentration, indicating that the diffusion rate within the adsorbent slows as the pollutant concentration rises [17].

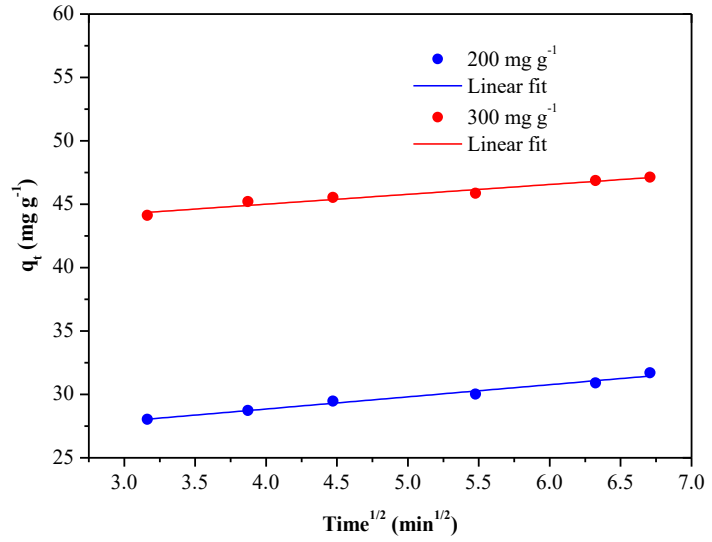

Figure V. 2. 7: Linear fitting of the intraparticle kinetic model of P-CPA adsorption onto K-AC_2

V. 2. 1. 6. Thermodynamic study of the adsorption of P-CPA by K-AC_2

Table V. 2. 4: Thermodynamic parameters of P-CPA adsorption by K-AC_2

C_o (mg L^{-1})	ΔH° (kJ mol^{-1})	ΔS° (kJ mol^{-1} K^{-1})	ΔG° (kJ mol^{-1})			
			293 K	298 K	303 K	313 K
200	34.207	0.139	-6.52	-7.215	-7.91	-9.3
300	38.103	0.151	-6.14	-6.895	-7.65	-9.16

Figure V. 2. 8 shows the good linearity of the plots of ln (K_d) = f (1/T) with coefficients of determination greater than 0.94 and 0.99 for the concentration of 200 and 300 mg L^{-1} respectively, which validates the estimated enthalpy ΔH° and entropy ΔS° values as obtained from the slope and intercept [80].

The negative ΔG° values (**Table V.1.4)** denote the spontaneous and thermodynamically favorable adsorption. Moreover, the decrease in the negative values of ΔG° with increasing temperature indicates that adsorption is more advantageous at higher temperatures [81].

A positive value for ΔH° of each concentration signifies that the process is endothermic and ranges between 20 and 80 kJ mol^{-1} [82], also less than 40 kJ mol^{-1} [83], revealing that P-chlorophenoxyacetic acid (P-CPA) adsorption by K-AC_2 activated carbon is physical. The positive value of ΔS^{o} indicated an increase in the randomness at the adsorbent/adsorbate interface during the adsorption process. In addition, this positive value shows the existing affinity of the prepared activated carbon toward the herbicide in an aqueous solution [31].

The adsorption power of K-AC_2 improves at higher temperatures, thanks to its high porosity and large surface area. Similar results for endothermic adsorption of herbicides have been previously demonstrated on KOH-based activated carbon [31].

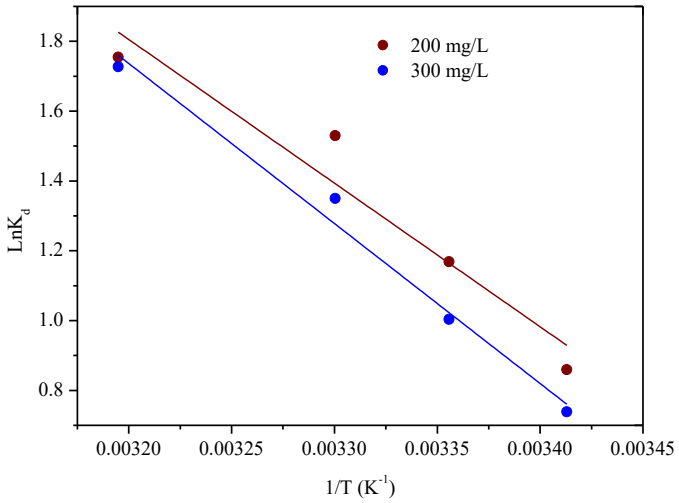

Figure V. 2. 8: van't Hoff plot lnK_d versus 1/T for P-CPA on K-AC_2

V. 2. 1. 7. Desorption test

A desorption study was carried out on the herbicide P-CPA, as this procedure is necessary if the adsorbent is to be reused. Desorption is the opposite of adsorption: it removes the pollutant bound to the adsorbent, making its pores available again. This enables us to understand how the pollutant is removed and recovered while allowing the adsorbent to be reused, thereby reducing costs and preserving the environment [65].

We studied the desorption process by mixing 250 mL of distilled water with 1 g of K-AC_2 that had absorbed 266.5 mg of P-CPA per gram. The mixture was placed in a special flask, and desorption was carried out using a Soxhlet apparatus, with fresh distilled water added every 2 hours. Over time, the water collected more of the released pollutant. The concentration of the desorbed pollutant in the solution was measured using a spectrophotometer at the same maximum wavelength.

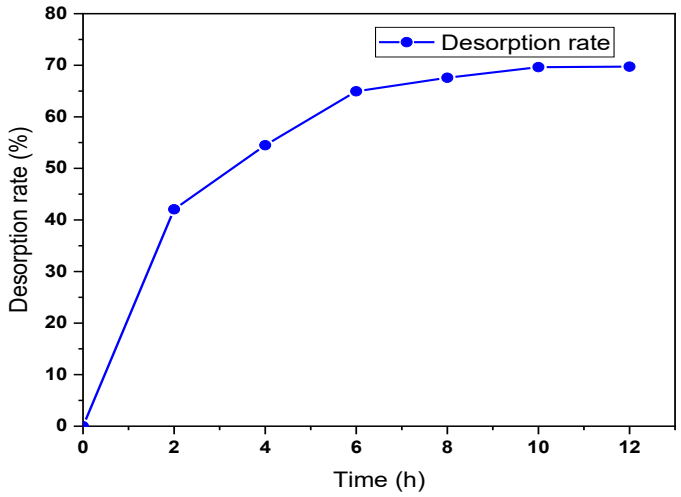

Figure V. 2. 9: Desorption rate of P-CPA from K-AC_2

As shown in **Figure V. 2. 9**, the amount desorbed was significantly higher at the start of extraction and stabilized thereafter, reaching a desorption rate of 69.72%. The results indicate that K-AC_2 can be recycled and reused for the adsorption of the herbicide P-CPA.

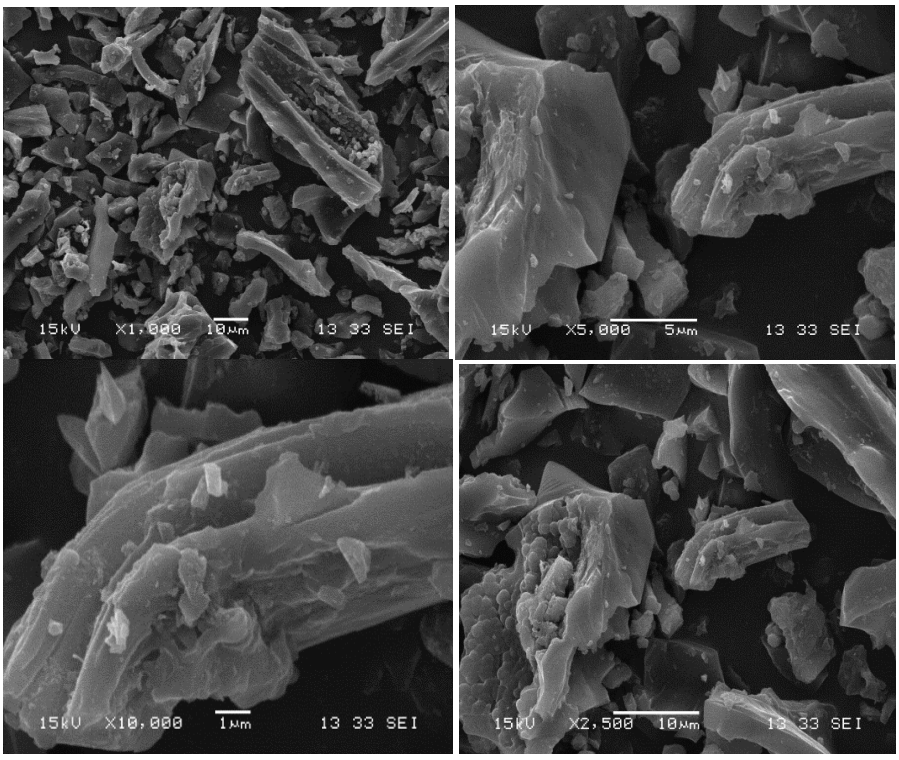

Figure V. 2. 10: SEM micrographs of K-AC_2 after adsorption of P-CPA

Figure V. 2. 10 shows that the P-CPA adsorbate occupied the pores and cavities of the K-AC_2-activated carbon. The EDS results further revealed a notable decrease in carbon content.

For the K-AC_2 activated carbon before P-CPA adsorption, the carbon content was 66.75% (**Figure V.1.10**), after adsorption, it was decreased to 56.6% in (**Figure V. 2. 11**) and an increase in oxygen content, shifting from 30.948 % (**Figure V. 1. 10**) to 31.773 % (**Figure V. 2. 11**), after P-CPA adsorption on K-AC_2. Additionally, the results confirm the presence of chlorine after the adsorption of P-CPA by K-AC_2. This occurrence is attributed to the binding of the adsorbate P-CPA on the porous surface of the adsorbent, confirming the adsorption mechanism of P-CPA.

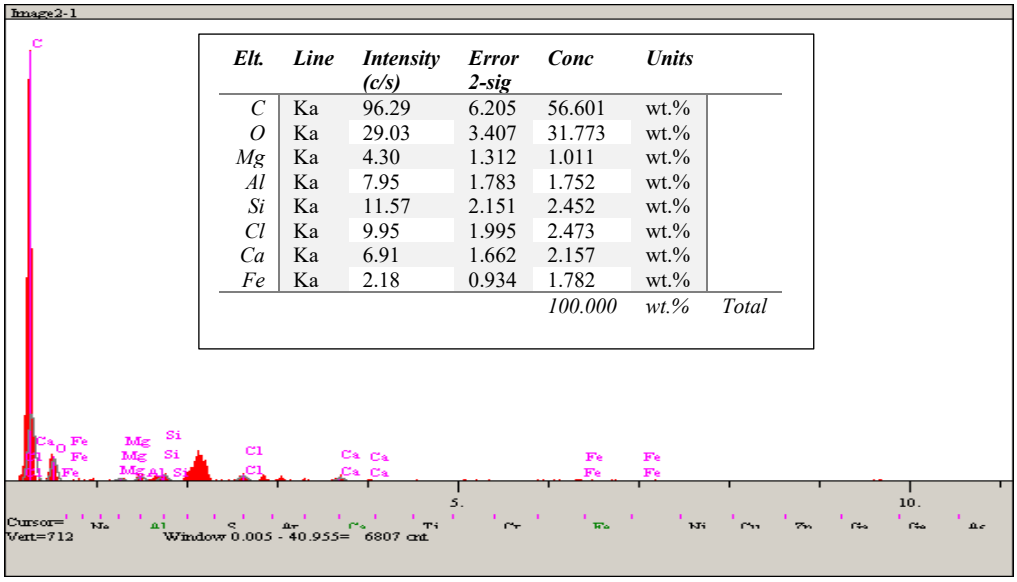

Figure V. 2. 11: EDS data of K-AC_2 after P-CPA adsorption

V. 2. 2. Lin removal from aqueous solution by K-AC_2 activated carbon

V. 2. 2. 1. Effect of contact time

Contact time is a key factor because it assesses the favorability of adsorption over time. We estimated the contact period required for the adsorption of Linuron (Lin) onto the prepared K-AC_2.

The removal process reached its maximum value at 90 min but decreased at 120 min for the 80 mg L^{-1} (86.89%). Thus, the optimum contact time was 90 min, with no substantial increase in removal rate observed beyond this time.

At the optimal contact time (90 min), the corresponding adsorption removal rates of P-CPA were 96.13 % for $C_{initial}$ = 70 mg L^{-1} and 90.24 % for $C_{initial}$ = 80 mg L^{-1} (**Figure V. 2. 12**).

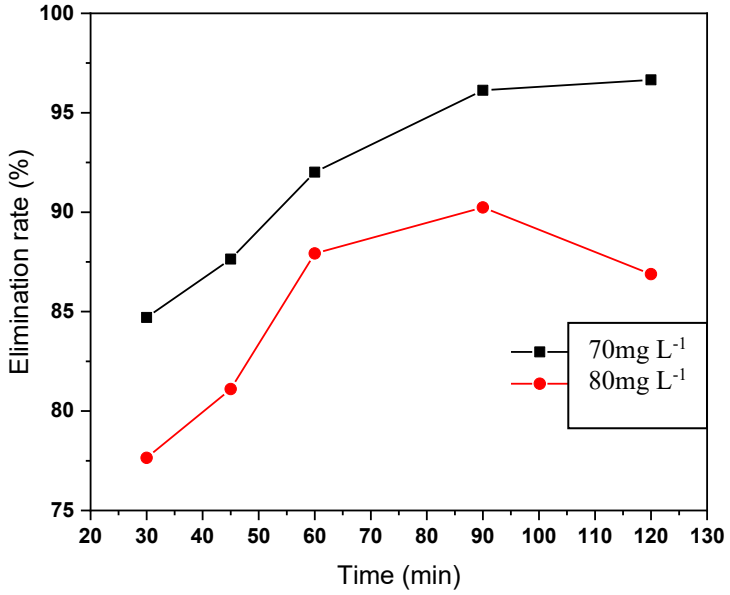

Figure V. 2. 12: Effect of contact time on Lin adsorption by K-AC_2

V. 2. 2. 2. Effect of adsorbent dose

To identify the optimal dose of K-AC_2 for maximum Lin removal, we tested an adsorbent dose range of 2 to 10 g/L at room temperature and initial solution pH for Lin concentrations of 70 and 80 mg L^{-1}. As shown in **Figure V. 2. 13**, the removal rate of Lin increased significantly as the activated carbon dose increased from 2 to 6 g L^{-1}. For the 70 mg L^{-1} Lin concentration, the removal efficiency improved from 52.68% to 98.54%, and for the 80 mg L^{-1} concentration, it increased from 48.05% to 98.79%. This enhancement can be attributed to the larger presence of active sites and free pores [65, 66]. However, at dose levels of 6 and 10 g L^{-1}, the adsorption process tends to stabilize, reaching a saturation point at 98.22% for 70 mg L^{-1} and 98.39% for 80 mg L^{-1}. Beyond this stabilization point, further increase in adsorbent dose did not lead to higher adsorption efficiency.

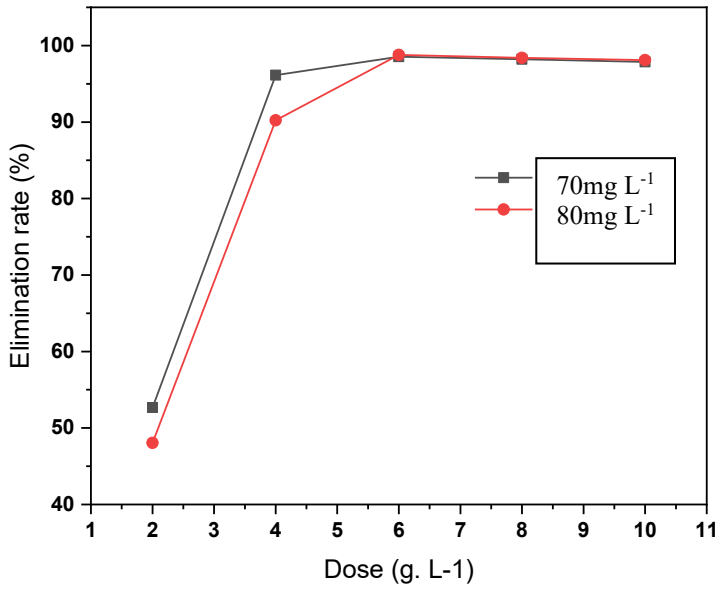

Figure V. 2. 13 : Effect of adsorbent dose on Lin adsorption by K-AC_2

Based on these results, the optimum activated carbon dose for Lin removal is 6 g L^{-1}.

V. 2. 2. 3. Effect of pH

To investigate the impact of pH on Lin removal by adsorption on K-AC_2, several experiments were conducted at 25 °C at fixed concentrations and an optimized adsorbent dose. **Figure V. 2. 14** depicts the adsorption of Lin as a function of pH.

A maximum removal rate of 99.84% and 99.61% was observed at pH values of 2.1 and 4.05, respectively, for an initial concentration of 80 mg L^{-1}. Similarly, at a concentration of 90 mg L^{-1}, removal rates of 98.49% and 98% were obtained at pH 2.1 and 7.07, respectively, with pH 7.07 representing the initial solution pH.

The pKa of Lin (12.13) corresponds to the deprotonation of the secondary amine (-NH) group. Below this pKa, Lin remains predominantly in its neutral (non-ionized) form. Adsorption decreased above pH 7.07, likely due to changes in Lin's charge state, the surface charge of K-AC_2, and competition with hydroxyl ions (OH^-).

The point of zero charge (pH_{pzc}) is a key factor in the adsorption mechanism. When pH < pH_{zpc} (7.6), the adsorbent surface becomes positively charged, which enhances adsorption due to interactions with polar functional groups on Lin. In acidic conditions, the high adsorption

capacity and possible interactions between K-AC_2 and Lin include van der Waals forces, electron donor-acceptor (EDA) interactions, and hydrogen bonding [84].

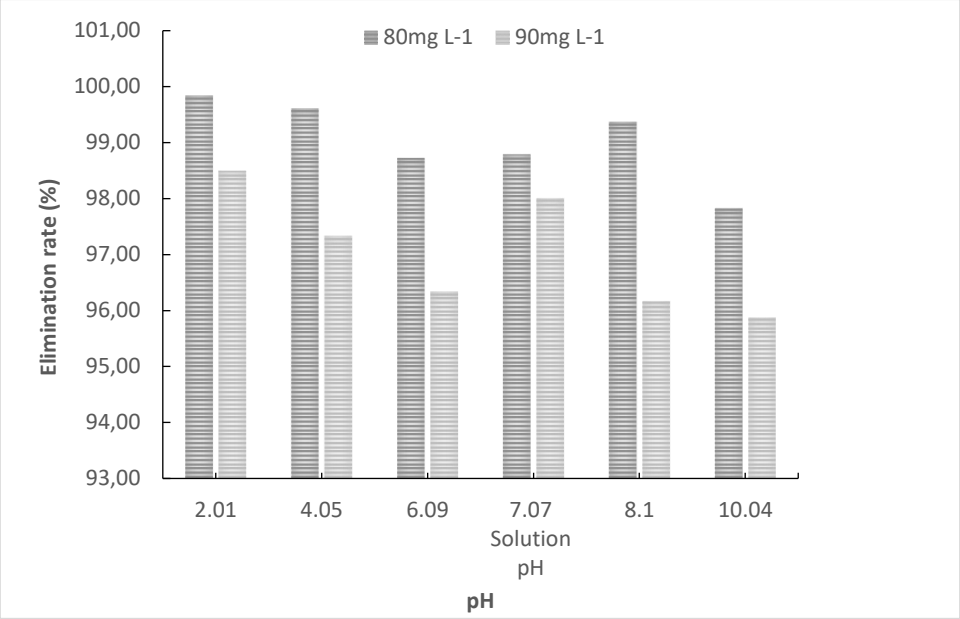

Figure V. 2. 14: Effect of pH on Lin adsorption by K-AC_2

Ⅴ. 2. 2. 4. Isotherms modeling

Table V. 2. 5: Fitting parameters of Linuron adsorption by K-AC_2 for the models investigated

Model	Isotherm modeling parameters				χ^2	RMSE	APE
Langmuir	R^2	K_L (mg g^{-1})	q_m (mg g^{-1})				
	0.84	0.53	43.76		38.10	6.17	16.95
Freundlich	R^2	n	K_F ((mg. L^{-1})^n. (mg· g^{-1}))				
	0.94	5.26	18.68		14.11	31.55	90
Temkin	R^2	B_T	b (J mol^{-1})	K_T			
	0.95	5.27	430.7	44.37	10.76	3.28	45.5
(D-R)	R^2	β (mol^2·J^{-2})	q_{mD-R}(mg g^{-1})	E			
	0.7	1.05	38.17	0.68	82.03	38	100
(R-P)	R^2	β (mol^2 J^{-2})	a_{r-p} (L g^{-1})	K_{RP} (L mg^{-1})			
	0.95	0.85	192.2	8.7	7.49	3.36	1.22

The adsorption data matched Langmuir's non-linear isothermal model for Lin removal by K-AC_2 activated carbon, with an R^2 greater than 0.84 but low error values. This model estimated a high maximum adsorption capacity of 43.76 mg per gram in a single layer.

The calculation of different initial concentrations reveals that R_L of Lin adsorption on the K-AC_2 is 0<R< 1 for the Langmuir model, which confirms that the adsorption process is favorable. The Freundlich model is a well-fitted Lin adsorption with a coefficient of determination of 0.94 and low error functions. The higher R^2 shows multi-layer adsorption between herbicide molecules and heterogeneous adsorbent surfaces. A value of n > 1 means that the prepared activated carbon has good adsorption properties (**Table V. 1. 5**).

The Temkin model describes the adsorption of Lin by K-AC_2 with 0.95 determination coefficient, and lower error functions.

For the Dubinin-Radushkevich (D-R) model, the determination coefficient $R^2 = 0.7$ and the high value of the error function mean that this model does not describe Lin adsorption using K-AC_2. The maximum adsorption capacity obtained by the Dubinin-Radushkevich (D-R) model was 38.17 mg g^{-1}. The value of adsorption energy obtained is lower than 8 kJ mol^{-1} (E = 0.68 kJ mol^{-1}) and denotes that the adsorption of Lin on Pines cones K-AC_2 is physical.

The Redlich-Peterson isotherm with a high coefficient of determination (0.95) and a low error function shows that this model well describes the adsorption study of Lin by K-AC_2. Furthermore, the Redlich-Peterson isotherm constant β is between 0 and 1 (**Table V. 1. 5**) indicating that the isotherm approaches the Freundlich isotherm (**Figure V. 2. 15**). The good fitting and the β value confirm that the Freundlich isotherm is the most fitted isotherm model for the adsorption process of Lin on K-AC_2

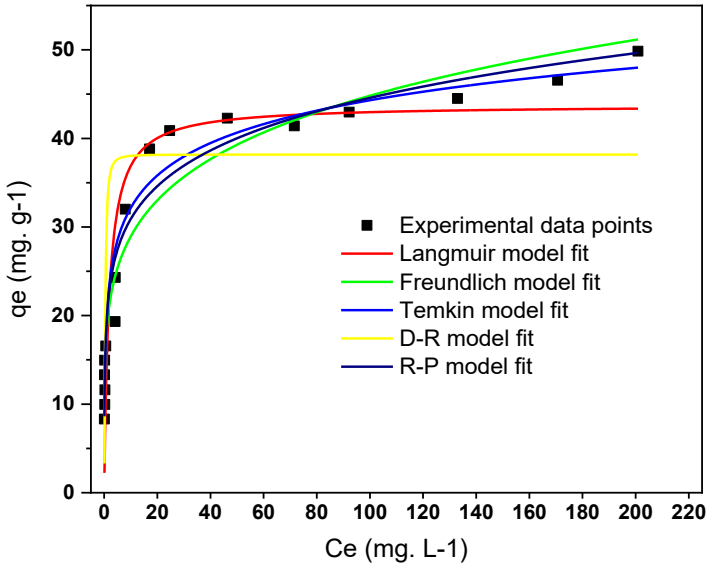

Figure V. 2. 15: Fit to the adsorption isotherm models of Lin by K-AC_2

Ⅴ. 2. 2. 5. Adsorption kinetics data of Linuron by K-AC_2

Table V. 2. 6: Adsorption fitting parameters for pseudo-first-order, pseudo-second-order kinetics and intraparticle diffusion models of Lin adsorption by K-AC_2

C_o (mg L^{-1})	**80**	**90**
$q_{e\ (exp)}$ (mg g^{-1})	**13.26**	**14.86**
Pseudo-first order	$R^2 = 0.99$	$R^2 = 0.99$
q_e(calc) (mg g^{-1})	**13.21**	**14.86**
K_1 (min^{-1})	1.013	0.516
Pseudo-second order	R^2=0.99	$R^2 = 0.99$
q_e(calc) (mg g^{-1})	**13.23**	**14.8**
K_2 (g mg^{-1} min^{-1})	1.5	1.3
Intraparticle diffusion	$R^2 = 0.96$	R^2=0.95
q_e(calc) (mg g^{-1})	**13.08**	**14.62**
K_{id} (min^{-1})	0.018	0.025

The high coefficient of determination values (**Table V. 1. 6**) (R^2>0.9) show that the pseudo-first-order kinetic model well describes the Lin adsorption by K-AC_2, moreover, the predicted adsorbed quantity values, q_{calc} (13.21 and 14.86 mg g^{-1} for 80 and 90 mg L^{-1} concentrations, respectively), are very near, and almost equal to the experimentally measured values, q_{exp} (13.26 and 14.86 mg g^{-1} for 80 and 90 mg L^{-1} concentrations, respectively) (**Figure V. 2. 16**). The pseudo-second-order equation is similar to the experimental data for both concentrations, with high coefficients of determination (R^2 = 0.99), and the values of q_{calc} computed (13.23 and 14.8 mg g^{-1} for 80 and 90 mg L^{-1} respectively) (**Figure V. 2. 17**).

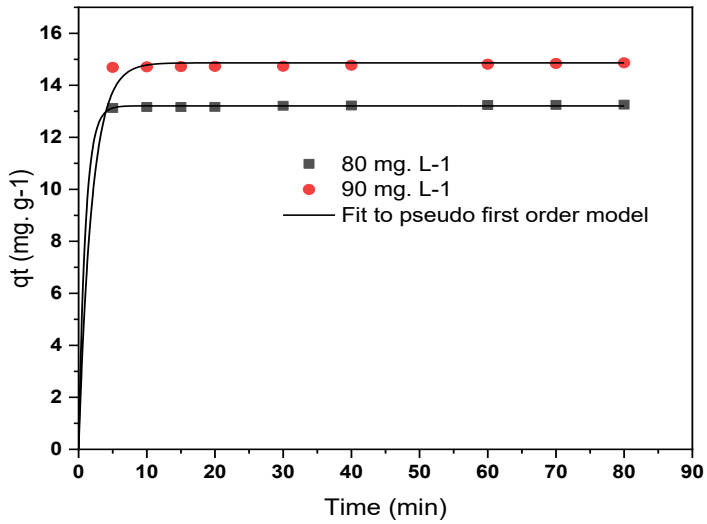

Figure V. 2. 16: Adsorption kinetics for K-AC_2 with pseudo-first-order fitted model

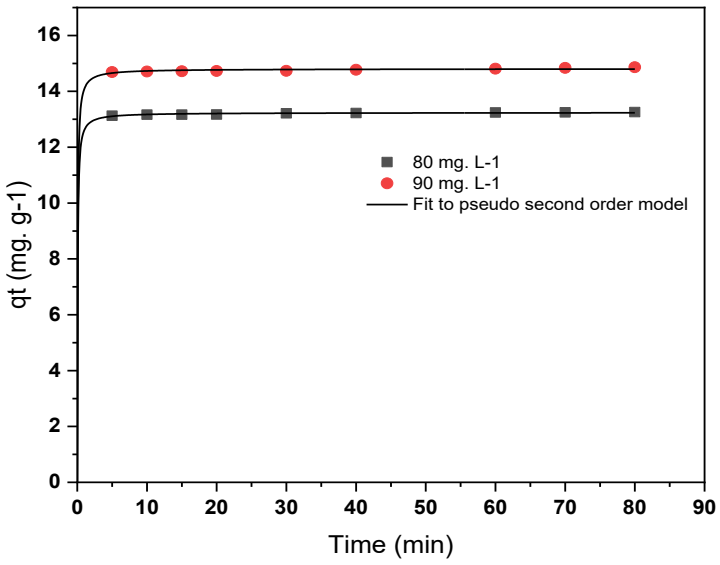

Figure V. 2. 17: Adsorption kinetics for K-AC_2 with pseudo-second order fitted model

We can say that intraparticle diffusion well controlled the Lin adsorption process by K-AC_2 (**Figure V. 2. 18**) as coefficient of determination was higher than 0.90. Additionally, we notice that the diffusion rate constant (k_{id}) values increased with increasing concentration, which indicates that the rate of diffusion into the K-AC_2 pores is faster when pollutant concentrations are higher [85] (**Table V. 1. 6**).

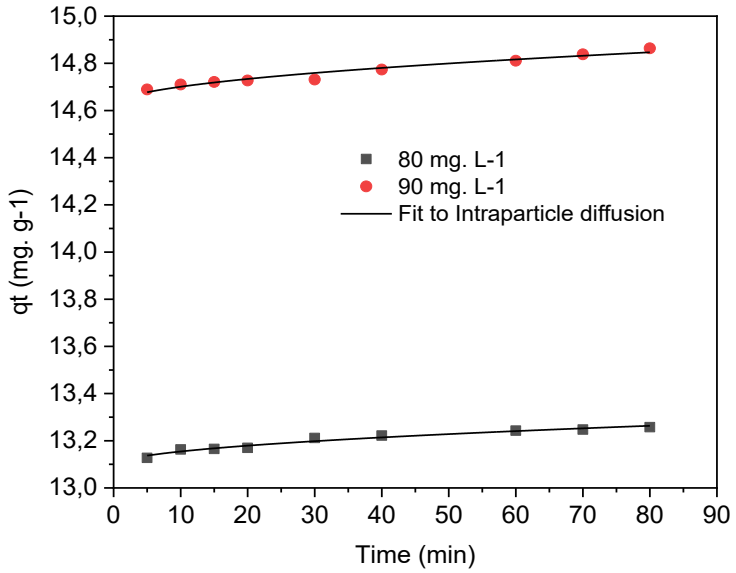

Figure V. 2. 18: Intraparticle diffusion fitting of Lin adsorption by K-AC_2

V. 2. 2. 6. Thermodynamic study of Linuron adsorption by K-AC_2

Table V. 2. 7: Thermodynamic parameters of Lin adsorption by K-AC_2

C_o (mg L^{-1})	ΔH° (kJ mol^{-1})	ΔS° (kJ mol^{-1} K^{-1})	ΔG° (kJ mol^{-1})			
			293 K	298 K	303 K	313 K
80	27.51	0.121	-7.943	-8.548	-9.153	-10.363
90	36.58	0.147	-6.491	-7.226	-7.961	-9.431

The plot of ln (K_d) = f (1/T) as depicted in **Figure V. 2. 19** shows the good linearity of the plots with coefficients of determination greater than 0.99 for both concentrations of 80 and 90 mg L^{-1}, demonstrating that the estimated enthalpy ΔH°, as well as entropy ΔS° values, were valid [80]. The negative ΔG° values in **Table V. 1. 7** are indicative of the spontaneous and thermodynamically favorable adsorption. Moreover, the increase in the negative values of ΔG° with increasing temperature indicates that adsorption was more advantageous at lower temperatures [81].

The positive value of ΔH° of each concentration signifies that the process is endothermic [82]. The obtained value lower than 40 kJ mol^{-1} and ranges between 20 and 80 kJ mol^{-1} [83] reveals that the Lin adsorption process by K-AC_2 was physical.

Table V. 2. 7 shows the positive value of ΔS^{o}, indicating an increase in the randomness at the adsorbent/adsorbate interface during the adsorption process. In addition, this positive value shows the existing affinity of the prepared activated carbon toward the herbicide in an aqueous solution[31].

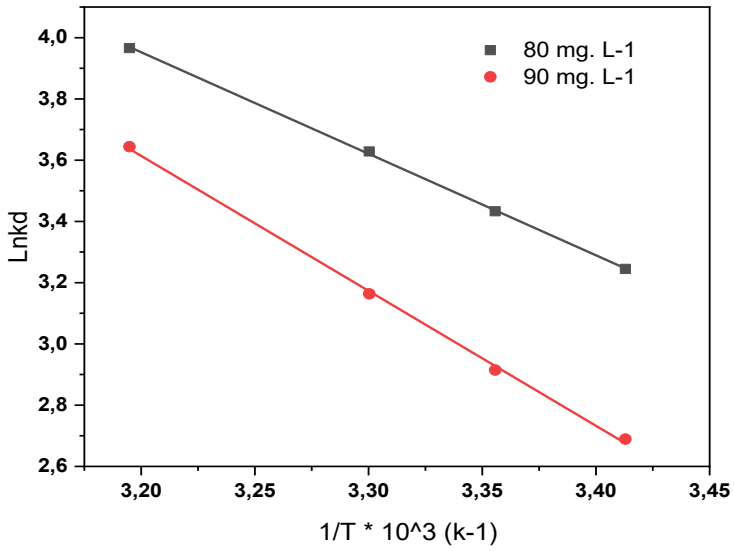

Figure V. 2. 19: Plot of ln(kd) versus 1/T for the determination of thermodynamic parameters of Lin adsorption by K-AC_2

V. 2. 3. P-CPA removal from aqueous solution by AC_2' activated carbon

V. 2. 3. 1. Contact time effect

As mentioned in the previous adsorption applications, it is essential to determine at first the contact time as the initial parameter before conducting the adsorption investigation. As it is clear from **Figure V. 2. 20**, the removal process onto AC_2' of P-CPA-herbicide progressively stabilized at 60 minutes. We fixed 45 minutes as the optimal contact duration, even though the corresponding adsorption elimination rates of P-CPA by AC_2' at this period were 97.35 % for $C_{initial}$ = 200 mg L^{-1} and 95.05 % for $C_{initial}$ = 300 mg L^{-1}. For the 60-minute contact time, these were 97.42 % for 200 mg L^{-1} and 96.67 % for 300 mg L^{-1}. The absorbance values observed were very close (0.035, 0.034, and 0.025 for the periods 45, 60, and 75, respectively, for 200 mg L^{-1} and 0.098, 0.066, and 0.074 for 45, 60, and 75 min, respectively, for the concentration

of 300 mg L^{-1}. Hence, we selected 45 minutes as optimal contact time for P-CPA adsorption by AC_2'.

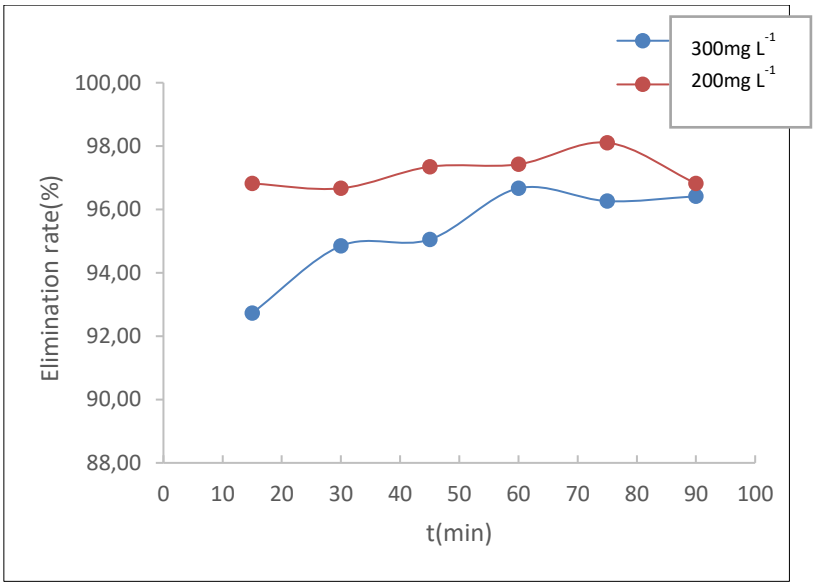

Figure V. 2. 20: Effect of contact time on P-CPA adsorption by AC_2'

V. 2. 3. 2. Dose effect

To determine the optimal dosage of AC_2' for maximum P-CPA removal, we varied the dose values from 2 to 10 g L^{-1} at ambient temperature and initial solution pH, with P-CPA concentrations of 300 and 400 mg L^{-1}. The results show (**Figure V. 2. 21)** a significant increase in the elimination rate of P-CPA as the AC_2' dose increased from 2 to 6 g L^{-1}. For the 300 mg L^{-1} P-CPA concentration, the removal efficiency improved from 83.18% to 98.64%, and for the 400 mg L^{-1} concentration, it increased from 87.2% to 97.16%. This improvement in the elimination rate can be attributed to the increased surface area and the presence of more active sites and contact surfaces on the AC_2' [65, 66]. However, at adsorbent dose levels from 6 to 10 g L^{-1}, the adsorption process tended to stabilize, reaching a saturation point at 97.78% for 300 mg/L and 97.92% for 400 mg L^{-1}. As in earlier sections, the optimum activated carbon dose for P-CPA removal is 6 g L^{-1}.

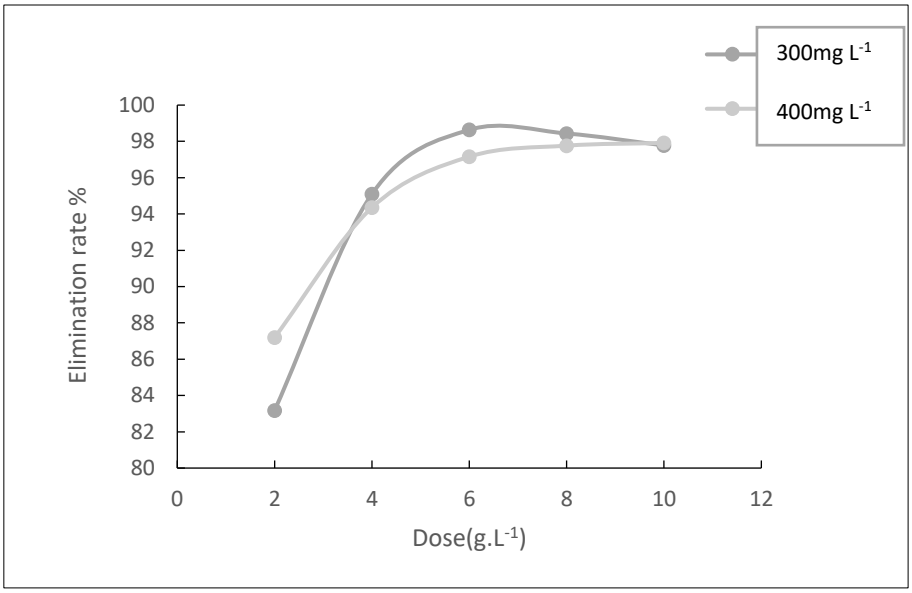

Figure V. 2. 21: Effect of adsorbent dose on the adsorption of P-CPA by AC_2'

V. 2. 3. 3. pH effect

The pH effect was studied in the range of 2–10. The results in **Figure V. 2. 22** show the adsorption elimination rate of P-CPA herbicides onto AC_2' as a function of pH. At pH 2.1, maximum elimination of the herbicide P-CPA was observed, reaching 99.36% for the 400 mg L^{-1} concentration and 99.27% for the 500 mg L^{-1} one. As the pH of the solution increased, the elimination rate decreased significantly, falling to 58.14% for 400 mg L^{-1} and 50% for 500 mg L^{-1} concentrations, respectively. At pH values above 3.56 (the pKa of P-CPA), the herbicide exists mainly in its deprotonated anionic form, reducing its interaction with the adsorbent surface. High adsorption at low pH is due to a strong electrostatic attraction between the positively charged AC_2' surface ($pH < pH_{pzc} = 7.7$) and the negatively charged P-CPA molecules. However, as pH increases above pH_{pzc}, the AC_2' surface becomes negatively charged, resulting in electrostatic repulsion and reduced adsorption.

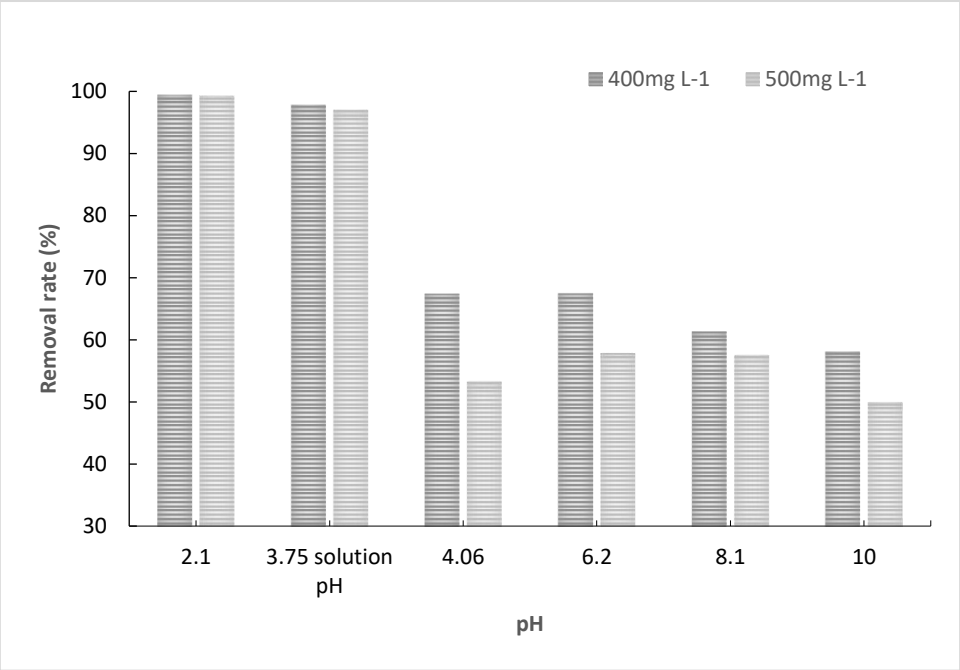

Figure V. 2. 22: Effect of pH on P-CPA adsorption by AC_2'

V. 2. 3. 4. Isotherm Models

Table V. 2. 8: Isotherm parameters of P-CPA adsorption by AC_2'

Nonlinear Model		**Adsorption Isotherm parameters**			**χ^2**	**RMSE**	**APE**
Langmuir	R^2	K_L (mg g^{-1})	q_m(mg g^{-1})		32.99	24.22	0.42
	0.87	0.12	284.8				
Freundlich	R^2	n	K_F ((mg. L^{-1})^n. (mg· g^{-1}))		10.34	12.35	4.53
	0.97	6.72	110.27				
Temkin	R^2	B_T	b (J mol^{-1})	K_T	5.36	9.08	3.27
	0.98	33.05	68.7	9.98			
(D-R)	R^2	β(mol^2 J^{-2})	q_{mD-R}(mg g^{-1})	E	79.59	36.41	13.73
	1	4.521×10^{-6}	270.35	0.13			
(R-P)	R^2	β(mol^2 J^{-2})	a_{r-p} (L g^{-1})	K_{RP} (L mg^{-1})	4.94	9.02	2.79
	0.98	0.9	102.94	0.73			

Figure V. 2. 23 shows that the experimental data for P-CPA adsorption on AC_2' does not fit the Langmuir isotherm model, with a coefficient of determination ($R^2 > 0.87$), a Chi-square error of 32.99, and an APE of 0.42. The maximum monolayer adsorption capacity was 284.8 mg g^{-1}.

The Freundlich isotherm had the highest R^2 value (>0.96), suggesting multilayer adsorption on a heterogeneous surface.

The Temkin model also accurately described adsorption, with a high coefficient of determination and low error values, indicating that interactions between the adsorbate and adsorbent are crucial in the process.

The Dubinin-Radushkevich (D-R) model also gave good results, with a predicted adsorption capacity of 270.3 mg g^{-1}, which is close to the Langmuir value. Adsorption energy (E = 0.13 kJ mol^{-1}) was less than 8 kJ mol^{-1}, confirming that P-CPA adsorption on AC_2' is physisorption (**Table V. 1. 8**).

The Redlich-Peterson fit was superimposed on the Freundlich fit, thus confirming that Freundlich is the best fit for P-CPA adsorption by AC_2'.

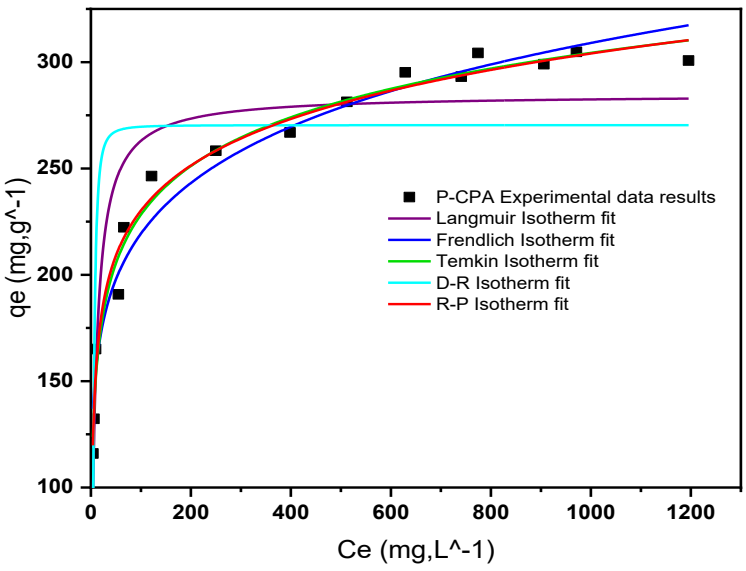

Figure V. 2. 23: Isotherm fitting of P-CPA adsorption by AC_2'

V. 2. 3. 5. Kinetic Study

Table V. 2. 9: Adsorption fitting parameters for pseudo-first-order, pseudo-second-order kinetics and intraparticle diffusion models of P-CPA adsorption by AC_2'

C_0 (mg L^{-1})	400	500
$q_{e\ (exp)}$ (mg g^{-1})	**66.62**	**83.13**
Pseudo-first order	$R^2 = 0.99$	$R^2 = 0.99$
$q_{e\ (calc)}$ (mg g^{-1})	**66.38**	**82.95**
k_1 (min^{-1})	0.976	0.926
Pseudo-second order	$R^2 = 1$	$R^2 = 1$
$q_{e(calc)}$ (mg g^{-1})	**66.58**	**83.22**
k_2 (g·mg^{-1}·min^{-1})	0.257	0.183
Intraparticle diffusion	$R^2 = 0.97$	$R^2 = 0.99$
$q_{e(calc)}$ (mg g^{-1})	**65.83**	**82.48**
k_{id} (min^{-1})	0.112	0.097

To clarify the adsorption kinetics of P-CPA on AC_2', two different concentrations (400 mg L^{-1} and 500 mg L^{-1}) were tested using the non-linear form. The results, summarized in **Table V. 1. 9**, show high coefficients of determination ($R^2 = 0.99$) for the pseudo-first-order model and ($R^2 = 1$) for the pseudo-second-order model at both concentrations (**Figure V. 2. 24**). In addition, the experimental adsorption capacity (q_e(exp) = 66.62 mg g^{-1} for 400 mg L^{-1} and 83.13 mg g^{-1} for 500 mg L^{-1} closely matched the calculated capacities (q_e(calc) = 66.38 mg g^{-1} and 82.95 mg g^{-1} for the pseudo-first-order model, and q_e(calc) = 66.58 mg g^{-1} and 83.22 mg g^{-1} for the pseudo-second-order model) (**Figure V. 2. 25**).

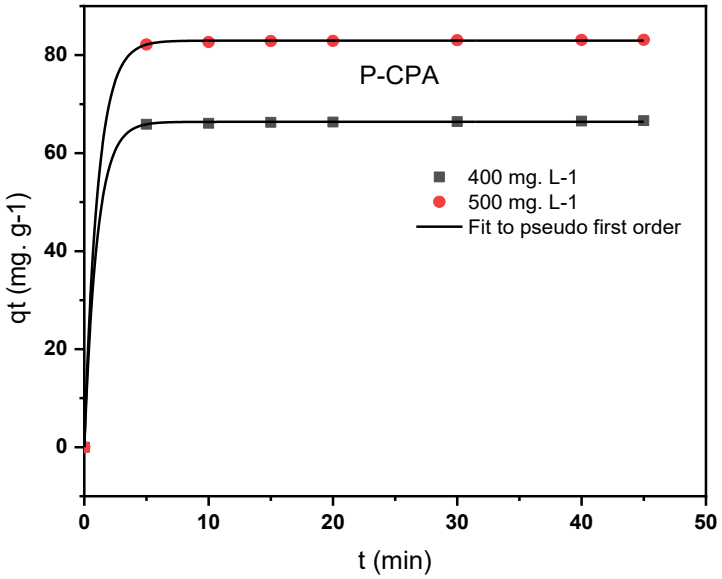

Figure V. 2. 24: Adsorption kinetics for P-CPA adsorption by AC_2' with pseudo-first order fitted model

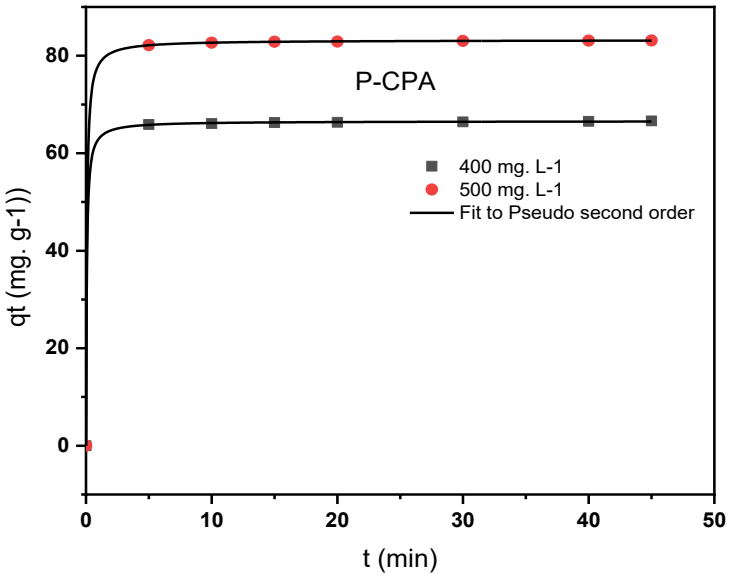

Figure V 2. 25: Adsorption kinetics for P-CPA adsorption by AC_2' with pseudo-second order fitted model

The intraparticle diffusion model also indicates that diffusion plays a role in adsorption, with the diffusion rate constant (k_{id}) increasing from 0.112 min^{-1} for the 400 mg L^{-1} concentration to 0.097 min^{-1} for the 500 mg L^{-1} concentration. This result suggests that the

adsorption mechanism is faster at low concentrations and becomes slow at higher concentrations (**Table V. 1. 9** and **Figure V. 2. 26**).

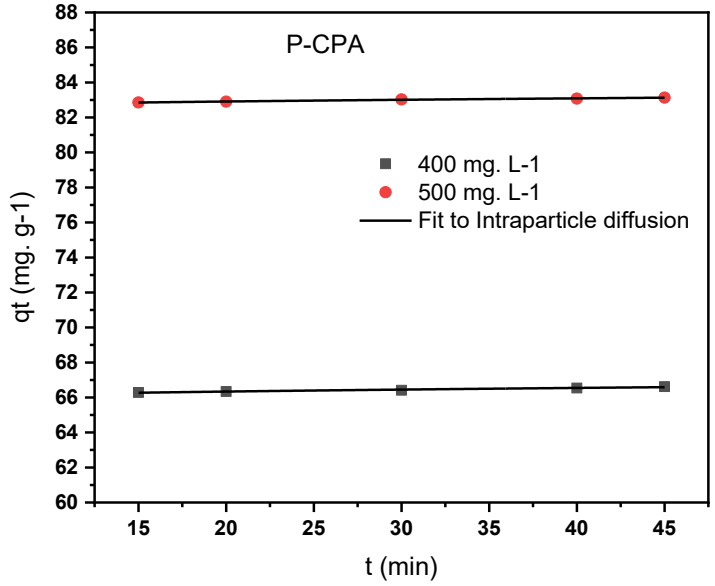

Figure V. 2. 26: Intraparticle diffusion model of P-CPA adsorption by AC_2'

V. 2. 3. 6. Thermodynamic Study

Table V. 2. 10: Thermodynamic parameters of P-CPA adsorption by AC_2'

Herbicide	C_o (mg L^{-1})	ΔH° (kJ mol^{-1})	ΔS° (kJ mol^{-1} K^{-1})	-ΔG° (kJ mol^{-1})			
				293 K	298 K	303 K	313 K
P-CPA	400	33.072	0.131	5.311	5.966	6.621	7.931
	500	40.217	0.157	5.784	6.569	7.354	8.924

The good linearity observed in the ln Kd = f(1/T) plots (**Figure V. 2. 27**), with coefficients of determination exceeding 0.99 for P-CPA (400 and 500 mg L^{-1}), confirms the reliability of the estimated thermodynamic parameters.

The positive values of enthalpy (ΔH°), 33.072 kJ. mol^{-1} and 40.217 kJ. mol^{-1} for the concentrations 400 and 500 mg. L^{-1} respectively, indicate that the adsorption process is endothermic.

The positive entropy (ΔS°) values, 0.131 kJ mol^{-1} for 400 mg L^{-1} and 0.157 kJ $mol^{-1}·K^{-1}$ for 500 mg L^{-1}, suggests increased randomness at the AC_2'/P-CPA interface during adsorption (**Table V. 2. 10**). The negative Gibbs free energy (ΔG°) values at all temperatures, such as -5.311 kJ mol^{-1} at 293 K and -7.931 kJ mol^{-1} at 313 K for 400 mg L^{-1} and -6.569 kJ mol^{-1} at 298 K and -8.924 kJ mol^{-1} at 313 K for 500 mg L^{-1}, confirms that the process is spontaneous and thermodynamically favorable (**Table V. 2. 10**). The decrease in the magnitude of ΔG° with increasing temperature shows improved adsorption at higher temperatures, likely due to the high porosity and large surface area of AC_2'.

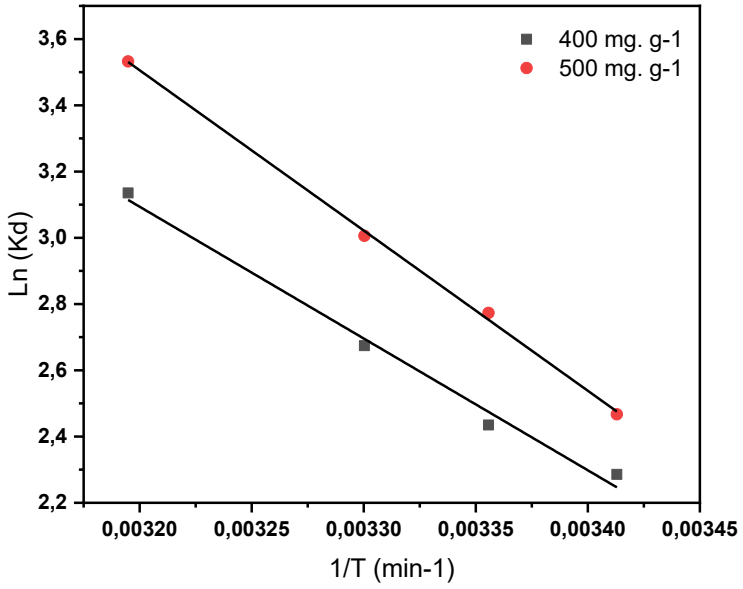

Figure V. 2. 27: Thermodynamic fitting of P-CPA adsorption by AC_2'

V. 2. 4. Lin removal from aqueous solution by AC_2' activated carbon

V. 2. 4. 1. Contact time effect

Depending on the results depicted in **Figure V. 2. 28,** it is noticed that the maximum adsorption elimination rate was at 90 minutes as an equilibrium rate is observed beyond this period, the removal rate at that time was 99.66% for the 70 mg L^{-1} and 99.83% for the 75 mg L^{-1} concentrations. After that, the equilibrium reached 99.41% and 99.11% for 70 and 75 mg L^{-1} respectively.

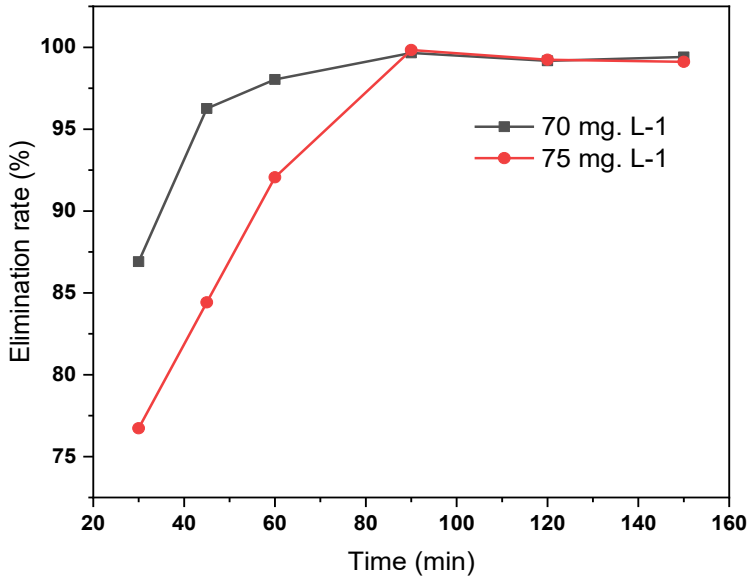

Figure V. 2. 28: Contact time effect of Lin adsorption by AC_2'

V. 2. 4. 2. Dose effect

The optimum dose of AC_2' is 4 g L^{-1} as shown in the following figure with maximum adsorption rates of 96.66 % for 70 mg L^{-1} and 96.95 % for 75 mg L^{-1} solute concentrations. A constant rate was then observed reaching 98.94 % for both concentrations at 12 g L^{-1} adsorbent dose, hence the optimum AC_2' dose is found to be 4 g L^{-1}.

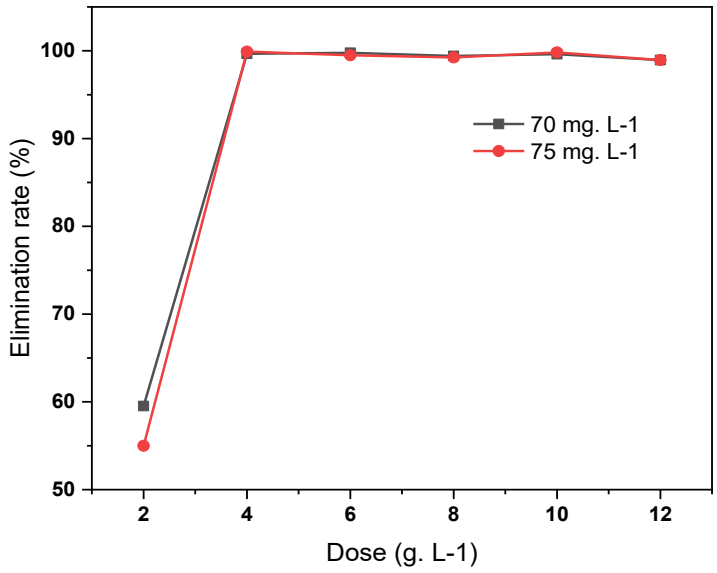

Figure V. 2. 29: Effect of adsorbent dose on the adsorption of Lin by AC_2'

V. 2. 4. 3. pH effect

The pH impact was investigated in the range of 2 to 10. **Figure V. 2. 30** shows the adsorption elimination rate of Lin herbicide onto AC_2' as a function of pH. Lin herbicide showed strong adsorption at acidic pH levels. The removal rate remained stable at 99% from pH 2 up to solution pH (7.07) for both concentrations (80 and 90 mg L^{-1}). Adsorption began to decrease above pH 7.07 due to changes in Lin's ionization state. With a pKa of 12.1, Lin remains in its non-ionized form at pH values below this value. The high adsorption efficiency below pH_{zpc} = 7.7 suggests that electrostatic interactions play a minor role in Lin adsorption and that other mechanisms such as van der Waals forces, electron donor-acceptor interactions, and hydrogen bonding contribute significantly. Above pH 7.07, adsorption decreased as the AC_2' surface becomes negatively charged, affecting interactions with Lin molecules.

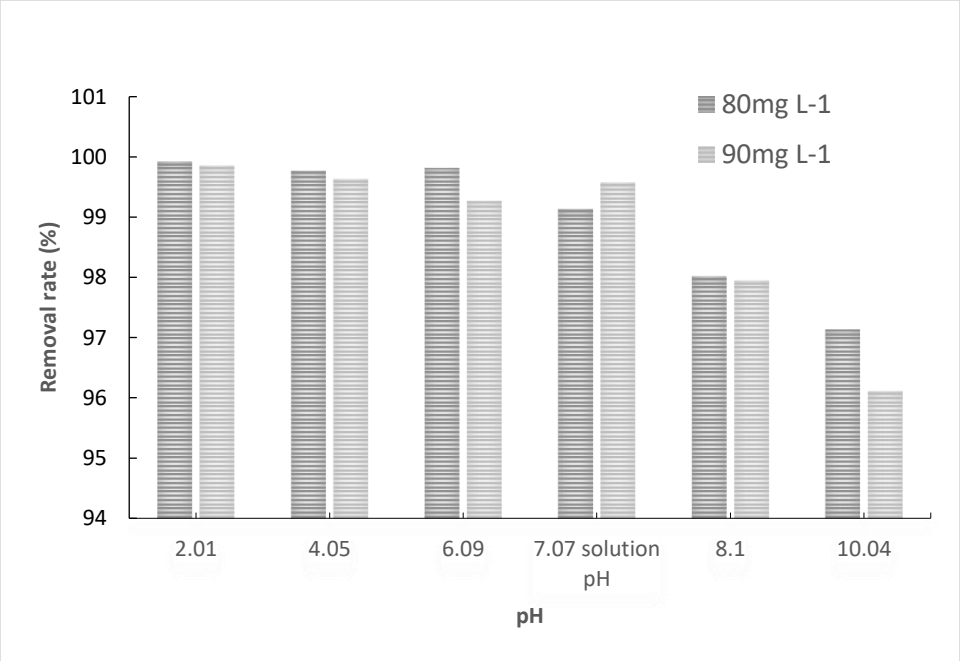

Figure V. 2. 30 : pH effect of Lin adsorption by AC_2'

V. 2. 4. 4. Isotherm models

Table V. 2. 11: Isotherm applied models of Lin adsorption by AC_2'

	Isotherm parameters				χ^2	RMSE	APE
Langmuir	R^2	K_L (mg g^{-1})	q_m (mg g^{-1})		6.18	5.29	2.66
	0.95	0.766	62.37				
Freundlich	R^2	n	K_F ((mg. $L^{-1})^n$. (mg· g^{-1}))		3.33	4.11	5.9
	0.93	3.62	21.12				
Temkin	R^2	B_T	b (J mol^{-1})	K_T	6.76	4.15	9.51
	0.89	9.86	230.19	9.63			
(D-R)	R^2	β (mol^2 J^{-2})	q_{mD-R}(mg g^{-1})	E	88.1	53.62	100
	0.87	0.2	59.33	1.6			
(R-P)	R^2	β (mol^2 J^{-2})	a_{r-p} (L g^{-1})	K_{RP} (L mg^{-1})	3.34	4.11	5.95
	0.93	0.72	7.55 x 10^{10}	3.58 x 10^9			

The Langmuir isotherm model provided a good fit, with $R^2 > 0.94$ (**Figure V. 2. 31**), a Chi-square error of 6.18, and an APE of 2.66. The maximum monolayer adsorption capacity was 62.37 mg g^{-1}.

The Freundlich isotherm provided the best fit ($R^2 > 0.97$), suggesting multilayer adsorption on heterogeneous AC_2' surfaces.

The Temkin model also described Lin adsorption well, highlighting the role of adsorbate-adsorbent interactions in the process.

Lin adsorption did not fit well with the Dubinin-Radushkevich (D-R) model ($R^2 = 0.87$), due to high error values ($\chi^2 = 88.1$, APE = 100), confirming that this model is not suitable for describing Lin adsorption. Adsorption energy (E = 1.6 kJ mol^{-1}) was less than 8 kJ mol^{-1}, confirming that Lin adsorption on AC_2' is mainly physisorption (**Table V. 2. 11**).

The Redlich-Peterson isotherm aligned well with the Freundlich model (R^2 up to 0.93), underscoring the fact that Lin adsorption follows a multilayer adsorption process.

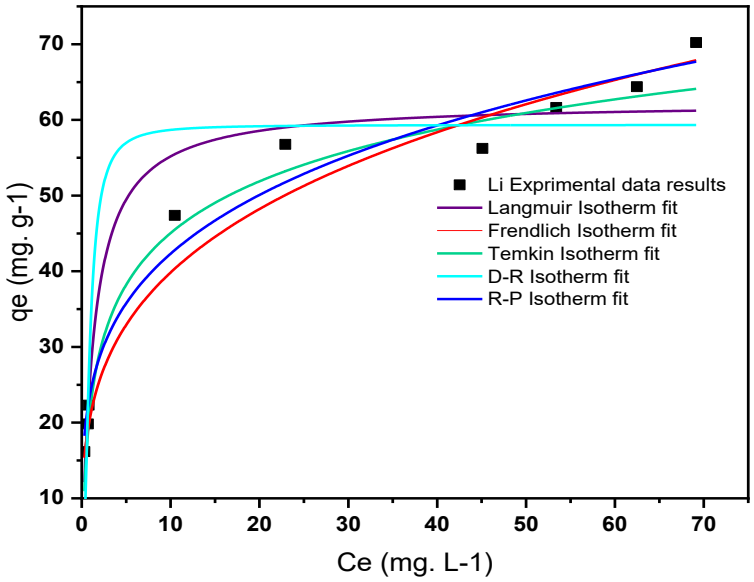

Figure V. 2. 31: Adsorption isotherm of Lin by AC_2'

V. 2. 4. 5. Kinetic study

Table V. 2. 12: Fitting parameters for the pseudo-first-order, the pseudo-second order adsorption kinetic and intraparticle diffusion models Lin adsorption by AC_2'

C_o (mg L^{-1})	**80**	**90**
$q_{e\ (exp)}$ (mg g^{-1})	**19.98**	**22.44**
Pseudo-first order	$R^2 = 0.98$	$R^2 = 0.96$
$q_{e\ (cal)}$ (mg g^{-1})	**19.32**	**21.92**
k_1 (min^{-1})	0.362	0.134
Pseudo-second order	$R^2 = 0.99$	$R^2 = 0.97$
$q_{e(cal)}$ (mg g^{-1})	**20.13**	**23.97**
k_2 (g mg^{-1} min^{-1})	0.04	0.009
Intraparticle diffusion	$R^2 = 0.94$	$R^2 = 0.83$
$q_{e(calc)}$ (mg g^{-1})	**19.29**	**21.12**
k_{id} (min^{-1})	0.077	0.152

Table V. 2. 12 shows that Lin adsorption kinetics by AC_2' had high R^2 values of 0.98 and 0.96 for the pseudo-first-order model (**Figure V. 2. 32**) and 0.99 and 0.97 for the pseudo-second-order model at initial concentrations of 80 mg L^{-1} and 90 mg L^{-1}, respectively. The experimental adsorption capacities (q_e(exp)) were 19.98 mg g^{-1} and 22.44 mg g^{-1}, closely aligned with the calculated values (q_e(calc)) from the pseudo-first-order model, 19.32 mg g^{-1} and 21.92 mg g^{-1}, and corresponding values for the pseudo-second-order model (**Figure V. 2. 33**): 20.13 mg g^{-1} and 23.97 mg g^{-1}. This confirms the applicability of these kinetic models.

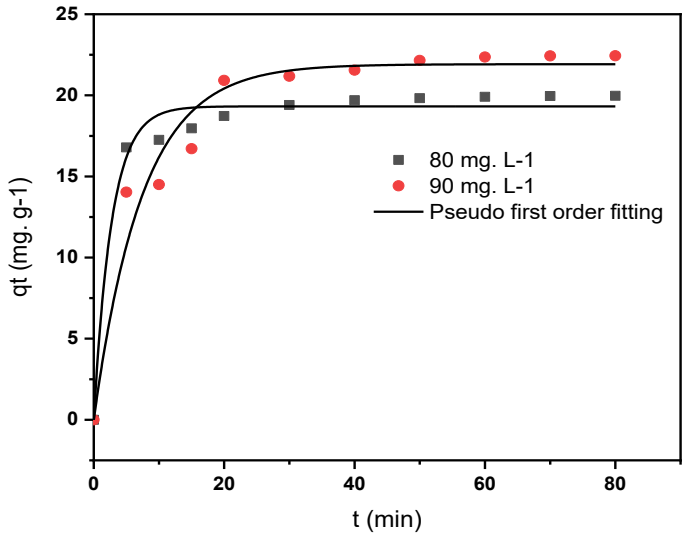

Figure V. 2. 32: Pseudo-first-order model for the adsorption of Lin on AC_2'

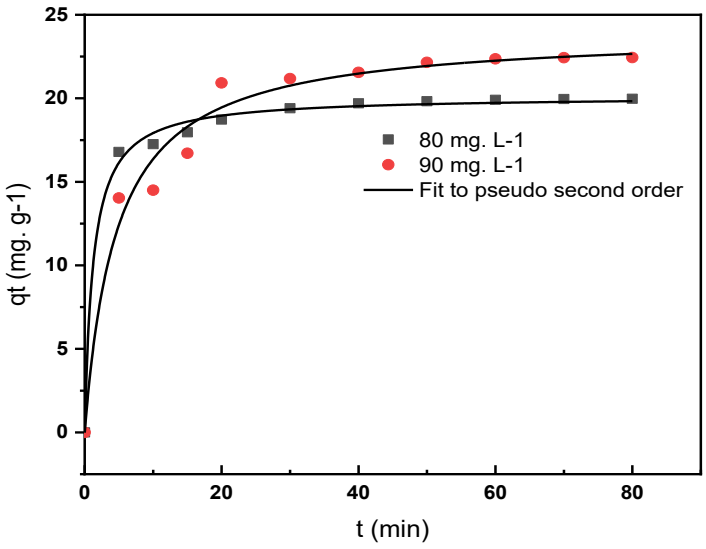

Figure V. 2. 33: Pseudo-second-order model for the adsorption of Lin on AC_2'

The intraparticle diffusion model suggests that diffusion significantly influences the adsorption process, as indicated by the calculated values of q_e(calc) (19.29 mg g^{-1} and 21.12 mg g^{-1}). It shows that the diffusion rate constant (k_{id}) increased from 0.077 min^{-1} to 0.152 min^{-1} with the initial concentration, which means that the adsorption procedure of Lin by AC_2' is faster at a higher concentration (**Table V. 2. 12** and **Figure V. 2. 34**).

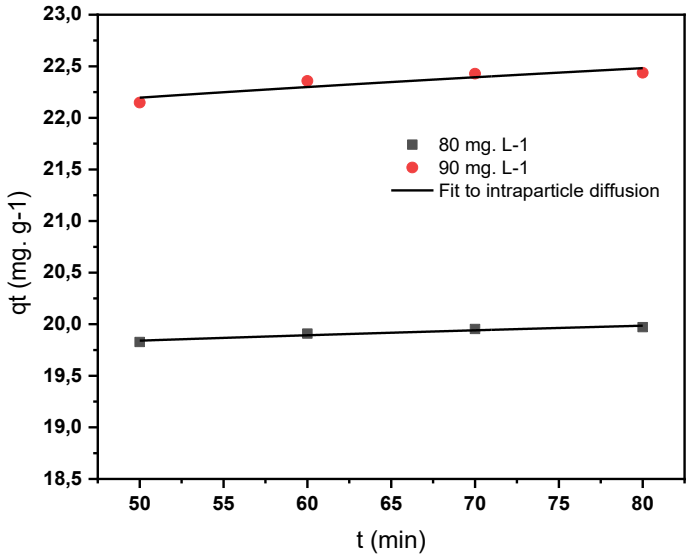

Figure V. 2. 34: Fit to intraparticle diffusion model of Lin adsorption by AC_2'

V. 2. 4. 6. Thermodynamic Study

Table V. 2. 13: Thermodynamic parameters of Lin adsorption by AC_2'

Herbicide	C_o (mg L^{-1})	ΔH° (kJ mol^{-1})	ΔS° (kJ mol^{-1} K^{-1})	-ΔG° (kJ mol^{-1})			
				293 K	298 K	303 K	313 K
Lin	80	-54.526	-0.145	12.041	11.316	10.591	9.141
	90	-65.565	-0.183	11.946	11.031	10.116	8.286

The ln (K_d) = f(1/T) plots for Lin adsorption at 80 and 90 mg L^{-1} (**Figure V. 2. 35**) showed high coefficients of determination exceeding 0.98, supporting the reliability of the thermodynamic parameters.

The negative enthalpy (ΔH°) values of -54.526 kJ mol^{-1} and -65.565 kJ mol^{-1} for 80 and 90 mg L^{-1}, respectively, indicate that the process is exothermic. The negative entropy (ΔS°) value is -0.145 kJ $mol^{-1}K^{-1}$ for the concentration 80 mg L^{-1} and -0.183 kJ mol^{-1} K^{-1} for the concentration 90 mg L^{-1}, which indicates decreased randomness at the AC_2'/Lin interface (**Table V. 2. 13**). The Gibbs free energy (ΔG°) values remain negative across all temperatures, such as -12.041 kJ mol^{-1} at 293 K and -9.141 kJ mol^{-1} at 313 K for 80 mg. L^{-1} and 11.946 kJ mol^{-1} at 293 K and 8.286 kJ mol^{-1} at 313 K for the concentration of 90 mg L^{-1}, confirming that Lin adsorption is spontaneous and thermodynamically favorable. However, the decrease in the value of ΔG° with higher temperatures indicates reduced adsorption efficiency at elevated temperatures (**Table V. 2. 13**).

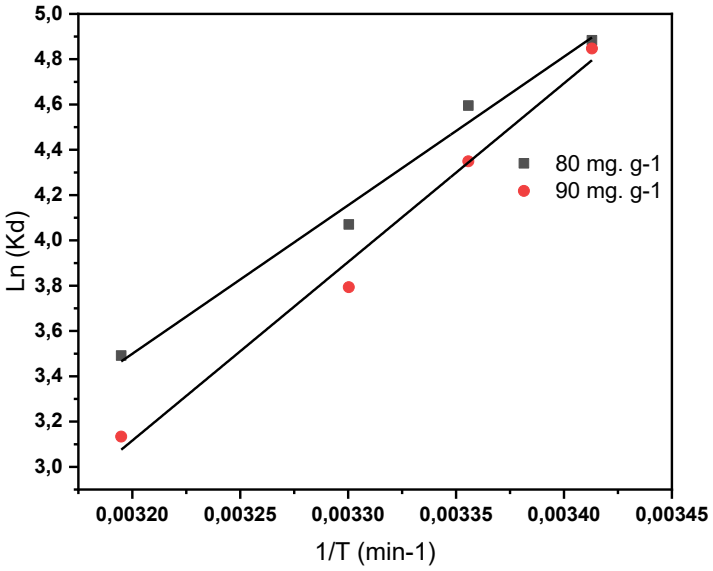

Figure V. 2. 35: Thermodynamic fitting of Lin adsorption by AC_2'

V. 3. Part 3: Theoretical Study Results of P-CPA ($C_8H_7O_3Cl$) molecule

In **Figure V. 3. 1.**, the gap energy of $C_8H_7O_3Cl$ (0) was calculated by the B3LYP approach using the 6 – 311 G(d,p) basis set, which is found to be 5.568 eV (**Table V. 3. 1**). The HOMO density distribution of the neutral molecule extends over its entire surface, excluding the carbonyl group. In contrast, the LUMO density is spread over the aromatic ring.

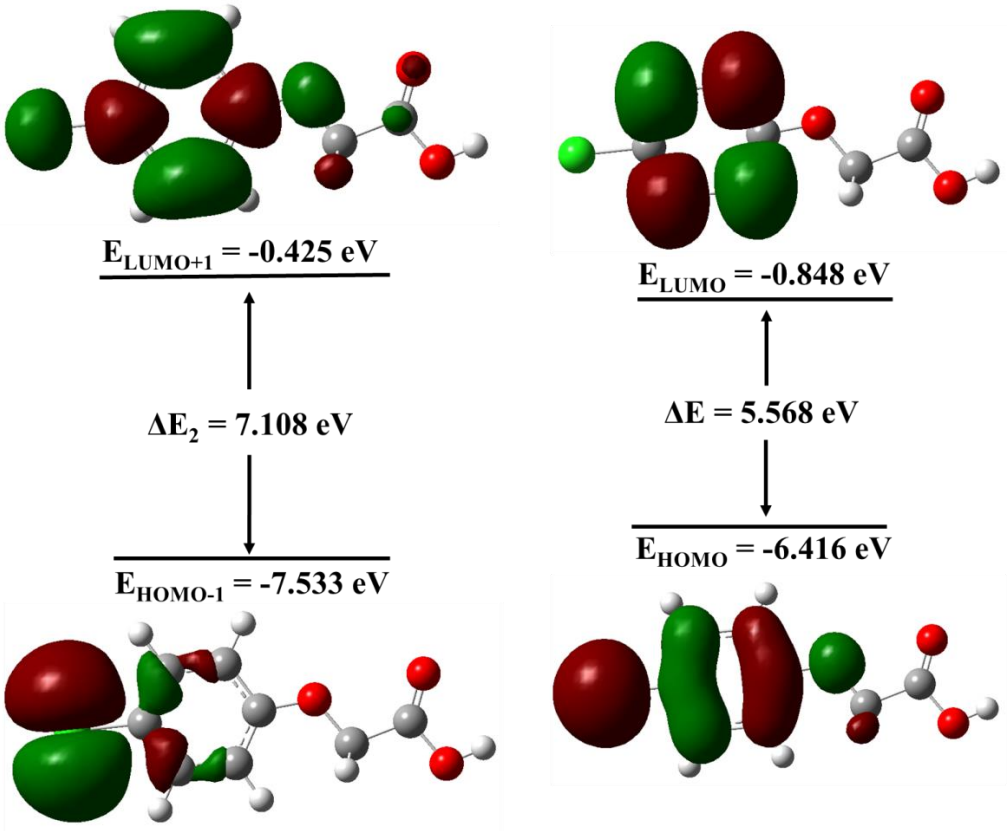

Figure V. 3. 1: The HOMO-LUMO diagram of P-CPA ($C_8H_7O_3Cl$) molecule

It can also be observed that the HOMO-1 density is strongly present in the chlorine atom and the region surrounding it. On the other hand, LUMO+ 1, is concentrated in the part of the aromatic ring and the chlorine atom. Indeed, once electrons are delocalized, they can interact more effectively with other compounds, forming preferred adsorption sites.

Table V. 3. 1: Global chemical reactivity descriptors of P-CPA ($C_8H_7O_3Cl$) molecule

Parameter	**P(1)**	**P(0)**	**P(-1)**
Dipole moment (Debye)	3.060	3.202	2.826
E_{HOMO} (eV)	-11,569	-6.416	-1.828
E_{LUMO} (eV)	-6.098	-0.848	3.716
ΔE (eV)	5.471	5.568	5.545
Electronegativity χ (eV)	8.834	3.632	-0.944
Chemical potential P (eV)	-8.834	-3.632	0.944
Chemical hardness η (eV^{-1})	2.736	2.784	2.772
Chemical softness S (eV)	0.182	0.179	0.180
Electrophilicity index ω (eV)	14.262	2.369	0.161
Nucleophilicity index N (eV)	0.949	6.102	10.690

Additionally, the small energy gap (5.471 eV) observed (**Table V. 3. 1)** in the $C_8H_7O_3Cl$ (1) molecule suggests that its cationic form is polarizable, resulting in increased reactivity compared to the other forms of $C_8H_7O_3Cl$.

Our calculation shows that the $C_8H_7O_3Cl$ (1) compound has the highest molecular electronegativity of 8.834 eV, which means that the compound of interest is more susceptible to gaining electrons rather than losing them. Additionally, the same molecule has a high electrophilicity index of 14.262 eV which is a good electrophile. Otherwise, the $C_8H_7O_3Cl$ (-1) indicates a high nucleophilicity index, suggesting its nucleophilicity character is higher than $C_8H_7O_3Cl$ and $C_8H_7O_3Cl$ (1). Moreover, other calculation results include chemical hardness and chemical softness values that confirm the stability of the $C_8H_7O_3Cl$ (0) molecule.

The dipole moment is a further measurement that was theoretically measured. It allows us to quantify how electric charges are distributed within a molecule. An increase in dipole moment intensifies the attraction between two molecules, as the opposite charges interact more strongly. The dipole moment is thus an important measure of molecule reactivity.

Our study assessed the dipole moment (μ) of the $C_8H_7O_3Cl$ molecule at 3.202 Debye in its neutral state. This measurement shows a large separation of charges within the molecule, which increases the contact between the molecules.

Table V. 3. 2: Quantum chemical parameter of P-CPA ($C_8H_7O_3Cl$) molecule

Atoms	P_k^+	P_k^-	ω_k	N_k
1C	0.0102	0.3078	0.0241	1.8780
2C	0.0874	0.1359	0.2071	0.8290
3C	0.1813	-0.0559	0.4296	-0.3410
4C	0.1323	0.2879	0.3135	1.7570
5C	-0.0590	0.1569	-0.1397	0.9573
6C	0.3157	-0.0639	0.7478	-0.3898
7H	-0.0020	-0.0208	-0.0047	-0.1271
8H	-0.0056	-0.0101	-0.0134	-0.0614
9H	0.0014	-0.0117	0.0032	-0.0714
10Cl	0.1418	-0.0005	0.3359	-0.0033
11O	0.1936	-0.0040	0.4587	-0.0246
12C	-0.0138	-0.0126	-0.0327	-0.0767
13H	0.0119	0.0346	0.0283	0.2109
14H	0.0119	0.0346	0.0283	0.2109
15C	0.0000	0.1637	0.0001	0.9986
16O	-0.0003	0.0716	-0.0007	0.4367
17O	0.0010	0.0062	0.0024	0.0378
18H	-0.0001	-0.0006	-0.0002	-0.0035
19H	-0.0079	-0.0190	-0.0187	-0.1158

Table V. 3. 2 and **Figure V. 3. 2** present the characteristics of the Parr functions for the nucleophiles of the cationic system, as well as the Parr P_k^+ functions for the electrophiles of the anionic system, in addition to the local electrophilicity and nucleophilicity values of the

compound under examination. In our case, chlorine (10Cl), oxygen (11O), and carbon (6C) atoms show the highest local electrophilicity (ωk) values, indicating that they are likely to be the preferred sites for nucleophilic attack. However, 15 C, 16 O, and the aromatic ring show the highest local nucleophilicity (N_k) values, indicating that such sites are the most suitable for electrophilic attack.

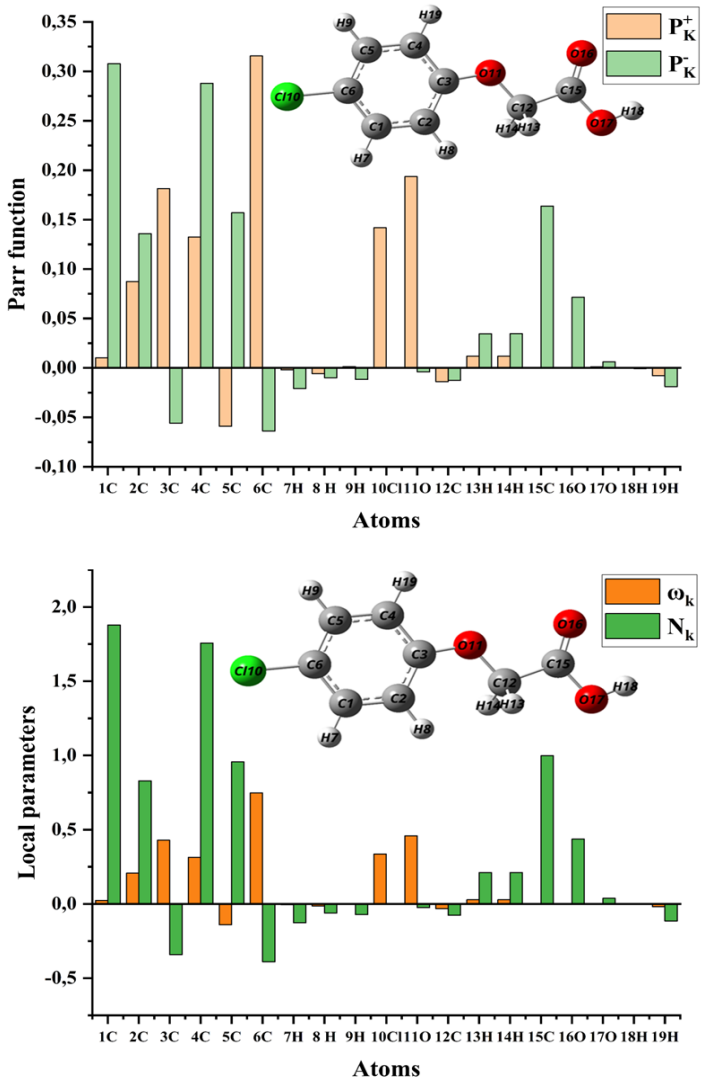

Figure V. 3. 2. The distribution of (a) the Parr functions, (b) electrophilicity (**ω_k**), and nucleophilicity (**N_k**) of $C_8H_7O_3Cl$

The results indicate that $C_8H_7O_3Cl$ (P-CPA) has more electrophilic sites than nucleophilic ones, but its nucleophilic sites are stronger in reactivity compared to its electrophilic regions. The chemical potential (μ) of the anionic form $C_8H_7O_3Cl$ (-1) (μ = 0.944 eV) is higher than that of the neutral $C_8H_7O_3Cl$ (0) (μ = −3.632 eV) and cationic $C_8H_7O_3Cl$ (1) (μ = −8.834 eV) forms, suggesting that the anionic form is more reactive.

The nucleophilicity index (N = 10.690 eV) of the anionic species is significantly greater than that of the neutral and cationic forms (N = 6.102 eV and −0.949 eV, respectively), confirming its strong nucleophilic character. A similar observation in the electrophilicity index values reinforces that the anionic form of P-CPA is highly reactive and less kinetically stable compared to the neutral and cationic species. This increased reactivity makes the anionic form more likely to participate in electron donation.

Furthermore, theoretical calculations suggest that P-CPA interacts strongly with activated carbon through electrostatic interactions when the adsorbent surface is positively charged (at pH below pH_{zpc} 7.6). The most nucleophilic centers, identified as C1, C2, C4, C5, and C15, play a crucial role in this interaction. Overall, the molecule exhibits a strong tendency to donate electrons rather than accept them, confirming its behavior as a nucleophile in chemical reactions.

References of Chapter V

[1] F. B. Benabed, S. Attouti, N. Douara, M. Termoul, M. İmamoğlu, A. Çoruh, N. Boukabcha, N. Benderdouche, B. Bestanı, Theoretical study of the herbicide parachlorophenoxyacetic acid molecule and its removal by activated carbon prepared from pine cone, Desalination and Water Treatment, 320 (2024).

[2] H. Mao, D. Zhou, Z. Hashisho, S. Wang, H. Chen, H. Wang, Preparation of pinewood-and wheat straw-based activated carbon via a microwave-assisted potassium hydroxide treatment and an analysis of the effects of the microwave activation conditions, BioResources, 10 (2015) 809-821.

[3] Z. Bahnes, Activation des noyaux de jujube pour l'obtention d'un charbon actif, Thesis, (2018).

[4] N. Kaya, Z.Y. Uzun, Investigation of effectiveness of pine cone biochar activated with KOH for methyl orange adsorption and CO_2 capture, Biomass Conversion and Biorefinery, 11 (2020) 1067-1083.

[5] B. B. Uzun, E. Yaman, Pyrolysis kinetics of walnut shell and waste polyolefins using thermogravimetric analysis, Journal of the Energy Institute, 90 (2017).

[6] M.A. Martín-Lara, G. Blázquez, A. Ronda, M. Calero, Kinetic study of the pyrolysis of pine cone shell through non-isothermal thermogravimetry: Effect of heavy metals incorporated by biosorption, Renewable Energy, 96 (2016).

[7] J.B. M. Gueye, C. Brunschwig, Etude de la synthèse des charbons actifs à partir de biomasses locales par activation chimique avec H_3PO_4, Journées Scientifiques du 2iE. Campus 2iE Ouagadougou, 6ème édition 4-8 avril (2011).

[8] I. K. Tetteh, I. Issahaku, A.Y. Tetteh, Recent advances in synthesis, characterization, and environmental applications of activated carbons and other carbon derivatives, Carbon Trends, (2024).

[9] D. Mohan, C.U. Pittman Jr, P.H. Steele, Pyrolysis of wood/biomass for bio-oil: a critical review, Energy & fuels, 20 (2006).

[10] O. W. Achaw, A study of the porosity of activated carbons using the scanning electron microscope, in: Scanning electron microscopy, IntechOpen, (2012).

[11] M.R. Yazdani, N. Duimovich, A. Tiraferri, P. Laurell, M. Borghei, J.B. Zimmerman, R. Vahala, Tailored mesoporous biochar sorbents from pinecone biomass for the adsorption of natural organic matter from lake water, Journal of Molecular Liquids, 291 (2019).

[12] R. Saleheen, M. Zaidi, S. Mehtab, K. Singhal, Sustainable Development of Pine Biocarbon Derived Thermally Stable and Electrically Conducting Polymer Nanocomposite Films, Renewable Energy for Sustainable Growth Assessment, (2022).

[13] S. Khalili, B. Khoshandam, M. Jahanshahi, Optimization of production conditions for synthesis of chemically activated carbon produced from pine cone using response surface methodology for CO 2 adsorption, RSC Advances, 5 (2015).

[14] S. Tyagi, A. Annachhatre, Solidification and Stabilization of Spent Pine-cone Biochar using Chemically Bonded Phosphate Cement, in: E3S Web of Conferences, EDP Sciences, (2023).

[15] A. Barroso-Bogeat, M. Alexandre-Franco, C. Fernández-González, A. Macías-García, V. Gómez-Serrano, Temperature dependence of the electrical conductivity of activated carbons prepared from vine shoots by physical and chemical activation methods, Microporous and Mesoporous Materials, 209 (2015).

[16] C. Saka, BET, TG–DTG, FT-IR, SEM, iodine number analysis and preparation of activated carbon from acorn shell by chemical activation with $ZnCl_2$, Journal of Analytical and Applied Pyrolysis, 95 (2012).

[17] S. Attouti, M. Termoul, Z. Bahnes, F. Baghdad-Benabed, N. Boukabcha, B. Bestani, N. Benderdouche, A. Chouaih, J. Srénscek-Nazzal, B. Michalkiewicz, Reduction of 2, 4-dichlorophenoxy acetic acid herbicide toxicity from aqueous media by adsorption: Experimental and theoretical study using DFT method, Journal of Dispersion Science and Technology, (2024).

[18] L. Rakhymbay, N. Bazybek, K. Kudaibergenov, S.-T. Myung, Z. Bakenov, A. Konarov, Present development and future perspectives on biowaste-derived hard carbon anodes for room temperature sodium-ion batteries, Journal of Power Sources, 602 (2024).

[19] A. Ghosh, C. do Amaral Razzino, A. Dasgupta, K. Fujisawa, L.H.S. Vieira, S. Subramanian, R.S. Costa, A.O. Lobo, O.P. Ferreira, J. Robinson, Structural and electrochemical properties of babassu coconut mesocarp-generated activated carbon and few-layer graphene, Carbon, 145 (2019).

[20] S.S. Mohtar, T.N.Z.T.M. Busu, A.M.M. Noor, N. Shaari, H. Mat, An ionic liquid treatment and fractionation of cellulose, hemicellulose and lignin from oil palm empty fruit bunch, Carbohydrate polymers, 166 (2017).

[21] S.M. Hafyana, A.F. Elsheikh, R. Hausler, Batch biosorption removal of total organic carbon from laundry aqueous media using raw pine and acid/microwave irradiation treated pine cone powder, Desalination and Water Treatment, 183 (2020).

[22] S.K. Singh, P.L. Dhepe, Isolation of lignin by organosolv process from different varieties of rice husk: Understanding their physical and chemical properties, Bioresource technology, 221 (2016).

[23] M. Lewoyehu, Comprehensive review on synthesis and application of activated carbon from agricultural residues for the remediation of venomous pollutants in wastewater, Journal of Analytical and Applied Pyrolysis, 159 (2021).

[24] L. Azzouz, D. Belaoui, N. Bouchemal Valorisation des cônes du pin pignon *Pinus pinea* L., par la synthèse du charbon actif, étude de caractérisation,2170-1652 (2022).

[25] N. Kaya, Z. Yildiz Uzun, Investigation of effectiveness of pyrolysis products on removal of alizarin yellow GG from aqueous solution: a comparative study with commercial activated carbon, Water Science and Technology, 81 (2020).

[26] R. Yang, J. Zhou, L. Wu, S. Ping, Fabrication of developed porous carbon derived from bluecoke powder by microwave-assisted KOH activation for simulative organic wastewater treatment, Diamond and Related Materials, 124 (2022).

[27] Y. Fu, Y. Shen, Z. Zhang, X. Ge, M. Chen, Activated bio-chars derived from rice husk via one- and two-step KOH-catalyzed pyrolysis for phenol adsorption, Sci Total Environ, 646 (2019).

[28] M. Lewoyehu, Comprehensive review on synthesis and application of activated carbon from agricultural residues for the remediation of venomous pollutants in wastewater, Journal of Analytical and Applied Pyrolysis, 159 (2021).

[29] P.J. Lodewyckx, The influence of water on the adsorption of organic vapours by activated carbon, Universitaire Instelling Antwerpen (Belgium), 1998.

[30] I. Gouaich, B. Bestani, Z. Bouberka, J. S. Nazza, A. Boucherdoud, N. Benderdouche Characterization of a low-cost Eucalyptus camaldulensis leaves based activated carbon for pharmaceutical residues removal from aqueous solutions, Desalination and Water Treatment, (2023).

[31] A. Pandiarajan, R. Kamaraj, S. Vasudevan, S. Vasudevan, OPAC (orange peel activated carbon) derived from waste orange peel for the adsorption of chlorophenoxyacetic acid herbicides from water: Adsorption isotherm, kinetic modelling and thermodynamic studies, Bioresour Technol, (2018).

[32] Q.H. Lin, H. Cheng, G.Y. Chen, Preparation and characterization of carbonaceous adsorbents from sewage sludge using a pilot-scale microwave heating equipment, Journal of Analytical and Applied Pyrolysis, 93 (2012).

[33] L. Zhang, Z. Yao, L. Zhao, Z. Li, W. Yi, K. Kang, J. Jia, Synthesis and characterization of different activated biochar catalysts for removal of biomass pyrolysis tar, Energy, 232 (2021).
[34] J.J. Manyà, B. González, M. Azuara, G. Arner, Ultra-microporous adsorbents prepared from vine shoots-derived biochar with high CO2 uptake and CO2/N2 selectivity, Chemical Engineering Journal, 345 (2018).
[35] J. Han, L. Zhang, B. Zhao, L. Qin, Y. Wang, F. Xing, The N-doped activated carbon derived from sugarcane bagasse for CO2 adsorption, Industrial Crops and Products, 128 (2019) 290-297.
[36] S. Rajkumar, S. Murugesh, V. Sivasankar, A. Darchen, T. Msagati, T. Chaabane, Low-cost fluoride adsorbents prepared from a renewable biowaste: syntheses, characterization and modeling studies, Arabian Journal of Chemistry, 12 (2019.
[37] İ. Demiral, C. Samdan, H. Demiral, Enrichment of the surface functional groups of activated carbon by modification method, Surfaces and Interfaces, 22 (2021).
[38] J. Bento, L. Senra, L. Maia, L. Almeida, L.M. Ferreira, M. Faria, D.d.S. Rosa, D.R. Mulinari, Prediction of Cr^{+6} Removal on the Biosorbent from Pine Cone Residue with Machine Learning Simulation (2025).
[39] M. Termoul, B. Bestani, N. Benderdouche, M.A. Chemrak, S. Attouti, Surface Modification of Olive Stone-based Activated Carbon for Nickel Ion removal from synthetic wastewater, Algerian Journal of Environmental Science and Technology, (2022).
[40] A. Ainane, Z. Shybat, F.M. Abdoul-Latif, R. Abbi, M. Achira, T. Ainane, Investigation into the effectiveness of activated carbon derived from chickpeas infected with anthracnose for the adsorption of methylene blue, Journal of Applied Science and Environmental Studies, 5 (2022) Appl. Sci. Envir. Stud. (2022).
[41] A.B. Alemayehu, E. Alemayehu, Optimization of reactive black 5 dye removal onto kaolin filter cake activated carbon using response surface methodology, (2024).
[42] X. Yang, Y. Wan, Y. Zheng, F. He, Z. Yu, J. Huang, H. Wang, Y.S. Ok, Y. Jiang, B. Gao, Surface functional groups of carbon-based adsorbents and their roles in the removal of heavy metals from aqueous solutions: a critical review, Chemical Engineering Journal, 366 (2019) 608-621.
[43] C. Li, K. Sun, Y. Sun, Y. Shao, G. Gao, L. Zhang, S. Zhang, X. Hu, Sustainable production of porous carbon from biomass: Influence of pre-carbonization on pore evolution and environment impact, Chemical Engineering Journal, 480 (2024).
[44] D. Bergna, Activated carbon from renewable resources: carbonization, activation and use, (2019).

[45] Y.X. Seow, Y.H. Tan, N. Mubarak, J. Kansedo, M. Khalid, M.L. Ibrahim, M. Ghasemi, A review on biochar production from different biomass wastes by recent carbonization technologies and its sustainable applications, Journal of Environmental Chemical Engineering, 10 (2022).

[46] M. Gayathiri, T. Pulingam, K. Lee, K. Sudesh, Activated carbon from biomass waste precursors: Factors affecting production and adsorption mechanism, Chemosphere, 294 (2022) 133764.

[47] R. Nandi, M.K. Jha, S.K. Guchhait, D. Sutradhar, S. Yadav, Impact of KOH activation on rice husk derived porous activated carbon for carbon capture at flue gas alike temperatures with high CO2/N2 selectivity, ACS omega, 8 (2023.

[48] N.A. Anuwar, P.F.M. Khamaruddin, Optimization of Chemical Activation Conditions for Activated Carbon From Coconut Shell Using Response Surface Methodology (RSM) and Its Ability to Adsorb CO_2, in: Third International Conference on Separation Technology 2020 (ICoST 2020), Atlantis Press, (2020).

[49] M. Şirazi, S. Aslan, Comprehensive characterization of high surface area activated carbon prepared from olive pomace by KOH activation, Chemical Engineering Communications, 208 (2021).

[50] J. Liu, K. Zhang, H. Wang, L. Lin, J. Zhang, P. Li, Q. Zhang, J. Shi, H. Cui, Advances in micro-/mesopore regulation methods for plant-derived carbon materials, Polymers, 14 (2022) 4261.

[51] W. Barszcz, M. Łożyńska, J. Molenda, Impact of pyrolysis process conditions on the structure of biochar obtained from apple waste, Scientific Reports, 14 (2024).

[52] T. Xu, K. Cui, S. Jin, Temperature-Driven Structural Evolution during Preparation of MCM− 41 Mesoporous Silica, Materials, 17 (2024).

[53] O.K. Strong, E. Nazari, T. Roy, K. Scotland, P.R. Pede, A.J. Vreugdenhil, Transforming micropores to mesopores by heat cycling KOH activated petcoke for improved kinetics of adsorption of naphthenic acids, Heliyon, 9 (2023).

[54] T. Li, J. Wu, X. Wang, H. Huang, Particle size effect and temperature effect on the pore structure of low-rank coal, ACS omega, 6 (2021).

[55] J. Choma, J. Jagiello, M. Jaroniec, Assessing the contribution of micropores and mesopores from nitrogen adsorption on nanoporous carbons: Application to pore size analysis, Carbon, 183 (2021).

[56] P. Liu, S. Sun, S. Huang, Y. Wu, X. Li, X. Wei, S. Wu, KOH Activation Mechanism in the Preparation of Brewer's Spent Grain-Based Activated Carbons, Catalysts, 14 (2024).

[57] W. S. Chen, Y. C. Chen, C.H. Lee, Modified activated carbon for copper ion removal from aqueous solution, Processes, 10 (2022).

[58] Y. Mu, W. He, H. Ma, Enhanced adsorption of tetracycline by the modified tea-based biochar with the developed mesoporous and surface alkalinity, Bioresource Technology, 342 (2021).

[59] A.M. Dehkhoda, E. Gyenge, N. Ellis, A novel method to tailor the porous structure of KOH-activated biochar and its application in capacitive deionization and energy storage, Biomass and Bioenergy, 87 (2016).

[60] J. Wang, S. Kaskel, KOH activation of carbon-based materials for energy storage, Journal of materials chemistry, 22 (2012).

[61] G. Dobele, A. Volperts, A. Plavniece, A. Zhurinsh, D. Upskuviene, A. Balciunaite, G. Niaura, L.C. Colmenares-Rausseo, L. Tamasauskaite-Tamasiunaite, E. Norkus, Thermochemical Activation of Wood with NaOH, KOH and H3PO4 for the Synthesis of Nitrogen-Doped Nanoporous Carbon for Oxygen Reduction Reaction, Molecules, 29 (2024) 2238.

[62] M. Yuan, Y. Kim, C.Q. Jia, Feasibility of recycling KOH in chemical activation of oil-sands petroleum coke, The canadian journal of chemical engineering, 90 (2012).

[63] J.O. Ighalo, Y. Zhou, Y. Zhou, C.A. Igwegbe, I. Anastopoulos, M.A. Raji, K.O. Iwuozor, A review of pine-based adsorbents for the adsorption of dyes, Biomass-derived materials for environmental applications, (2022).

[64] A. Nurhidayah, N. Zaini, M. Zulhaziman, M. Salleh, N. Zulbadli, N.A. Mohamad, S. Ezaty, N. Shafie, D.M. Sahri, S.S.A.M. Najib, Evaluation of physically modified kenaf core adsorbent for carbon dioxide adsorptive study, in: Journal of Physics: Conference Series, IOP Publishing, (2022).

[65] Z. Mekibes, B. Bestani, N. Douara, N. Benderdouche, M. Benzekri-Benallou, Simultaneous activation of Ficus carica L. leaves for the removal of emerging pollutants from aqueous solutions, Desalination and Water Treatment, 222 (2021).

[66] F. Ahmadijokani, H. Molavi, A. Peyghambari, A. Shojaei, M. Rezakazemi, T.M. Aminabhavi, M. Arjmand, Efficient removal of heavy metal ions from aqueous media by unmodified and modified nanodiamonds, J Environ Manage, 316 (2022).

[67] R. Boumaraf, S. Khettaf, F. Benmahdi, R. Masmoudi, A. Ferhati, Removal of 2,4-dichlorophenoxyacetic acid from aqueous solutions by nanofiltration and activated carbon, Biomass Conversion and Biorefinery, (2022).

[68] F.Z. Soufal, A. Zehhaf, B.A. Reguig, F. Chouli, Adsorption efficiency of malachite green dye (MG) using a novel composite adsorbent based on synthesized alumina/acid-activated clay, Desalination and Water Treatment, 273 (2022).

[69] E.G. Lemraski, S. Sharafinia, Kinetics, equilibrium and thermodynamics studies of Pb2+ adsorption onto new activated carbon prepared from Persian mesquite grain, Journal of Molecular Liquids, 219 (2016.

[70] L. H. Mendoza-huizar, C.H. Rios-reyes, G.A. álvarez-romero M.T. Ramírez-silva, M.E. Palomar-pardavé, Electrophilic and nucleophilic chemical reactivity of neutral and anionic forms of 4-CPA, 24D-CPA, 34-CPA and 245T-CPA through conceptual DFT reactivity descriptors., (2017)

[71] S.M. Yakout, Mohamed R. Hassan, b Mohamed E. El-Zaidy, and Omar H. Shair,c and Abdalrhaman M. Salih Kinetic Study of Methyl Orange Adsorption on Activated Carbon Derived from Pine (Pinus strobus) Sawdust, (2019).

[72] A. Naboulsi, L. El Mersly, H. Yazid, M. El Himri, S. Rafqah, M. El Haddad, Adsorption behaviors and mechanisms by theoretical study of herbicide 2,4,5-Trichlorophenoxyacetic on activated carbon as a new biosorbent material, Journal of the Taiwan Institute of Chemical Engineers, 142 (2023).

[73] T.S. Khayyun, A.H. Mseer, Comparison of the experimental results with the Langmuir and Freundlich models for copper removal on limestone adsorbent, Applied Water Science, 9 (2019) 170.

[74] K.P. Kuśmierek, Maciej Biniak, Stanislaw Świątkowski, Andrzej Dąbek, Lidia, Adsorption and Electrodegradation of Phenoxyacetic Acids on Various Activated Carbons, International Journal of Electrochemical Science, 15 (2020).

[75] F. Dhaouadi, L. Sellaoui, S. Taamalli, F. Louis, A. El Bakali, M. Badawi, J. Georgin, D.S. Franco, L.F. Silva, A. Bonilla-Petriciolet, Enhanced adsorption of ketoprofen and 2, 4-dichlorophenoxyactic acid on Physalis peruviana fruit residue functionalized with H2SO4: Adsorption properties and statistical physics modeling, Chemical Engineering Journal, 445 (2022).

[76] G.A. Sayğılı, Conversion of a renewable bio-resource to a functional composite material: Product design, comprehensive characterization and adsorption of 2, 4-D herbicide, Sustainable chemistry and pharmacy, 18 (2020).

[77] S. Mandal, B. Sarkar, A.D. Igalavithana, Y.S. Ok, X. Yang, E. Lombi, N. Bolan, Mechanistic insights of 2, 4-D sorption onto biochar: Influence of feedstock materials and biochar properties, Bioresource technology, 246 (2017).

[78] K.Y. Lim, K.Y. Foo, One-step synthesis of carbonaceous adsorbent from soybean bio-residue by microwave heating: Adsorptive, antimicrobial and antifungal behavior, Environmental research, 204 (2022.

[79] T. Si, L. Liu, X. Liang, H. Duo, L. Wang, S. Wang, Solid-phase extraction of phenoxyacetic acid herbicides in complex samples with a zirconium(IV)-based metal-organic framework, J Sep Sci, 42 (2019).

[80] F.M. Machado, C.P. Bergmann, T.H. Fernandes, E.C. Lima, B. Royer, T. Calvete, S.B. Fagan, Adsorption of Reactive Red M-2BE dye from water solutions by multi-walled carbon nanotubes and activated carbon, J Hazard Mater, 192 (2011).

[81] S. Arif, S. Zafar, M.I. Khan, S. Manzoor, A. Shanableh, J.F. Garcia, M. Hayat, Removal of chromium (VI) by commercial anion exchange membrane BII from an aqueous solution: Adsorption kinetic, equilibrium and thermodynamic studies, Inorganic Chemistry Communications, 152 (2023).

[82] L. Ding, B. Zou, W. Gao, Q. Liu, Z. Wang, Y. Guo, X. Wang, Y. Liu, Adsorption of Rhodamine-B from aqueous solution using treated rice husk-based activated carbon, Colloids and Surfaces A: Physicochemical and Engineering Aspects, 446 (2014).

[83] M. Li, Y. Wang, Y. Liu, H. Wang, H. Song, Preparation of active carbon through one-step NaOH activation of coconut shell biomass for phenolic wastewater treatment, Research on Chemical Intermediates, 48 (2022).

[84] J. Shah, M.R. Jan, Magnetic chitosan graphene oxide composite for solid phase extraction of phenylurea herbicides, Carbohydrate polymers, 199 (2018).

[85] S. Attouti, B. Bestani, N. Benderdouche, Chemical surface modification of seaweed species for cationic dyes removal from simulated water, Indian J. Environ. Prot, 40 (2020)

CONCLUSION AND PERSPECTIVES

Conclusion

This study successfully prepared activated carbon from pine cones using chemical activation with potassium hydroxide. The results confirmed that the two-step activation process produced activated carbon with superior porosity and higher yields compared to the one-step method. Among the prepared materials, K-AC_2 and AC_2' activated carbons exhibited the best textural and adsorption properties, making them highly effective for pollutant removal.

K-AC_2, which was synthesized using two-step KOH activation in a muffle furnace at 800°C for 30 minutes with a 1:1 impregnation ratio, achieved a yield of 72.25%, a BET surface area of 430.504 $m^2\ g^{-1}$, a micropore surface area of 270.52 $m^2\ g^{-1}$, an iodine number of 666.38 mg g^{-1}, and a Methylene blue index of 72.77 mg g^{-1}. On the other hand, AC_2', which was prepared in a tube furnace under nitrogen atmosphere using a 1:2 impregnation propotion, offered even greater microporosity with a micropore surface area of 1039.22 $m^2\ g^{-1}$, an iodine number of 888.51 mg g^{-1}, a Methylene blue index of 50.60 mg g^{-1}, and a yield of 72.57%.

The parametric study confirmed that activation temperature, contact time, and impregnation ratio had a significant impact on the yield and porosity of the activated carbon. Increasing temperature and activation time improved porosity but led to greater material loss, reducing the final yield. The highest yields were obtained for $AC_{600.45}$ (77.65%), $AC_{700.45}$ (75.01%), $AC_{600.30}$ (74.75%), $AC_{700.30}$ (72.25%), $AC_{800.45}$ (71.63%), K-AC_2 (66.95%), and K-AC_2' (65.06%), confirming that a two-step activation approach provides a balance between material retention and enhanced porosity.

Pesticides, particularly herbicides, are important for modern agriculture, however, they pose serious hazards to the environment and human health. Their persistence in soil and water requires effective removal procedures to mitigate their negative impacts. Activated carbon adsorption has proven to be one of the most successful techniques for removing pesticides from wastewater, serving to maintain ecosystems and provide clean water for future generations.

In our research, the adsorption experiments demonstrated the effectiveness of these activated carbons in removing herbicides from aqueous solutions.

The findings showed that adsorption of para-chlorophenoxyacetic acid followed several models (Langmuir, Freundlich, Temkin, Dubinin-Radushkevich, and Redlich-Paterson), with

the Freundlich model providing the best fit. K-AC_2 achieved a maximum adsorption capacity of 266.5 mg g^{-1}, while AC_2' exhibited an even higher adsorption capacity of 284.8 mg g^{-1}.

Similarly, for the adsorption of Linuron (Lin), K-AC_2 reached a maximum adsorption capacity of 43.76 mg g^{-1}, whereas AC_2' gave a superior performance with an adsorption capacity of 62.37 mg g^{-1}. The adsorption kinetics followed a pseudo-second-order model, indicating that both physical and chemical interactions can play a role in the adsorption process. The thermodynamic study confirmed that adsorption was spontaneous and endothermic for P-CPA adsorption by AC_2' as well as for P-CPA and Lin adsorption by K-AC_2, but exothermic for Lin adsorption by AC_2'. Furthermore, the desorption study showed that K-AC_2 could be regenerated, achieving a 69.72% desorption rate, which improves its applicability for reuse in multiple adsorption cycles.

Perspectives

To further enhance the performance of pine cone-based activated carbon, several aspects could be investigated.

First, optimizing the activation process by optimizing the impregnation ratio using another ratio or using another activating agent, such as phosphoric acid or sodium hydroxide, could further improve the adsorption capacity and material stability.

Moreover, introducing CO_2/steam in a tubular furnace with nitrogen (N_2) could improve the activated carbon porosity. In addition, testing these activated carbons on other contaminants, inorganic elements such as heavy metals, could enlarge the potential applications of this material in environmental remediation.

Another important perspective is to test the applicability of these materials in real wastewater treatment systems. Since this study focused on synthesized solutions, future research should evaluate the adsorption performance in complex wastewater containing multiple organic and inorganic contaminants.

Also, long-term stability and regeneration efficiency of the activated carbon after multiple adsorption-desorption cycles would be essential for practical applications.

Finally, combining adsorption by activated carbon with other treatment techniques, such as advanced oxidation processes or membrane filtration, could also enhance the overall efficiency of water purification systems.

To realize these prospects, the findings of this study could contribute to the development of a more sustainable and efficient approach to wastewater treatment using renewable-based activated carbons (Pine cone-based activated carbon).

Appendix I

I. 1. Muffle Furnace

Used for carbonization and activation of precursors at high temperatures to prepare activated carbons. A muffle furnace operates on the principle of controlled heating in an insulated chamber, providing a high-temperature environment for thermal processes. It is commonly used in the preparation of materials for processes such as carbonization and activation.

The characteristics of the muffle furnace, such as uniform temperature distribution, precise temperature control, and insulation, make it ideal for these processes, guaranteeing consistent material properties for the activated carbon obtained.

Figure I .1: Muffle furnace used for pyrolysis and activation (Carbolite furnace)

I. 2. Tube furnace under an inert nitrogen atmosphere

The tubular furnace was used for carbonization under an inert nitrogen atmosphere to avoid oxidation and effectively monitor the pyrolysis environment. This ensures that the precursor material is efficiently converted into activated carbon, and the activation process is completely performed under an inert and unoxidized atmosphere.

Figure I. 2: Tube furnace used under nitrogen atmosphere (Protherm furanace)

I. 3. Laboratory grinder

The laboratory grinder was used to reduce the size of the raw material before activation and to homogenize the activated carbon samples to conduct uniform characterization and adsorption experiments.

Figure I. 3: Laboratory grinder used for sample preparation (**Fritsch pulverisette**)

I. 4. Laboratory siever

The laboratory siever was used to get specific particle size fractions for the precursor and the prepared activated carbon, guaranteeing uniformity for further characterization and adsorption tests.

Figure I. 4: Laboratory Siever used during the preparation of the activated carbons **(Retsch)**

I. 5. Drying oven

The drying oven was used to remove moisture from the precursor material and activated carbon samples before further processing or characterization. This equipment provided an accurate assessment of adsorption characteristics.

Figure I. 5: Drying oven used in the Laboratory (HRDH-71 and venticell)

I. 6. pH meter

The pH meter was used to measure the pH of solutions during adsorption experiments and parametric adsorption studies. It also measured the point of zero charge pH (pH_{pzc}) of activated carbon, which is an important parameter for understanding adsorption behavior.

Figure I. 6: pH meter used for pH measurement (ADWA Hungary pH and Conductivity Meter)

I. 7. Centrifuge

The centrifuge was used to separate the solid and liquid phases of the activated carbon during the depollution tests, ensuring effective isolation of the material.

Figure I. 7: Centrifuge used for solid-liquid separation in our study (Hettich EBA III centrifuge)

Appendix II

Scientific Contributions

International Publications

1. **Fatma Baghdad Benabed**, Salima Attouti, Nadia Douara, Mourad Termoul, Mustafa İmamoğlu, Ali Çoruh, Nourdine Boukabcha, Nouredine Benderdouche, Benaouda Bestani. "Theoretical study of the herbicide parachlorophenoxyacetic acid molecule and its removal by activated carbon prepared from pine cone". Journal of Desalination and Water Treatment 320 (2024) 100719. https://doi.org/10.1016/j.dwt.2024.100719

2. Salima Attouti, Mourad Termoul, Zohra Bahnes, **Fatma Baghdad-Benabed**, Nourdine Boukabcha, Benaouda Bestani, Nouredine Benderdouche, Abdelkader Chouaih, Joanna Srénscek-Nazzal & Beata Michalkiewicz. "Reduction of 2,4-dichlorophenoxy acetic acid herbicide toxicity from aqueous media by adsorption: Experimental and theoretical study using DFT method" Journal of Dispersion Science and Technology. https://doi.org/10.1080/01932691.2024.2414276

International Conferences

1. **Fatma BAGHDAD BENABED**, Salima ATTOUTI, Nadia DOUARA, Mokhtar Benallou BENZEKRI, Mourad TERMOUL, Benaouda BESTANI, Nouredine BENDERDOUCHE. "PREPARATION OF MICROPOROUS ACTIVATED CARBON FROM LIGNOCELLULOSIC RAW MATERIAL FOR WASTEWATER TREATMENT". 3rd BİLSEL INTERNATIONAL WORLD SCIENCE AND RESEARCH CONGRESS" 17-18 February 2024, İSTANBUL/TÜRKİYE

2. **Fatma BAGHDAD BENABED**, Nadia DOUARA, Salima ATTOUTI, Mokhtar Benallou BENZEKRI, Mourad TERMOUL, Benaouda BESTANI, Noureddine BENDERDOUCHE. "DEVELOPMENT OF POROUS ADSORBENT MATERIAL DERIVED FROM ORGANIC WASTE FOR WASTEWATER PROCESSING". ASES INTERNATIONAL VAN SCIENTIFIC RESEARCH CONFERENCE held in Van, Türkiye, on September 22-24, 2023

3. **Fatma BAGHDAD BENABED**, Salima ATTOUTI, Nadia DOUARA, Mokhtar Benallou BENZEKRI, Mourad TERMOUL, Benaouda BESTANI, Noureddine BENDERDOUCHE. "PRODUCTION OF A NOVEL ADSORBENT MATERIAL FROM ORGANIC RESIDUE". 4th Baskent International Conference on Multidisciplinary Studies held online and in-person on August 4-6, 2023 / Ankara, Türkiye 05-08-2023

4. **Fatma BAGHDAD BENABED**, Nadia DOUARA, Salima ATTOUTI, Mokhtar Benallou BENZEKRI, Mourad TERMOUL, Benaouda BESTANI, Nouredine BENDERDOUCHE. "Preparation of activated carbon by chemical activation from vegetal waste". 1st BİLSEL INTERNATIONAL SUMELA SCIENTIFIC RESEARCHES CONGRESS" 22-23 JULY 2023, TRABZON/TURKEY

5. **Fatma BAGHDAD BENABED**, Salima ATTOUTI, Nadia DOUARA, Mourad TERMOUL, Mokhtar Benallou BENZEKRI, Benaouda BESTANI, Nouredine BENDERDOUCHE. "The study of the porosity of prepared activated carbons". 4th

INTERNATIONAL HASANKEYF SCIENTIFIC RESEARCH AND INNOVATION CONGRESS 29-30 APRIL 2023/ Turkey.

6. **Fatma BAGHDAD BENABED**, Asmae BENABBOU, Halima DELALI, Salima ATTOUTI, Nadia DOUARA, Mourad TERMOUL, Mokhtar Benallou BENZEKRI, Benaouda BESTANI, Nouredine BENDERDOUCHE. "The study of the influence of the carbonization temperature on the activation of a raw material". 4th International Dicle Scientific Research and Innovation Congress 18-19 April 2023- Diyarbakir-Türkiye

7. **Fatma BAGHDAD BENABED**, Asmae BENABBOU, Salima ATTOUTI, Nadia DOUARA, Mourad TERMOUL, Mokhtar Benallou BENZEKRI, Benaouda BESTANI, Nouredine BENDERDOUCHE. "The influence of the carbonization process on the performance of prepared activated carbons". 4th International Cappadocia Scientific Research Congress April 16-17, 2023 / Nevşehir-Türkiye

8. **Fatma BAGHDAD BENABED**, Asmae BENABBOU, Halima DELALI, Iman GOUAICH, Salima ATTOUTI, Nadia DOUARA, Mourad TERMOUL, Mokhtar Benallou BENZEKRI, Benaouda BESTANI, Noureddine BENDERDOUCHE. "Comparison between one-step and two-step chemical activation for the preparation of activated carbon". 5th International Palandoken Scientific Studies Congress 18-19 March 2023 Erzurum/Turkey

9. **Fatma BAGHDAD BENABED**, Asmae BENABBOU, Salima ATTOUTI, Nadia DOUARA, Mourad TERMOUL, Mokhtar Benallou BENZEKRI, Benaouda BESTANI, Nouredine BENDERDOUCHE. "The efficiency of the carbonization step on the activation of an adsorbent material". 3rd International Dicle Scientific Research And Innovation Congress 26-27 November 2022- Diyarbakir/ Turkey

National Conferences

1. **Fatma Baghdad Benabed**, Salima Attouti, Nadia Douara, Mourad Termoul, Nouredine BENDERDOUCHE, Benaouda BESTANI. "Removal of the herbicide Parachlorophenoxyacetic acid by activated carbon prepared from pine cone". 3eme Séminaire National Environnement et Gestion Durable 8-9 Décembre 2024 / Mostaganem, Algérie

2. **Fatma BAGHDAD BENABED**, Asmae BENABBOU, Halima DELALI, Salima ATTOUTI, Nadia DOUARA, Mourad TERMOUL, Mokhtar Benallou BENZEKRI, Benaouda BESTANI, Nouredine BENDERDOUCHE. "The influence of the activation parameters on the porosity of activated carbon". Le $\mathbf{1}^{er}$ Séminaire National sur les Matériaux pour l'Environnement et le Développement Durable (MEDD) Webinaire 9 &10 Mai 2023 / Relizane, Algérie

Workshop

Fatma BAGHDAD BENABED, Salima ATTOUTI, Nadia DOUARA, Mokhtar Benallou BENZEKRI, Mourad TERMOUL, Benaouda BESTANI, Noureddine BENDERDOUCHE. "Transformation Process of Lignocellulosic Raw Material into Porous Activated Carbon for Wastewater Treatment". Workshop on Durability and Advanced Technologies May 21-22, 2024, Mostaganem, Algeria

- Certificate of participation in "Experimental Design" in Workshop on Durability and Advanced Technologies May 21-22, 2024, Mostaganem, Algeria
- Certificate of participation in "Successful Completion of the thesis" in Workshop on Durability and Advanced Technologies May 21-22, 2024, Mostaganem, Algeria